SAPIENZA
UNIVERSITÀ DI ROMA

High Precision Flavour Physics

Scuola di dottorato Vito Volterra

Dottorato di Ricerca in Fisica – XXXIII Ciclo

Candidate

Matteo Di Carlo
ID number 1556257

Thesis Advisor

Prof. Guido Martinelli

October 31, 2020

High Precision Flavour Physics
Ph.D. thesis. Sapienza – University of Rome

This thesis has been typeset by LaTeX and the Sapthesis class.

Version: January 20, 2021

Author's email: matteo.dicarlo@uniroma1.it

Abstract

Flavour Physics is a very powerful tool to test the Standard Model and quantify the effects of New Physics by exploring possible departures from the model. It is necessary, however, to increase the level of precision of the experimental measurements and of the theoretical predictions in order to be sensitive to possible deviations. In this thesis we address this issue by providing theoretical improvements for both non-perturbative and perturbative calculations of some relevant flavour observables. On the one hand, we present a new strategy to renormalize lattice operators in QCD+QED in the RI-MOM scheme, fully including the non perturbative dynamics of QCD, and QED at $\mathcal{O}(\alpha_{\rm em})$. We show how to keep systematically into account all contributions not separable between the two interactions, thus overcoming the factorization approximation in which the mixed effects are neglected. A numerical analysis in the electro-quenched approximation is carried out for quark bilinear operators and for the case of the matrix elements relevant for $K_{\ell 2}$ and $\pi_{\ell 2}$ processes and for semileptonic decays like $K_{\ell 3}$. A detailed discussion of the calculation of the leading isospin breaking corrections to the leptonic decay rates $\Gamma(K_{\mu 2})$ and $\Gamma(\pi_{\mu 2})$ is presented. On the other hand, we compute for the first time the anomalous dimension matrices of quark bilinear and weak four-fermions semileptonic operators at $\mathcal{O}(\alpha_{\rm s}\alpha_{\rm em})$, thus improving the evolution and matching of the matrix elements related to such operators in Effective Field Theories.

Contents

Introduction **1**

I Non-perturbative calculations **7**

1 Isospin breaking effects on the lattice **9**
1.1 QED on the lattice 10
1.2 Photon propagator 12
1.3 Electromagnetic corrections to hadronic observables 14
1.4 Path integral expansion at $\mathcal{O}(\alpha_{\rm em})$ 17
1.5 Defining QCD in the full QCD+QED theory 20
1.5.1 Renormalization of the full theory 20
1.5.2 Defining observables in QCD 23

2 QED corrections to hadronic decay rates **29**
2.1 The method 30
2.2 From Standard Model to W-regularization 31
2.3 From W-regularization to Lattice 33
2.4 Evaluation of the leptonic decay amplitude 35
2.4.1 Quark-quark photon exchange diagrams and scalar and pseudoscalar insertions 42
2.4.2 Crossed diagrams and lepton self-energy 47

3 Non-perturbative renormalization in QCD+QED **51**
3.1 Renormalization conditions in QCD+QED 53
3.1.1 RI'-MOM renormalization conditions 53
3.1.2 Beyond factorization approximation 54
3.1.3 Ingredients of the calculation 55
3.2 Renormalization of fermion fields 56
3.3 Corrections to the amputated and projected Green function 58
3.4 The strategy for a QCD+QED calculation 59
3.4.1 Sequential quark propagators 60
3.4.2 Pure QED calculation 61
3.5 Renormalization of quark bilinear operators 62
3.6 Renormalization of the weak operator O_1 64
3.7 A hint of the RI-SMOM scheme 67

4 Numerical Analysis of RCs in QCD+QED **69**
4.1 Lattice Setup . . . 69
4.1.1 ETMC $N_f = 4$ configurations . . . 69
4.1.2 Tuning of the mass counterterms . . . 71
4.2 Numerical Procedure . . . 73
4.3 Numerical results . . . 83
4.3.1 Results for quark bilinear operators . . . 90
4.3.2 Results for semileptonic weak-operators . . . 90

5 Light-meson leptonic decay rates in QCD+QED: results **91**
5.1 Chirality mixing and Twisted Mass fermions . . . 91
5.2 Calculation of $\delta R_P^{\rm ren}$ . . . 94
5.2.1 Dealing with the lepton self-energy . . . 95
5.3 Finite volume effects at order $\mathcal{O}(\alpha_{\rm em})$ . . . 97
5.4 Results for the charged pion and kaon decays into muons . . . 99

II Perturbative calculations **105**

6 Perturbative evolution in QCD+QED **107**
6.1 General formalism . . . 107
6.2 Determination of the matrix $\hat{W}$ . . . 110
6.3 Evolution matrix at NLO in QCD+QED . . . 112
6.3.1 Pure QCD evolution matrix . . . 112
6.3.2 QED correction . . . 113
6.3.3 Expanding the resummed logarithms . . . 113
6.4 Evolution matrix in pure QCD . . . 114

7 Two-loop anomalous dimensions in QCD+QED **117**
7.1 The master formulae . . . 118
7.2 Evanescent operators . . . 119
7.3 Diagrams and counterterms . . . 121
7.3.1 Current-current diagrams at one-loop . . . 124
7.3.2 Current-current diagrams at two loops . . . 127
7.3.3 Self-energy diagrams at one and two loops . . . 129
7.4 Anomalous dimension matrices . . . 131
7.4.1 One-loop anomalous dimension matrix $\hat{\gamma}_e^{(0)}$ . . . 131
7.4.2 Two-loop anomalous dimension matrix $\hat{\gamma}_{se}^{(1)}$ . . . 131
7.5 Scheme dependence of the matrix $\hat{\gamma}_{se}^{(1)}$ . . . 132

8 Future perspectives **135**

Conclusions **137**

A Divergent part of two-loop current-current diagrams **141**
A.1 Bilinear operators . . . 141
A.2 Weak four-fermions operators . . . 143

Introduction

The discovery of the Higgs boson at LHC in 2013 established the Standard Model (SM) of particle physics as the most accurate description of nature in terms of elementary particles and their interactions, except gravity. So far, the SM has been proven to be very successful in reproducing the experimental data, even considering the recent and impressively precise measurements from the LHC experiments. However, despite its remarkable success, there are several reasons to believe that the SM is not a complete theory of particle interactions, but just a low-energy approximation to a more fundamental theory. One of the most evident limits of the SM is perhaps its inability to describe the gravitational interaction. Other problems of the model are also the following: the lack of a mechanism that explains baryogenesis and the masses of the neutrinos, the absence of a candidate for dark matter, the instability of the Higgs mass to radiative corrections and the failure to unify all the fundamental forces.

In addition, several issues related to the flavour structure of the SM remain still unanswered. In particular, the fact that the model, although parametrizing the observed hierarchy of particles masses and mixing angles through free parameters (for quark sector we have: 6 masses, 3 angles and 1 complex phase), does not explain it.

All (or part of) these questions could find an answer in an underlying theory, that manifests itself at some higher energy scale. The strategy for discovering New Physics (NP) at the fundamental level is based on three pillars: the energy frontier (LHC), the intensity frontier (LHCb, BelleII, rare decays experiments, etc.) and astrophysics (XENON, Darkside, axion searches, etc.). Within the intensity frontier, flavour physics is a very powerful tool to test the SM and to quantify the effects of NP by exploring possible departures from the SM, given its highly non-trivial structure.

In the hadronic sector, quark flavour mixing is described by the Cabibbo-Kobayashi-Maskawa (CKM) matrix and the accurate determination of its elements, obtained by combining experimental inputs with theoretical calculations, represents one of the most powerful tests of the limits of the SM, allowing to put stringent lower bounds on the NP energy scale. Since, up to now, no sign of NP has been observed both in direct and indirect searches, we expect that the contributions of NP to SM processes are rather tiny, certainly smaller than the actual experimental and theoretical precision. Therefore, in order to observe a sensible deviation of the experimental measurements from the theoretical predictions it is necessary to increase the level of precision on both sides.

Theoretical calculations are usually complicated by hadronic effects due to

strong interactions, which are described by quantum chromodynamics (QCD) and become very intense at low energies. The general mathematical approach to compute correlation functions in interacting quantum field theories is perturbation theory, which consists in performing an expansion in the coupling constant, thus linearizing the theory and making it solvable analytically. When it comes to strongly coupled theories, however, an expansion in the coupling constant is not appropriate any more. As regards QCD, the only available method which allows to compute hadronic observables in a non-perturbative way from first principles is Lattice QCD (LQCD). It consists in the simulation of QCD by formulating the Lagrangian on a discrete and finite Euclidean space-time, that allows for numerical computations of path integrals via Monte Carlo methods.

Most of the theoretical predictions on phenomenologically relevant hadronic observables have been derived assuming the exact validity of the isospin symmetry and completely neglecting the effects of electromagnetic (e.m.) interactions. The up (u) and down (d) mass difference is indeed small with respect to the confinement scale $\Lambda_{\rm QCD}$. Also the e.m. isospin breaking (IB) effects are small on hadronic observables because in the low energy regime $\alpha_{\rm em} \ll 1$. For several quantities relevant for flavour physics phenomenology, LQCD has recently reached the impressive level of precision of $\mathcal{O}(1\%)$, or even better. Important examples are the ratio f_K/f_π of kaon and pion leptonic decay constants and the $K_{\ell 3}$ vector form factor $f^+(0)$ [1], which play a central role in the accurate determination of the CKM entries $|V_{us}/V_{ud}|$ and $|V_{us}|$, respectively. Since both $\alpha_{\rm em}$ and $(m_d - m_u)/\Lambda_{\rm QCD}$ are of $\mathcal{O}(1\%)$, IB effects need to be included in lattice simulations to make further progress in flavour physics phenomenology, beyond the currently impressive precision obtained in iso-symmetric QCD.

A possible way to include such effects in lattice simulations is to use a perturbative approach (the RM123 method proposed in Refs. [2, 3]) in which the lattice path-integral is expanded in terms of the two small parameters $\alpha_{\rm em}$ and $(m_d - m_u)/\Lambda_{\rm QCD}$ and IB corrections to observables computed in the iso-symmetric limit are evaluated at first order in these parameters. Such a perturbative approach also allows one to control the subtraction of infrared (IR) divergences arising when evaluating the corrections to hadron decay rates introduced by quantum electrodynamics (QED). While IR divergences are cancelled by including both virtual corrections and the real emission of photons, ultraviolet (UV) divergences have to be treated by including QED corrections in the renormalization procedure.

Non-perturbative renormalization of lattice operators is a long-time known procedure in pure QCD, but it has never been extended before to the QCD+QED context. Renormalization constants (RCs) at $\mathcal{O}(\alpha_{\rm s}\alpha_{\rm em})$ were indeed computed separately (e.g. in Refs. [4, 5]): the QCD RCs non-perturbatively on the lattice and the pure QED ones at one loop in perturbation theory. However, in this *factorization approximation* mixed non-factorizable QCD+QED contributions to the RCs are not taken into account and hence a systematic error is introduced in the calculation. A central part of this thesis will be the formulation of a strategy to extend the renormalization procedure on the lattice in order to fully include the non perturbative dynamics of QCD, and QED corrections at $\mathcal{O}(\alpha_{\rm em})$, thus overcoming the factorization approximation and improving the precision of the RCs. This strategy will be applied to quark bilinear operators and to the four-fermion

operators involved in the calculation of light-meson leptonic decay rates.

A first calculation of IB corrections to the ratio $\Gamma(K_{\mu 2})/\Gamma(\pi_{\mu 2})$ was done in Ref. [6]. In the ratio of the decay rates there was a large cancellation of renormalization corrections and the factorization approximation only affected the quark mass RCs. However, to obtain a separate determination of the first order corrections to the decay rates $\Gamma(K_{\mu 2})$ and $\Gamma(\pi_{\mu 2})$ it is necessary to overcome the factorization approximation and renormalize the operator mediating the process non-perturbatively in QCD and at $\mathcal{O}(\alpha_{\rm em})$ in QED, taking into account its possible mixing with other lattice operators. Such calculation and its results will be described in details in the first part of this thesis work. We anticipate here some key results: after extrapolation of the data to the physical pion mass, and to the continuum and infinite-volume limits, the IB corrections to the leptonic decay rates can be written in the form [7]

$$\begin{aligned}\Gamma(\pi^\pm \to \mu^\pm \nu_\ell[\gamma]) &= (1.0153 \pm 0.0019)\,\Gamma^{(0)}(\pi^\pm \to \mu^\pm \nu_\ell)\ , \\ \Gamma(K^\pm \to \mu^\pm \nu_\ell[\gamma]) &= (1.0024 \pm 0.0010)\Gamma^{(0)}(K^\pm \to \mu^\pm \nu_\ell)\ ,\end{aligned}$$

where $\Gamma^{(0)}$ is the leptonic decay rate at tree level in the Gasser-Rusetsky-Scimemi (GRS) scheme which is a particular definition of QCD [8] (see Sec. 1.5.2 below). The corrections are about 1.5% for the pion decays and 0.2% for the kaon decay. Taking the experimental value of the rate for the $K_{\mu 2}$ decay, our result for the IB correction together with $\Gamma^{(0)}(K^\pm \to \mu^\pm \nu_\ell)$ obtained using the lattice determination of the kaon decay constant we obtain $|V_{us}| = 0.22567(42)$, in agreement with the latest estimate $|V_{us}| = 0.2253(7)$, recently updated by the Particle Data Group (PDG) [9], but with better precision. Alternatively, by taking the ratio of $K_{\mu 2}$ and $\pi_{\mu 2}$ decay rates and the updated value $|V_{ud}| = 0.97420\,(21)$ from super-allowed nuclear beta decays [10], we obtain $|V_{us}| = 0.22538(46)$. The unitarity of the first row of the CKM matrix is satisfied at the per-mille level, e.g. taking the value of V_{us} from the ratio of decay rates and $|V_{ub}| = 0.00413(49)$ [9], we obtain $|V_{ud}|^2 + |V_{us}|^2 + |V_{ub}|^2 = 0.99988(46)$. See Sec. 5.4 for a more detailed discussion of our results and their implications.

An important step for the calculation of the decay rates is the matching of the lattice renormalized operator mediating the process to the W-regularization scheme, in which the theory has to be renormalized in order to be consistent at $\mathcal{O}(\alpha_{\rm em})$ with the value of G_F extracted from the lifetime of the muon and exploit the matching of the effective theory to the Standard Model made in Ref. [11]. The matching is done in perturbation theory and, in order to consistently evolve the operator renormalized in QCD+QED from one scale to another, the knowledge of the two-loop anomalous dimension matrix (ADM) at $\mathcal{O}(\alpha_{\rm s}\alpha_{\rm em})$ is necessary. Both for bilinear operators and the complete mixing matrix of the weak four fermion operators studied in this work, the ADMs were absent in the literature. Therefore, we have produced a Mathematica package in which such ADMs have been computed in the $\overline{\rm MS}$-scheme in naive dimensional regularization. The anomalous dimensions are extracted from the single poles of two loop diagrams in which one gluon and one photon are exchanged, after the subtraction of eventual one-loop counterterms and contaminations of evanescent operators [12, 13]. The introduction of the mixed two-loop anomalous dimension in the evolution of the operator mediating light-meson leptonic decays made it possible to reduce the residual truncation error in the matching to the W-regularization scheme. The residual uncertainty is now of

$\mathcal{O}(\alpha_{\rm em}\alpha_{\rm s}(M_W))$, reduced from $\mathcal{O}(\alpha_{\rm em}\alpha_{\rm s}(1/a))$ of Ref. [14]. The typical size of the inverse lattice spacing is of order $\mathcal{O}(2-4)$ GeV, much smaller than $M_W \sim 80GeV$, and thus $\alpha_{\rm s}(M_W) < \alpha_{\rm s}(1/a)$. As a consequence, we expect that higher order corrections will be smaller at a larger scale. The perturbative calculation of two-loop anomalous dimensions and the discussion of the NLO QCD+QED renormalization group evolution is discussed in the second part of the thesis.

This thesis work is organized as follows:

Part I: Non-perturbative calculations

- In **Chapter 1** we describe how to include IB corrections in LQCD calculations using the RM123 method and discuss the non-compact implementation of QED on the lattice, thus giving a regularized prescription for the photon propagator. We also discuss the relation between the *full* QCD+QED theory, including e.m. and strong IB effects, and isosymmetric QCD without electromagnetism.

- In **Chapter 2** we present the calculation of the relevant amplitudes for the calculation of leptonic decay rates of light-mesons. Furthermore, we discuss how the operator mediating the process is renormalized in the W-regularization scheme and its relation to the corresponding lattice operator(s) renormalized non-perturbatively in QCD+QED.

- **Chapter 3** contains a detailed description of a novel framework to renormalize lattice operators with the inclusion of $\mathcal{O}(\alpha_{\rm em})$ corrections. The procedure is presented in the RI-MOM scheme and is then applied to quark bilinear operators and to the four-fermion operators entering the calculation of leptonic decay rates.

- In **Chapter 4** we describe the numerical analysis of the QCD+QED renormalization constants in the RI-MOM scheme and report the results for the quark bilinear and the four-fermion operators. The analysis is performed using lattice gauge configurations with $N_f = 4$ degenerate sea quarks produced by the ETM Collaboration.

- In **Chapter 5** we include renormalization corrections into the calculation of leptonic decay rates. We describe the final steps of the lattice calculation: the extrapolation to the physical pion mass, the continuum and infinite volume limits. Finally, we present the first results of the leading e.m. and strong IB corrections to the leptonic decay rates of pions and kaons into muons and we discuss their implication.

Part II: Perturbative calculations

- In **Chapter 6** we derive the renormalization group evolution function for renormalized operators at next-to-leading order in QCD+QED, including contributions from the mixed anomalous dimension of order $\mathcal{O}(\alpha_{\rm s}\alpha_{\rm em})$.

- **Chapter 7** is devoted to the calculation of the two-loop anomalous dimension matrices of order $\mathcal{O}(\alpha_s \alpha_{em})$ for quark bilinear operators and the weak four-fermion operators studied in Part I of the thesis. The computation is done in the $\overline{\text{MS}}$ scheme using a self-produced Mathematica package. The results of the calculation of two-loop diagrams are reported in **Appendix A**.
- In **Chapter 8** we investigate a further possible extension of the calculation of anomalous dimensions to *penguin* operators and discuss possible related phenomenological implications.

Part I

Non-perturbative calculations

1 | Isospin breaking effects on the lattice

Isospin is an almost exact symmetry of strong interactions as described by the QCD Lagrangian. This symmetry is based on the assumption that the up (u) and down (d) quarks are strictly identical particles. In nature, however, such symmetry is only approximate and it is broken by two effects: the different electric charge of u and d quarks and their mass difference, which exists also in the absence of electromagnetic interactions. We will refer to these effects respectively as *electromagnetic* and *strong isospin breaking* (IB) *effects*. The IB is driven by two small parameters: the fine structure constant,

$$\widehat{\alpha}_{\rm em} \simeq 1/137.036 \ , \tag{1.1}$$

and the up-down quark mass splitting,

$$\frac{\widehat{m}_d - \widehat{m}_u}{\Lambda_{\rm QCD}} \lesssim 0.01 \ , \tag{1.2}$$

yielding in general small corrections of $\mathcal{O}(1\%)$ to hadronic observables. Here and through all the chapter we indicate renormalized quantities with an "hat", e.g. $\widehat{m}_{u,d}$, to distinguish them from the corresponding bare quantities. For the above reasons isospin symmetry can be considered as a good approximation of reality with an $\mathcal{O}(1\%)$ relative error. Nevertheless, it is interesting to note that these small IB corrections are crucial to describe the structure of atomic matter in the Universe. Indeed, the hydrogen atom is stable because $\Delta M_n = M_n - M_p = 1.29333205\,(51)$ MeV is greater then the electron mass $M_e = 0.5109989461\,(31)$ MeV [9] and hence the electron capture $p + e^- \to n + \nu_e$ is forbidden.

In flavour physics, the precision reached so far by experimental measurements of many hadronic observables related to weak processes is smaller than $\mathcal{O}(1\%)$. On the theoretical side, lattice simulations performed in the isospin symmetric limit of QCD, i.e. by considering the masses of u and d quarks to be equal and the e.m. interactions switched off, allow in principle to reach a precision of $\mathcal{O}(1\%)$ or even smaller on many hadronic observables [1]. However, the precision of such results is limited by the systematic uncertainty given by the missing IB effects, which are expected to be of the same order of magnitude. Therefore, at this level of precision, strong IB effects and e.m. corrections cannot be neglected in lattice simulations. In the past, IB effects due to the light quark mass difference, also called *strong* IB (SIB) effects, have been accommodated within the chiral perturbation theory (ChPT) framework or relying on model-dependent approximations (see for example

Refs. [15–18]), while several attempts to compute e.m. corrections to the hadron spectrum in lattice QCD have been presented [19–22].

Over the past decade several approaches to include QED effects in lattice simulations have been pursued by different collaborations, following mainly two methods. In the all-order (or "stochastic") approach, QED is added directly to the action, and dedicated QCD+QED simulations are performed, with the result of including the IB corrections to all orders (see, e.g., Refs. [23–25]). In the perturbative approach, also called RM123 approach, presented in Refs. [2, 3, 26] and adopted in this work, the lattice path-integral is expanded at first order in the two small parameters $\hat{\alpha}_{\rm em}$ and $(\widehat{m}_d - \widehat{m}_u)/\Lambda_{\rm QCD}$, and the IB corrections to observables are evaluated in the isospin symmetric theory, with no need to perform new dedicated simulations. Moreover, as it will be described later in Chap. 2, the perturbative approach allows one to control the subtraction of infrared divergences arising when evaluating the QED corrections to charged hadron observables.

In the following we explain how we included electromagnetism in our lattice simulations using a non-compact formulation of QED, i.e. by using the electromagnetic field $\mathcal{A}_\mu$ as a dynamical variable on the lattice. As we will see, the expansion of the lattice path-integral in powers of $\hat{\alpha}_{\rm em}$ leads to correlators containing the integral over the whole space-time lattice volume of two insertions of the quark electromagnetic currents multiplied by the lattice photon propagator. These quantities have both infrared and ultraviolet divergences that must be removed by providing an infrared safe finite volume definition of the lattice photon propagator and by imposing suitable renormalization conditions. These issues will be discussed in detail. We illustrate our method explaining how we performed the expansion in terms of $(\widehat{m}_d - \widehat{m}_u)$ and $\hat{\alpha}_{\rm em}$ of physical observables and how to calculate corrections to the lattice path-integral.

The method is applicable in principle to any hadronic observable which can be computed on the lattice and it was tested applying it to the computation of leading IB effects for several physical quantities of interest: the pseudoscalar meson masses [26], the neutron-proton mass splitting [3], the light meson decay constants [6, 7], the form factors of semileptonic $K_{\ell 3}$ decays [2] and the hadronic vacuum polarization contribution to the lepton anomalous magnetic moments [4, 5]. All the results presented in this work have been obtained within the so-called *electro-quenched* approximation, which will be introduced later in this chapter and consists in considering dynamical sea quarks as neutral with respect to electromagnetism. We then dedicate the final part of this chapter to the issue of defining QCD within the full QCD+QED (physical) theory. In particular, we discuss different prescriptions to define QCD and introduce the hadronic schemes, advocating their use in future lattice simulations.

1.1 QED on the lattice

We start our discussion by describing how QED can be regularized on the lattice and we discuss the issues associated with the expansion of the quark action with respect to the electric charge. In particular we present a safe prescription for the definition of the IR regularized finite volume lattice photon propagator which can be conveniently used in numerical calculations by working directly in coordinate space,

in such a way to eliminate the infrared divergence associated with the photon zero momentum mode.

In this work we have adopted a non-compact formulation of lattice QED, that consists in treating the electromagnetic gauge potential $\mathcal{A}_\mu(x)$ in a fixed QED gauge (e.g. Feynman gauge) as a dynamical variable. The field $\mathcal{A}_\mu(x)$ is introduced as a free field with the kinetic Maxwell action (in the Feynman gauge)

$$\begin{aligned} S^{\mathcal{A}} &= \frac{1}{2}\sum_x \sum_{\mu,\nu} \mathcal{A}_\mu(x)\left[-\nabla^-_\nu \nabla^+_\nu\right]\mathcal{A}_\mu(x) \\ &= \frac{1}{2}\sum_k \sum_{\mu,\nu} \tilde{\mathcal{A}}^\star_\mu(k)\left[2\sin(k_\nu/2)\right]^2 \tilde{\mathcal{A}}_\mu(k)\,, \end{aligned} \tag{1.3}$$

where $\tilde{\mathcal{A}}_\mu(k)$ denotes the Fourier transform of the real field $\mathcal{A}_\mu(x)$ and satisfies the condition $\tilde{\mathcal{A}}^\star_\mu(k) = \tilde{\mathcal{A}}_\mu(-k)$. The operators $\nabla^\pm_\mu$ are defined as follows

$$\begin{aligned} &\nabla^+_\mu f(x) = f(x+\hat{\mu}) - f(x) \\ &\nabla^-_\mu f(x) = f(x) - f(x-\hat{\mu}) \end{aligned} \quad \longrightarrow \quad \nabla_\mu = \frac{\nabla^+_\mu + \nabla^-_\mu}{2}\,. \tag{1.4}$$

The interaction between quarks and photons is described in terms of quark covariant derivatives by introducing the QED link through exponentiation[1],

$$\mathcal{A}_\mu(x) \;\to\; E_\mu(x) = \frac{\mathbb{1}+\tau^3}{2}\,\mathrm{e}^{-ie_u e\mathcal{A}_\mu(x)} + \frac{\mathbb{1}-\tau^3}{2}\,\mathrm{e}^{-ie_d e\mathcal{A}_\mu(x)}\,, \tag{1.5}$$

where e_f is the fractional electric charge of the quark of flavour f, i.e. $e_u = 2/3$ for up-type quarks and $e_d = -1/3$ for down-type quarks. In the previous expression we have considered the up and down quarks as components of a flavour doublet. The covariant derivatives are obtained by multiplying the QCD links $U_\mu(x)$ for the appropriate $U(1)_{\mathrm{em}}$ factor,

$$\mathcal{U}^f_\mu(x) = E^f_\mu(x) U_\mu(x) \quad \text{with} \quad E^f_\mu(x) = \mathrm{e}^{-ie_f e\mathcal{A}_\mu(x)}\,, \tag{1.6}$$

thus obtaining

$$\begin{aligned} \mathcal{D}^+_\mu[U,\mathcal{A}]\,\psi_f(x) &= \mathcal{U}^f_\mu(x)\,\psi_f(x+\hat{\mu}) - \psi(x)\,, \\ \mathcal{D}^-_\mu[U,\mathcal{A}]\,\psi_f(x) &= \psi_f(x) - \mathcal{U}^{f\,\dagger}_\mu(x)\,\psi(x-\hat{\mu})\,. \end{aligned} \tag{1.7}$$

Exact electromagnetic gauge invariance is obtained if the fields are transformed as follows

$$\begin{aligned} \psi_f(x) &\to \mathrm{e}^{ie_f e\lambda(x)}\,\psi_f(x)\,, \\ \bar{\psi}_f(x) &\to \bar{\psi}_f(x)\,\mathrm{e}^{-ie_f e\lambda(x)}\,, \\ A_\mu(x) &\to A_\mu(x) + \nabla^+_\mu \lambda(x)\,. \end{aligned} \tag{1.8}$$

We want to treat electromagnetism at fixed order with respect to $\hat{\alpha}_{em}$ and, to this end, we need to expand the quarks action in powers of e. The e.m. corrections

[1] Here and in the following equations the variable x has to be considered as a lattice discretized variable.

involving one photon propagator can be obtained by starting from the explicit expression of the lattice Dirac operator $D_f[U, \mathcal{A}; \vec{g}]$ and by calculating

$$\sum_x \bar{\psi}_f(x) \left\{ D_f[U, \mathcal{A}; \vec{g}] - D_f[U, 0; \vec{g}] \right\}\Big|_{\mathcal{O}(e^2)} \psi_f(x) = \tag{1.9}$$
$$= \sum_{x,\mu} \left\{ e_f e\, \mathcal{A}_\mu(x) V_f^\mu(x) + \frac{(e_f e)^2}{2}\, \mathcal{A}_\mu(x)\mathcal{A}_\mu(x) T_f^\mu(x) \right\} ,$$

where $V_f^\mu(x)$ is the (non-local) conserved vector current corresponding to the quark with flavour f while $T_f^\mu(x)$ is the "tadpole" vertex, and $\vec{g}$ is a compact vector notation for the bare parameters of the theory,

$$\vec{g} = \left(e^2, g_s^2, m_u, m_d, m_s, m_c, \ldots \right) . \tag{1.10}$$

Clearly, both the conserved vector current and the tadpole vertex depend upon the particular choice made for the discretization of the fermion action. Their definitions are given in Eq. (37) of Ref. [3] for the Twisted Mass action in the physical basis at maximal twist. Once the fermion action has been expanded, the leading QED corrections to a given lattice correlator are obtained by considering the time product of the original operators with two insertions of the combination $\mathcal{A}_\mu(x) V_f^\mu(x)$ or with a single insertion of $\mathcal{A}_\mu(x)\mathcal{A}_\mu(x) T_f^\mu(x)$[2]. To give an example, let us consider the electromagnetic corrections to the kaon two-point correlator. One of the contributions one has to compute is

$$-$$ 
$$= \left\langle \sum_{x,y} \mathcal{A}_\mu(x)\mathcal{A}_\nu(y)\; T \langle 0|\; [\bar{u}\gamma_5 s](t)\, V_s^\mu(x)\, V_u^\nu(y)\, [\bar{s}\gamma_5 u](0)\; |0\rangle \right\rangle^{\mathcal{A}}$$
$$= \sum_{x,y} D_{\mu\nu}(x-y)\; T \langle 0|\; [\bar{u}\gamma_5 s](t)\, V_s^\mu(x)\, V_u^\nu(y)\, [\bar{s}\gamma_5 u](0)\; |0\rangle \;, \tag{1.11}$$

where the notation $\langle \cdots \rangle^{\mathcal{A}}$ represents the path integral average over the gauge potential $\mathcal{A}_\mu$, $D_{\mu\nu}(x-y)$ is the lattice *photon propagator* and a factor $e_s e_u e^2$ has to be understood. Here we have neglected the disconnected quark contributions coming from the contraction of the vector currents among themselves. As anticipated, the corrected correlators are expressed in terms of the photon propagator and thus have both infrared and ultraviolet divergences. For this reason, now we have to give a prescription for treating the zero mode of the photon propagator.

1.2 Photon propagator

The lattice action of the QED gauge field (in the Feynman gauge) defined in Eq. (1.3) is explicitly reported in momentum space to highlight the well-known problem with the definition of the lattice photon propagator, i.e. the infrared divergence associated to the zero momentum mode. Indeed, the propagator of the field $\mathcal{A}_\mu$ is defined

[2] Here we have used a compact notation for V_f^μ and T_f^μ in which they seem to depend only on the point x. It should be stressed that these vertices are non-local and connect different lattice points.

as the inverse of the kinetic term and, in order to define the inverse of the lattice Laplace operator $-\nabla^-_\mu\nabla^+_\mu$, one has to provide a prescription to cope with its kernel.

One possibility, originally proposed in Ref. [19], is to make the zero momentum mode to vanish identically. The resulting theory is called $\mathrm{QED}_{\mathrm{TL}}$ and has been widely used in the literature [3, 19, 27]. Although this scheme is simple, it introduces some strong finite-volume effects which can be hard to control [28]. Alternative regularizations of the zero momentum mode of the photon propagator results into different finite volume behaviours (for a recent review on QED simulations in a finite box, see Ref. [29]). In our calculation we have adopted the so called $\mathrm{QED}_{\mathrm{L}}$ prescription, which consists in removing all spatial zero-modes, i.e. to set to zero all the photon modes k with $\vec{k}=\vec{0}$, $\tilde{\mathcal{A}}_\mu(k_0,\vec{0})=0$. This scheme is inspired from Ref. [30] where QED is formulated in a finite spatial volume directly with an infinite temporal dimension.

We define the infrared regularized photon propagator as the expectation value of the time-ordered product of two photon fields:

$$G_{\mu\nu}(x_1,x_2)=\langle\mathcal{A}_\mu(x_1)\,\mathcal{A}_\nu(x_2)\rangle\ , \tag{1.12}$$

where the photon field $\mathcal{A}_\mu(x)$ is generated according to the distribution probability

$$P(\mathcal{A})\,\mathrm{d}\mathcal{A}\propto\exp\left[-\mathcal{A}_\mu(x_1)\,G^{-1}_{\mu\nu}(x_1,x_2)\,\mathcal{A}_\nu(x_2)\right]\ . \tag{1.13}$$

Being the action Gaussian distributed it is easier to generate photon fields in momentum space, in which the probability distribution is diagonal with respect to k, namely

$$P(\tilde{\mathcal{A}})\,\mathrm{d}\tilde{\mathcal{A}}\propto\exp\left[-\tilde{\mathcal{A}}_\mu(k)\,\tilde{G}^{-1}_{\mu\nu}(k)\,\tilde{\mathcal{A}}_\nu(k)\right]\ . \tag{1.14}$$

The local change of variable $\tilde{\mathcal{B}}_\mu(k)=\sqrt{\tilde{G}^{-1}_{\mu\rho}(k)}\,\tilde{\mathcal{A}}_\rho(k)$ allows to further simplify the calculation drawing each component of $\tilde{\mathcal{B}}$ independently:

$$P(\tilde{\mathcal{B}})\,\mathrm{d}\tilde{\mathcal{B}}\propto\exp\left[-\tilde{\mathcal{B}}^2_\mu(k)\right]\ , \tag{1.15}$$

and the value of $\tilde{\mathcal{A}}$ can be reconstructed as

$$\tilde{\mathcal{A}}_\mu(k)=\sqrt{\tilde{G}_{\rho\mu}(k)}\,\tilde{\mathcal{B}}_\rho(k)\ . \tag{1.16}$$

The matrix $\tilde{G}_{\mu\nu}(k)$ for the Wilson (Plaquette) action in a generic covariant gauge is given by [31]

$$\tilde{G}_{\mu\nu}(k)=\left[\delta_{\mu\nu}\,\frac{1}{\hat{k}^2}-(1-\xi)\,\frac{\hat{k}_\mu\hat{k}_\nu}{(\hat{k}^2)^2}\right] \tag{1.17}$$

where $\hat{k}_\mu$ is the lattice shortcut for

$$\hat{k}_\mu=\frac{2}{a}\sin\left(\frac{k_\mu a}{2}\right) \tag{1.18}$$

and the gauge parameter $\xi=0\,(1)$ corresponds to the Landau (Feynman) gauge. Once the field $\tilde{\mathcal{A}}_\mu(k)$ is determined, the real space configuration can be recovered by Fourier transform.

1.3 Electromagnetic corrections to hadronic observables

In this Section we describe the general strategy to calculate leading IB corrections to hadronic observables according to the RM123 approach proposed in Refs. [2, 3, 26]. We compute strong IB effects and QED corrections on the lattice by performing a combined perturbative expansion of the lattice path-integral of the *full theory* in the two small parameters: $(\widehat{m}_d - \widehat{m}_u)/\Lambda_{\rm QCD} \sim \hat{\alpha}_{\rm em} \sim \mathcal{O}(\varepsilon)$, neglecting contributions of order $\mathcal{O}(\varepsilon^2)$. We denote as "full" the theory with both QCD and QED interactions switched on and, consequently, with $\widehat{m}_d \neq \widehat{m}_u$, while we call "isosymmetric QCD" or simply "isosymmetric" the theory without electromagnetic interactions and with $\widehat{m}_d = \widehat{m}_u$. We anticipate here that the separation of QCD and QED effects is prescription dependent. Indeed, since the electric charges of the up and down quarks are different, the presence of electromagnetism itself induces a difference in their masses, in addition to any explicit difference in the bare masses input into the action being simulated. Therefore, the separation of IB effects into strong and e.m. components requires a convention. This topic will be discussed in details later in Sec. 1.5. In order to compute $\mathcal{O}(\hat{\alpha}_{\rm em})$ corrections to a given observable we have to take into account correlators containing two insertions of the electromagnetic current or one insertion of the tadpole vertex, multiplied by the IR regularized photon propagator and integrated over the space-time volume. In the first case, the correction to a given correlator is proportional to

$$T\langle O(x_i)\rangle \longrightarrow T\int d^4y d^4z\; D_{\mu\nu}(y-z)\;\langle O(x_i)J_\mu(y)J_\nu(z)\rangle\;, \tag{1.19}$$

where $T\langle O(x_i)\rangle$ is the T–product of a certain number of local operators, $D_{\mu\nu}(y-z)$ is the photon propagator in a fixed QED gauge and $J_\mu(x)$ is the sum of the electromagnetic currents of all the flavours. Because of the contact interaction of the electromagnetic currents, the equation is UV divergent and need to be regularized. The introduction of electromagnetism induce a (divergent) shift of quark masses, of the strong coupling constant and, if chirality is broken, also of the critical masses. By neglecting for the moment the contribution of the critical mass shift and the tadpole vertex, let consider the short distance expansion of the product of two electromagnetic currents, namely

$$J^\mu(x)J^\mu(0) \;\;\sim\;\; c_1(x)\mathbb{1} + \sum_f c_m^f(x) m_f \bar{\psi}_f\psi_f + c_{g_s}(x)G^{\mu\nu}G^{\mu\nu} + \cdots\;. \tag{1.20}$$

The "counterterm" coefficients c_1, c_m^f and c_{g_s} are divergent quantities that must be fixed by fixing appropriate renormalization prescriptions. In particular, the terms proportional to c_m^f can be reabsorbed by a redefinition of each quark mass m_f, the term proportional to c_{g_s} can be reabsorbed by a redefinition of the strong coupling constant (i.e. of the lattice spacing) while the term proportional to c_1 corresponds to the vacuum polarization and the associated divergence cancels by taking the fully connected part of the right hand side of eq. (1.19).

Let us consider a generic *physical* quantity O in the full QCD+QED theory,

$$O(\vec{g}) \;=\; O(e^2, g_s^2, m_u, m_d, \dots) \;=\; \langle O\rangle^{\vec{g}}\;, \tag{1.21}$$

where we have used the compact vector notation for the bare parameters of the theory, $\vec{g} = (e^2, g_s^2, m_u, m_d, \dots)$, and where the notation $\langle \cdots \rangle^{\vec{g}}$ means that the path-integral average is performed in the full theory. The RM123 method consists in expanding the observable $O(\vec{g})$ with respect to the isosymmetric QCD result $O(\vec{g}^{\,0})$ as follows,

$$\begin{aligned} O(\vec{g}) &= O(\vec{g}^{\,0}) + \left\{ e^2 \frac{\partial}{\partial e^2} + \left[g_s^2 - (g_s^0)^2 \right] \frac{\partial}{\partial g_s^2} + \left[m_f - m_f^0 \right] \frac{\partial}{\partial m_f} \right\} O(\vec{g}) \, \Big|_{\vec{g}=\vec{g}^{\,0}} \\ &= \langle O \rangle^{\vec{g}^{\,0}} + \boldsymbol{\Delta} O \, , \end{aligned} \tag{1.22}$$

where

$$\vec{g}^{\,0} = \left(0, (g_s^0)^2, m_{ud}^0, m_{ud}^0, \dots \right) \tag{1.23}$$

and the notation $\langle \cdots \rangle^{\vec{g}^{\,0}}$ means that the path-integral average is performed in the isosymmetric theory. Note that since physical observables are QED and QCD gauge invariant and depend on e^2 and g_s^2, terms linear in e and g_s are absent in Eq. (1.22). The parameters of the physical QCD+QED theory can be fixed by using a suitable number of experimental inputs. On the other hand, as already anticipated, "unphysical" parameters of the isosymmetric theory have to be set by giving some renormalization prescription. Here we follow the procedure of Ref. [3], where IB effects are defined by using an intermediate renormalization scheme and a matching procedure. Once the full theory renormalized parameters $\hat{g}_i(\mu) = Z_i(\mu)\, g_i$ have been tuned by using experimental inputs, the renormalized couplings of the isosymmetric theory ($\hat{\alpha}_{\rm em} = \widehat{m}_d - \widehat{m}_u = 0$), $\hat{g}_i^0(\mu) = Z_i^0(\mu)\, g_i^0$, are fixed by the matching condition $\hat{g}_i^0(\mu^\star) \equiv \hat{g}_i(\mu^\star)$ at a given scale $\mu^\star$. Note that the renormalized parameters of the two theories, although equal in this scheme at the scale $\mu^\star$, are different at any other scale. More precisely, we impose the following matching conditions

$$\begin{aligned} &\hat{g}_s^0(\mu^\star) = \hat{g}_s(\mu^\star) \, , \\ &\widehat{m}_{ud}^0(\mu^\star) = \widehat{m}_{ud}(\mu^\star) = \frac{\widehat{m}_d(\mu^\star) + \widehat{m}_u(\mu^\star)}{2} \, , \\ &\widehat{m}_s^0(\mu^\star) = \widehat{m}_s(\mu^\star) \, . \end{aligned} \tag{1.24}$$

This is known as the Gasser-Rusetsky-Scimemi (GRS) prescription [8] and has been widely used in the past [3, 6, 26]. In this work we rely on this prescription by matching the couplings renormalized in the $\overline{\rm MS}$ scheme at the scale $\mu^\star = 2$ GeV. A detailed discussion on the GRS scheme and possible alternative prescriptions is postponed to Sec. 1.5.

By using the property that a physical observable is a Renormalization Group Invariant (RGI) quantity, i.e. $O(g_i) = O(\hat{g}_i)$ and $O(g_i^0) = O(\hat{g}_i^0)$, the perturbative expansion of Eq. (1.22) can be expressed in terms of the renormalized couplings according to

$$\boldsymbol{\Delta} O = \left\{ \hat{e}^2 \frac{\partial}{\partial \hat{e}^2} + \left[\hat{g}_s^2 - \left(\frac{Z_{g_s}}{Z_{g_s}^0} \hat{g}_s^0 \right)^2 \right] \frac{\partial}{\partial \hat{g}_s^2} + \left[\hat{m}_f - \frac{Z_{m_f}}{Z_{m_f}^0} \widehat{m}_f^0 \right] \frac{\partial}{\partial \widehat{m}_f} \right\} O(\hat{g}_i) \Bigg|_{\hat{g}_i = \frac{Z_i}{Z_i^0} \hat{g}_i^0} \, . \tag{1.25}$$

From the comparison of the previous equation with Eq. (1.20) we find that the divergent quantities $Z_{m_f}/Z^0_{m_f}$ and $Z_{g_s}/Z^0_{g_s}$ correspond respectively to the counter-terms c^f_m and c_{g_s}. In practice, these counter-terms appear because the renormalization constants of the full theory are different from the corresponding quantities in pure QCD, the theory in which we perform the numerical simulations. Once the counter-terms have been properly tuned, this procedure can be interpreted as the expansion of the full theory in the renormalized parameters $\hat{\alpha}_{em}$ and $\widehat{m}_d - \widehat{m}_u$. The electric charge e does not need to be renormalized at this order,

$$\hat{e}^2 = e^2 = 4\pi\hat{\alpha}_{\rm em} \sim \frac{4\pi}{137.036} \ . \tag{1.26}$$

The problem of the electric charge renormalization would arise in the calculation of next-to-leading IB corrections, which can be safely neglected by now from the phenomenological point of view.

In Eq. (1.20) we did not take into account the shift of the critical mass induced by electromagnetism when a Wilson term is introduced in the fermionic action. To do this we re-write Eq. (1.20) by adding to the left-hand side a contribution from tadpole vertices of the different quarks, and to the right-hand side an additional divergent contribution that have to be reabsorbed in the definition of the critical masses, namely

$$\begin{aligned} &J^\mu(x)J^\mu(0) + \sum_\mu T^\mu(x) \\ &\quad\sim\ c_1(x)\mathbb{1} + \sum_f c^f_k(x)\bar{\psi}_f i\gamma_5\tau^3\psi_f + \sum_f c^f_m(x) m_f \bar{\psi}_f\psi_f + c_{g_s}(x)G^{\mu\nu}G^{\mu\nu} + \cdots \ , \end{aligned}$$

where the coefficients $c^f_k(x)$ are the critical mass counter-terms.

The determination of the counter-term associated with the electromagnetic shift of the critical mass can be done by using the Ward-Takahashi identity (WTI) of the continuum theory (see Ref. [3] for the explicit calculation).

We can generalize the operator $\mathbf{\Delta}$ in Eq. (1.22) by taking into account also the dependence of a generic lattice observable on the critical mass m^{cr}_f. More precisely, we have to add new parameters to the full theory,

$$\vec{g} = \left(e^2, g_s^2, m_u, m_d, m^{cr}_u, m^{cr}_d, \dots\right) \ , \tag{1.27}$$

and by calling m^{cr}_0 the single critical mass parameter of the symmetric theory, we have that isosymmetric QCD simulations correspond to the set of parameters

$$\vec{g}^{\,0} = \left(0, (g^0_s)^2, m^0_{ud}, m^0_{ud}, m^{cr}_0, m^{cr}_0, \dots\right) \ . \tag{1.28}$$

Therefore, the generalization of Eq. (1.22) to the case in which Wilson fermions are used is

$$\mathbf{\Delta}O = \left\{ e^2\frac{\partial}{\partial e^2} + \left[g_s^2 - (g^0_s)^2\right]\frac{\partial}{\partial g_s^2} + [m_f - m^0_f]\frac{\partial}{\partial m_f} + [m^{cr}_f - m^{cr}_0]\frac{\partial}{\partial m^{cr}_f} \right\} O(\vec{g})\Big|_{\vec{g}=\vec{g}^{\,0}} \ . \tag{1.29}$$

1.4 Path integral expansion at $\mathcal{O}(\alpha_{\rm em})$

In this section, we discuss in detail the derivation of the formulas necessary to calculate the LIB corrections to a specific observable by following the strategy outlined in the previous section. We start by discussing the separation of the QCD action from that in the full theory.

The lattice action in the full QCD+QED theory is given by

$$S^{\rm full} = \frac{1}{g_s^2} S^{\rm YM} + S^{\mathcal{A}} + \sum_f \left(S_f^{\rm kin} + m_f\, S_f^m \right) + \sum_\ell \left(S_\ell^{\rm kin} + m_\ell\, S_\ell^m \right) \ . \tag{1.30}$$

Here $S^{\rm YM}$ is a discretisation of the gluon action, $S^{\mathcal{A}}$ is the preferred discretization of the Maxwell action of the photon (see Eq. (1.3)), $S_f^{\rm kin}$ is the kinetic term for the quark with flavour f, including the interaction with the gluon and photon fields, $m_f S_f^m = m_f \sum_x \overline{q}_f(x) q_f(x)$ is the mass term, $S_\ell^{\rm kin}$ and S_ℓ^m are respectively the kinetic and mass terms for the lepton ℓ. For fermion actions which break chiral symmetry, such as the Wilson action, a counterterm is needed to remove the critical mass and $m_f S_f^m$ has to be replaced with $m_f S_f^m + m_f^{\rm cr} S_f^{\rm cr}$. A mass counterterm is in principle needed also in the case of the lepton, but at leading order in α_{em} the lepton critical mass can be ignored. It is useful to rewrite the full action in Eq. (1.30) by factorizing the isosymmetric QCD action

$$S^{\rm QCD} = \frac{1}{g_0^2} S^{\rm YM} + \sum_f \left(S_{f,0}^{\rm kin} + m_{f,0} S_f^m \right) \ , \tag{1.31}$$

where the kinetic term only includes gluon links and the subscripts 0 indicate that the bare coupling and masses are different from those in the full theory of Eq. (1.30).

The lattice action in the full theory then takes the form

$$S^{\rm full} = S^{\rm QCD} + \sum_\ell S_{\ell,0} + S^{\mathcal{A}} + S^{\rm ct} + \Delta S \,, \tag{1.32}$$

where $S_{\ell,0} = S_{\ell,0}^{\rm kin} + m_\ell S_\ell^m$, while the counter-term $S^{\rm ct}$ and the QED part ΔS are given by

$$S^{\rm ct} = \left(\frac{1}{g_s^2} - \frac{1}{g_0^2} \right) S^{\rm YM} + \sum_f \left[(m_f^{\rm cr} - m_0^{\rm cr}) S_f^{\rm cr} + (m_f - m_{f,0}) S_f^m \right] \ , \tag{1.33}$$

$$\Delta S = \sum_\ell \left(S_\ell^{\rm kin} - S_{\ell,0}^{\rm kin} \right) + \sum_f \left(S_f^{\rm kin} - S_{f,0}^{\rm kin} \right) \ . \tag{1.34}$$

We now consider these terms in detail using Wilson fermions for illustration. The kinetic term for the quark with flavour f, $S_f^{\rm kin}$, is given by:

$$S_f^{\rm kin} = \sum_x \bar{\psi}_f(x) \left(\gamma_\mu \frac{\mathcal{D}_\mu^+[U,\mathcal{A}] + \mathcal{D}_\mu^-[U,\mathcal{A}]}{2} - \frac{\mathcal{D}_\mu^+[U,\mathcal{A}]\mathcal{D}_\mu^-[U,\mathcal{A}]}{2} \right) \psi_f(x) \,, \tag{1.35}$$

where ψ_f is the quark field and the modified covariant derivatives $\mathcal{D}_\mu^\pm[U,\mathcal{A}]$ are defined in Eq. (1.7). On the other hand, the leptonic action is given by

$$S_\ell^{\rm kin} + S_\ell^m = \sum_{x,\ell} \bar{\psi}_\ell(x) \left(\gamma_\mu \frac{\mathcal{D}_\mu^+[\mathcal{A}] + \mathcal{D}_\mu^-[\mathcal{A}]}{2} - \frac{\mathcal{D}_\mu^+[\mathcal{A}]\mathcal{D}_\mu^+[\mathcal{A}]}{2} + m_\ell \right) \psi_\ell(x) \tag{1.36}$$

with ψ_ℓ being the lepton field and $\mathcal{D}_\mu^\pm[\mathcal{A}]$ corresponding to the covariant derivatives in Eq. (1.7) with the QCD links set to 1 and $E_\mu^\ell(x) = \exp\{-ie_\ell e\mathcal{A}_\mu(x)\}$. In pure QCD, the kinetic term only includes the gluon links so that for Wilson fermions

$$S_{f,0}^{\text{kin}} = \sum_x \bar{\psi}_f(x)\left(\gamma_\mu \frac{\mathcal{D}_\mu^+[U] + \mathcal{D}_\mu^-[U]}{2} - \frac{\mathcal{D}_\mu^+[U]\mathcal{D}_\mu^-[U]}{2}\right)\psi_f(x)\,, \tag{1.37}$$

and the derivatives are defined in Eq. (1.7) with the QED link $E_\mu^f = 1$. Since for leptonic and semileptonic decays, leptonic spinors are present even in the absence of electromagnetism, it is also convenient to define the kinetic action for free leptons (all links set to 1):

$$S_{\ell,0}^{\text{kin}} = \sum_x \bar{\psi}_\ell(x)\left(\gamma_\mu \frac{\mathcal{D}_\mu^+[1] + \mathcal{D}_\mu^-[1]}{2} - \frac{\mathcal{D}_\mu^+[1]\mathcal{D}_\mu^-[1]}{2}\right)\psi_\ell(x)\,. \tag{1.38}$$

Physical observables are determined from correlation functions evaluated from lattice computations in the full theory. For a generic observable O evaluated in the full theory up to $\mathcal{O}(\alpha_{\text{em}})$ we write:

$$\begin{aligned}\langle O\rangle &= \frac{\int_{U,\mathcal{A},\psi_f,\psi_\ell} \mathrm{e}^{-S^{\text{full}}} O[\psi_f,\psi_\ell,U,\mathcal{A}]}{\int_{U,\mathcal{A},\psi_f,\psi_\ell} \mathrm{e}^{-S^{\text{full}}}} \qquad (1.39)\\ &= \frac{\int_{U,\psi_f} \mathrm{e}^{-S^{\text{QCD}}} \int_{\mathcal{A},\psi_\ell} \mathrm{e}^{-S^{\mathcal{A}} - \sum_\ell S_{\ell,0}} \left\{1 - S^{\text{ct}} - \Delta S + \frac{(\Delta S)^2}{2}\right\} O[\psi_f,\psi_\ell,U,\mathcal{A}]}{\int_{U,\psi_f} \mathrm{e}^{-S^{\text{QCD}}} \int_{\mathcal{A},\psi_\ell} \mathrm{e}^{-S^{\mathcal{A}} - \sum_\ell S_{\ell,0}} \left\{1 - S^{\text{ct}} - \Delta S + \frac{(\Delta S)^2}{2}\right\}}\,,\end{aligned}$$

where in the integrand O is a generic multilocal composite operator. In general, the determination of physical observables requires the processing of correlation functions of the form of Eq. (1.39). Hadronic masses, for example are obtained from behaviour in the time separation of two interpolating operators.

We now turn to the definition of correlation functions in QCD defined in a generic scheme. For a generic observable O we define its value in QCD by:

$$\langle O\rangle^{\text{QCD}} \equiv \frac{\int_{U,\psi_f} \mathrm{e}^{-S^{\text{QCD}}} \int_{\mathcal{A},\psi_\ell} \mathrm{e}^{-S^{\mathcal{A}} - \sum_\ell S_{\ell,0}} O[\psi_f,\psi_\ell,U,\mathcal{A}]}{\int_{U,\psi_f} \mathrm{e}^{-S^{\text{QCD}}} \int_{\mathcal{A},\psi_\ell} \mathrm{e}^{-S^{\mathcal{A}} - \sum_\ell S_{\ell,0}}}\,. \tag{1.40}$$

The free QED action is included in the numerator and the denominator of Eq. (1.40) since, even without radiative corrections, the physical quantities such as $\Gamma(K_{\ell 2})$ and $\Gamma(\pi_{\ell 2})$ studied in this work are obtained by combining the results for hadronic matrix elements obtained from QCD simulations with leptonic spinors. Moreover, for other quantities, for example the long-distance contributions to the amplitude for the rare kaon decay $K^+ \to \pi^+\nu\bar{\nu}$, there are internal free lepton propagators even in the absence of isospin breaking [32, 33].

Comparing Eqs. (1.39) and (1.40) we arrive at

$$\begin{aligned}\langle O\rangle^{\text{full}} &= \langle O\rangle^{\text{QCD}} - \left\langle O\, S^{\text{ct}}\right\rangle^{\text{QCD}} - \left\langle O\left(\Delta S - \frac{(\Delta S)^2}{2}\right)\right\rangle^{\text{QCD}} \qquad (1.41)\\ &\equiv \langle O\rangle^{\text{QCD}} + \langle \delta O\rangle^{\text{QCD}}\,,\end{aligned}$$

where $\langle \delta O \rangle^{\rm QCD}$ coincides with the correction $\mathbf{\Delta} O$ in Eq. (1.22).

Before closing this section we clarify a subtlety which we must account for. We need to convert the results obtained from simulations in lattice units (i.e. in units of the lattice spacing) into values given in physical units (such as MeV). Eq. (1.41) is also written in lattice units. Let us consider an observable O with mass dimension n and rewrite Eq. (1.41) with the lattice spacing included explicitly:

$$\langle a^n O \rangle^{\rm full} = \langle a_0^n O \rangle^{\rm QCD} + \langle a_0^n \delta O \rangle^{\rm QCD} \ , \tag{1.42}$$

where, since we are working to first order in isospin breaking, in the second term on the right-hand side we do not need to distinguish between the lattice spacing in the full theory (a) and that obtained in QCD (a_0). The quantity which we wish to determine, $\langle O \rangle^{\rm phys}$ in physical units, is therefore given by

$$\langle O \rangle^{\rm phys} \equiv \frac{\langle aO \rangle^{\rm full}}{a} = \frac{\langle a_0^n O \rangle^{\rm QCD}}{a_0^n} + \frac{\langle a_0^n \delta O \rangle^{\rm QCD}}{a_0^n} - \frac{n\,\delta a}{a_0^{n+1}} \langle a_0^n O \rangle^{\rm QCD} \ , \tag{1.43}$$

where $\delta a = a - a_0$. The three expectation values on the right-hand side of Eq. (1.43) are directly computed in QCD simulations.

A concrete example of the above procedure is represented by the correction to the quark propagator S_f, which has been explicitely computed in Ref. [3] using the Twisted Mass action at maximal twist and in the *physical basis*[3]:

$\mathbf{\Delta}($  $) =$ (1.44)

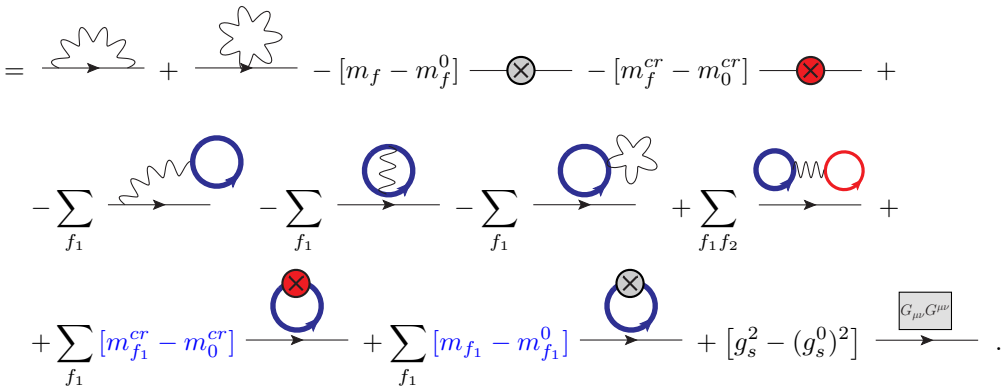

Here the diagram  represents the propagator of a quark with flavour f with the insertion of the local scalar operator $\sum_y \bar{\psi}_f(y)\psi_f(y)$, while  the propagator with the insertion of the local pseudoscalar operator $i \sum_y \bar{\psi}_f(y)\gamma_5\psi_f(y)$ [4]. Quark propagators of different flavours have been drawn with different colours and different lines and $f_{1,2}$ denotes the flavour of sea quarks. We have reported here the explicit expression of the correction to the quark propagator to define the *quenched QED* (qQED) or *electro-quenched* approximation and visualize its effect. Quark disconnected diagrams are in general noisy and difficult to calculate and therefore the usual solution to this problem consists in forcing the sea quarks to be neutral with respect to electromagnetic interactions. In practice, such approximation neglects the

[3] For simplicity we show the result for a fixed value of the Wilson parameter, namely $r = 1$.

[4] In the case of standard Wilson fermions the red and grey "blobs" would coincide.

contribution of disconnected diagrams in the evaluation of the lattice path-integrals of Eq. (1.41). In addition to completely disconnected diagrams (i.e. the vacuum polarization diagrams), also the polarization diagrams proportional to the charges of the valence quarks, which are a flavour $SU(3)$ breaking effect, are neglected in the qQED approximation.

Therefore, in such approximation the propagator in Eq. (1.45) becomes[5]

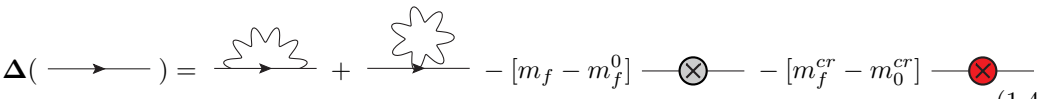

(1.45)

1.5 Defining QCD in the full QCD+QED theory

Before concluding the chapter and presenting the detailed description of our calculation of leptonic decay rates, we find it useful to further discuss the relation between the "full" QCD+QED theory, that includes explicit e.m. and strong IB effects, and QCD without electromagnetism.

At the level of precision to which we are currently working it is only the full theory, described by the action of Eq. (1.30), which is expected to reproduce physical results and that is therefore unambiguous. Nevertheless, one could wonder what is the difference between the results for a physical quantity computed in the full theory and in pure QCD, and how big are the strong isospin-breaking effects with respect to the e.m. corrections. We underline that in order to properly formulate such questions it is necessary to carefully define what is meant by QCD. It is naturally to be expected that in QCD alone physical quantities will not be reproduced with a precision of better than $\mathcal{O}(\alpha_{\rm em}) \simeq 1\%$ and this of course is the motivation for including QED corrections in lattice calculations. In order to define what is meant by QCD at this level of precision, it is necessary to state the conditions which are used to determine the quark masses and the lattice spacing. The separation of the full theory into QCD and the rest is therefore prescription dependent.

In Ref. [3] the issue of a precise definition of QCD has been discussed by using the GRS scheme originally proposed in Ref. [8]. In the following we present an extended and detailed discussion by introducing the *hadronic schemes*. Indeed, in light of the fact that hadron masses can nowadays be computed very precisely, we strongly suggest using hadronic schemes in future lattice calculations of QED radiative corrections. At the end of this section we discuss the connection with the GRS scheme that has been adopted at the time in which this calculation was started and that, for this reason, has been used in this work.

1.5.1 Renormalization of the full theory

The main difference in the steps required to renormalize the full theory compared to the procedure in QCD is the presence of a massless photon and the corresponding finite-volume (FV) corrections which appear as inverse powers of L, where L is the

[5] We stress that this result is obtained in Ref. [3] using the Twisted Mass action at maximal twist and in the *physical basis*. In Sec. 4.1.1 we will find a similar expression, but with different coefficients. This is due to the use of the *twisted* basis for fermions, instead of the *physical* one.

spatial extent of the lattice, and the volume $V = L^3$. By contrast, in QCD for leptonic and semileptonic decays the FV corrections are exponentially small in the volume.

A possible strategy to renormalize the full QCD+QED theory, in principle, is the following:

1. Fix the number of lattice points N, e.g. $L = aN$ and $T = 2L$, where L and T are the spatial and temporal extents of the lattice and the lattice spacing a will be determined later[6].

2. Using a four-flavour theory for illustration, we now need to determine the four physical bare quark masses, the bare electric charge and the lattice spacing. To this end we need to compute six quantities, e.g. the five dimensionless ratios[7]

$$\begin{aligned} R_1(aN; g_s, e, \mathbf{m}) &= \frac{aM_{\pi^+}}{aM_\Omega}(aN; g_s, e, \mathbf{m}) \ , \\ R_2(aN; g_s, e, \mathbf{m}) &= \frac{aM_{K^0}}{aM_\Omega}(aN; g_s, e, \mathbf{m}) \\ R_3(aN; g_s, e, \mathbf{m}) &= \frac{aM_{D_s}}{aM_\Omega}(aN; g_s, e, \mathbf{m}) \ , \\ R_4(aN; g_s, e, \mathbf{m}) &= \frac{aM_{K^+} - aM_{K^0}}{aM_\Omega}(aN; g_s, e, \mathbf{m}) \ , \\ R_5(aN; g_s, e, \mathbf{m}) &= \frac{aM_{D^0} - aM_{D^+}}{aM_\Omega}(aN; g_s, e, \mathbf{m}) \ , \end{aligned} \tag{1.46}$$

   as well as a dimensionful quantity, e.g. the mass of the Ω baryon, computed in lattice units, from which the lattice spacing can be determined after extrapolation to the infinite volume limit (see below):

$$R_0(aN; g_s, e, \mathbf{m}) = \frac{aM_\Omega(aN; g_s, e, \mathbf{m})}{M_\Omega^{\rm phys}} \ , \tag{1.47}$$

   where $M_\Omega^{\rm phys} = 1.672\,\text{GeV}$ is the physical value of the mass of the Ω baryon [9]. For illustration we are considering the masses of QCD+QED stable pseudoscalar mesons in the numerators of the dimensionless ratios (1.46) and using $M_\Omega^{\rm phys}$ to determine the lattice spacing, but of course other quantities can be used instead. For example, in the four-flavour theory that we are considering here one can in principle avoid potentially noisy baryon observables by using one of the charmed mesons masses already considered above to set the scale. In Eqs. (1.46) - (1.47) we have used aN instead of L to highlight that the infinite-volume limit should be taken at fixed lattice spacing (see Eq. (1.48) below). The quantity $\mathbf{m}$ represents the vector of bare quark masses $\mathbf{m} \equiv \{m_u, m_d, m_s, m_c\}$. Note that in the RM123 strategy, since one works at first order in $\alpha_{\rm em}$, it is not necessary to impose a renormalization condition to

[6] The specific choice $T = 2L$ is convenient for illustration but not strictly necessary for the following argument.

[7] An alternative procedure to determine the bare electric charge would be the evaluation of the hadronic corrections to a leptonic observable.

fix the e.m. coupling [3, 26]. In this case the electric charge can simply be fixed to the Thomson limit, i.e. $e = \sqrt{4\pi/137.036}$, and R_5 becomes a predictable quantity. For the remainder of this section, we assume that we are working to $\mathcal{O}(\alpha_{\rm em})$ and only consider the four ratios R_i $(i = 1, 2, 3, 4)$ as well as R_0 when discussing the calibration of the lattices. Notice also that at first order in $\alpha_{\rm em}$ the π^0 cannot decay in two photons, so that it can also be used in the calibration procedure (see Sec. 2.4 below).

3. Up to this point the procedure is the standard one used in QCD simulations. The difference here is in the FV effects which behave as inverse powers of L. We therefore suggest to extrapolate the ratios R_i to the infinite-volume limit by taking the lattice spacing fixed:

$$R_i(g_s, e, \mathbf{m}) \equiv \lim_{N\to\infty} R_i(aN; g_s, e, \mathbf{m}) \ , \qquad i = 0, 1, 2, 3, 4, 5 \ . \tag{1.48}$$

4. For a given discretization and choice of the coupling g_s, the *physical* bare quark masses, $\mathbf{m}^{\rm phys}(g_s)$, and the electric charge, $e^{\rm phys}(g_s)$, are defined by requiring that the five ratios $R_{1,2,3,4,5}$ take their physical values

$$R_i(g_s, e^{\rm phys}(g_s), \mathbf{m}^{\rm phys}(g_s)) = R_i^{\rm phys} \ , \qquad i = 1, 2, 3, 4, 5 \ . \tag{1.49}$$

   In practice, of course, depending on the specific choice of the ratios R_i, this will require some extrapolations of results obtained at different values of the bare quark masses and electric charge.

5. The lattice spacing a at this value of g_s can now be defined to be

$$a(g_s) = R_0(g_s, e^{\rm phys}(g_s), \mathbf{m}^{\rm phys}(g_s)) \ . \tag{1.50}$$

   Note that with such a procedure the bare parameters and the lattice spacing a do not depend on the lattice volume.

6. At leading order in the two IB parameters, i.e. $\mathcal{O}(\alpha_{\rm em}, m_d - m_u)$, the renormalization of the lepton masses is performed perturbatively, by requiring that the on-shell masses correspond to the physical ones. If one wishes to go beyond first order, when hadronic effects first enter, then the physical lepton masses should be added to the quantities used in the non-perturbative calibration. The bare lepton masses, together with the other parameters, should be chosen such that, in addition to satisfying the conditions in Eq. (1.46), the lepton-lepton correlators decay in time as $\mathrm{e}^{-m_\ell t}$, where m_ℓ is the physical mass of the lepton ℓ.

In Eq. (1.48) we have taken the infinite-volume limit of the computed hadron masses. By working in the QED$_L$ finite-volume formulation of QED, if for each hadron H the FV corrections of order $\mathcal{O}(e^2/(M_H L)^3, e^4)$ can be neglected, then the extrapolation to the infinite-volume limit can be avoided by making use of the formula [23, 30]

$$\frac{aM_H(L; g_s, e, \mathbf{m})}{aM_H(g_s, e, \mathbf{m})} = 1 - \kappa\, \alpha_{\rm em}\, e_H^2 \left\{ \frac{1}{2L\, M_H(g_s, e, \mathbf{m})} + \frac{1}{L^2\, M_H^2(g_s, e, \mathbf{m})} \right\} \ , \tag{1.51}$$

where e_H is the charge of the hadron H and $\kappa = 2.837297\,(1)$ is a known universal constant, independent of the structure of the hadron H. Similar formulae also exist for other finite-volume formulations of the theory, see e.g. Ref. [34] in the case of C* boundary conditions. Equation (1.51) can be used to determine the infinite-volume mass of the hadron H from the value measured on the finite-volume L^3, up to corrections of order of $\mathcal{O}(e^2/(m_H L)^3, e^4)$.

1.5.2 Defining observables in QCD

The procedure discussed above in Sec. 1.5.1 provides a full framework in which to perform lattice simulations of QCD together with isospin-breaking effects including radiative corrections. Under the assumption that isospin breaking effects are not negligible, QCD by itself is an unphysical theory and requires a definition. Different prescriptions are possible and, of course, lead to different results in QCD. In this section we propose and advocate *hadronic schemes*, based on the non-perturbative evaluation of a set of hadronic masses in lattice simulations, and compare them with schemes like the GRS one, which is based on equating the renormalized strong coupling and masses in some renormalization scheme and at a particular renormalization scale.

We recall that the QCD action is given by Eq. (1.31), which is evaluated with bare coupling and masses different from those in the full theory, described instead by the action of Eq. (1.30). Indeed the two theories have different dynamics that, in turn, generate a different pattern of ultraviolet divergences. The difference in the bare parameters of the two theories, for all schemes used to define QCD, can in fact be related to the necessity of reabsorbing the different ultraviolet singularities. In what follows we present two different approaches to making the choice of the parameters g_0 and $m_{f,0}$.

Hadronic schemes

In hadronic schemes we choose a value of g_0 and determine the bare quark masses $\mathbf{m}_0^{\rm phys}$ and the lattice spacing a_0 imposing the same conditions as for the full theory with the ratios $R_{0,\ldots,4}$ evaluated at vanishing electric charge, i.e. following steps 1 - 5 in Sec. 1.5.1 without imposing any constraint on the ratio R_5. These parameters differ by terms of order $\mathcal{O}(\alpha_{\rm em})$ from those in the full theory. For this discussion, we make the natural and convenient choice $g_0 = g_s$. With this choice, the lattice spacings in QCD (a_0) and in the full theory (a) can be obtained as

$$a_0 = \frac{\langle a_0 M_\Omega\rangle^{\rm QCD}}{M_\Omega^{\rm phys}} \quad \text{and} \quad a = \frac{\langle a M_\Omega\rangle^{\rm full}}{M_\Omega^{\rm phys}} \equiv a_0(1+\delta a)\ . \tag{1.52}$$

To illustrate the procedure imagine that we wish to calculate an observable O of mass dimension 1, for example the mass of a hadron which has not been used for the calibration. At a fixed value of $g_s = g_0$, we denote the best estimate of the observable O, which is the one obtained in the full theory, by $O^{\rm phys}$, and that obtained in QCD as defined above by $O^{\rm QCD}$:

$$O^{\rm phys} \equiv \frac{\langle aO\rangle^{\rm full}}{a} \quad \text{and} \quad O^{\rm QCD} \equiv \frac{\langle a_0 O\rangle^{\rm QCD}}{a_0}\ . \tag{1.53}$$

We *define* the difference of the two as being due to QED effects, $\delta O^{\rm QED} \equiv O^{\rm phys} - O^{\rm QCD}$. By using the result obtained in Eq. (1.43) with $n = 1$, we get

$$O^{\rm phys} = O^{\rm QCD} + \frac{\langle a_0\, \delta O\rangle^{\rm QCD}}{a_0} - \frac{\delta a}{a_0^2}\langle a_0 O\rangle^{\rm QCD} \ , \tag{1.54}$$

where we have combined the contributions to the correlation functions from the exchange of virtual photons and from the insertion of the mass counterterms into $\langle a_0 \delta O\rangle^{\rm QCD}$ and the last term comes from the difference in the lattice spacings $\delta a = a - a_0$ in the full theory and QCD. The first term on the right-hand side is one that can be calculated within QCD alone. This term allows us to define what is the difference between QCD (defined as above) and the full theory in the hadronic scheme: $\delta O^{\rm QED} = O^{\rm phys} - O^{\rm QCD}$.

An important feature of the RM123 approach which we follow in the numerical study presented below, is that the $\mathcal{O}(\alpha_{\rm em})$ terms are computed explicitly and so we do not have to take the difference between numerical calculations performed in the full theory and in QCD. Each of the terms on the right-hand side of Eq. (1.54) is calculated directly. We now explain the procedure in some more detail by assuming that terms of order $\mathcal{O}(\alpha_{\rm em}^2)$ are negligible.

a. Correlation functions corresponding to diagrams with the exchange of a virtual photon and to the insertion of the mass counterterms are already of $\mathcal{O}(\alpha_{\rm em})$ and are calculated directly in QCD. The term proportional to the time separation in the correlation functions gives us the mass shift δM_{H_i} $(i = 1, 2, 3, 4)$ and δM_Ω for the five masses (or mass differences) in the ratios R_i $(i = 1, 2, 3, 4)$ in Eq. (1.46);

b. In the hadronic scheme being used for illustration, we impose the condition that the four ratios $R_i = m_{H_i}/m_\Omega$ are the same in QCD and in the full theory. This corresponds to requiring that

$$\frac{\delta M_{H_i}}{M_{H_i}} - \frac{\delta M_\Omega}{M_\Omega} = 0 \qquad (i = 1, 2, 3, 4) \ . \tag{1.55}$$

The QED contribution to the left-hand side is different from zero (and also ultraviolet divergent) and we require the terms proportional to the counterterms to cancel this contribution. We therefore (in principle) scan the values of the four mass counterterms $\delta m_f = m_f - m_{f,0}$ $(f = u, d, s, c)$ until the four conditions (1.55) are satisfied. Also in this case no subtraction of results obtained in the full theory and in QCD is necessary.

c. Finally we determine the difference $\delta a \equiv a - a_0$ in the lattice spacing. Having determined the bare masses using item b, we can calculate the shift in the Ω mass (δM_Ω) due to both QED and the mass counterterms and use Eq. (1.52).

We have discussed in detail the definition of the isospin-breaking effects due to electromagnetism, $\delta O^{\rm QED}$. Having done this, the subsequent definition of the strong isospin breaking effects is straightforward. To do this, however, we need to define the isosymmetric theory (labelled by "ISO") by imposing appropriate conditions to determine the bare quark masses and the lattice spacing. Since $m_u = m_d$, in the

$N_f = 2 + 1 + 1$ theory we need to determine only three quark masses and hence we only need three conditions, e.g. we can use the ratios $R_{1,2,3}$ in Eq. (1.46) to determine the physical bare quark masses. For the determination of the lattice spacing we have two options. The simplest one is to work in a mass–independent scheme and set the lattice spacing in the isosymmetric theory, $a_0^{\rm ISO}$, equal to the one of QCD with $m_u \neq m_d$, i.e. $a_0^{\rm ISO} = a_0$. The other option is that we set the lattice spacing in the isosymmetric theory by using R_0 in Eq. (1.50). The difference between the two options is due to cutoff effects that disappear once the continuum limit is taken consistently. The strong isospin breaking correction $\delta O^{\rm SIB}$ to the observable O can now be defined by

$$\delta O^{\rm SIB} = O^{\rm QCD} - O^{\rm ISO} \ , \tag{1.56}$$

where $O^{\rm ISO} = \frac{\langle a_0^{\rm ISO} O\rangle^{\rm ISO}}{a_0^{\rm ISO}}$ is the value of the observable obtained in isosymmetric QCD. With these definitions we have the natural relation $O^{\rm phys} = O^{\rm ISO} + \delta O^{\rm QED} + \delta O^{\rm SIB}$.

The GRS scheme

A different prescription consists in using the GRS scheme already introduced in Sec. 1.3. This was originally proposed in Ref. [8] (see also Ref. [35]) to relate the bare quark masses and bare coupling of QCD (m_f^0 and g_0) to those in the full theory (m_f and g_s). This prescription has been adopted in Refs. [3, 26]. In the GRS approach, instead of determining the bare parameters of QCD by requiring that the chosen hadronic masses in QCD are equal to their physical values, one imposes that the renormalized parameters in a given short-distance scheme (e.g. the $\overline{\rm MS}$ scheme) and at a given scale are equal in the full and QCD theories.

A consistent procedure is the following:

1. The full theory is renormalized by using a physical hadronic scheme as discussed in subsection 1.5.1. This means that for each chosen value of g_s, the corresponding physical value of the bare electric charge $e^{\rm phys}(g_s)$ and of the lattice spacing $a(g_s)$ are known.

2. The renormalization constants (RCs) of the strong coupling constant and of the quark masses are computed in a short-distance mass-independent scheme both in the full theory and in the theory with $e = 0$.

3. In order to set the bare parameters of QCD at a given value of the lattice spacing we choose a matching scale μ and impose that the renormalized strong coupling constant and quark masses are the same as in the full theory. In practice we might want to simulate QCD at the same values of the lattice spacing used in the full theory simulations. In this case the matching conditions are

$$\begin{aligned} \hat{g}_0(\mu) &= Z_g(0, g_0, a(g_s)\mu) g_0 = Z_g(e^{\rm phys}(g_s), g_s, a(g_s)\mu) g_s = \hat{g}_s(\mu) \ , \\ \widehat{m}_f^0(\mu) &= Z_{m_f}(0, g_0, a(g_s)\mu) m_f^0(g_0) = Z_{m_f}(e^{\rm phys}(g_s), g_s, a(g_s)\mu) m_f(g_s) = \widehat{m}_f(\mu) \, , \end{aligned} \tag{1.57}$$

   where the hat ($\widehat{\ }$) indicates renormalized quantities. Notice that quarks with the same electric charge have the same RC, e.g. $Z_{m_u}(e, g_s, \mu) = Z_{m_c}(e, g_s, \mu)$, and that the quark mass RC at vanishing electric charge is flavour independent, $Z_{m_f}(0, g_0, \mu) = Z_m(g_0, \mu)$.

4. In order to define isosymmetric QCD by using this approach, the bare up-down quark mass is determined from

$$Z_m(g_0, a(g_s)\mu)\, m^0_{ud}(g_0) = \frac{\widehat{m}_u(\mu) + \widehat{m}_d(\mu)}{2} \ . \tag{1.58}$$

The GRS scheme is a short-distance matching procedure that can also be used to match the theories at unphysical values of the renormalized electric charge and/or quark masses with the physical theory. By following the procedure outlined above one can perform lattice simulations of the full theory and of isosymmetric QCD at the same value of the lattice spacing but, consequently, at different values of the bare strong coupling constant. This is different from the strategy outlined in the previous subsection where, by using hadronic schemes, it was more natural to choose the same value of the bare strong coupling ($g_0 = g_s$) at the price of having two different lattice spacings. The absence of the lattice spacing counterterm (see Eq. (1.54) above) in the GRS scheme is compensated from the presence of the counterterm $(1/g_0^2 - 1/g_s^2)S^{\rm YM}$ originating from the difference of the bare strong coupling constants in the two theories.

A remark of some practical relevance concerns the possibility of implementing hadronically the GRS scheme. To this end, note that in the GRS scheme the dimensionless ratios R_i will not be equal to the corresponding physical values and the difference can be parametrized as follows

$$R_i^{\text{QCD-GRS}} = R_i^{\rm phys}(1 + \epsilon_i^{\rm GRS}), \tag{1.59}$$

where the $\epsilon_i^{\rm GRS}$ are order $\mathcal{O}(\alpha_{\rm em})$ and depend on the chosen matching scheme and also on the chosen matching scale. Once the $\epsilon_i^{\rm GRS}$ (and hence the $R_i^{\text{QCD-GRS}}$) are known, for example from a particularly accurate lattice simulation, then they can be used in other lattice computations. The bare quark masses are then determined by requiring that the R_i in isosymmetric QCD reproduce $R_i^{\text{QCD-GRS}}$ as given by Eq. (1.59), and, at this stage, the GRS scheme can be considered to be a hadronic one as it is defined in terms of non-perturbatively computed quantities (in this case meson masses). We stress however that this requires prior knowledge of the $\epsilon_i^{\rm GRS}$.

Of course other schemes are also possible. In general, the ϵ_i provide a unifying language to discuss the different schemes for the definition of (isosymmetric) QCD in the presence of electromagnetism; in physical hadronic schemes the $\epsilon_i = 0$, while in the GRS and other schemes they are of order $\mathcal{O}(\alpha_{\rm em})$. For later use, we make the simple observation that two schemes can be considered to be equivalent in practice if the ϵ_i in the two schemes are equal within the precision of the computations.

Although the GRS scheme is perfectly legitimate, we advocate the use of physical hadronic schemes in future lattice calculations. For lattice simulations of physical quantities, a non-perturbative calibration of the lattice is necessary in general, but the renormalization required for the GRS conditions in Eq. (1.57) is not generally necessary (except perhaps for the determination of the renormalized coupling and quark masses themselves). Now that hadronic masses are calculated with excellent precision in lattice simulations and their values are well known from experimental measurements, it is natural to use hadronic schemes. By contrast, the renormalized couplings and masses are derived quantities which are not measured directly in

experiments. In spite of this, as explained above, at the time that the computation of leptonic decay rates was started, the GRS scheme was adopted. Of course the physical results in the full theory do not depend on this choice.

2 | QED corrections to hadronic decay rates

The study of weak processes play a crucial role in exploring the limits of the Standard Model of particles and in searching signals of new physics. Leptonic and semileptonic decays of hadrons allow one to extract the entries of the CKM matrix by comparing theoretical determinations with experimental measurements. The precision in extracting CKM matrix elements is generally limited by our ability to quantify hadronic effects and the main goal of large-scale simulations using the lattice formulation of QCD is the *ab initio* evaluation of the non-perturbative QCD effects in physical processes. The recent improvement in lattice computations has led to a precision approaching $\mathcal{O}(1\%)$ for a number of quantities (see e.g. Ref. [1] and references therein) and therefore in order to make further progress electromagnetic and strong isospin-breaking effects, which are of the same order of magnitude, have to be considered. The inclusion of IB effects in lattice calculations, described in the previous Chapter 1 following the RM123 approach of Refs. [2, 3, 26], has been first applied with great success to the calculation of the hadron spectrum. The issue of how to include electromagnetic effects in the hadron spectrum and in the determination of quark masses from lattice calculations was addressed for the first time in Ref. [19]. Using a variety of different methods to include QED effects in lattice QCD simulations, several collaborations have recently obtained remarkably precise results for the hadron spectrum, such as the determination of the charged-neutral mass splittings of light pseudoscalar mesons and baryons [2, 3, 21, 27, 36–42] (see Refs. [28, 29, 43] for recent reviews on the subject). However, the computation of the hadron spectrum is much simplified by the absence of infrared (IR) divergences. The same is not true when computing hadronic amplitudes, where electromagnetic IR divergences are present and cancel only for well defined, measurable physical quantities only after including diagrams containing both real and virtual photons, as first understood by Bloch and Nordsieck in Ref. [44]. This is the case, for instance, for the leptonic $\pi_{\ell 2}$ and $K_{\ell 2}$ and semileptonic $K_{\ell 3}$ decay rates. The presence of IR divergences in intermediate steps of the calculation requires in this case a new strategy beyond those developed for the calculation of IB effects in the hadron spectrum. Such a new strategy was proposed in Ref. [14], where the lattice determination of the decay rate of a charged pseudoscalar meson ($P^{\pm}$) into either a final $\ell^{\pm}\nu_{\ell}$ pair or $\ell^{\pm}\nu_{\ell}\gamma$ state was addressed.

In this chapter we discuss in full detail such strategy, focusing on the leptonic decay of a pseudoscalar meson with positive charge, P^{+}.

2.1 The method

Let Γ_0 be the partial width for the decay $P^+ \to \ell^+ \nu_\ell$ where the charged lepton ℓ is an electron or a muon (or possibly a τ) and ν_ℓ is the corresponding neutrino. The subscript 0 is used to indicate that there are no photons in the final state. In the absence of electromagnetism, the non-perturbative QCD effects are contained in a single number, the decay constant $f_P^{(0)}$, which is defined in the continuum and in a given scheme in terms of the matrix element of the QCD axial current $A_P^{(0)}$ as

$$A_P^{(0)} \equiv \langle 0 | \, \bar{q}_2 \, \gamma_0 \gamma_5 \, q_1 \, | P^{(0)} \rangle \equiv f_P^{(0)} M_P^{(0)} \ , \tag{2.1}$$

where the initial state meson $P^{(0)}$ (considered at rest) is composed of the valence quarks $\bar{q}_1$ and q_2, and $M_P^{(0)}$ is the P-meson mass defined in isosymmetric QCD in the chosen scheme as well. Many calculations of decay constants $f_\pi, f_K, f_{D_{(s)}}$ and $f_{B_{(s)}}$ have been done in the last years in isosymmetric QCD [1], some of which approaching $\mathcal{O}(1\%)$ precision. As noted above, at such a level of precision isospin breaking effects, including electromagnetic corrections, have to be taken into account. However, as it has been stressed in Refs. [45, 46], it is not possible to give a physical definition of the decay constant f_P in the presence of electromagnetism, because of the contributions from diagrams in which the photon is emitted by the hadron and absorbed by the charged lepton. Thus the physical width can only be obtained by a full calculation of the electromagnetic corrections at a given order in $\alpha_{\rm em}$. The immediate difficulty one encounters when including electromagnetic corrections is that Γ^0 contains IR divergences and by itself is therefore unphysical. In order to solve the problem, as mentioned above, one has to include the contributions from real photons. We therefore define Γ_1 to be the partial witdh for the decay $P^+ \to \ell^+ \nu_\ell \gamma$, the subscript 1 indicating that there is one photon in the final state. The e.m. corrections due to the exchange of a virtual photon and to the emission of a real one can be both computed non-perturbatively, by numerical simulations, on a finite lattice with the corresponding uncertainties. The exchange of a virtual photon depends on the structure of the decaying meson, since all momentum modes are included, and the corresponding amplitude must therefore be computed non-perturbatively. The non-perturbative evaluation of the emission of a real photon is very challenging and first promising results have been recently obtained [47, 48]. However, it is possible to compute the real emission amplitudes in perturbation theory by limiting the maximum energy of the emitted photon in the meson rest-frame to a value ΔE_γ small enough so that the internal structure of the decaying meson is not probed and the meson P^+ can be treated as a pointlike particle[1]. The IR divergences in the non-perturbative calculation of the corrections due to the exchange of a virtual photon are cancelled by the corrections due to the real photon emission even when the latter is computed perturbatively, because IR divergences do not depend on the structure of the decaying hadron. Such a strategy, which requires an experimental cut on the energy of the real photon, is the one originally proposed in Ref. [14] and it will be the one adopted in this thesis. It is necessary to ensure that the cancellation

[1] On the other hand, ΔE_γ must be sufficiently large that the decay rate can be measured experimentally.

of IR divergences between Γ_0 and $\Gamma(\Delta E_\gamma)$ occurs with good numerical precision, since they are computed in a Monte-Carlo simulation and in perturbation theory respectively. An intermediate step is therefore needed, in which an IR regulator is introduced. The inclusive rate $\Gamma(P^+ \to \ell^+\nu_\ell[\gamma])$ can be expressed as [14]

$$\begin{aligned}\Gamma(P^\pm \to \ell^\pm\nu_\ell[\gamma]) &= \Gamma_0 + \Gamma_1^{\rm pt}(\Delta E_\gamma) \\ &= \lim_{L\to\infty}\Big[\Gamma_0(L) - \Gamma_0^{\rm pt}(L)\Big] + \lim_{\mu_\gamma\to 0}\Big[\Gamma_0^{\rm pt}(\mu_\gamma) + \Gamma_1^{\rm pt}(\Delta E_\gamma,\mu_\gamma)\Big]\ ,\end{aligned} \tag{2.2}$$

where the subscripts $0, 1$ indicate the number of photons in the final state, while the superscript pt denotes the point-like approximation of the decaying meson and μ_γ is an IR regulator. In the first term on the r.h.s. of Eq. (2.2) the quantities $\Gamma_0(L)$ and $\Gamma_0^{\rm pt}(L)$ are evaluated on the lattice. Both have the same IR divergences which therefore cancel in the difference. We use the lattice size L as the intermediate IR regulator by working in the $\rm QED_L$ finite-volume formulation of QED [30] (see Sec. 1.2). The difference $\Big[\Gamma_0 - \Gamma_0^{\rm pt}\Big]$ is independent of the regulator as this is removed [49]. As already pointed out, since all momentum modes contribute to it, $\Gamma_0(L)$ depends on the structure of the decaying meson and must be computed non-perturbatively. In the second term on the r.h.s. of Eq. (2.2), the meson is treated as point-like and both $\Gamma_0^{\rm pt}(\mu_\gamma)$ and $\Gamma_1^{\rm pt}(\Delta E_\gamma,\mu_\gamma)$ can be calculated directly in infinite volume in perturbation theory, using a photon mass μ_γ as the IR regulator. Each term is IR divergent, but the sum is convergent [44] and independent of the IR regulator. The explicit perturbative calculations of $\Big[\Gamma_0^{\rm pt} + \Gamma_1^{\rm pt}(\Delta E_\gamma)\Big]$ and $\Gamma_0^{\rm pt}(L)$ have been performed in Refs. [14] and [49], respectively.

The first application of this method to the calculation of leptonic decay rates has been done in Ref. [6], where e.m. and IB corrections to the ratio of K_{μ_2} and π_{μ_2} decay rates of charged kaons and pions into muons, $\Gamma[K \to \mu\nu_\mu(\gamma)]/\Gamma[\pi \to \mu\nu_\mu(\gamma)]$, was evaluated. The ratio is less sensitive to various sources of uncertainty than the IB corrections to π_{μ_2} and K_{μ_2}, since the e.m. corrections coming from the renormalization of the operator mediating the decay process cancel out in the ratio. However, in order to obtain a separate evaluation of IB corrections to the π_{μ_2} and K_{μ_2} decay rates such contributions must be included in the calculation. Therefore, in the following we describe how to renormalize the weak effective Hamiltonian in the presence of e.m. interactions. Then, in Sec. 2.4 we will describe the structure of the calculation of leptonic decay amplitudes, including the leading order IB effects.

2.2 From Standard Model to W-regularization

At the lowest order in the e.m. and strong perturbation theory, the process $P^+ \to \ell^+\nu_\ell$ takes place by an s-channel exchange of a W boson between the constituent quarks of the meson and the lepton pair, see left-hand diagram of Fig. 2.1. Since the energy-momentum carried by the W boson in this process is much smaller than the W-boson mass M_W, it is standard practice to rewrite the amplitude in terms of a four-fermion local interaction, described by the effective Hamiltonian

$$\mathcal{H}_W = \frac{G_F}{\sqrt{2}}\, V_{q_1q_2}^*\ O_1 \equiv \frac{G_F}{\sqrt{2}}\, V_{q_1q_2}^*\ (\bar{q}_2\gamma_\mu(1-\gamma_5)q_1)\ (\bar{\nu}_\ell\gamma^\mu(1-\gamma_5)\ell)\ , \tag{2.3}$$

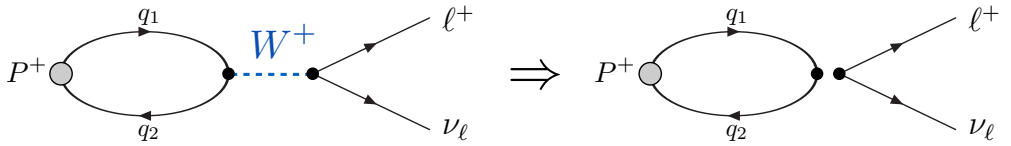

Figure 2.1. Tree-level diagram for the process $P^+ \to \ell^+\nu_\ell$ (left-hand diagram). In the effective theory the interaction is given by a local four-fermion operator (right-hand diagram).

where G_F is the Fermi constant and $V_{q_1q_2}$ is an element of the CKM matrix. At lowest order in $\alpha_{\rm em}$ the two full dots in the right-hand diagram of Fig. 2.1 represent the two currents in the bare four-fermion operator

$$O_1 = \left(\bar{q}_2\gamma_\mu(1-\gamma_5)q_1\right)\left(\bar{\nu}_\ell\gamma^\mu(1-\gamma_5)\ell\right) \ . \tag{2.4}$$

In order to compute the rate on the lattice, such a replacement is necessary, since the lattice spacing a is much greater than $1/M_W$. When including first order QED corrections, the ultraviolet (UV) contributions to the matrix element of the local operator in the effective theory are different from those in the Standard Model. Therefore, a matching between the two theories is necessary. The Fermi constant G_F is conventionally taken from the measured value of the muon lifetime using the expression [50, 51]

$$\frac{1}{\tau_\mu} = \frac{G_F^2 m_\mu^5}{192\pi^3}\left[1-\frac{8m_e^2}{m_\mu^2}\right]\left[1+\frac{\alpha_{\rm em}}{2\pi}\left(\frac{25}{4}-\pi^2\right)\right] \ , \tag{2.5}$$

leading to the value $G_F = 1.16634 \times 10^{-5}\,\text{GeV}^{-2}$. For an extension of Eq. (2.5) to $\mathcal{O}(\alpha_{\rm em}^2)$ and the inclusion of higher powers of $\rho \equiv (m_e/m_\mu)^2$ see Sec. 10.2 of Ref. [9]. The Particle Data Group [9] quote the corresponding value of the Fermi constant to be $G_F = 1.1663787(6) \times 10^{-5}\,\text{GeV}^{-2}$.

Eq. (2.5) can be taken as the definition of G_F at $\mathcal{O}(\alpha_{\rm em})$. When calculating the Standard Model corrections to the muon lifetime many of the contributions are absorbed into G_F and the remaining terms on the right-hand side of Eq. (2.5) come from the diagrams in Fig. 2.2, in which the factor $1/k^2$ in the Feynman-gauge photon propagator is replaced by $1/k^2 \times M_W^2/(M_W^2-k^2)$, where k is the momentum in the propagator. This is called the *W-regularisation* of UV divergences [52]. The diagrams are evaluated in the effective theory with the local four-fermion operator $(\bar{\nu}_\mu\gamma^\mu(1-\gamma^5)\mu)\,(\bar{e}\gamma^\mu(1-\gamma^5)\nu_e)$, the two currents being represented by the filled black circles in Fig. 2.2. In such regularization, the photon propagator is rewritten as

$$\frac{1}{k^2} \to \frac{1}{k^2-M_W^2} + \frac{M_W^2}{M_W^2-k^2}\,\frac{1}{k^2} \tag{2.6}$$

and the UV divergent contributions absorbed in the definition of G_F come from the first term. In addition, the Standard-Model γ-W box diagram is ultra-violet convergent and is equal to the corresponding diagram in the effective theory (i.e. the third diagram in Fig. 2.2) with the W-regularisation, up to negligible corrections

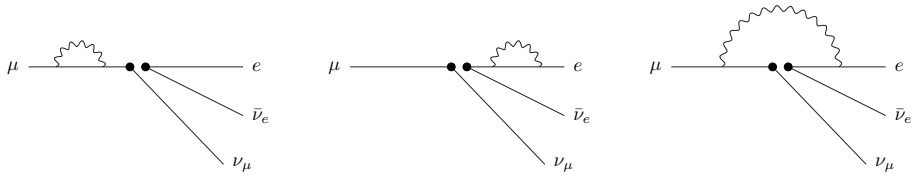

Figure 2.2. Diagrams contributing to the $\mathcal{O}(\alpha_{\rm em})$ corrections to muon decay; see Eq. (2.5). The curly line represents the photon.

of $O(q^2/M_W^2)$, where q is the four-momentum of the electron and its neutrino. Other electroweak corrections not explicitly mentioned above are all absorbed into G_F.

The helpful feature of W-regularization is that most of the terms which are absorbed into G_F are common to other processes, including leptonic decays of pseudoscalar mesons [11, 53]. There are however, some short-distance contributions which do depend on the electric charges of the individual fields in the four-fermion operators and these lead to a correction factor of $(1 + \frac{2\alpha_{\rm em}}{\pi} \log \frac{M_Z}{M_W})$ to Γ_0 [11].

The conclusion of the above discussion is that the evaluation of the amplitude for the process $P^+ \to \ell^+ \nu_\ell$ up to $\mathcal{O}(\alpha_{\rm em})$ can be performed in the effective theory with the effective Hamiltonian

$$\mathcal{H}_W = \frac{G_F}{\sqrt{2}} V^*_{q_1 q_2} \left[1 + \frac{\alpha_{\rm em}}{\pi} \log\left(\frac{M_Z}{M_W}\right)\right] O_1^{\text{W-reg}}(M_W) \,, \tag{2.7}$$

where G_F is obtained from the muon lifetime and $O_1^{\text{W-reg}}(M_W)$ is the operator O_1 of Eq. (2.3) renormalized in the W-regularization scheme and with the Feynman-gauge photon propagator in the W-regularization. At order $\mathcal{O}(\alpha_{\rm em})$, the two full dots in the right-hand diagram of Fig. 2.1 denote instead the insertion of $O_1^{\text{W-reg}}(M_W)$.

2.3 From W-regularization to Lattice

Since the W-boson is too large to be simulated on the lattice, the inverse lattice spacing being much smaller than the W-boson mass, a matching between the lattice weak operator O_1 and the one renormalized in the W-regularization scheme is necessary. Moreover, for lattice formulations which break chiral symmetry, like the one used in the present work, the lattice weak operator O_1 mixes with other four-fermion operators of different chirality. The calculation of $O_1^{\text{W-reg}}$ takes place in two steps: we start by renormalizing the lattice four-fermion operator O_1 defined in Eq. (2.4) in the RI'-MOM scheme [54], at all orders in QCD and first order in QED, obtaining $O_1^{\text{RI'}}(\mu)$, and then perturbatively match the operator $O_1^{\text{RI'}}(\mu)$ to the one in the W-regularization [14]

$$O_1^{\text{W-reg}}(M_W) = Z^{\text{W-RI'}}\left(\frac{M_W}{\mu}, \alpha_s(\mu), \alpha_{\rm em}\right) O_1^{\text{RI'}}(\mu) \,. \tag{2.8}$$

The coefficient $Z^{\text{W-RI'}}\left(M_W/\mu, \alpha_s(\mu), \alpha_{\rm em}\right)$ can be computed by first evolving the operator in the RI' scheme to the scale M_W and then matching it to the corresponding

operator in the W-scheme. The coefficient can therefore be written as the product of a matching coefficient and an evolution operator

$$Z^{\text{W-RI'}}\left(\frac{M_W}{\mu},\alpha_s(\mu),\alpha_{\text{em}}\right) = Z^{\text{W-RI'}}\left(1,\alpha_s(M_W),\alpha_{\text{em}}\right) U^{\text{RI'}}\left(M_W,\mu;\alpha_{\text{em}}\right) . \quad (2.9)$$

Below we will only consider terms of first order in α_{em} and, therefore we will consistently neglect the running of α_{em}.

We note that the original bare lattice operators and $O_1^{\text{W-reg}}(M_W)$ are gauge invariant, and thus the corresponding matching coefficients are gauge invariant. This is not the case for $O_1^{\text{RI'}}(\mu)$ that instead depends not only on the external states chosen to define the renormalization conditions, but also on the gauge. Consequently the matching coefficient $Z^{\text{W-RI'}}\left(\frac{M_W}{\mu},\alpha_s(\mu),\alpha_{\text{em}}\right)$ and the evolution operator $U^{\text{RI'}}\left(M_W,\mu,\alpha_{\text{em}}\right)$ are in general gauge dependent. However, at the order of perturbation theory to which we are working, the evolution operator turns out to be both scheme and gauge independent.

In the following, we discuss the matching coefficient, $Z^{\text{W-RI'}}\left(1,\alpha_s(M_W),\alpha_{\text{em}}\right)$, and give the result for the evolution operator $U^{\text{RI'}}\left(M_W,\mu,\alpha_{\text{em}}\right)$, while the calculation of the renormalized operator $O_1^{\text{RI'}}(\mu)$ obtained non-perturbatively on the lattice will be the subject of Chapters 3 and 4. A detailed calculation of the evolution operator at NLO in QCD+QED is done in Chapter 6.

The matching coefficient. At first order (one loop) in α_{em}, the matching coefficient takes the form

$$Z^{\text{W-RI'}}\left(1,\alpha_{\text{s}}(M_W),\alpha_{\text{em}}\right) = 1 + \frac{\alpha_{\text{em}}}{4\pi} C^{\text{W-RI'}} , \quad (2.10)$$

where the strong interaction corrections for the RI'-MOM operator vanish, at this order, because of the Ward identities of the quark vector and axial vector currents appearing in the operator O_1 in the massless limit. We stress that we currently do not include terms of $\mathcal{O}(\alpha_{\text{s}}(M_W)\alpha_{\text{em}})$ in the matching coefficient $Z^{\text{W-RI'}}$. The inclusion of such terms would require the knowledge of the three-loops anomalous dimension matrix in QCD+QED, which we have not computed. The specific value of $C^{\text{W-RI'}}$ used in this work will be given later in Eq. (5.17).

The evolution operator. The evolution operator $U^{\text{RI'}}\left(M_W,\mu;\alpha_{\text{em}}\right)$ is the solution of the renormalization group equation

$$\left[\mu^2\frac{\partial}{\partial\mu^2} + \beta(\alpha_{\text{s}},\alpha_{\text{em}})\frac{\partial}{\partial\alpha_{\text{s}}}\right] U^{\text{RI'}}\left(M_W,\mu;\alpha_{\text{em}}\right) = \frac{\gamma(\alpha_{\text{s}},\alpha_{\text{em}})}{2} U^{\text{RI'}}\left(M_W,\mu;\alpha_{\text{em}}\right) , \quad (2.11)$$

where $U^{\text{RI'}}\left(M_W,\mu;\alpha_{\text{em}}\right)$ satisfies the initial condition $U^{\text{RI'}}\left(M_W,M_W,\alpha_{\text{em}}\right) = 1$, $\gamma(\alpha_{\text{s}},\alpha_{\text{em}})$ is, in general, the anomalous dimension matrix [12, 13], although in our particular case it is actually a number (and not a matrix), and $\beta(\alpha_{\text{s}},\alpha_{\text{em}})$ is the QCD β-function with the inclusion of e.m. corrections. A detailed discussion on the calculation at NLO in QCD+QED of the evolution operator $U^{\text{RI'}}$ for a given set of operators is done in Chap. 6, while the calculation of the anomalous dimension matrix $\gamma(\alpha_{\text{s}},\alpha_{\text{em}})$ is carried on in Chap. 7.

According to Eqs. (6.50) - (6.52), together with the results obtained for the anomalous dimension of the operator $O_1^{\mathrm{RI'}}$ in Eqs. (7.57), the evolution operator has the form

$$\begin{aligned} U^{\mathrm{RI'}}(M_W,\mu;\alpha_{\mathrm{em}}) &= 1-\frac{\alpha_{\mathrm{em}}}{4\pi}\frac{\gamma_e^{(0)}}{2}\log\left(\frac{M_W^2}{\mu^2}\right)-\frac{\alpha_s(\mu)\alpha_{\mathrm{em}}}{(4\pi)^2}\frac{\gamma_{se}^{(1)}}{2}\log\left(\frac{M_W^2}{\mu^2}\right) \\ &= 1+\frac{\alpha_{\mathrm{em}}}{4\pi}2\left(1-\frac{\alpha_{\mathrm{s}}(\mu)}{4\pi}\right)\log\left(\frac{M_W^2}{\mu^2}\right)\ . \end{aligned} \tag{2.12}$$

Note that at this order the evolution operator is independent of the QCD β-function. This is a consequence of the fact that the QCD anomalous dimension vanishes for the operator O_1.

Combining Eqs. (2.8)-(2.10) and (2.12) we obtain the relation between the operator O_1 in the W-regularization scheme and the one in the RI' scheme,

$$O_1^{\text{W-reg}}(M_W)=\left\{1+\frac{\alpha_{\mathrm{em}}}{4\pi}\left[2\left(1-\frac{\alpha_{\mathrm{s}}(\mu)}{4\pi}\right)\log\left(\frac{M_W^2}{\mu^2}\right)+C^{\text{W-RI'}}\right]\right\}O_1^{\mathrm{RI'}}(\mu)\ , \tag{2.13}$$

which is valid at first order in α_{em} and up to (and including) terms of $\mathcal{O}(\alpha_{\mathrm{em}}\alpha_{\mathrm{s}}(M_W))$ in the strong coupling constant.

The calculation of the renormalized operator $O_1^{\mathrm{RI'}}(\mu)$, computed non-perturbatively on the lattice in the RI'-MOM scheme at all orders in α_{s} and up to first order in α_{em} is the only missing step for the determination of $O_1^{\text{W-reg}}(M_W)$ in Eq. (2.8). A new strategy to renormalize lattice operators in QCD+QED fully including the non perturbative dynamics of QCD, and QED at $\mathcal{O}(\alpha_{\mathrm{em}})$ will be presented in Chap. 3, while in Chap. 4 we will show the details of the numerical analysis performed in the electro-quenched approximation using gauge ensembles produced by the ETM collaboration with $N_f=4$ dynamical quarks.

2.4 Evaluation of the leptonic decay amplitude

At first order in α_{em} and $(m_d-m_u)/\Lambda_{\mathrm{QCD}}$ the inclusive decay rate (2.2) can be written as

$$\Gamma(P^\pm\to\ell^\pm\bar\nu_\ell[\gamma])=\Gamma^{\mathrm{QCD}}\left(1+\overline{\delta R}_P\right)+\mathcal{O}\left[\alpha_{\mathrm{em}}^2,(m_d-m_u)^2,\alpha_{\mathrm{em}}(m_d-m_u)\right]\ , \tag{2.14}$$

where Γ^{QCD} is the tree-level decay rate given by

$$\begin{aligned} \Gamma^{\mathrm{QCD}} &= \frac{G_F^2}{8\pi}|V_{q_1q_2}|^2\frac{m_\ell^2}{M_P^{(0)}}\left(1-\frac{m_\ell^2}{M_P^{(0)\,2}}\right)^2|A_P^{(0)}|^2 \\ &= \frac{G_F^2}{8\pi}|V_{q_1q_2}|^2m_\ell^2\left(1-\frac{m_\ell^2}{M_P^{(0)\,2}}\right)^2 f_P^{(0)\,2}M_P^{(0)}\ , \end{aligned} \tag{2.15}$$

with $M_P^{(0)}$ and $f_P^{(0)}$ being the mass and decay constant of the charged P-meson defined in isosymmetric QCD in the chosen scheme. The decay constant $f_P^{(0)}$ is defined in terms of the matrix element of the QCD axial current $A_P^{(0)}$ as in Eq. (2.1).

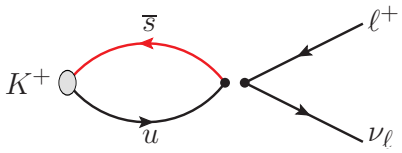

Figure 2.3. Feynman diagram for the process $K^+ \to \ell^+\nu_\ell$. In the effective theory the interaction is given by a local four-fermion operator denoted by the two full dots in the figure.

The decay rate is obtained from the insertion of the lowest-order effective Hamiltonian $\mathcal{H}_W$ of Eq. (2.3), as depicted in the Feynman diagram of Fig. 2.3, where the decay of a charged kaon is shown as an example. At lowest order in $\alpha_{\rm em}$ the two full dots in the figure represent the two currents in the bare four-fermion operator O_1 in Eq. (2.4), whereas at order $\mathcal{O}(\alpha_{\rm em})$ they will denote the insertion of the renormalized operator in the W-regularisation, $O_1^{\text{W-reg}}$.

In order to compare our results for the e.m. and strong IB corrections to those obtained in Ref. [18] and adopted by the PDG [9, 55], however, we will use a modified expression:

$$\Gamma(P^\pm \to \ell^\pm \bar{\nu}_\ell[\gamma]) = \Gamma^{(0)}\,(1+\delta R_P) + \mathcal{O}\left[\alpha_{\rm em}^2, (m_d-m_u)^2, \alpha_{\rm em}(m_d-m_u)\right] \ , \quad (2.16)$$

where $\Gamma^{(0)}$ is given by

$$\begin{aligned}\Gamma^{(0)} &= \frac{G_F^2}{8\pi}|V_{q_1q_2}|^2\frac{m_\ell^2}{M_P^2}\left(1-\frac{m_\ell^2}{M_P^2}\right)^2|\bar{A}_P|^2 \\ &= \frac{G_F^2}{8\pi}|V_{q_1q_2}|^2 m_\ell^2\left(1-\frac{m_\ell^2}{M_P^2}\right)^2 f_P^{(0)\,2} M_P \ , \end{aligned} \quad (2.17)$$

and M_P this time is the *physical* mass of the charged P-meson, including both e.m. and leading-order strong IB corrections. In the above Eq. (2.17) we have defined the matrix element of the hadronic axial current between the vacuum and the physical P ground state as

$$\bar{A}_P = \frac{p_P^\mu}{M_P}\,\langle 0|\,\bar{q}_2\gamma_\mu\gamma_5 q_1\,|P\rangle \equiv f_P^{(0)} M_P \ . \quad (2.18)$$

The quantity δR_P in Eq. (2.16) encodes both the e.m. and the strong IB leading-order corrections to the tree-level decay rate. Its value depends on the prescription used for the separation between the QED and QCD corrections, while the quantity

$$\mathcal{F}_P^2 \equiv \frac{\Gamma(P^\pm \to \ell^\pm\bar{\nu}_\ell[\gamma])}{\frac{G_F^2}{8\pi}|V_{q_1q_2}|^2 m_\ell^2\left(1-\frac{m_\ell^2}{M_P^2}\right)^2 M_P} = \left[f_P^{(0)}\right]^2(1+\delta R_P) \quad (2.19)$$

is prescription independent [46] to all orders in both $\alpha_{\rm em}$ and (m_d-m_u).

The quantity $\mathcal{F}_\pi$ may be used to set the lattice scale instead of the Ω baryon mass. Indeed, the physical value $\mathcal{F}_\pi^{\rm phys}$ can be obtained by taking the experimental pion decay rate $\Gamma(\pi^- \to \mu^-\bar{\nu}_\mu[\gamma]) = 3.8408(7)\cdot 10^7\ \text{s}^{-1}$ from the PDG [9] and the

result for $|V_{ud}| = 0.97420(21)$ determined accurately from super-allowed β-decays in Ref. [10]. Consequently, one may replace M_Ω with $\mathcal{F}_\pi$ (as the denominator of the ratios $R_{1,\ldots,4}$ in Eqs. (1.46)), M_{π^+} with M_{π^0} in the ratio R_1 (when working at leading order in $\alpha_{\rm em}$) and set the electron charge directly to its Thomson's limit (instead of using the ratio R_5), namely

$$
\begin{aligned}
R_1(aN; g_s, e, \mathbf{m}) &= \frac{aM_{\pi^0}}{a\mathcal{F}_\pi}(aN; g_s, e, \mathbf{m})\,, \\
R_2(aN; g_s, e, \mathbf{m}) &= \frac{aM_{K^0}}{a\mathcal{F}_\pi}(aN; g_s, e, \mathbf{m}) \\
R_3(aN; g_s, e, \mathbf{m}) &= \frac{aM_{D_s}}{a\mathcal{F}_\pi}(aN; g_s, e, \mathbf{m})\ , \\
R_4(aN; g_s, e, \mathbf{m}) &= \frac{aM_{K^+} - aM_{K^0}}{a\mathcal{F}_\pi}(aN; g_s, e, \mathbf{m})\ .
\end{aligned}
\tag{2.20}
$$

For the present study, however, we were unable to use M_Ω to determine the lattice spacing because the corresponding baryon correlators were unavailable. Numerical calculations of M_Ω by the ETM Collaboration are currently ongoing. The choice of using $\mathcal{F}_\pi$ instead to set the scale clearly prevents us from being able to predict the value of $|V_{ud}|$. This is one of the reasons why the use of hadronic schemes with hadron masses as experimental inputs is strongly suggested for future lattice calculations. However, as already explained above in Sec. 1.5, in this work we renormalize the QCD theory using the same set of hadronic inputs adopted in the analysis of quark-masses performed in Ref. [56], since the present calculations started applying the RM123 method on previously generated isosymmetric QCD gauge configurations from ETMC. The bare parameters of these QCD gauge ensembles were fixed in Ref. [56] by using the hadronic scheme corresponding to

$$
\begin{aligned}
M_\pi^{(0),\rm FLAG} &= 134.98 \text{ MeV} && (2.21)\\
M_K^{(0),\rm FLAG} &= 494.2\,(3) \text{ MeV} && (2.22)\\
f_\pi^{(0),\rm FLAG} &= 130.41\,(20) \text{ MeV} && (2.23)\\
M_{D_s}^{(0),\rm FLAG} &= 1.9690\,(14) \text{ GeV} && (2.24)
\end{aligned}
$$

where $M_{D_s}^{(0)}$ was chosen to be equal to the experimental D_s^+-meson mass [9]. Note that in the absence of QED radiative corrections $\mathcal{F}_\pi$ reduces to the conventional definition of the pion decay constant $f_\pi^{(0)}$. The superscript FLAG has been used because the chosen values of three out of the four hadronic inputs had been suggested in the previous editions of the FLAG review [1]. For this reason we refer to the scheme defined from these inputs as the FLAG scheme.

The same input parameters (2.20) used in the FLAG scheme have been computed in Ref. [7] also in the GRS scheme (corresponding to the $\overline{\rm MS}$ scheme at $\mu = 2$ GeV)

obtaining[2]:

$$M_\pi^{(0),\mathrm{GRS}} = 135.0\,(2)\ \mathrm{MeV}\ , \tag{2.29}$$
$$M_K^{(0),\mathrm{GRS}} = 494.6\,(1)\ \mathrm{MeV}\ , \tag{2.30}$$
$$f_\pi^{(0),\mathrm{GRS}} = 130.65\,(12)\ \mathrm{MeV}\ , \tag{2.31}$$
$$M_{D_s}^{(0),\mathrm{GRS}} = 1.9667\,(15)\ \mathrm{GeV}\ . \tag{2.32}$$

For the result of $f_\pi^{(0),\mathrm{GRS}}$, see Eq. (5.49) in Chap. 5 below. It follows that the values of the inputs determined in the GRS scheme differ at most by $\sim 0.15\%$ from the corresponding values adopted in Ref. [56] for the isosymmetric QCD theory and the differences are at the level of our statistical precision. Thus, the result of our analysis of the scheme dependence can be summarized by the conclusion that the FLAG and GRS schemes can be considered to be equivalent at the current level of precision. Nevertheless, we have used the results of this analysis to estimate the systematic error on our final determinations of the isospin breaking corrections δR_P induced by residual scheme uncertainties (see the discussion at the end of Chap. 5). In light of this quantitative analysis, given the numerical equivalence of the two schemes at the current level of precision, in the rest of the paper we shall compare our results obtained in the GRS scheme with the results obtained by other groups using the FLAG scheme and we shall not use superscripts to distinguish between the two schemes.

The correction to the decay rate δR_P, defined in Eq. (2.16), gets to kind of contributions and can be written as

$$\delta R_P = \delta R_P^{\mathrm{ren}} + \delta R_P^{\mathrm{ampl}}\ . \tag{2.33}$$

The term $\delta R_P^{\mathrm{ren}}$ comes from the e.m. corrections in the matching of the renormalized weak four-fermion lattice operator to the W-regularization scheme, described by Eq. (2.13), and from the (eventual) mixing of the operator O_1 with other bare lattice four-fermion operators in the case chiral symmetry breaking actions are used for fermions. On the other hand, $\delta R_P^{\mathrm{ampl}}$ comes from the strong IB and e.m. corrections to the leptonic decay rate, computed with the insertion of the QCD-renormalized weak four-fermion operator into the amplitude. We focus now on the calculation of $\delta R_P^{\mathrm{ampl}}$ and postpone the evaluation of $\delta R_P^{\mathrm{ren}}$ to Chap. 5, after the discussion on how to renormalize lattice operators non perturbatively in QCD+QED.

[2]These values differ slightly from those obtained in Ref. [26], since now we include the non-factorizable corrections of order $\mathcal{O}(\alpha_{\mathrm{em}}\alpha_s^n)$ (with $n \geq 1$) to the mass renormalization constant (see the coefficient $\mathcal{Z}_m^{\mathrm{fact}}$ in Eq. (2.51) and in Table 2.1 below). The updated results for Eqs. (8), (10), (14) and (15) of Ref. [26] are reported in Ref. [7] and are given by

$$\epsilon_{\pi^0} = 0.01\,(4)\ , \tag{2.25}$$
$$\epsilon_{K^0} = 0.01\,(2)\ , \tag{2.26}$$
$$\delta M_{D^+} + \delta M_{D^0} = 1.7\,(1.0)\ \mathrm{MeV}\ , \tag{2.27}$$
$$\delta M_{D_s^+} = 2.3\,(4)\ \mathrm{MeV}\ . \tag{2.28}$$

The correction $\delta R_P^{\rm ampl}$, can be written as (see Ref. [6, 7])

$$\begin{aligned}\delta R_P^{\rm ampl} &= \frac{\alpha_{\rm em}}{\pi}\log\left(\frac{M_Z^2}{M_W^2}\right) + 2\,\delta\left[\frac{A_P}{\bar{A}_P}\right] + \delta\Gamma^{(\rm pt)}(\Delta E_\gamma) \\ &= \frac{\alpha_{\rm em}}{\pi}\log\left(\frac{M_Z^2}{M_W^2}\right) + 2\,\frac{\delta A_P}{A_P^{(0)}} - 2\,\frac{\delta M_P}{M_P^{(0)}} + \delta\Gamma^{(\rm pt)}(\Delta E_\gamma)\ ,\end{aligned} \tag{2.34}$$

where

i) the term containing $\log(M_Z^2/M_W^2)$ comes from the short-distance matching between the full theory (the Standard Model) and the effective theory in the W-regularisation (see Eq. (2.7)) [11];

ii) the quantity $\delta\Gamma_P^{(\rm pt)}(\Delta E_\gamma)$ represents the $\mathcal{O}(\alpha_{\rm em})$ correction to the tree-level decay rate for a point-like meson including the contributions of the emissions of both virtual and real photons (see Eq. (2.2)) evaluated using a photon mass for the IR regulation. The cut-off on the final-state photon's energy, ΔE_γ, must be sufficiently small for the point like-approximation to be valid. The expression of $\delta\Gamma_P^{(\rm pt)}(\Delta E_\gamma)$ can be read off from Eq. (51) of Ref. [14] and one has explicitely

$$\begin{aligned}\delta\Gamma^{(\rm pt)}(\Delta E_\gamma) &= \frac{\alpha_{\rm em}}{4\pi}\left(3\log\left(\frac{m_\pi^2}{M_W^2}\right) - 8\log(1-r_\ell^2) - \frac{3r_\ell^4}{(1-r_\ell^2)^2}\log(r_\ell^2) + \right. \\ &\quad - 8\,\frac{1+r_\ell^2}{1-r_\ell^2}\,{\rm Li}_2(1-r_\ell^2) + \frac{13-19\,r_\ell^2}{2\,(1-r_\ell^2)} + \\ &\quad \left. + \frac{6-14\,r_\ell^2-4(1+r_\ell^2)\log(1-r_\ell^2)}{1-r_\ell^2}\,\log(r_\ell^2)\right)\end{aligned} \tag{2.35}$$

where $r_\ell = m_\ell/M_P$;

iii) δA_P is the e.m. and strong IB correction to the decay amplitude $P\to\ell\nu_\ell$ with the subtraction of the corresponding correction evaluated for a point-like meson using the finite lattice volume as the infrared regulator. The subtraction term is added back in $\delta\Gamma_P^{(\rm pt)}(\Delta E_\gamma)$, see Eq. (2.2). We remind that such procedure makes both $\delta\Gamma_P^{(\rm pt)}(\Delta E_\gamma)$ and δA_P infrared finite quantities and independent on the specific infrared regularization;

iv) δM_P encodes the e.m. and strong IB corrections to the mass of the P-meson, $M_P = M_P^{(0)} + \delta M_P$. The correction proportional to $2\,\delta M_P/M_P^{(0)}$ is present because of the relation between the amplitudes $\bar{A}_P$ and $A_P^{(0)}$, namely

$$\bar{A}_P = A_P^{(0)}\left(1 + \frac{\delta M_P}{M_P^{(0)}}\right)\ . \tag{2.36}$$

Since we adopt the qQED approximation, which neglects the effect of the sea-quark electric charges, the calculation of δA_P and δM_P only requires the evaluation of

connected diagrams. In the following we consider twisted-mass fermions, as in the numerical calculation of Ref. [6, 7]. The diagrams to be evaluated are shown in Figs. 2.3-2.7 for the case of $K_{\ell 2}$ decays. As already pointed out, at $\mathcal{O}(\alpha_{\rm em})$ the renormalized operator, defined in the W-renormalization scheme, is inserted in the diagram of Fig. 2.3. As for the diagrams of Figs. 2.4 - 2.7, which are already of order $\mathcal{O}(\alpha_{\rm em})$ and $\mathcal{O}((m_d - m_u)/\Lambda_{\rm QCD})$, it is sufficient to insert the weak current operator renormalized in QCD only.

In Eq. (2.35), $\delta A_P^{\rm ampl}$ and δM_P contain both the e.m. and the strong IB leading-

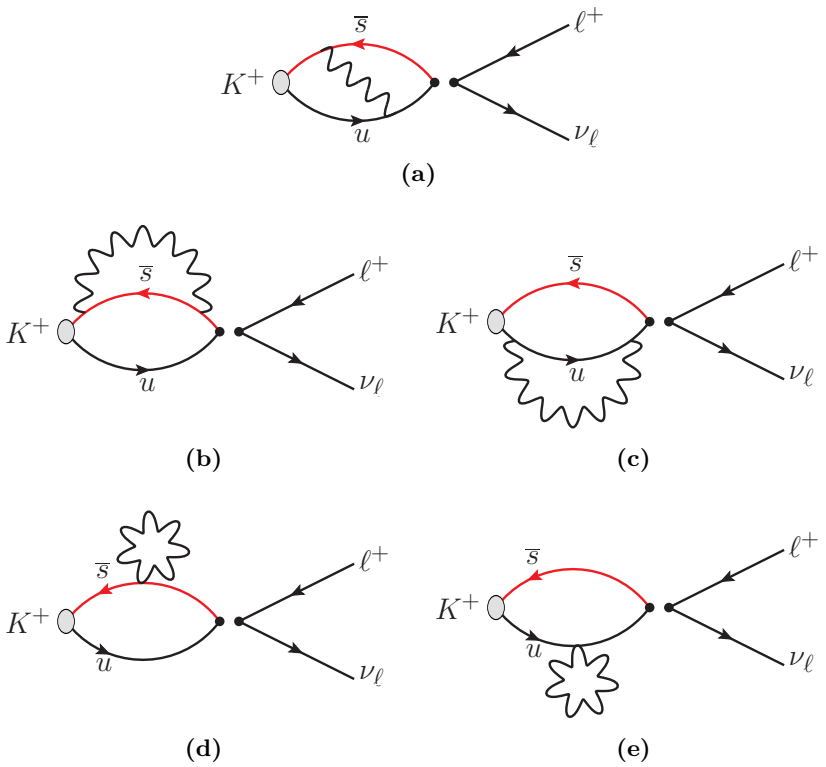

Figure 2.4. Connected diagrams contributing at $\mathcal{O}(\alpha_{\rm em})$ to the $K^+ \to \ell^+\nu_\ell$ decay amplitude, in which the photon is attached to quark lines: (a) *exchange*, (b, c) *self-energy* and (d, e) *tadpole* diagrams. The labels are introduced to identify the individual diagrams when describing their evaluation in the text.

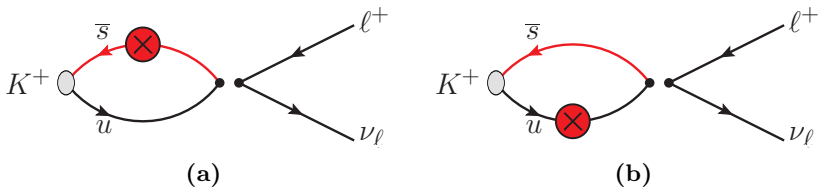

Figure 2.5. Connected diagrams contributing at $\mathcal{O}(\alpha_{\rm em})$ to the $K^+ \to \ell^+\nu_\ell$ decay amplitude corresponding to the insertion of the pseudoscalar density related to the e.m. shift of the critical mass, $\delta m_f^{\rm crit}$, determined in Ref. [26].

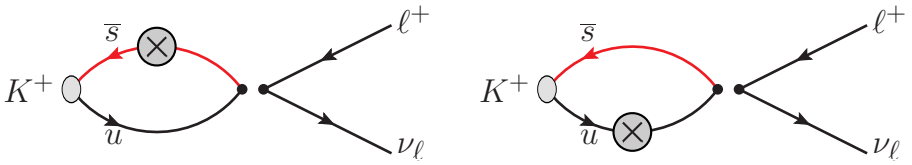

Figure 2.6. Connected diagrams contributing at $\mathcal{O}(\alpha_{\rm em})$ and $\mathcal{O}(m_d - m_u)$ to the $K^+ \to \ell^+\nu_\ell$ decay amplitude related to the insertion of the scalar density (see Ref. [26]).

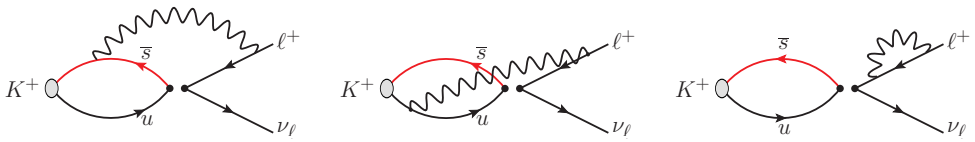

Figure 2.7. Connected diagrams contributing at $\mathcal{O}(\alpha_{\rm em})$ to the $K^+ \to \ell^+\nu_\ell$ decay amplitude corresponding to photon exchanges involving the final-state lepton.

order corrections

$$\delta A_P^{\rm ampl} = \delta A_P^{\rm SIB} + \sum_{i=J,T,P,S} \delta A_P^i + \delta A_P^\ell + \delta A_P^{\ell,\rm self} , \tag{2.37}$$

$$\delta M_P = \delta M_P^{\rm SIB} + \sum_{i=J,T,P,S} \delta M_P^i . \tag{2.38}$$

The quantity $\delta A_P^{\rm SIB}$ ($\delta M_P^{\rm SIB}$) represents the strong IB corrections proportional to $m_d - m_u$ and to the diagram of Fig. 2.6(b), while the other terms are QED corrections coming from the insertions of the e.m. current and tadpole operators, of the pseudoscalar and scalar densities (see Refs. [2, 3]). The term δA_P^J (δM_P^J) is generated by the diagrams of Fig. 2.4(a-c), δA_P^T (δM_P^T) by the diagrams of Fig. 2.4(d-e), δA_P^P (δM_P^P) by the diagrams of Fig. 2.5(a-b) and δA_P^S (δM_P^S) by the diagrams of Fig. 2.6(a-b). The term δA_P^ℓ corresponds to the exchange of a photon between the quarks and the final-state lepton and arises from the diagrams in Fig. 2.7(a-b). The term $\delta A_P^{\ell,\rm self}$ corresponds to the contribution to the amplitude from the lepton's wave function renormalization and arises from the self-energy diagram of Fig. 2.7(c). Such correction can be in principle computed in perturbation theory, since the hadronic amplitude factorizes and coincides with its tree-level value. Therefore, the contribution of $\delta A_P^{\ell,\rm self}$ cancels out in the difference $\Gamma_0(L) - \Gamma_0^{\rm pt}(L)$ in Eq. (2.2) and could be omitted in the calculation (this cancellation happens in any regularization scheme when using the same value of the decay constant $f_P^{(0)}$). Such cancellation will be discussed later in Sections 4.3 and 5.2. The different insertions of the scalar density encode the strong IB effects together with the counter terms necessary to fix the masses of the quarks. We stress that the insertion of the pseudoscalar density (diagrams in Fig. 2.5) is peculiar to twisted mass quarks and would be absent in standard Wilson (improved) formulations of QCD.

In the following subsections we discuss the calculation of all the diagrams contributing to $\delta A_P^{\rm ampl}$.

2.4.1 Quark-quark photon exchange diagrams and scalar and pseudoscalar insertions

In the calculation of δA_P^i, with $i = J, T, P, S$, the contribution of the leptonic part of the amplitude, namely $[\bar{u}(p_{\nu_\ell})\gamma_\nu(1-\gamma^5)v(p_\ell)]$ is factorized. Therefore, the corrections δA_P^i can be evaluated through the study of purely hadronic lattice correlators.

Let us consider first the evaluation of the tree-level amplitude. Following Ref. [3], the tree-level correlator can be defined as

$$C_P^{(0)}(t) \equiv \sum_{\vec{x}} \langle 0|T\left\{J_W^\rho(0)\phi_P^\dagger(\vec{x},-t)\right\}|0\rangle \frac{p_P^\rho}{M_P} \ . \tag{2.39}$$

Here $J_W^\rho(x)$ is the local version of the hadronic $(V-A)$ weak current renormalized in QCD only[3]

$$J_W^\rho(x) = \overline{q}_{f_2}(x)\gamma^\rho\left[\mathcal{Z}_V^{\rm QCD} - \mathcal{Z}_A^{\rm QCD}\gamma^5\right] q_{f_1}(x) \ , \tag{2.40}$$

and $\phi_P^\dagger(\vec{x},-t) = i\,\overline{q}_{f_1}(\vec{x},-t)\gamma_5 q_{f_2}(\vec{x},-t)$ is the interpolating field for a P-meson composed by two valence quarks f_1 and f_2 with charges $e_1 e$ and $e_2 e$. The Wilson r-parameters r_{f_1} and r_{f_2} are always chosen to be opposite $r_{f_1} = -r_{f_2}$. We will denote in the following renormalization constants in the *physical* basis as "$\mathcal{Z}$", to distinguish them from the RCs "Z" defined (and computed in Chap. 4) for operators in the *twisted* basis. At large time distance $t \gg a$ and $(T-t) \gg a$, i.e. when t and $T-t$ are sufficiently large to suppress the contributions from heavier states and from the backward propagating P meson, one has

$$C_P^{(0)}(t) \to \frac{G_P^{(0)} A_P^{(0)}}{2\,M_P^{(0)}}\left(\mathrm{e}^{-M_P^{(0)}t} - \mathrm{e}^{-M_P^{(0)}(T-t)}\right) \ , \tag{2.41}$$

where $A_P^{(0)}$ is the QCD renormalized axial amplitude defined in Eq. (2.1) and $G_P^{(0)} \equiv \langle 0|\,\phi_P(0)\,|P^{(0)}\rangle$ is the coupling of the interpolating field of the P meson with its ground state in isosymmetric QCD. In Eq. (2.41), the quantity $A_P^{(0)}$ corresponds to the matrix element of the local axial current on the lattice and therefore it needs to be renormalized, namely

$$\delta_{\mu,0}\,A_P^{(0)} \equiv \mathcal{Z}_A^{\rm QCD}\ \langle 0|\,\bar{q}_2\gamma_\mu\gamma_5 q_1\,|P^{(0)}\rangle \ . \tag{2.42}$$

The same renormalization constant $\mathcal{Z}_A^{\rm QCD}$ should be applied also to the e.m. correction δA_P.

The IB corrections δA_P^i and δM_P^i $(i = J, T, P, S)$ can be extracted from the

[3] In our maximally twisted-mass setup, in which the Wilson r-parameters r_{f_1} and r_{f_2} are always chosen to be opposite $r_{f_1} = -r_{f_2}$, the vector (axial) weak current in the *physical basis* renormalizes multiplicatively with the RC Z_A (Z_V) of the axial (vector) current for Wilson-like fermions, i.e. $\mathcal{Z}_V = Z_A$ and $\mathcal{Z}_A = Z_V$ (see Sec. 5.1).

following correlators:

$$\frac{\delta C_P^J(t)}{4\pi} = \frac{1}{2}\,\alpha_{\rm em} \sum_{\vec{x},y_1,y_2} \langle 0|T\left\{J_W^\rho(0)\; j_\mu^{\rm em}(y_1) j_\nu^{\rm em}(y_2)\; \phi_P^\dagger(\vec{x},-t)\right\}|0\rangle \Delta_{\mu\nu}^{\rm em}(y_1,y_2)\frac{p_P^\rho}{M_P}\;, \tag{2.43}$$

$$\frac{\delta C_P^T(t)}{4\pi} = \alpha_{\rm em} \sum_{\vec{x},y} \langle 0|T\left\{J_W^\rho(0)\; T_\mu^{\rm em}(y)\; \phi_P^\dagger(\vec{x},-t)\right\}|0\rangle \Delta_{\mu\mu}^{\rm em}(y,y)\frac{p_P^\rho}{M_P}\;, \tag{2.44}$$

$$\frac{\delta C_P^P(t)}{4\pi} = \alpha_{\rm em} \sum_{f=f_1,f_2} \delta m_f^{\rm crit} \cdot \sum_{\vec{x},y} \langle 0|T\left\{J_W^\rho(0)\; i\overline{q}_f(y)\gamma_5 q_f(y)\; \phi_P^\dagger(\vec{x},-t)\right\}|0\rangle \frac{p_P^\rho}{M_P}\;, \tag{2.45}$$

$$\frac{\delta C_P^S(t)}{4\pi} = -\alpha_{\rm em} \sum_{f=f_1,f_2} m_f \frac{\Delta\mathcal{Z}_m^f}{\mathcal{Z}_m^{\rm QCD}} \cdot \sum_{\vec{x},y} \langle 0|T\left\{J_W^\rho(0)\;\left[\overline{q}_f(y)q_f(y)\right]\;\phi_P^\dagger(\vec{x},-t)\right\}|0\rangle \frac{p_P^\rho}{M_P}\;, \tag{2.46}$$

where $\Delta_{\mu\nu}^{\rm em}(y_1,y_2)$ is the photon propagator, $J_W^\rho(x)$ is the $(V-A)$ weak current of Eq. (2.40), $j_\mu^{\rm em}$ is the (lattice) conserved e.m. current and $T_\mu^{\rm em}$ is the tadpole operator[4]. In Eq. (2.46) $\mathcal{Z}_m^{\rm QCD}$ is the mass RC in pure QCD, which in the maximally twisted-mass setup is given by $\mathcal{Z}_m^{\rm QCD} = 1/Z_P^{\rm QCD}$, where $Z_P^{\rm QCD}$ is the QCD RC of the pseudoscalar density determined in Ref. [56] and in Chap. 4 of this thesis[5]. The quantity $\Delta\mathcal{Z}_m^f$ is the e.m. correction to the mass RC, which can be written in QCD+QED as

$$\mathcal{Z}_m^{\rm QCD+QED} = \left(1 + \frac{\alpha_{\rm em}}{4\pi}\Delta\mathcal{Z}_m^f\right)\mathcal{Z}_m^{\rm QCD}\;. \tag{2.47}$$

Since $\mathcal{Z}_m = 1/Z_P$, it follows that the correction $\Delta\mathcal{Z}_m^f$ is related to the e.m. correction of the pseudoscalar current RC as

$$\Delta\mathcal{Z}_m^f = -e_f^2\,\Delta Z_P\;, \tag{2.48}$$

where e_f is the fractional charge of the quark q_f and ΔZ_P is the e.m. correction to the RC of the pseudoscalar current (evaluated with equal unitary charges). As it will be discussed in great detail in the next chapter, the e.m. correction ΔZ_P (or equivalently ΔZ_m^f) can be decomposed as

$$\Delta Z_P = \Delta Z_P^{\rm QED} + \eta_P\;, \tag{2.49}$$

where $\Delta Z_P^{\rm QED}$ is the pure QED contribution at leading order in $\alpha_{\rm em}$ and η_P takes into account all the non-factorizable corrections of order $\mathcal{O}(\alpha_{\rm em}\alpha_{\rm s}^n)$ with $n \geq 1$. The quantity $\Delta Z_P^{\rm QED}$ is given in the $\overline{\rm MS}$ scheme at a renormalization scale μ by [57, 58]

$$\Delta Z_P^{\rm QED}(\overline{\rm MS},\mu) = 6\log(a\mu) - 22.5954\;. \tag{2.50}$$

[4]The use of the conserved e.m. current guarantees the absence of additional contact terms in the product $j_\mu^{\rm em}(y_1)j_\nu^{\rm em}(y_2)$. For twisted mass fermions at maximal twist in the physical basis, the conserved e.m. current and the tadpole operator read

$$\begin{aligned} j_\mu^{\rm em}(y) &= \sum_f \frac{e_f}{2}\left[\bar{q}_f(y)(\gamma_\mu - i\tau^3\gamma_5)U_\mu(y)q_f(y+a\hat{\mu}) + \bar{q}_f(y+a\hat{\mu})(\gamma_\mu + i\tau^3\gamma_5)U_\mu^\dagger(y)q_f(y)\right] \\ T_\mu^{\rm em}(y) &= \sum_f \frac{e_f^2}{2}\left[\bar{q}_f(y)(\gamma_\mu - i\tau^3\gamma_5)U_\mu(y)q_f(y+a\hat{\mu}) - \bar{q}_f(y+a\hat{\mu})(\gamma_\mu + i\tau^3\gamma_5)U_\mu^\dagger(y)q_f(y)\right]\;. \end{aligned}$$

[5]Notice that the pseudoscalar current in the physical basis renormalizes multiplicatively with the RC Z_P of the pseudoscalar current for Wilson-like fermions, i.e. $\mathcal{Z}_P = Z_P$.

On the other hand, the quantity η_P, which will be introduced and discussed in Chap. 3, is computed non-perturbatively on the lattice in Chap. 4. It encodes the QCD corrections to the "naive factorisation" approximation $\Delta\mathcal{Z}_m^f = \Delta\mathcal{Z}_m^{\mathrm{QED}\,f}$ introduced in Refs. [4, 26]. In Ref. [7] the e.m. correction $\Delta\mathcal{Z}_m^f$ is expressed in the alternative form

$$\Delta\mathcal{Z}_m^f = \Delta\mathcal{Z}_m^{f\,\mathrm{QED}} \cdot \mathcal{Z}_m^{\mathrm{fact}} \ , \tag{2.51}$$

where $\mathcal{Z}_m^{\mathrm{fact}}$ is a different way to quantify the violation of the naive factorization approximation, corresponding to $\mathcal{Z}_m^{\mathrm{fact}} = 1$. The values of the correction $\mathcal{Z}_m^{\mathrm{fact}}$ to $\Delta\mathcal{Z}_m^f(\overline{\mathrm{MS}}, 2\ \mathrm{GeV})$ for the three inverse lattice spacings β used in the calculation are reported in Table 2.1. The values are obtained from the results of η_P, whose calculation is carried out in the RI'-MOM scheme in Chap. 4 (see Table 4.3). The two methods M1 and M2 correspond to different treatments of the $\mathcal{O}(a^2\mu^2)$ discretization effects and are described in Sec. 4.2. The results in Table 2.1 show that the non-factorisable corrections to the mass RC $\Delta\mathcal{Z}_m^f$ are significant, being of $\mathcal{O}$(40-60%).

Table 2.1. Values of the coefficient Z_m^{fact} corresponding to the non-factorisable e.m. correction to the mass RC in the $\overline{\mathrm{MS}}(2\,\mathrm{GeV})$ (see Eq. (2.51)), calculated for the three values of the inverse coupling β adopted in this work. These values are obtained from the results of η_P computed in the RI'-MOM scheme using the methods M1 and M2 and reported in Table 4.3 (at the scale $\mu = 1/a$).

β	$\mathcal{Z}_m^{\mathrm{fact}}(\overline{\mathrm{MS}}, 2\ \mathrm{GeV})$	
	M1	M2
1.90	1.629 (41)	1.637 (14)
1.95	1.514 (33)	1.585 (12)
2.10	1.459 (17)	1.462 (6)

In analogy with Eqs. (2.43) - (2.46), the terms $[\delta A_P]^{\mathrm{SIB}}$ and $[\delta M_P]^{\mathrm{SIB}}$ can be extracted from the correlator

$$\delta C_P^{\mathrm{SIB}}(t) = -\sum_{f=f_1,f_2} \frac{\widehat{m}_f - m_f}{\mathcal{Z}_m^{\mathrm{QCD}}} \cdot \sum_{\vec{x},y} \langle 0|T\left\{ J_W^\rho(0)\ \ [\overline{q}_f(y)q_f(y)]\ \ \phi_P^\dagger(\vec{x},-t)\right\}|0\rangle \frac{p_P^\rho}{M_P} \ , \tag{2.52}$$

where, following the notation of Ref. [26], we indicate with $\widehat{m}_f$ the renomalized mass of the quark with flavour f in the full theory and with and m_f the one renormalized in isosymmetric QCD only. We stress again that the separation between QCD and QED corrections is prescription dependent and in this work we adopt the GRS prescription of Refs. [3, 6, 26], where

$$\begin{aligned} \widehat{m}_u(\overline{\mathrm{MS}}, 2\,\mathrm{GeV}) + \widehat{m}_d(\overline{\mathrm{MS}}, 2\,\mathrm{GeV}) &= 2\,\widehat{m}_{ud}(\overline{\mathrm{MS}}, 2\,\mathrm{GeV}) = 2\,m_{ud}(\overline{\mathrm{MS}}, 2\,\mathrm{GeV})\,, \\ \widehat{m}_s(\overline{\mathrm{MS}}, 2\,\mathrm{GeV}) &= m_s(\overline{\mathrm{MS}}, 2\,\mathrm{GeV})\,, \\ \widehat{m}_c(\overline{\mathrm{MS}}, 2\,\mathrm{GeV}) &= m_c(\overline{\mathrm{MS}}, 2\,\mathrm{GeV})\ . \end{aligned} \tag{2.53}$$

Thus, in Eq. (2.52), the only relevant quark mass difference is $\widehat{m}_d - m_{ud} = -(\widehat{m}_u - m_{ud})$, whose value in the $(\overline{\mathrm{MS}}, 2\,\mathrm{GeV})$ scheme was found to be equal to

1.19 (9) MeV [26] using as inputs the experimental values of the charged and neutral kaon masses.

Given the correction $\delta C_P^i(t)$, its large time behaviour (i.e. when $t \gg a$ and $(T-t) \gg a$) will be

$$\begin{aligned} \delta C_P^i(t) \;\to\; & \delta\left[\frac{G_P^i A_P^i}{2M_P^i}\right]\left(\mathrm{e}^{-M_P^{(0)}t} - \mathrm{e}^{-M_P^{(0)}(T-t)}\right) + \\ & - \frac{G_P^{(0)} A_P^{(0)}}{2\,M_P^{(0)}}\,\delta M_P^i\,\frac{T}{2}\left(\mathrm{e}^{-M_P^{(0)}t} - \mathrm{e}^{-M_P^{(0)}(T-t)}\right) + \\ & + \frac{G_P^{(0)} A_P^{(0)}}{2\,M_P^{(0)}}\,\delta M_P^i\left(\frac{T}{2}-t\right)\left(\mathrm{e}^{-M_P^{(0)}t} - \mathrm{e}^{-M_P^{(0)}(T-t)}\right)\,. \end{aligned} \tag{2.54}$$

Therefore, by combining Eqs. (2.41) and (2.55) one obtains at large time distances t we obtain ($i = J, T, P, S, \mathrm{SIB}$)

$$\frac{\delta C_P^i(t)}{C_P^{(0)}(t)} \;\to\; \frac{\delta[G_P^i A_P^i]}{G_P^{(0)} A_P^{(0)}} + \frac{\delta M_P^i}{M_P^{(0)}} f(t)\;, \tag{2.55}$$

with

$$f(t) = \left[M_P^{(0)}\left(\frac{T}{2}-t\right)\frac{\mathrm{e}^{-M_P^{(0)}t} + \mathrm{e}^{-M_P^{(0)}(T-t)}}{\mathrm{e}^{-M_P^{(0)}t} - \mathrm{e}^{-M_P^{(0)}(T-t)}} - 1 - M_P^{(0)}\frac{T}{2}\right]\,. \tag{2.56}$$

The function $f(t)$, which is related to the e.m. and strong IB corrections of the meson mass, is almost linear in t. Thus, the correction to the P-meson mass can be extracted from the slope of the ratio $\delta C_P^i(t)/C_P^{(0)}(t)$ and the quantity $\delta[G_P^i A_P^i] = \delta G_P^i A_P^{(0)} + G_P^{(0)}\delta A_P^i$. As explained in Ref. [14], in order to obtain the quantity δA_P^i the correction δG_P^i is separately determined by evaluating a correlator similar to those of Eqs. (2.43)-(2.46), in which the weak operator $J_W^\rho p_P^\rho / M_P$ is replaced by the P-meson interpolating field ϕ_P.

For illustration, in Fig. 2.8 we report the ratios $\delta C_P^i/C_P^{(0)}$ for the charged kaon ($P = K$) obtained in Ref. [7] at a fixed value of lattice spacing, volume and sea quark mass. The top panel contains the ratio $\delta C_K^{\mathrm{SIB}}(t)/C_K^{(0)}(t)$, the ratio $\delta C_K^J(t)/C_K^{(0)}(t)$ is shown in the middle panel and the ratios $\delta C_K^T(t)/C_K^{(0)}(t)$ and $\delta C_K^P(t)/C_K^{(0)}(t)$ are presented in the bottom panel. We observe that the contributions $\delta C_K^T(t)/C_P^{(0)}(t)$ and $\delta C_K^P(t)/C_P^{(0)}(t)$ are separately large, but strongly correlated, since the tadpole insertion dominates the values of the e.m. shift of the critical mass $\delta m_f^{\mathrm{crit}}$ (see Ref. [26]). In the chiral limit they would cancel, but at finite masses the sum is small and linear in t. Because of the correlations, it can nevertheless be determined quite precisely. Moreover, the time dependence of the ratio $\delta C_K^J(t)/C_K^{(0)}(t)$ is almost linear in the time interval where the ground state is dominant.

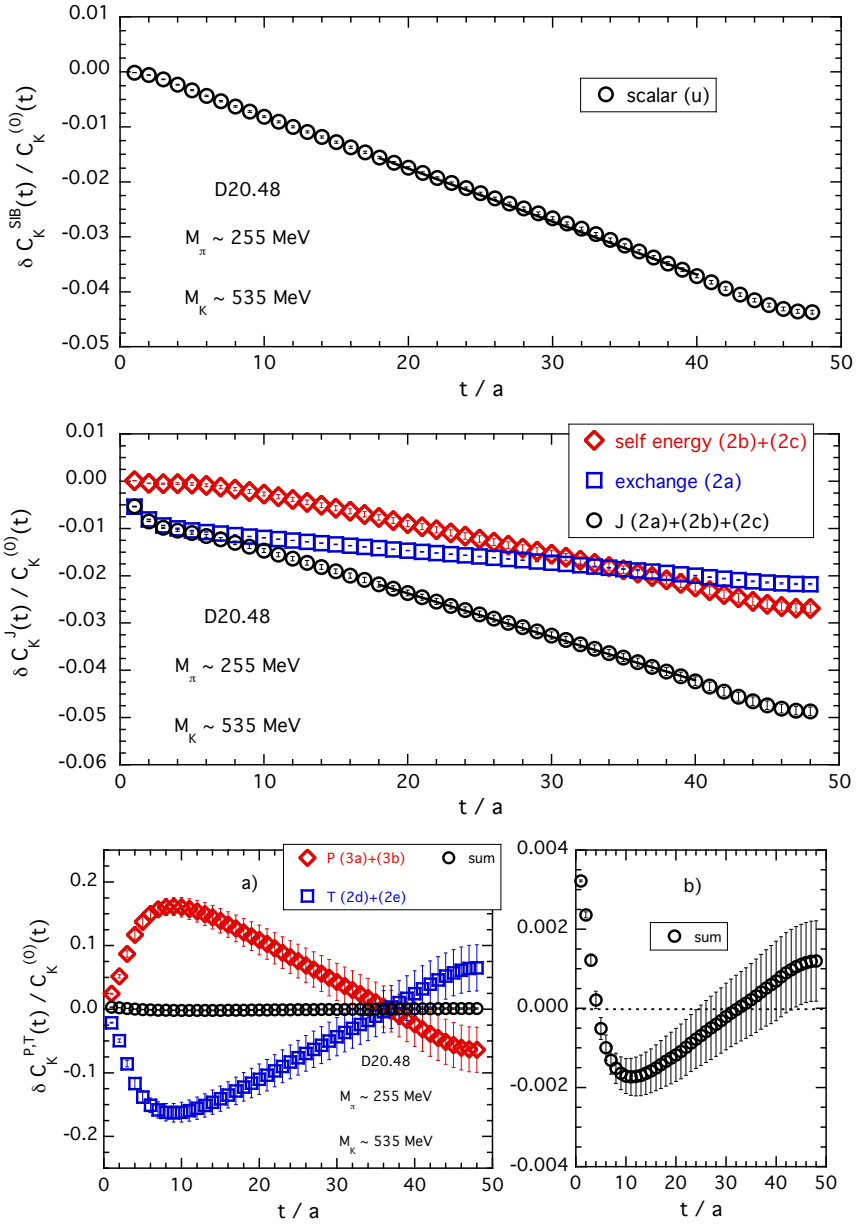

Figure 2.8. TOP PANEL: The strong IB correction $\delta C_K^{\rm SIB}(t)/C_K^{(0)}(t)$ for the charged kaon obtained on the ensemble D20.48 (see Appendix A of Ref. [7]). The solid line is the "linear" fit (2.55) applied in the time interval where the ground-state is dominant. MIDDLE PANEL: contributions of the exchange (2.4a) and self-energy (2.4b)+(2.4c) diagrams. The circles represent the sum (2.4a)+(2.4b)+(2.4c), i.e. the ratio $\delta C_K^J(t)/C_K^{(0)}(t)$. BOTTOM PANEL: contributions of the tadpole operator $\delta C_K^T(t)/C_K^{(0)}(t)$, i.e. diagrams (2.4d)+(2.4e), and of the e.m. shift of the critical mass $\delta C_K^P(t)/C_K^{(0)}(t)$, i.e. diagrams (2.5a)+(2.5b). The sum $\delta[C_K^T(t)+C_K^P(t)]/C_K^{(0)}(t)$, shown by the circles, is non vanishing and it is determined quite precisely (see the right-hand plot where it is presented on an expanded scale). Errors are statistical only.

2.4.2 Crossed diagrams and lepton self-energy

The evaluation of the diagrams 2.7(a) - (b), corresponding to the term δA_P^ℓ in Eq. (2.37), can be obtained by studying the correlator [14]

$$\begin{aligned}\delta C_P^\ell(t) &= -4\pi\alpha_{\rm em}\sum_{\vec{x},x_1,x_2}\langle 0|\,T\left\{J_W^\rho(0)j_\mu^{\rm em}(x_1)\phi_P^\dagger(\vec{x},-t)\right\}|0\rangle\Delta_{\mu\nu}^{\rm em}(x_1,x_2)e^{E_\ell t_2-i\vec{p}_\ell\cdot\vec{x}_2}\\ &\quad\cdot\,\overline{u}(p_\nu)\gamma_\rho(1-\gamma_5)S^\ell(0,x_2)\gamma_\nu v(p_\ell)\left[\overline{v}(p_\ell)\gamma_\sigma(1-\gamma_5)u(p_\nu)\frac{p_P^\sigma}{M_P}\right]\,, \qquad (2.57)\end{aligned}$$

where $S^\ell(0,x_2)$ stands for the free twisted-mass propagator of the charged lepton. In the numerical analysis done in Ref. [7], it has been found convenient to saturate the Dirac indices by inserting on the r.h.s. of Eq. (2.57) the factor $[\overline{v}(p_\ell)\gamma_\sigma(1-\gamma_5)u(p_\nu)]$, which represents the lowest order "conjugate" leptonic $(V-A)$ amplitude, and to sum over the lepton polarizations. In this way it is possible to study the time behaviour of a single function $\delta C_P^\ell(t)$.

The corresponding correlator at lowest order $\mathcal{O}(\alpha_{\rm em}^0)$ is

$$C_P^{\ell(0)}(t)=\sum_{\vec{x}}\langle 0|\,T\left\{J_W^\rho(0)\phi_P^\dagger(\vec{x},-t)\right\}|0\rangle\,\overline{u}(p_\nu)\gamma_\rho(1-\gamma_5)v(p_\ell)\left[\overline{v}(p_\ell)\gamma_\sigma(1-\gamma_5)u(p_\nu)\frac{p_P^\sigma}{M_P}\right]. \qquad (2.58)$$

In Eqs. (2.57) and (2.58) the contraction between the weak hadronic current $J_W^\rho(0)$ [see Eq. (2.40)] and its leptonic $(V-A)$ counterpart gives rise to two terms corresponding to the product of either the temporal or spatial components of these two weak currents, which are odd and even under time reversal, respectively. Thus, on a lattice with finite time extension T, for $t\gg a$ and $(T-t)\gg a$ one has

$$\delta C_P^\ell(t)\;\to\;\frac{G_P^{(0)}}{2\,M_P^{(0)}}\sum_{\sigma=0}^{4}\delta A_P^{\ell,\sigma}\;X_P^{\ell,\sigma}\;\left[e^{-M_P^{(0)}t}+s_\nu e^{-M_P^{(0)}(T-t)}\right]\,, \qquad (2.59)$$

where $s_0=-1$, $s_{1,2,3}=1$ and

$$X_P^{\ell,\sigma}={\rm Tr}\left[\gamma_\sigma(1-\gamma_5)\ell\overline{\ell}\gamma_0(1-\gamma_5)\nu\overline{\nu}\right] \qquad (2.60)$$

is the relevant leptonic trace evaluated on the lattice using for the charged lepton the free twisted-mass propagator and for the neutrino the free Wilson propagator in the P-meson rest frame, $p_P=(M_P,\vec{0})$.

Similarly, for the lowest-order correlator one has

$$C_P^{\ell(0)}(t)\;\to\;\frac{G_P^{(0)}A_P^{(0)}}{2\,M_P^{(0)}}\;X_P^{\ell,0}\;\left[{\rm e}^{-M_P^{(0)}t}-{\rm e}^{-M_P^{(0)}(T-t)}\right]\,, \qquad (2.61)$$

where $A_P^{(0)}$ is the axial amplitude evaluated on the lattice in isosymmetric QCD in the P-meson rest frame, to be renormalized with the QCD axial RC $\mathcal{Z}_A$ in the physical basis (see Eq. (2.42)).

The effect of the different signs of the backward-propagating signal in Eq. (2.59) can be removed by introducing the following new correlators:

$$\begin{aligned}\delta\overline{C}_P^\ell(t) &\equiv \frac{1}{2}\left\{\delta C_P^\ell(t)+\frac{\delta C_P^\ell(t-1)-\delta C_P^\ell(t+1)}{{\rm e}^{M_P^{(0)}}-{\rm e}^{-M_P^{(0)}}}\right\}\;\to\;\frac{G_P^{(0)}}{2M_P^{(0)}}\,\delta A_P^\ell\,X_P^{\ell,0}\,{\rm e}^{-M_P^{(0)}t}\,,\\ \overline{C}_P^{\ell(0)}(t) &\equiv \frac{1}{2}\left\{C_P^{\ell(0)}(t)+\frac{C_P^{\ell(0)}(t-1)-C_P^{\ell(0)}(t+1)}{{\rm e}^{M_P^{(0)}}-{\rm e}^{-M_P^{(0)}}}\right\}\;\to\;\frac{G_P^{(0)}}{2M_P^{(0)}}A_P^{(0)}X_P^{\ell,0}\,{\rm e}^{-M_P^{(0)}t}\,, \qquad (2.62)\end{aligned}$$

where

$$\delta A_P^\ell = \frac{1}{X_P^{\ell,0}} \sum_{\sigma=0}^{4} \delta A_P^{\ell,\sigma} \; X_P^{\ell,\sigma} \; . \tag{2.63}$$

Thus, the quantity $\delta A_P^\ell / A_P^{(0)}$ can be extracted from the plateau of the ratio $\delta \overline{C}_P^\ell(t) / \overline{C}_P^{\ell(0)}(t)$ at large time separations $(t \gg a, (T-t) \gg a)$,

$$\frac{\delta \overline{C}_P^\ell(t)}{\overline{C}_P^{\ell(0)}(t)} \; \to \; \frac{\delta A_P^\ell}{A_P^{(0)}} \; . \tag{2.64}$$

Note that the diagrams in Fig. 2.7(a)-(b) do not contribute to the electromagnetic corrections to the masses of the mesons and therefore the ratio (2.64) has no slope in t in contrast to the ratios (2.55).

In terms of the lattice momenta $a\widetilde{p}_\ell$ and $a\overline{p}_\ell$, defined as [7]

$$a\widetilde{p}_\ell = \sqrt{\sum_{k=1,2,3} \sin^2\left(a p_{\ell k}\right)} \; , \qquad a\overline{p}_\ell = 2 \sqrt{\sum_{k=1,2,3} \sin^2\left(\frac{a p_{\ell k}}{2}\right)} \; , \tag{2.65}$$

the energy-momentum dispersion relations for the charged lepton and the neutrino in the P-meson rest frame are given by

$$a\widetilde{E}_\ell = 2 \, \mathrm{arcsinh}\left[\frac{1}{2}\sqrt{\frac{a^2 m_\ell^2 + a^2 \widetilde{p}_\ell^{\,2} + a^4 \overline{p}_\ell^{\,4}/4}{1 + a^2 \overline{p}_\ell^{\,2}/2}}\right] \; , \quad a\widetilde{E}_\nu = \mathrm{arcsinh}(a\widetilde{p}_\ell) \, . \tag{2.66}$$

The 3-momentum of the final-state lepton $\vec{p}_\ell = -\vec{p}_\nu$ is chosen to satisfy the equation

$$\widetilde{E}_\ell + \widetilde{E}_\nu = M_P^{(0)} \, . \tag{2.67}$$

for any given simulated P-meson mass $M_P^{(0)}$. By using the above definitions, the leptonic trace $X_P^{\ell,0}$ can be written as

$$X_P^{\ell,0} = \mathrm{Tr}\left[\gamma_0(1-\gamma_5)\ell\overline{\ell}\gamma_0(1-\gamma_5)\nu\overline{\nu}\right] = 8 a\widetilde{p}_\ell \left[\sinh(a\widetilde{E}_\ell) - a\widetilde{p}_\ell\right] \; . \tag{2.68}$$

The quality of the signal for the ratio $\delta \overline{C}_P^\mu(t) / \overline{C}_P^{\mu(0)}(t)$ is illustrated in Fig. 2.9 for charged kaon and pion decays into muons for the case of two different ensembles.

Finally, the calculation of the correction $A_P^{\ell,\mathrm{self}}$ due to the diagram 2.7(c) is straightforward, since it can be obtained by simply multiplying the lowest order amplitude, $A_P^{(0)}$, renormalized in pure QCD, by the one-loop lepton self-energy evaluated on the lattice.

The evaluation of the correction $\delta R_P^{\mathrm{ampl}}$ is completely determined from the study of the correlators described in this Section. The additional correction $\delta R_P^{\mathrm{ren}}$ to the leptonic decay rate, instead, requires the determination of the operator $O_1^{\mathrm{RI'}}(\mu)$ in Eq. (2.13) renormalized non-pertubatively on the lattice in QCD+QED in the RI'-MOM scheme. Therefore, in the next Chapter, we describe a novel formalism to determine renormalization constants of lattice operators with the inclusion of QED corrections at $\mathcal{O}(\alpha_{\mathrm{em}})$. The calculation of $\delta R_P^{\mathrm{ren}}$, and hence of δR_P, is then addressed in Chap. 5.

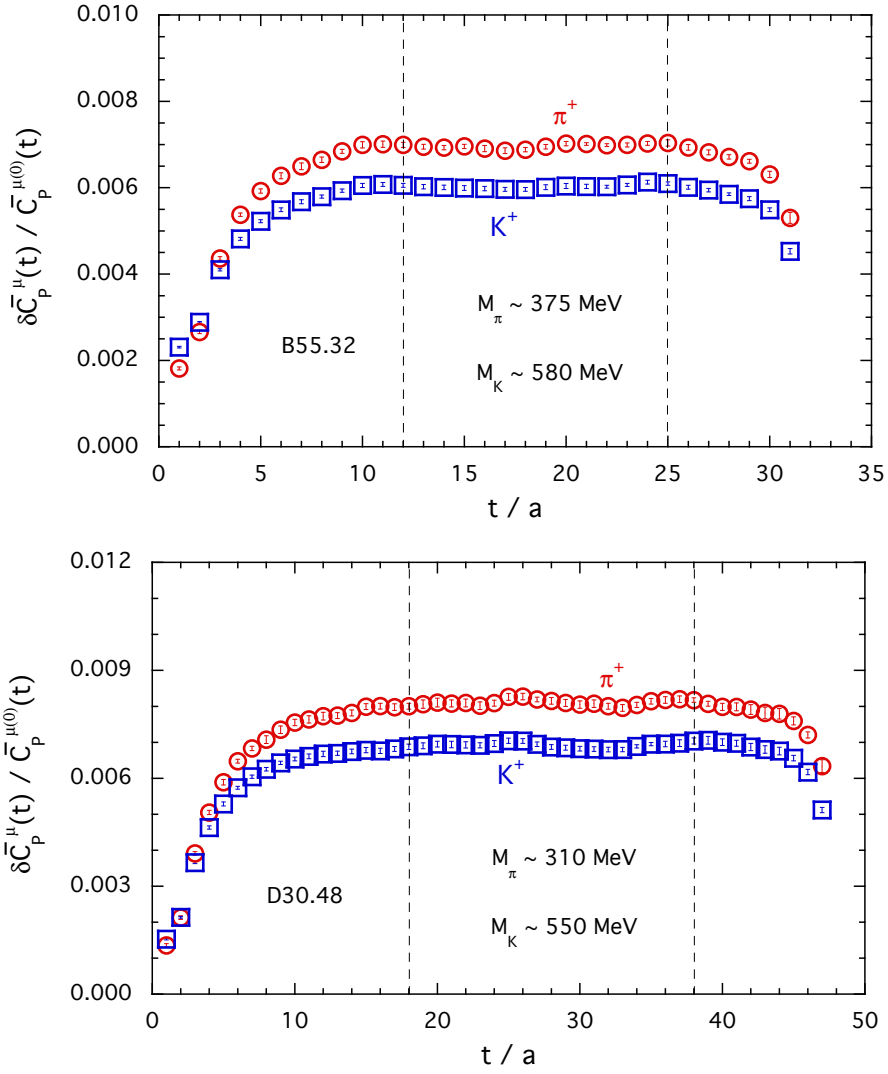

Figure 2.9. Results for the ratio $\delta\overline{C}_P^{\mu}(t)/\overline{C}_P^{\mu(0)}(t)$, given by Eq. (2.64), for $K_{\mu 2}$ and $\pi_{\mu 2}$ decays obtained from the gauge ensembles B55.32 (top panel) and D30.48 (bottom panel) [7]. The vertical dashed lines indicate the time region used for the extraction of the ratio $\delta A_P^{\mu}/A_P^{(0)}$. Errors are statistical only.

3 | Non-perturbative renormalization in QCD+QED

In this Chapter, we present a new strategy to renormalise lattice operators in QCD+QED fully including the non perturbative dynamics of QCD, and QED at $\mathcal{O}(\alpha_{\rm em})$. We show how to keep systematically into account all contributions not separable between the two interactions, thus overcoming the factorization approximation in which the mixed effects are neglected. A numerical analysis in the electro-quenched approximation is carried out for quark bilinear operators and for the case of the matrix elements relevant for $K_{\ell 2}$ process and will be presented in Chap. 4. We will show that the effects of adding the mixed QCD+QED effects in the renormalization constants (RCs) are estimated to amount to up 8% of the overall QED corrections to the process. The procedure is presented here for the RI'-MOM scheme, but with appropriate changes can be applied to other schemes such as RI-SMOM.

When e.m. corrections at first order in $\alpha_{\rm em}$ are added to QCD, RCs can be written in the form

$$Z = \left(1 + \frac{\alpha_{\rm em}}{4\pi}\,\Delta Z\right) Z^{\rm QCD}\ , \tag{3.1}$$

where $Z^{\rm QCD}$ is the RC computed in pure QCD ($\alpha_{\rm em} = 0$) and ΔZ represents the correction introduced by e.m. interactions. As it is well known, perturbation theory works poorly on the lattice [59], so it is customary to recur to non-pertubative schemes to compute the renormalization constants. For pure QCD this procedure is long-time known, and several schemes are available, the most popular relying on variations of RI-MOM [54], such as RI-SMOM [60]. On the other hand, the calculation of ΔZ has been so far performed in the so-called *factorization approximation*, in which the correction to the RC is simply evaluated as $\Delta Z \equiv \Delta Z^{\rm QED}$, namely the correction of $\mathcal{O}(\alpha_{\rm em})$ to the RC computed in pure QED. This quantity can be easily obtained in perturbation theory through the evaluation of one-loop diagrams, see for example Refs. [57, 58] for what concerns the renormalization constants of bilinear operators. Clearly the renormalization constants so computed take into account QCD and QED renormalization separately, which at perturbative level amounts to considering only the one-particle reducible diagrams like the one presented in Fig. 3.1(a), in which gluon and photon loops can be separated by cutting a single fermionic line. This approximation introduces systematic effects due to the missed non-factorizable contributions to the RCs. In order to overcome the factorization approximation,

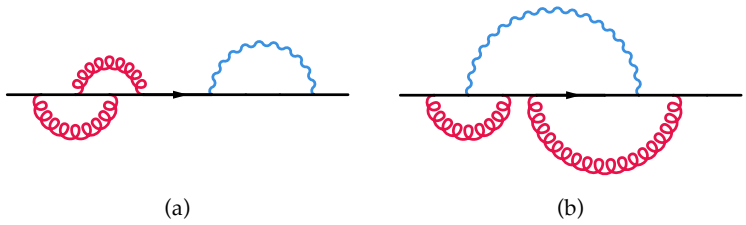

Figure 3.1. Examples of (a) *factorizable* and (b) *non-factorizable* diagrams in perturbative QCD+QED at $\mathcal{O}(\alpha_s^2\alpha_{em})$.

the renormalization condition must be imposed considering simultaneously both interactions. In perturbation theory one would proceed by including the diagrams like the one in Fig. 3.1(b). The scope of this Chapter is to present extensively a novel framework for the non-perturbative calculation of RCs with the inclusion of e.m. corrections at first order in α_{em}, consistent with the RM123 approach used for the calculation of the matrix element corrections (see Chap. 1). Such new framework has been used for the first time in Ref. [7], where the method has been briefly introduced in Sec. IV and in Appendix C. The presentation will recur to RI'-MOM scheme for concreteness, but can be applied to other schemes (such as RI-SMOM) with appropriate modifications. In the phenomenological papers [4, 26] the deviation from the factorization approximation has been included in the systematic error, by defining a correction to renormalization constants as

$$\Delta Z \equiv Z^{\text{fact}}\,\Delta Z^{\text{QED}} \tag{3.2}$$

and introducing an estimate for the factorization-violation coefficient Z^{fact}. The factorization approximation corresponds to $Z^{\text{fact}} = 1$ and large deviations from such a value amount to large non-factorizable effects of QCD+QED. Another possible way to quantify non-factorization of renormalization constants is by computing the ratio $\mathcal{R}$ of the full QCD+QED RC and the pure QCD and QED ones,

$$\mathcal{R} = (Z^{\text{QED}})^{-1} Z (Z^{\text{QCD}})^{-1} \,, \tag{3.3}$$

which encodes by definition all the non-perturbative contributions of order $\mathcal{O}(\alpha_{em}\alpha_s^n)$ with $n \geq 1$, other than the *factorizable* terms given by the product $Z^{\text{QED}} Z^{\text{QCD}}$. This decomposition is especially convenient if together with QCD+QED, also pure QED is evaluated numerically at finite lattice spacing by repeating closely the calculation made in the full theory. In this case, in fact, using $\mathcal{R}$ to determine the non-factorizable contributions to the RCs allows to reduce the statistical fluctuations and systematic uncertainties in their calculation. Indeed, by dividing the full QCD+QED Z by the pure QCD and QED RCs, the ratio $\mathcal{R}$ is automatically free from QED cut-off effects of $\mathcal{O}(\alpha_{em}a^n)$ and the pure QCD ones, thus avoiding the need to compute such effects analytically. Furthermore, for those operators having a non-vanishing anomalous dimension matrix, the pure QCD and the QED anomalous dimensions at lowest order cancel out in the ratio, leaving only the contribution of the non-factorizable mixed term $\gamma_{se}^{(1)}$ of order $\mathcal{O}(\alpha_{em}\alpha_s)$. Lastly, the noise arising from the stochastic representation of the photon propagator (see Sec. 3.4) greatly cancels between numerator and denominator.

In the following we present a new strategy to compute the non-factorizable contributions to the correction ΔZ and its application to quark bilinear operators and the four-fermion operators entering the calculation of the leptonic decay rates of light-mesons. In our work the electro-quenched approximation is employed but the same methodology can be applied, with appropriate changes, to the unquenched case as well.

3.1 Renormalization conditions in QCD+QED

In this section we provide the general formalism to compute renormalization constants of a given operator non-perturbatively in the RI'-MOM scheme, with the inclusion of e.m. corrections of order $\mathcal{O}(\alpha_{\rm em})$. The same procedure can be easily adapted to other renormalization schemes, such as RI-SMOM [60], by changing kinematical conditions and with a proper choice of projectors.

3.1.1 RI'-MOM renormalization conditions

In the RI-MOM scheme RCs of operators are defined by imposing that suitable Green functions, computed between external fermionic states with exceptional external momenta (i.e. all external fields have equal momentum, $p_i^2 = p^2$), in a fixed gauge, coincide at a given scale μ with their tree-level values [54]. This condition can be written in terms of the amputated and projected Green function of the operator,

$$\Gamma_O(pa) = \mathrm{Tr}\left[\Lambda_O(pa)\, P_O\right] , \tag{3.4}$$

with P_O being a suitable combination of Dirac matrices projecting the amputated Green function $\Lambda_O(pa)$ on its tree-level value. The renormalization condition then reads

$$Z_{\Gamma_O}(\mu a)\Gamma_O(\mu a) \equiv Z_{\Gamma_O}(\mu a)\Gamma_O(pa)|_{p^2=\mu^2} = 1 , \tag{3.5}$$

where

$$Z_{\Gamma_O}(\mu a) = Z_O(\mu a) \prod_f Z_f^{-1/2}(\mu a) . \tag{3.6}$$

In Eq. (3.6), Z_O and $Z_f^{1/2}$ are respectively the operator and the fermion field RCs necessary to renormalize the amputated Green function. The product is over all the fermionic fields entering the operator and renormalizing under the action of QCD and/or QED, namely quarks (q_i) and charged leptons (ℓ_i). The RC Z_O is defined as

$$O^{\rm RI'}(\mu) = Z_O(\mu a)\, O^{\rm bare}(a) \tag{3.7}$$

and in the presence of operator mixing is a matrix. To remain as general as possible, we will treat Z_O as a generic matrix unless otherwise specified. The RC Z_f is proportional to the identity matrix, i.e. $[\hat{Z}_f]_{ij} = Z_f\, \delta_{ij}$.

In the RI'-MOM scheme the fermion field RC is defined as

$$Z_f = -\frac{i}{12}\,\mathrm{Tr}\left[\frac{\not{p}\,\langle S_f(p)\rangle^{-1}}{p^2}\right]_{p^2=\mu^2} , \tag{3.8}$$

where $\langle S_f(p) \rangle$ is the traslational invariant fermion propagator in momentum space averaged over the gauge configurations and the trace is done over color and spin indices. On a fixed gauge configuration, the propagator in momentum space is defined as

$$S_f(p) = \int \mathrm{d}^4x \, S_f(x,0) \, \mathrm{e}^{-ip\cdot x} \ . \tag{3.9}$$

In QCD+QED the RCs Z_{q_i} and Z_O depend in general both on the strong and e.m. coupling constants, while for leptons Z_{ℓ_i} only gets corrections from e.m. interactions and can be in principle easily computed in perturbation theory. Since neutrinos do not interact neither strongly nor electromagnetically, it follows that $Z_{\nu_\ell} = 1$.

3.1.2 Beyond factorization approximation

We find it particularly convenient to decompose any renormalization constant Z in the terms of the ratio $\mathcal{R}$ introduced in Eq. (3.3),

$$Z = Z^{\mathrm{QED}} \left[(Z^{\mathrm{QED}})^{-1} Z (Z^{\mathrm{QCD}})^{-1} \right] Z^{\mathrm{QCD}} \equiv Z^{\mathrm{QED}} \, \mathcal{R} \, Z^{\mathrm{QCD}} \ , \tag{3.10}$$

where Z^{QCD} is the RC, in general a matrix, in pure QCD (corresponding to the case $\alpha_{\mathrm{em}} = 0$),

$$Z^{\mathrm{QCD}} = \prod_f \left[Z_f^{\mathrm{QCD}}(\mu a) \right]^{-1/2} \left[\Gamma_O^{\mathrm{QCD}}(pa) \Big|_{p^2=\mu^2} \right]^{-1} \ , \tag{3.11}$$

and

$$Z^{\mathrm{QED}} \equiv 1 + \frac{\alpha_{\mathrm{em}}}{4\pi} \Delta Z^{\mathrm{QED}} \tag{3.12}$$

is the pure, perturbative QED mixing matrix (corresponding to $\alpha_{\mathrm{s}} = 0$) at first order in α_{em}. The ratio $\mathcal{R}$ can be expanded in terms of α_{em} as well,

$$\mathcal{R} = (Z^{\mathrm{QED}})^{-1} Z (Z^{\mathrm{QCD}})^{-1} \equiv 1 + \frac{\alpha_{\mathrm{em}}}{4\pi} \eta \ , \tag{3.13}$$

so that, at the first order in α_{em}, the RCs can be written as

$$\begin{aligned} Z &= \left[1 + \frac{\alpha_{\mathrm{em}}}{4\pi} \left(\Delta Z^{\mathrm{QED}} + \eta \right) \right] Z^{\mathrm{QCD}} \\ &\equiv \left(1 + \frac{\alpha_{\mathrm{em}}}{4\pi} \Delta Z \right) Z^{\mathrm{QCD}} \ , \end{aligned} \tag{3.14}$$

where we have defined

$$\Delta Z = \Delta Z^{\mathrm{QED}} + \eta \ . \tag{3.15}$$

The first term in Eq. (3.15), ΔZ^{QED}, represents the pure QED contribution to the RC at order $\mathcal{O}(\alpha_{\mathrm{em}})$, whereas η contains the $\mathcal{O}(\alpha_{\mathrm{em}})$ *non-factorizable* QCD+QED corrections. The case $\eta = 0$ corresponds to the factorization approximation in which the RC simply reduces to $Z = Z^{\mathrm{QED}} Z^{\mathrm{QCD}}$. We stress that the quantities appearing in Eq. (3.10) are in general non-commuting matrices, which reduce to 1×1 matrices in the case of non-mixing operators, and thus the order of the factors must be consistently handled. The introduction of the non-factorization estimator η is particularly useful. Indeed, the pure QCD and the pure $\mathcal{O}(\alpha_{\mathrm{em}})$ QED anomalous

dimensions cancel in the ratio, so that the scale dependence of η is related only to the non-factorizable mixed anomalous dimension $\gamma_{se}^{(1)}$ of $\mathcal{O}(\alpha_{\rm em}\alpha_{\rm s})$. The anomalous dimension $\gamma_{se}^{(1)}$ has been computed for the specific operators studied in this work and the details are given in Chapter 7.

Moreover, leading QCD and QED cut-off effects cancel in the ratio, provided that pure QED is computed on the lattice with the same regularization used for the QCD+QED calculation. In fact, at one loop in lattice perturbation theory, the RCs computed in pure QCD, in pure QED and in the full theory would have respectively the form

$$\begin{aligned} Z^{\rm QED} &= 1 + \frac{\alpha_{\rm em}}{4\pi}\,\Delta Z^{\rm QED}_{(0)} + \mathcal{O}(\alpha_{\rm em}a^2)\ , \\ Z^{\rm QCD} &= 1 + \frac{\alpha_{\rm s}}{4\pi}\,\Delta Z^{\rm QCD}_{(0)} + \mathcal{O}(\alpha_{\rm s}a^2)\ , \\ Z &= 1 + \frac{\alpha_{\rm em}}{4\pi}\,\Delta Z^{\rm QED}_{(0)} + \frac{\alpha_{\rm s}}{4\pi}\,\Delta Z^{\rm QCD}_{(0)} + \frac{\alpha_{\rm em}\alpha_{\rm s}}{(4\pi)^2}\,\Delta Z^{\rm QED}_{(0)}\Delta Z^{\rm QCD}_{(0)} + \frac{\alpha_{\rm em}}{4\pi}\,\eta_{(0)} \\ &\quad + \mathcal{O}(\alpha_{\rm em}a^2, \alpha_{\rm s}a^2, \alpha_{\rm em}\alpha_{\rm s}a^2)\ , \end{aligned} \tag{3.16}$$

where the subscript (0) denotes the contribution to the RC at order $\mathcal{O}(a^0)$. From Eq. (3.13) it follows that η is automatically free from pure QCD and pure QED cut-off effects, retaining only subleading corrections of $\mathcal{O}(\alpha_{\rm em}\alpha_{\rm s}a^2)$, namely

$$\eta = \frac{4\pi}{\alpha_{\rm em}}\,(\mathcal{R}-1) = \eta_{(0)} + \mathcal{O}(\alpha_{\rm em}\alpha_{\rm s}a^2)\ . \tag{3.17}$$

The result remains valid also when $Z^{\rm QCD}$ is computed non-perturbatively, its contribution being completely cancelled in the ratio.
The introduction of η therefore makes the extraction of e.m. corrections to RCs cleaner and more precise than the direct calculation of the quantity $\Delta Z^{(\rm QED)}$. As will be discussed later in Sec. 3.4, further improvement can be achieved by using stochastic photon propagators in the computation of ΔZ and $\Delta Z^{\rm QED}$.

Once η is determined nonperturbatively, the full RC Z can obtained as

$$Z = \left[1 + \frac{\alpha_{\rm em}}{4\pi}\left(\Delta Z^{\rm QED}_{\rm an} + \eta\right)\right]\, Z^{\rm QCD}\ , \tag{3.18}$$

where this time $\Delta Z^{\rm QED}_{\rm an}$ is computed *analytically* at one-loop in perturbation theory. This quantity is known for both bilinear operators [57] and the four fermion operators studied in this work [14]. The measure of non-factorization of the RC $Z^{\rm fact}$, introduced in Eq. (3.2), is then given by

$$Z^{\rm fact} = 1 + \eta\,(\Delta Z^{\rm QED}_{\rm an})^{-1}\ . \tag{3.19}$$

3.1.3 Ingredients of the calculation

We are interested in computing non-perturbatively the non-factorization estimator η for the RC of a given operator. From the above discussion, it is clear that in order to compute η, the correction ΔZ and $\Delta Z^{\rm QED}$ have to be first computed on the lattice in QCD+QED and in pure QED respectively. Being the RI-MOM condition

in Eq. (3.5) valid at each order in both $\alpha_{\rm s}$ and $\alpha_{\rm em}$, we can obtain the condition for the e.m. correction to the RCs by expanding it in terms of $\alpha_{\rm em}$.

We now proceed to derive the correction to the RC of a generic composite operator O. By expressing Z_{Γ_O} as in Eq. (3.14) and using the RI-MOM condition evaluated in pure QCD, the $\mathcal{O}(\alpha_{\rm em})$ expansion of Eq. (3.5) reads

$$\begin{aligned} Z_{\Gamma_O}(\mu a)\,\Gamma_O(pa)|_{p^2=\mu^2} &= \left[1+\frac{\alpha_{\rm em}}{4\pi}\,\Delta Z_{\Gamma_O}(\mu a)\right] Z^{\rm QCD}_{\Gamma_O}(\mu a)\,\times \\ &\quad \times\left[\Gamma^{\rm QCD}_O(\mu a)+\frac{\alpha_{\rm em}}{4\pi}\,\Delta\Gamma_O(\mu a)\right] \\ &= 1+\frac{\alpha_{\rm em}}{4\pi}\,\left[\Delta Z_{\Gamma_O}(\mu a)+Z^{\rm QCD}_{\Gamma_O}(\mu a)\Delta\Gamma_O(\mu a)\right] \quad (3.20) \\ &\equiv 1\,. \end{aligned}$$

The RI-MOM renormalization condition is then satisfied at $\mathcal{O}(\alpha_{\rm em})$ by imposing that

$$\Delta Z_{\Gamma_O}(\mu a) = -Z^{\rm QCD}_{\Gamma_O}(\mu a)\Delta\Gamma_O(\mu a)\,. \tag{3.21}$$

This relation can be expressed in terms of the e.m. corrections to Z_O and Z_f expanding the definition of Z_{Γ_O} in Eq. (3.6), thus obtaining the $\mathcal{O}(\alpha_{\rm em})$ correction to the RC of the operator O,

$$\Delta Z_O(\mu a) = -\prod_f\left[Z^{\rm QCD}_f(\mu a)\right]^{-1/2}\,Z^{\rm QCD}_O(\mu a)\,\Delta\Gamma_O(\mu a)+\frac{1}{2}\sum_f\Delta Z_f(\mu a)\,. \tag{3.22}$$

To summarize, the $\mathcal{O}(\alpha_{\rm em})$ correction ΔZ_O is a combination of the corrections to the fermion field RCs ΔZ_f, the corrections to the projected Green function $\Delta\Gamma_O$ and the pure QCD RCs.

This applies also to $\Delta Z^{\rm QED}_O$, where all the ingredients must be evaluated in the absence of QCD, namely

$$\Delta Z^{\rm QED}_O(\mu a) = -\Delta\Gamma^{\rm QED}_O(\mu a)+\frac{1}{2}\sum_f\Delta Z^{\rm QED}_f(\mu a)\,. \tag{3.23}$$

We stress that the corrections ΔZ_f and $\Delta Z^{\rm QED}_f$ are proportional to the identity matrix, and therefore they contribute only to the diagonal entries of ΔZ_O and $\Delta Z^{\rm QED}_O$ respectively.

Now we discuss how to compute the e.m. corrections to the fermion field RCs, ΔZ_f, and to the amputated and projected Green function of a generic composite operator, $\Delta\Gamma_O$. The calculation of $\Delta\Gamma_O$ for the specific cases of bilinear operators and the four-fermion operator O_1 mediating light-meson leptonic decays will be discussed later in Sec. 3.5 and Sec. 3.6.

3.2 Renormalization of fermion fields

The corrections to the RCs of fermion fields are fundamental ingredients for the calculation of ΔZ_O, as shown in Eq. (3.22). In this section we focus on the renormalization of *quark* fields, which require a non-perturbative calculation. The $\mathcal{O}(\alpha_{\rm em})$

RCs of charged lepton fields are instead computable in perturbation theory, while neutrinos are irrelevant in the calculation since they are neutral with respect to both strong and e.m. interactions.

Let us define the full propagator of a quark of flavour q as

$$S_q(pa) = S^{\rm QCD}(pa) + \frac{\alpha_{\rm em}}{4\pi}\,\Delta S_q(pa)\ , \tag{3.24}$$

where $S^{\rm QCD}(pa) \equiv \left[S^{\rm QCD}\right]^{AB}_{\alpha\beta}(pa)$ is the pure QCD quark propagator and $\Delta S_q(pa)$ is the sum of the $\mathcal{O}(\alpha_{\rm em})$ electromagnetic corrections to the quark propagator, both evaluated in a given gluon field background with fixed gauge. These corrections depend on the fractional electric charge of the propagating quark, e_q, which can however be factorized in the calculation. For Wilson fermions, the e.m. correction to the quark propagator in the *electro-quenched approximation*, in which dynamical sea quarks are considered as neutral with respect to electromagnetism, can be written as

$\Delta S_q(pa)$ =

$+ [m_{\rm w} - m^0_{\rm w}]$

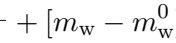

$$\equiv\ \Delta S_q^{\rm self}(pa) + \Delta S_q^{\rm T}(pa) + [m_{\rm w} - m^0_{\rm w}]\ \Delta S^{\rm S}(pa) \tag{3.25}$$

where we have exhibited explicitly the counter-term for the quark mass, which can be rewritten as $[m_{\rm w} - m^0_{\rm w}] \equiv e_q^2\,\delta m_{\rm w}$, together with the self-energy and tadpole corrections. Details on the calculation of ΔS_q as a sequential propagator and the stochastic representation of the photon propagator are discussed in Sec. 3.4. Once averaged over the gauge configurations, the inverse quark propagator reads

$$\langle S_q(pa)\rangle^{-1} \equiv \langle S^{\rm QCD}(pa)\rangle^{-1} + \frac{\alpha_{\rm em}}{4\pi}\,\Delta\Sigma_q(pa)\ , \tag{3.26}$$

where we have defined the amputated one-particle irreducible two-point vertex

$$\Delta\Sigma_q(pa) = -\ \langle S^{\rm QCD}(pa)\rangle^{-1}\,\langle \Delta S_q(pa)\rangle\,\langle S^{\rm QCD}(pa)\rangle^{-1}\,. \tag{3.27}$$

From Eq. (3.8) it follows that the correction to the quark field RC in the RI'-MOM scheme is given by

$$\Delta Z_q(\mu a) = -\frac{i}{12}\,\left(Z_q^{\rm QCD}(\mu a)\right)^{-1}\,{\rm Tr}\left[\frac{\not{p}\,\Delta\Sigma_q(pa)}{p^2}\right]_{p^2=\mu^2}\ , \tag{3.28}$$

with

$$Z_q^{\rm QCD}(\mu a) = -\frac{i}{12}\,{\rm Tr}\left[\frac{\not{p}\,\langle S^{\rm QCD}(pa)\rangle^{-1}}{p^2}\right]_{p^2=\mu^2}\ . \tag{3.29}$$

In order to avoid discretization effects in the calculation of Z_q, whose precision is crucial for an accurate determination of the RCs of composite operators, we find it more practical to substitute the projector $(\not{p}/p^2)$ in the RI'-MOM conditions (3.28) and (3.29) with $(\gamma_\nu/\tilde{p}_\nu)$ and define Z_q as

$$Z_q^{\rm QCD}(\mu a) = -\frac{i}{12\,N_p}\,{\sum_\nu}'\,{\rm Tr}\left[\frac{\gamma_\nu\,\langle S^{\rm QCD}(pa)\rangle^{-1}}{\tilde{p}_\nu}\right]_{\tilde{p}^2=\mu^2}\ , \tag{3.30}$$

where

$$\tilde{p}_\nu \equiv \frac{1}{a}\sin(p_\nu a) \tag{3.31}$$

and the sum $\sum'$ is over the N_p non-vanishing components of the four-momentum $\tilde{p}$. In this way, since the tree-level lattice quark propagator, in the massless theory, is given by

$$S_q^{\text{free}}(p) = -i\frac{\tilde{\not{p}}}{\tilde{p}^2}\ , \tag{3.32}$$

it follows that $Z_q^{\text{free}} = 1$ in the free theory, without discretization errors. The prescription adopted in Eq. (3.30) has been first proposed in Ref. [61] as an alternative to the usual RI'-MOM definition (3.29). The two choices differ by discretization effects of order $\mathcal{O}(a^2)$, but it has been observed that Eq. (3.30) reduces $O(4)$-breaking effects, thus making the numerical calculation of Z_q more clean.

3.3 Corrections to the amputated and projected Green function

We now address the calculation of the e.m. correction to the amputated and projected Green function of a generic composite operator, $\Delta\Gamma_O$, which is the other essential ingredient for the calculation of the $\mathcal{O}(\alpha_{\text{em}})$ contribution to the RC of the operator, ΔZ_O. From the definition of $\Delta\Gamma_O$ in Eq. (3.4), it follows that it can be obtained from the correction at $\mathcal{O}(\alpha_{\text{em}})$ to the amputated Green function by projecting it on the tree-level structure of the operator O, namely

$$\Delta\Gamma_O(pa) = \text{Tr}\left[\Delta\Lambda_O(pa)\, P_O\right]\ . \tag{3.33}$$

The projector P_O depends on the operator inserted in the Green function and must be defined in such a way that $\text{Tr}\left[\Lambda_O^{\text{tree}}\, P_O\right] = 1$ at tree-level. Nevertheless, the choice of P_O is not unique and different choices produce different discretization effects in the RCs. We stress that, given a set of n bare composite operators $\{O_i\}$, with amputated Green functions $\Delta\Lambda_{O_i}$, it is possible that under the action of QCD and QED interactions the amputated Green function of O_i gives a non-vanishing result when projected on the tree-level Dirac structure of a different operator O_j with the projector P_{O_j}. Therefore, the correction to the amputated and projected Green function has to be considered in general as a $n \times n$ matrix.

The amputated Green function $\Lambda_O(pa)$ is obtained from the Green function $G_O(pa)$ by removing the external legs with the inverse propagators $\langle S_f(pa)\rangle^{-1}$. Hence, at $\mathcal{O}(\alpha_{\text{em}})$, the e.m. corrections to the amputated Green function comes either from the corrections to the Green function $\Delta G_O(pa)$, or from the e.m. corrections to the inverse quark propagator (i.e. $\Delta\Sigma_f(pa)$ of Eq. (3.27)). In the first case case, $\Delta G_O(pa)$ is obtained by evaluating all possible corrections at $\mathcal{O}(\alpha_{\text{em}})$ to the QCD Green function: in addition to the e.m. corrections to individual propagators, also the exchange of a photon between pairs of charged fermions must be included. The calculation of these diagrams relies on the evaluation of the propagator $\Delta S_f^{\mathcal{A}}$ in Fig. 3.2, representing the interaction of a photon with a fermion line. The calculation of $\Delta\Lambda_O$ for quark bilinear operators and the weak four-fermion operator O_1 defined in Eq. (2.4) is carried out in Sec. 3.5 and Sec. 3.6 respectively.

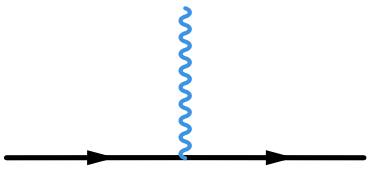

Figure 3.2. Representation of the sequential fermion propagator $\Delta S_f^{\mathcal{A}}$ with the insertion of a photon field.

Before closing this section, we anticipate a subtle feature of Green functions of operators involving pseudoscalar currents. When working with exceptional kinematics, as in the RI-MOM scheme, the zero momentum transfer ($q^2 = 0$) does not prevent the contribution of infrared poles due to the coupling of the current to the would-be Goldstone boson. Such Goldstone poles go as inverse power of the quark mass and vanishes at large momenta as $1/p^2$ in pure QCD [54] and the usual way to remove them is to fit the amputated and projected Green function at fixed external momentum with a term proportional to $1/M_P^2$, where $M_P \equiv M_P(\mu_1, \mu_2)$ is the mass of the pseudoscalar meson composed of valence quarks with masses μ_1 and μ_2 (see also Refs. [62, 63]). When including QED corrections, Goldstone poles occurring in QCD generate double poles in the correction to the Green function of the pseudoscalar operator and therefore the fit Ansatz has to be properly modified. Details on the chiral extrapolation of bilinear and four-fermion Green functions in QCD+QED will be provided in the numerical analysis, see Chap. 4.

3.4 The strategy for a QCD+QED calculation

In this work we consider QED corrections at $\mathcal{O}(\alpha_{\rm em})$, within the electro-quenched approximation in which the sea quarks are considered electrically neutral. Among the 1-loop diagrams appearing when expanding the path integral in powers of $\alpha_{\rm em}$, those in which a photon is exchanged by quark lines have a numerical cost that scales badly with the volume ($\sim V^2$). To make the calculation feasible and avoid computing explicitly the integral over the beginning and end of the photon propagator, the cost of which would be exceedingly too large for realistic volumes, the use of stochastic approaches is necessary. We adopt here a technique to compute such diagrams similar to the one used in Ref. [26], with an improvement of the numerical cost. By observing the diagrams in Eq. (3.25), and analogous diagrams appearing in the calculation of the corrections to the Green functions (see Sec. 3.5 and Sec. 3.6), one can notice that the building blocks of the calculation in QCD+QED are 6 propagators: the pure QCD quark propagator ($S^{\rm QCD}$), the QCD propagator with the insertion of a single photon ($\Delta S^{\mathcal{A}}$ in Fig. 3.2) and the propagators contributing to ΔS_q, namely the ones with the insertion of the scalar density ($\Delta S^{\rm S}$), of the tadpole operator ($\Delta S^{\rm T}$) and the self-energy correction ($\Delta S^{\rm self}$). The approach we used in this work to compute such diagrams relies on the stochastic definition of the photon propagator in Sec. 1.2.

3.4.1 Sequential quark propagators

The stochastic definition of the photon propagator in Sec. (1.2) can be exploited to reduce the calculation of diagrams with the exchange of a photon to the calculation of sequential propagators. In addition to the pure QCD quark propagator $S^{\rm QCD}(x,0)$, four additional sequential propagators are needed for Wilson fermions (see Eq. (3.25)), namely

$$\Delta S^{\rm S}(x,0) = -\sum_y S^{\rm QCD}(x,y)\,\mathbb{1}\,S^{\rm QCD}(y,0)\ , \tag{3.34}$$

$$\Delta S_q^{\rm T}(x,0) = \sum_y S^{\rm QCD}(x,y)\,T_q(y)\,S^{\rm QCD}(y,0)\ , \tag{3.35}$$

$$\Delta S_q^{\mathcal{A}}(x,0) = \sum_y S^{\rm QCD}(x,y)\,V_q^\mu(y)\mathcal{A}_\mu(y)\,S^{\rm QCD}(y,0)\ , \tag{3.36}$$

$$\Delta S_q^{\rm self}(x,0) = \sum_y S^{\rm QCD}(x,y)\,V_q^\mu(y)\mathcal{A}_\mu(y)\,\Delta S_q^{\mathcal{A}}(y,0)\ , \tag{3.37}$$

where $V_q^\mu(y) \equiv e_q\,V^\mu(y)$ is the conserved vector current and $T_q(y) \equiv e_q^2\,T^\mu(y)G_{\mu\mu}(y,y)$ the tadpole vertex, specific to the chosen lattice regularization[1]. Following the approach of Ref. [26], the calculation of such propagators would require the solution of five Dirac equations:

$$\sum_y D(x,y)\,S^{\rm QCD}(y,0) = \mathbb{1}\,\delta(x-0)\ , \tag{3.38}$$

$$\sum_y D(x,y)\,\Delta S^{\rm S}(y,0) = -\,\mathbb{1}\,S^{\rm QCD}(x,0)\ , \tag{3.39}$$

$$\sum_y D(x,y)\,\Delta S_q^{\rm T}(y,0) = T_q(x)\,S^{\rm QCD}(x,0)\ , \tag{3.40}$$

$$\sum_y D(x,y)\,\Delta S_q^{\mathcal{A}}(y,0) = V_q^\mu(x)\mathcal{A}_\mu(x)\,S^{\rm QCD}(x,0)\ , \tag{3.41}$$

$$\sum_y D(x,y)\,\Delta S_q^{\rm self}(y,0) = V_q^\mu(x)\mathcal{A}_\mu(x)\,\Delta S_q^{\mathcal{A}}(x,0)\ , \tag{3.42}$$

where $D(x,y)$ is the QCD Dirac operator. However, it is useful to remark that due to linearity of Dirac equation it is always possible to directly compute the sum of $(\Delta S_q^{\rm T} + \Delta S_q^{\rm self})$ entering ΔS_q in Eq. (3.25) by solving the equation

$$\sum_y D(x,y)\left(\Delta S_q^{\rm T} + \Delta S_q^{\rm self}\right)(y,0) = T_q(x)\,S^{\rm QCD}(x,0) + V_q^\mu(x)\mathcal{A}_\mu(x)\,\Delta S_q^{\mathcal{A}}(x,0)\ . \tag{3.43}$$

In general, the mass counterterm $[m_{\rm w} - m_{\rm w}^0] = e_q^2\,\delta m_{\rm w}$ in Eq. (3.25) must be determined by imposing a suitable renormalization condition as a part of the calculation of QED corrections, as discussed in Sec. 4.1.2. However, if the value of the counterterm is already known, it is possible to compute directly the full correction to the propagator, ΔS_q in Eq. (3.25), by solving the Dirac equation

$$\sum_y D(x,y)\Delta S_q(y,0) = \Phi_q(x,0)\ , \tag{3.44}$$

[1] The definitions of $V^\mu(y)$ and $T^\mu(y)$ are given in Eq. (37) of Ref. [3] for the Twisted Mass action in the physical basis at maximal twist.

where the sequential source $\Phi_q(x,0)$ is given by

$$\Phi_q(x,0) \equiv V_q^\mu(x)\mathcal{A}_\mu(x)\,\Delta S_q^{\mathcal{A}}(x,0) + \Big(T_q(x) - [m_{\rm w} - m_{\rm w}^0]\,\mathbb{1}\Big)\,S^{\rm QCD}(x,0)\ . \quad (3.45)$$

Dirac equations are solved in a specific gluon and photon gauge configuration, and the Green functions computed in such backgrounds. The average over different photon and gluon configurations leads to the desired e.m. correction to the Green function. Since averages over gluon and photon configurations commute, it is not needed to carry out the two averages independently. In practice, for each gluon configuration, we have employed a single photon configuration, and performed the two averages simultaneously. A schematic representation of the procedure adopted to compute the e.m. correction to the quark propagator ΔS_q is reported in Fig. 3.3, where include also the insertion of the pseudoscalar current typical of the twisted-mass regularization, which will be discussed in Sec. 4.1.

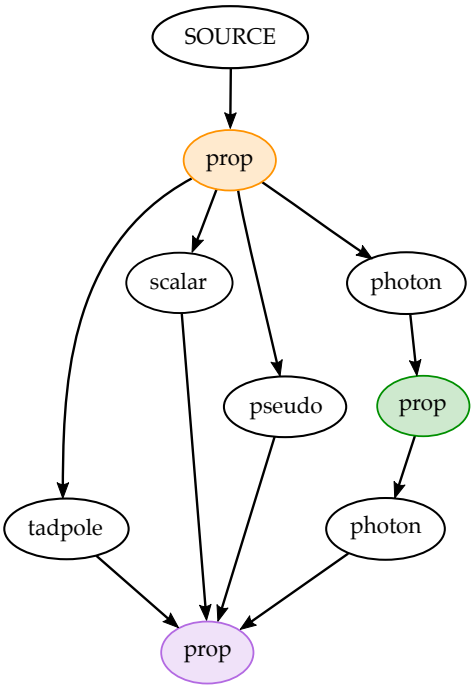

Figure 3.3. Schematic representation of the construction of the propagator ΔS_q. The nodes labeled as "prop" correspond to an inversion of the Dirac operator, that produces respectively (starting from the top) the QCD propagator $S^{\rm QCD}$ (orange), the sequential propagator $\Delta S_q^{\mathcal{A}}$ (green) and the complete correction ΔS_q (purple). Here we include the insertion of the pseudoscalar current typical of the twisted-mass regularization, which will be discussed in Sec. 4.1.

3.4.2 Pure QED calculation

We have shown how in QCD+QED the basic ingredients for the calculation are just three propagator, $S^{\rm QCD}$, $\Delta S^{\mathcal{A}}$ and ΔS_q, each obtained with an inversion of the Dirac operator. The same ingredients are needed in the pure QED analysis and these are obtained by following the same steps described above with the substitution

$S^{\rm QCD} \to S^{\rm free}$ in Eqs. (3.34)-(3.37) and (3.45), $S^{\rm free}$ being the quark propagator in the free theory.

Since the non-factorizable correction to RCs is defined according to Eq. (3.15) as the difference

$$\eta = \Delta Z - \Delta Z^{\rm QED} \ , \tag{3.46}$$

it is highly convenient to compute ΔZ and $\Delta Z^{\rm QED}$ individually in such a way that their statistical uncertainties are maximally correlated. This can be achieved by computing the two quantities using the *same* stochastic photon fields. To our experience, such a procedure yields a reduction of the statistical uncertainty on η by approximatively a factor 5, as it will be illustrated in Chap. 4.

3.5 Renormalization of quark bilinear operators

We discuss now the renormalization of lattice quark bilinear operators. Let us consider the local, flavour non-singlet quark field bilinear operators of the form

$$O_\Gamma \equiv \bar{q}_2 \, \Gamma \, q_1 \ , \tag{3.47}$$

where Γ is a matrix of the Clifford algebra[2], $\Gamma = \mathbb{1}, \gamma_5, \gamma_\mu, \gamma_\mu\gamma_5, \sigma_{\mu\nu}$, which we denote according to their Lorentz symmetry as S, P, V, A, T, respectively. The fields q_1 (ingoing) and q_2 (outgoing) are considered here to be generic quark fields in a given lattice regularization of QCD with masses μ_{q_1} and μ_{q_2} respectively. In our numerical analysis, described in Chap. 4, we adopt Twisted Mass fermions in the *twisted basis*, with opposite Wilson parameters $r_1 = -r_2$. Moreover, the two quarks are considered having equal electric fractional charge, namely $e_{q_1} = e_{q_2} = 1$.
For a bilinear operator, the renormalization condition (3.5) yields

$$Z_{O_\Gamma} = \frac{Z_{q_1}^{1/2} Z_{q_2}^{1/2}}{\Gamma_{O_\Gamma}} \ , \tag{3.48}$$

where $Z_{q_{1,2}}$ are the RCs of the quark fields computed as in Eq. (3.8) and $\Gamma_{O_\Gamma}^{\rm QCD}$ is the amputated, projected one-particle irreducible vertex, expressed in terms of the amputated Green function Λ_{O_Γ} as in Eq. (3.4). The pure QCD RCs of quark bilinear operators have been obtained in Ref. [56] using the same ETMC gauge configurations with $N_f = 4$ degenerate flavors of sea quarks used in this work. However, the QCD calculation in Ref. [56] differs in the number of ensembles used and the numerical procedure adopted, which will be described in Chap. 4.

The e.m. correction ΔZ_{O_Γ} can be obtained from Eq. (3.22) and reads

$$\Delta Z_{O_\Gamma} = -(Z_{q_1}^{\rm QCD})^{-1/2} (Z_{q_2}^{\rm QCD})^{-1/2} \, Z_{O_\Gamma}^{\rm QCD} \ \Delta\Gamma_{O_\Gamma} + \frac{1}{2} \left(\Delta Z_{q_1} + \Delta Z_{q_2} \right) \ , \tag{3.49}$$

where $Z_{q_1}^{\rm QCD} = Z_{q_2}^{\rm QCD}$ in pure QCD and

$$\Delta\Gamma_{O_\Gamma} = {\rm Tr}[\Delta\Lambda_{O_\Gamma} \, P_{O_\Gamma}] \ . \tag{3.50}$$

[2] We use Euclidean Dirac matrices in the chiral representation, in which γ_5 is diagonal and $\gamma_\mu = \gamma_\mu^\dagger = \gamma_\mu^{-1}$.

The set of projectors P_{O_Γ} used in Eq. (3.50) is chosen in such a way that

$$\mathrm{Tr}[\Lambda^{\mathrm{tree}}_{O_\Gamma} P_{O_\Gamma}] = \mathrm{Tr}[\Gamma\, P_{O_\Gamma}] = 1 \ , \tag{3.51}$$

the trace acting on spin and colour indices. For bilinear operators we adopt the usual set of projectors

$$P_{O_\Gamma} = \frac{\Gamma^\dagger}{\mathfrak{L}_\Gamma} \tag{3.52}$$

where $\mathfrak{L}_\Gamma \equiv \mathrm{Tr}[\Gamma\,\Gamma^\dagger]$ ensures the correct normalization of the trace at tree-level. In particular, for bilinear operators we get $\mathfrak{L}_\Gamma = 12\, N_\Gamma$, where the factor 12 comes from the trace of color and spin identity matrices and $N_\Gamma = \{1, 1, 4, 4, 6\}$ is the number of independent Lorentz components of the matrix $\Gamma = \{S, P, V, A, T\}$ coming from the sum over the repeated Lorentz indices in the product $\Gamma\,\Gamma^\dagger$.

Since bilinear operators do not mix with each other neither in the presence of electromagnetic interactions, the RCs are real numbers and not matrices.

In order to compute the e.m. correction to the amputated Green function, $\Delta\Lambda_{O_\Gamma}$ in Eq. (3.50), we need first to construct the Green function of the operator O_Γ between external quark fields with equal momenta $p_1^2 = p_2^2 = p^2$. The Green function in pure QCD in momentum space is given by

$$G^{\mathrm{QCD}}_{O_\Gamma}(pa) = \langle S^{\mathrm{QCD}}_{q_2}(pa)\,\Gamma\,\gamma_5 S^{\mathrm{QCD}\,\dagger}_{q_1}(pa)\gamma_5\rangle \ , \tag{3.53}$$

where we have used the γ_5-hermiticity $S_i(x,y) = \gamma_5 S_i(y,x)^\dagger\gamma_5$ and $\langle\cdots\rangle$ stands for the average over the gauge configurations. The two quark propagators computed in pure QCD are labelled, as well as their corresponding RCs, with a different flavour index to remind that in the intermediate steps of the calculation, i.e. before any average or chiral extrapolation, they are distinguished by the quark mass and, eventually, by the Wilson parameter ($r_1 = -r_2$).

At order $\mathcal{O}(\alpha_{\mathrm{em}})$, the diagrams that contribute are those in which:

- one photon is emitted from the *ingoing* quark and absorbed by the *outgoing* one,
- either the *ingoing* or the *outgoing* quark propagator gets an order $\mathcal{O}(\alpha_{\mathrm{em}})$ correction.

We can write such corrections as

$\Delta G_{O_\Gamma}(pa)$ = ⟨ 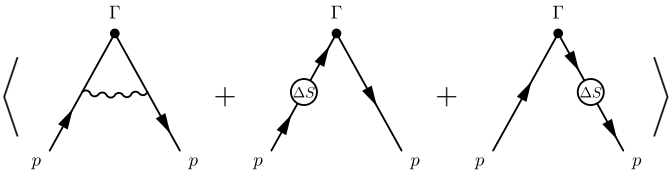 ⟩ (3.54)

$$\equiv \quad \Delta G^{\mathrm{exc}}_{O_\Gamma}(pa) \quad + \quad \Delta G^{\mathrm{in}}_{O_\Gamma}(pa) \quad + \quad \Delta G^{\mathrm{out}}_{O_\Gamma}(pa) \ ,$$

where

$$\Delta G^{\mathrm{exc}}_{O_\Gamma}(pa) = \left\langle \Delta S^{\mathcal{A}}_{q_2}(pa)\,\Gamma\,\gamma_5 \left(\Delta S^{\mathcal{A}}_{q_1}(pa)\right)^\dagger \gamma_5 \right\rangle \ , \tag{3.55}$$

$$\Delta G^{\mathrm{in}}_{O_\Gamma}(pa) = \left\langle \Delta S_{q_2}(pa)\ \Gamma\,\gamma_5 \left(S^{\mathrm{QCD}}_{q_1}(pa)\right)^\dagger \gamma_5 \right\rangle , \tag{3.56}$$

$$\Delta G^{\mathrm{out}}_{O_\Gamma}(pa) = \left\langle S^{\mathrm{QCD}}_{q_2}(pa)\,\Gamma\,\gamma_5 \left(\Delta S_{q_1}(pa)\right)^\dagger \gamma_5 \right\rangle . \tag{3.57}$$

The propagator $\Delta S^{\mathcal{A}}$ is the propagator coupled to the photon field through the conserved vector current and its calculation is discussed in Sec. 3.4. In the combination of the two propagators $\Delta S^{\mathcal{A}}_{q_i}$ in Eq. (3.55), the average over the photon field configurations realizes the appropriate photon propagator. We remind that the average over the photon field configurations is done simultaneously with the one over the gluon configurations (see Sec. 3.4). Two kinds of corrections contribute to the amputated Green function: either the e.m. correction ΔG_{O_Γ} is amputated with QCD propagators, or the QCD Green function is amputated with the e.m. corrections to the inverse propagator. Thus we have

$$\begin{aligned}\Delta\Lambda_{O_\Gamma}(pa) \;=\; & \Delta\Sigma_{q_2}(pa)\, G^{\rm QCD}_{O_\Gamma}(pa)\,\gamma_5\,\langle S^{\rm QCD\,\dagger}_{q_1}(pa)\rangle^{-1}\,\gamma_5 + \qquad (3.58)\\ & + \langle S^{\rm QCD}_{q_2}(pa)\rangle^{-1}\, G^{\rm QCD}_{O_\Gamma}(pa)\,\gamma_5\,\Delta\Sigma^{\dagger}_{q_1}(pa)\,\gamma_5 \;+\\ & + \langle S^{\rm QCD}_{q_2}(pa)\rangle^{-1}\,\Delta G_{O_\Gamma}(pa)\,\gamma_5\langle S^{\rm QCD\,\dagger}_{q_1}(pa)\rangle^{-1}\,\gamma_5\;. \qquad (3.59)\end{aligned}$$

3.6 Renormalization of the weak operator O_1

In this section we discuss the non-perturbative QCD+QED renormalization in the RI'-MOM scheme of the semi-leptonic four-fermion operator

$$O_1 = \overline{q}_2\gamma^\mu(1-\gamma_5)q_1\;\overline{\nu}_\ell\gamma_\mu(1-\gamma_5)\ell\;, \qquad (3.60)$$

that enters the weak effective Hamiltonian in Eq. (2.3) describing the leptonic decay of a light-meson. As discussed in Sec. 2.2, the non-perturbative renormalization of O_1 in the RI'-MOM scheme is part of a two-steps process in which the operator is first renormalized on the lattice and then perturbatively matched to the W-regularization scheme in which the weak effective Hamiltonian is renormalized. Here we give the details on the non-perturbative lattice calculation.

When we include QCD and e.m. corrections at $\mathcal{O}(\alpha_{\rm em})$, since Wilson-like fermions explicitly break chiral symmetry, it follows that the operator O_1 on the lattice mixes with other 4 lattice operators with different chirality.

The complete basis for a left-handed neutrino is given by:

$$\begin{aligned}O_1^{\rm bare} &= \overline{q}_2\gamma^\mu(1-\gamma_5)q_1\;\overline{\nu}_\ell\gamma_\mu(1-\gamma_5)\ell\;,\\ O_2^{\rm bare} &= \overline{q}_2\gamma^\mu(1+\gamma_5)q_1\;\overline{\nu}_\ell\gamma_\mu(1-\gamma_5)\ell\;,\\ O_3^{\rm bare} &= \overline{q}_2(1-\gamma_5)q_1\;\overline{\nu}_\ell(1+\gamma_5)\ell\;, \qquad (3.61)\\ O_4^{\rm bare} &= \overline{q}_2(1+\gamma_5)q_1\;\overline{\nu}_\ell(1+\gamma_5)\ell\;,\\ O_5^{\rm bare} &= \overline{q}_2\sigma^{\mu\nu}(1+\gamma_5)q_1\;\overline{\nu}_\ell\sigma_{\mu\nu}(1+\gamma_5)\ell\,.\end{aligned}$$

The complete basis for a generic neutrino is made up of ten operators, the five additional operators being obtained from $O_1 - O_5$ by the exchange $(1-\gamma_5) \leftrightarrow (1-\gamma_5)$. Since the neutrino is electrically neutral its chirality is conserved and the operators $O_1 - O_5$ do not mix under renormalization with the remaining 5 operators and invariance under parity transformations ensures that the two 5×5 renormalization matrices are equal. In the following we focus the discussion on the five operators of Eq. (3.61), which are a complete basis for a left-handed neutrino.

The renormalized operators $\vec{O}^{\rm RI'}(\mu)$, with $\vec{O} = (O_1, \ldots, O_5)$, can be written in terms of bare lattice operators $\vec{O}^{\rm bare}(a)$ as

$$\vec{O}^{\rm RI'}(\mu) = Z_O(a\mu)\, \vec{O}^{\rm bare}(a) \ , \tag{3.62}$$

where $Z_O(a\mu)$ is a 5×5 renormalization matrix. We note that in pure QCD the operator O_1 mixes only with O_2, with scale independent coefficients, whereas the full 5×5 renormalization matrix is necessary in general when e.m. corrections are included. If instead of using Wilson-like fermions, we used a lattice formulation with good chiral properties, such as domain wall fermions, only $O_1^{\rm bare}(a)$ would appear on the right-hand side of Eq. (3.62), which transforms as the $(8,1)$ representation under the $SU(3)_L \times SU(3)_R$ chiral symmetry for quarks.

In the following it will be useful to define the Dirac structure associated to the operators

$$O_i = (\bar{q}_2\, X_i\, q_1)\, (\bar{\nu}_\ell\, Y_i\, \ell)\,, \tag{3.63}$$

as $\Gamma_i = X_i \otimes Y_i$, namely

$$\begin{aligned} \Gamma_1 &= \gamma^\mu(1-\gamma^5) \otimes \gamma_\mu(1-\gamma^5)\,, \qquad \Gamma_2 = \gamma^\mu(1+\gamma^5) \otimes \gamma_\mu(1-\gamma^5)\,, \\ \Gamma_3 &= (1-\gamma^5) \otimes (1+\gamma^5)\,, \qquad \Gamma_4 = (1+\gamma^5) \otimes (1+\gamma^5)\,, \\ \Gamma_5 &= \sigma^{\mu\,\nu}(1+\gamma^5) \otimes \sigma_{\mu\,\nu}(1+\gamma^5)\,. \end{aligned} \tag{3.64}$$

The renormalization matrix Z_O satisfies the renormalization condition

$$Z_O(\mu a)_{ik}\, \Gamma_O(\mu a)_{kj} = \delta_{ij}\, \sqrt{Z_{q_1}(\mu a)\, Z_{q_2}(\mu a)\, Z_\ell(\mu a)}\ , \tag{3.65}$$

where

$$\Gamma_O(\mu a)_{\,ij} = {\rm Tr}\left[\Lambda_{O_i}(pa) P_{O_j}\right]_{p^2=\mu^2} \tag{3.66}$$

and $\Lambda_{O_i}(pa)$ is the amputated Green function of the operator O_i with external momenta p. We choose to project the Green functions by tracing over the colour and spin indices of quarks and the spin indices of leptons separately. Therefore, the projectors $P_{O_i} = P_{X_i} \otimes P_{Y_i}$ are defined in such a way that at tree-level

$${\rm Tr}\left[X_i P_{X_j}\right] = {\rm Tr}\left[Y_i P_{Y_j}\right] = \delta_{ij}\ , \tag{3.67}$$

$${\rm Tr}\left[\Lambda_{O_i}^{\rm tree} P_{O_j}\right] = {\rm Tr}\left[X_i P_{X_j}\right]\, {\rm Tr}\left[Y_i P_{Y_j}\right] = \delta_{ij}\ . \tag{3.68}$$

For the Dirac structures $\Gamma_i = X_i \otimes Y_i$ reported in Eq. (3.64), we adopt the set of projectors

$$P_{X_i} \equiv \frac{X_i^\dagger}{\mathfrak{L}_{X_i}}, \qquad P_{Y_i} \equiv \frac{Y_i^\dagger}{\mathfrak{L}_{Y_i}}\ , \tag{3.69}$$

where $\mathfrak{L}_{X_i} \equiv {\rm Tr}[X_i\, X_i^\dagger]$ and $\mathfrak{L}_{Y_i} \equiv {\rm Tr}[Y_i\, Y_i^\dagger]$.

In the absence of QED interactions, the calculation is simplified by the factorization of the Green function into quark and lepton bilinear vertices. In this case we can simply project the two-fermion operators to obtain

$$\begin{aligned} \Gamma_O^{\rm QCD}(\mu a)_{\,ij} &= {\rm Tr}\left[\Lambda_{X_i}^{\rm QCD}(pa)\, P_{X_j}\right]\, {\rm Tr}\left[\Lambda_{Y_i}^{\rm QCD}(pa)\, P_{Y_j}\right]_{p^2=\mu^2} \\ &= {\rm Tr}\left[\Lambda_{X_i}^{\rm QCD}(pa)\, P_{X_j}\right]_{p^2=\mu^2}\ , \end{aligned} \tag{3.70}$$

where $\mathrm{Tr}\left[\Lambda_{Y_i}^{\mathrm{QCD}}(pa)\,P_{Y_j}\right] = \mathrm{Tr}\left[Y_i\,P_{Y_j}\right] = \delta_{ij}$ since the lepton propagators exactly cancel out and

$$\Lambda_{X_i}^{\mathrm{QCD}}(pa) = \langle S_{q_2}^{\mathrm{QCD}}(pa)\rangle^{-1}\,\langle S_{q_2}^{\mathrm{QCD}}(pa)\;X_i\,\gamma_5\,S_{q_1}^{\mathrm{QCD}\dagger}(pa)\,\gamma_5\rangle\,\gamma_5\,\langle S_{q_1}^{\mathrm{QCD}\dagger}(pa)\rangle^{-1}\gamma_5\ . \tag{3.71}$$

Combining Γ_O^{QCD} with the quark RC Z_q^{QCD} defined in Eq. (3.29), it is easy to show that the renormalization matrix Z_O in the absence of QED interactions reduces to the block diagonal matrix

$$Z_O^{\mathrm{QCD}} = \begin{pmatrix} Z_+^{\mathrm{QCD}} & Z_-^{\mathrm{QCD}} & 0 & 0 & 0 \\ Z_-^{\mathrm{QCD}} & Z_+^{\mathrm{QCD}} & 0 & 0 & 0 \\ 0 & 0 & \mathcal{Z}_+^{\mathrm{QCD}} & \mathcal{Z}_-^{\mathrm{QCD}} & 0 \\ 0 & 0 & \mathcal{Z}_-^{\mathrm{QCD}} & \mathcal{Z}_+^{\mathrm{QCD}} & 0 \\ 0 & 0 & 0 & 0 & Z_T^{\mathrm{QCD}} \end{pmatrix} \tag{3.72}$$

where

$$Z_\pm^{\mathrm{QCD}} = \frac{Z_V^{\mathrm{QCD}} \pm Z_A^{\mathrm{QCD}}}{2}\ , \quad \mathcal{Z}_\pm^{\mathrm{QCD}} = \frac{Z_S^{\mathrm{QCD}} \pm Z_P^{\mathrm{QCD}}}{2}\ , \tag{3.73}$$

with $Z_{O_\Gamma}^{\mathrm{QCD}}$ are the QCD RCs of the bilinear operators O_Γ defined in Eq. (3.47). As a consequence, we notice that pure QCD corrections only induce the mixing of the operator O_1 with the operator O_2, with scale independent coefficients since the quark vector and axial vector currents are protected by Ward identities in the massless limit. The mixing of O_1 produces the renormalized QCD operators

$$O_1^\chi = (Z_O^{\mathrm{QCD}}\,\vec{O}^{\mathrm{bare}})_1 = \bar{q}_2\gamma^\mu\left(Z_V^{\mathrm{QCD}} - Z_A^{\mathrm{QCD}}\,\gamma_5\right) q_1\ \bar{\nu}_\ell\gamma_\mu(1-\gamma_5)\ell\ , \tag{3.74}$$

$$O_2^\chi = (Z_O^{\mathrm{QCD}}\,\vec{O}^{\mathrm{bare}})_2 = \bar{q}_2\gamma^\mu\left(Z_V^{\mathrm{QCD}} + Z_A^{\mathrm{QCD}}\,\gamma_5\right) q_1\ \bar{\nu}_\ell\gamma_\mu(1-\gamma_5)\ell\ , \tag{3.75}$$

which, similarly to the corresponding continuum operators, belong, respectively, to the $(8,1)$ and $(1,8)$ chiral representations with respect to a rotation of the quark fields [64] .

When including QED at $\mathcal{O}(\alpha_{\mathrm{em}})$, the Green function can no longer be factorized, due to the appearance of crossed diagrams in which a photon is exchanged between a quark and the charged lepton. The e.m. corrections, neglecting terms of $\mathcal{O}(\alpha_{\mathrm{em}}^2)$, follow from Eqs. (3.22) and (3.33)

$$\Delta Z_O = -(Z_{q_1}^{\mathrm{QCD}})^{-1/2}(Z_{q_2}^{\mathrm{QCD}})^{-1/2}\,Z_O^{\mathrm{QCD}}\,\mathrm{Tr}[\Delta\Lambda_O\,P_O] + \frac{1}{2}\left(\Delta Z_{q_1} + \Delta Z_{q_2} + \Delta Z_\ell\right)\ , \tag{3.76}$$

where ΔZ_ℓ has purely electromagnetic origin and can be computed in perturbation theory. As in the case of bilinear operators, the correction to the amputated Green function gets two kinds of contributions and is given by

$$\begin{aligned} \Delta\Lambda_{O_i}(pa) \;=\; & \Delta\Sigma_{q_2}(pa)\,G_{O_i}^{\mathrm{QCD}}(pa)\;\gamma_5\,\langle S_{q_1}^{\mathrm{QCD}\dagger}(pa)\rangle^{-1}\,(S_\ell{}^\dagger(pa))^{-1}\,\gamma_5 + \\ & + \langle S_{q_2}^{\mathrm{QCD}}(pa)\rangle^{-1}\,G_{O_i}^{\mathrm{QCD}}(pa)\;\gamma_5\,\Delta\Sigma_{q_1}^\dagger(pa)\,(S_\ell{}^\dagger(pa))^{-1}\,\gamma_5\;+ \\ & + \langle S_{q_2}^{\mathrm{QCD}}(pa)\rangle^{-1}\,G_{O_i}^{\mathrm{QCD}}(pa)\;\gamma_5\langle S_{q_1}^{\mathrm{QCD}\dagger}(pa)\rangle^{-1}\Delta\Sigma_\ell^\dagger(pa)\;\gamma_5 \\ & + \langle S_{q_2}^{\mathrm{QCD}}(pa)\rangle^{-1}\,\Delta G_{O_i}(pa)\;\gamma_5\langle S_{q_1}^{\mathrm{QCD}\dagger}(pa)\rangle^{-1}\,(S_\ell{}^\dagger(pa))^{-1}\,\gamma_5\ , \end{aligned} \tag{3.77}$$

where S_ℓ^{-1} is the inverse charged lepton propagator in the absence of QED interactions and $\Delta\Sigma_\ell$ its e.m. correction, computed in analogy with Eq. (3.27). Neutrino's propagator plays no role in the calculation and is therefore considered already amputated both in $G_{O_i}^{\rm QCD}$ and ΔG_{O_i}.

The e.m. correction ΔG_{O_i} can be represented diagrammatically as

$\Delta G_{O_i}(pa) \;=\;$ 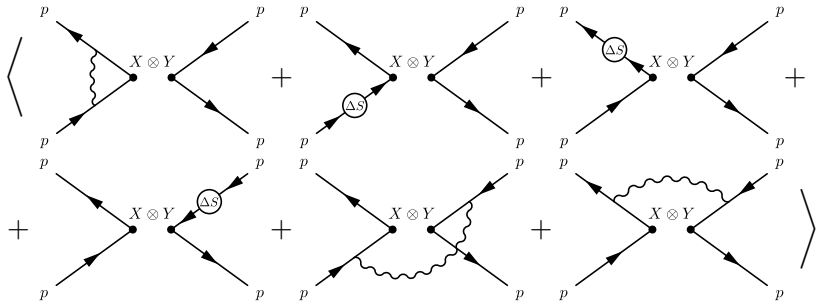

$$\equiv\; \Delta G^{\rm exc}_{O_i}(pa) + \Delta G^{①}_{O_i}(pa) + \Delta G^{②}_{O_i}(pa) + \\ +\, \Delta G^{\ell}_{O_i}(pa) + \Delta G^{\rm in}_{O_i}(pa) + \Delta G^{\rm out}_{O_i}(pa)\ .$$

Such corrections depend on the fermion charges: the charge of the lepton entering the Lagrangian is $e_\ell = -1$ and the fractional charges of the quarks are $e_u = 2/3$ for up-like quarks and $e_d = -1/3$ for down-like quarks. The fermionic lines on the left-hand side of the diagrams in Eq. (3.78) represent the *ingoing* and *outgoing* light quarks. On the right-hand side, the neutrino propagator is drawn for illustration but not actually included in the calculation. The terms $\Delta G^{{\rm exc},①,②,\ell}_{O_i}$ in Eq. (3.78) can be easily related to the Green functions of bilinear operators computed in Sec. 3.5. The two additional diagrams $\Delta G^{\rm in,out}_{O_i}$, representing the exchange of a photon between the charged lepton and a quark, can be computed using the sequential propagators defined in Sec 3.4,

$$\Delta G^{\rm in}_{O_i}(pa) = \Big\langle S^{\rm QCD}_{q_2}(pa)\, X_i\, \gamma_5 (\Delta S^{\mathcal{A}}_{q_1}(pa))^\dagger \gamma_5 \otimes Y_i\, \gamma_5 (\Delta S^{\mathcal{A}}_{\ell}(pa))^\dagger \gamma_5 \Big\rangle\ , \qquad (3.78)$$

$$\Delta G^{\rm out}_{O_i}(pa) = \Big\langle \Delta S^{\mathcal{A}}_{q_2}(pa)\, X_i\, \gamma_5 (S^{\rm QCD}_{q_1}(pa))^\dagger \gamma_5 \otimes Y_i\, \gamma_5 (\Delta S^{\mathcal{A}}_{\ell}(pa))^\dagger \gamma_5 \Big\rangle\ , \qquad (3.79)$$

where the average $\langle\cdots\rangle$ refers both to QCD and QED gauge field configurations and the neutrino external propagator is already amputated.

3.7 A hint of the RI-SMOM scheme

In practice it is not always easy to satisfy the bound imposed by the renormalization window $\Lambda_{\rm QCD} \ll \mu \ll 1/a$ in which the RI-MOM scheme works. The condition $\mu \gg \Lambda_{\rm QCD}$ ensures that perturbation theory is valid, but when spontaneous symmetry breaking occurs, as in the case of QCD, a large value of μ may not be sufficient, because of the presence of the Goldstone boson, the pion in our case. At low momentum transfer, $q = p_1 - p_2$, Green functions can receive a non-perturbative contribution from the pion pole. It has been proven in [54] that this contribution is proportional to $1/p^2 = 1/\mu^2$, even when $q^2 = 0$. In order to reduce the infrared chiral-symmetry breaking effects one should compute the RI-MOM renormalization constants at a very high scale. On the other hand, one is faced with the problem of

discretization errors if the value of μ is too high. One way to reduce this problem is to choose the kinematics without channels of exceptional momenta, i.e. with $q = p_1 - p_2 \neq 0$. One such choice is a variant of the RI-MOM scheme, called RI-SMOM [60, 65]. The scheme consists in the choice of "symmetric" external quark momenta such that

$$p_1^2 = p_2^2 = q^2 = \mu^2 \quad \text{and} \quad q = p_1 - p_2 \neq 0\,. \tag{3.80}$$

In this case the chiral symmetry breaking effects are better behaved and vanish with powers of order $1/p^6$ [60].

Another property of the RI-SMOM scheme is that the Ward-Takahashi identity (WTI) is satisfied by both the axial and the vector current, in contrast with the RI-MOM scheme in which the WTI for the axial current only holds at large μ^2.

Although the powerful features of the RI-SMOM scheme, in this work the renormalization procedure has been performed in the RI-MOM scheme. The reason of this choice is related to the difficulty in the implementation of the condition (3.80) on the lattice. In fact, if one requires for the momenta p_1 and p_2 to satisfy anti-periodic boundary conditions along the temporal direction, there is no way to obtain a temporal anti-periodic momentum q. The chiral-symmetry breaking effects which appear due to the pion contribution to the Feynman diagrams have to be properly taken into account and removed, as will be illustrated in Chap. 4.

4 | Numerical Analysis of RCs in QCD+QED

4.1 Lattice Setup

4.1.1 ETMC $N_f = 4$ configurations

In this section we discuss the numerical setup adopted to test the framework proposed to compute RCs of operators non-perturbatively on the lattice at all orders in QCD and first order in QED. We consider as a reference target the calculation of the leptonic decay rates for light mesons [7], which employs $N_f = 2 + 1 + 1$ ensembles with degenerate light-quarks (u, d) and almost physical mass strange and charm quarks. Since RI'-MOM is a mass independent scheme, the RCs are to be defined in the massless limit. Ensembles with fixed strange and charm sea quark masses are not well suited. We use therefore dedicated gauge configurations with $N_f = 4$ degenerate dynamical quarks produced by the ETM Collaboration [66, 67], with different values of valence and sea quark masses in order to have a controlled and reliable extrapolation to the chiral limit of the RC-estimators. Due to instabilities in the tuning to maximal twist, the $N_f = 4$ ensembles have been produced out of maximal twist and hence without an automatic cancellation of $\mathcal{O}(a)$ cut-off effects. However, it is still possible to achieve the $\mathcal{O}(a)$ improvement through the so-called *θ-average* method, introduced in Ref. [68] and based on averaging results obtained at opposite values of twist angle θ (and hence opposite PCAC quark masses). This procedure clearly requires a doubling of the ensembles, produced with the same renormalized quark mass parameters but opposite angle θ. We will refer in the following to the two sets of ensembles with the labels "p" or "m" according to the sign of the angle θ. The simulations have been performed at three different values of the inverse lattice coupling, namely $\beta = \{1.90, 1.95, 2.10\}$, corresponding to inverse lattice spacings $a^{-1} \simeq \{2.23, 2.42, 3.19\}$ GeV. The ensembles used in this work for the QCD+QED analysis, are a large subset of the original ones used in Ref. [56] and the details are reported in Table 4.1. With respect to the analysis performed in Ref. [56], the ensembles A2 and A3 at $\beta = 1.90$ are not used in the present analysis because they were unavailable. The gluon action used in QCD is the improved Iwasaki action, while the pure QED analysis has been performed using the Wilson gauge action with gauge links set to 1. We choose to work in the Landau gauge for gluons, as it is customary for RI'-MOM, and the same choice is adopted for photons. For this work we have used $N_{\text{conf}} = 150$ gauge configurations generated

Table 4.1. Details of the lattice setup for the QCD+QED analysis. Here $L_4 \equiv T$ and $L_{1,2,3} \equiv L$.

	$a\mu^{\rm sea}$	$\kappa^{\rm sea}$	$am^{\rm sea}_{\rm PCAC}$	$a\mu^{\rm val}$	$\kappa^{\rm val}$	$am^{\rm val}_{\rm PCAC}$
$\beta = 1.90$ ($L = 24$, $T = 48$) , $a^{-1} = 2.23$ GeV						
A4m	0.0080	0.163476	-0.0390(01)	{0.0060, 0.0080, 0.0120,	0.162113	-0.0142(02)
A4p		0.162689	0.0398(01)	0.0170, 0.0210,0.0260}	0.164817	+0.0147(02)
A1m	0.0080	0.163206	-0.0273(02)	{0.0060, 0.0080, 0.0120,	0.162549	-0.0163(02)
A1p		0.162876	+0.0275(04)	0.0170, 0.0210,0.0260}	0.163881	+0.0159(02)
$\beta = 1.95$ ($L = 24$, $T = 48$) , $a^{-1} = 2.42$ GeV						
B1m	0.0085	0.161739	-0.0413(02)	{0.0085, 0.0150, 0.0203,	0.160754	-0.0216(02)
B1p		0.160389	+0.0425(02)	0.0252, 0.0298}	0.162145	+0.0195(02)
B7m	0.0085	0.161585	-0.0353(01)	{0.0085, 0.0150, 0.0203,	0.160681	-0.0180(02)
B7p		0.160524	+0.0361(01)	0.0252, 0.0298}	0.161925	+0.0181(01)
B8m	0.0020	0.161585	-0.0363(01)	{0.0085, 0.0150, 0.0203,	0.160681	-0.0194(01)
B8p		0.160524	+0.0363(01)	0.0252, 0.0298}	0.161925	+0.0183(02)
B3m	0.0180	0.161229	-0.0160(02)	{0.0060,0.0085,0.0120,0.0150,	0.161229	-0.0160(02)
B3p		0.160826	+0.0163(02)	0.0180,0.0203,0.0252,0.0298}	0.160826	+0.0162(02)
B2m	0.0085	0.161229	-0.0209(02)	{0.0085, 0.0150, 0.0203,	0.161229	-0.0213(02)
B2p		0.160826	+0.0191(02)	0.0252, 0.0298}	0.160826	+0.0191(02)
B4m	0.0085	0.161095	-0.0146(02)	{0.0060,0.0085,0.0120,0.0150,	0.161095	-0.0146(02)
B4p		0.160870	+0.0151(02)	0.0180,0.0203,0.0252,0.0298}	0.160870	+0.0151(02)
$\beta = 2.10$ ($L = 32$, $T = 64$) , $a^{-1} = 3.19$ GeV						
C5m	0.0078	0.156291	-0.00821(11)	{0.0048,0.0078,0.0119,	0.156291	-0.0082(01)
C5p		0.155949	+0.00823(08)	0.0190,0.0242,0.0293}	0.155949	+0.0082(01)
C4m	0.0064	0.156250	-0.00682(13)	{0.0039,0.0078,0.0119,	0.156250	-0.0068(01)
C4p		0.155983	+0.00685(12)	0.0190,0.0242,0.0293}	0.155983	+0.0069(01)
C3m	0.0046	0.156209	-0.00585(08)	{0.0025,0.0046,0.0090,0.0152,	0.156209	-0.0059(01)
C3p		0.156017	+0.00559(14)	0.0201,0.0249,0.0297}	0.156017	+0.0056(01)
C2m	0.0030	0.156157	-0.00403(14)	{0.0013,0.0030,0.0080,0.0143,	0.156157	-0.0040(01)
C2p		0.156042	+0.00421(13)	0.0195,0.0247,0.0298}	0.156042	+0.0042(01)

by Monte Carlo simulations and statistical errors have been evaluated using the jackknife procedure (for details on the jackknife method we refer to Refs. [69–71]).

For each ensemble in Table 4.1, each mass (or combination of masses in the case of composite operators) and each gauge configuration we compute the estimators of the RCs at values of momenta, $p_\mu = (2\pi/L_\mu)\, n_\mu$, with components lying in the following intervals

$$\begin{aligned} \vec{n} &= ([0,3]\,,[0,3]\,,[0,3]\,,[0,7])\,, \quad \text{for } \beta = 1.95, \\ \vec{n} &= ([0,5]\,,[0,5]\,,[0,5]\,,[0,9])\,, \quad \text{for } \beta = 1.90 \quad \text{and} \quad 2.10\,, \end{aligned} \tag{4.1}$$

with L_μ denoting the lattice size in the direction μ. Anti-periodic boundary conditions on the quark fields in the time direction are adopted and they are implemented by a shift of the time component of the four-momentum by the constant $\Delta p_4 = \pi/L_4$.

The four-momenta have been selected by imposing a "democratic" momentum cut defined by

$$\Delta_4(p) \equiv \frac{\sum_\mu \tilde{p}_\mu^4}{(\sum_\mu \tilde{p}_\mu^2)^2} < 0.29, \tag{4.2}$$

where $\tilde{p}$ is defined in Eq. (3.31), thus minimizing the contribution of Lorentz non-invariant discretization effects. In order to increase the statistics, the restriction on the momenta has been loosened to $\Delta_4(p) < 2.0$ when all the components of the vector lie in the intervals $n_\mu = [0, 1]$ and $n_\mu = [1, 2]$ and, in addition, a bigger list of momenta has been generated by starting from the "democratically" filtered ones and considering all the momenta obtained by a reflection across one of the four axes. All the quantities of interest have been calculated using the extended list of momenta and then averaged over the equivalent momenta. The choice of *anti-periodic* boundary conditions guarantees that zero modes of quark propagators do not appear in the massless limit, being the minimum momentum equal to the shift $\Delta p_4 = \pi/L_4$.

When using Twisted Mass fermions, the quark mass μ_q appearing in such regularization undergoes renormalization as well. Therefore, the correction to the propagator ΔS_q in Eq. (3.25) includes an additional term and in the *twisted basis* it reads as

$\Delta S_q(pa)$ = 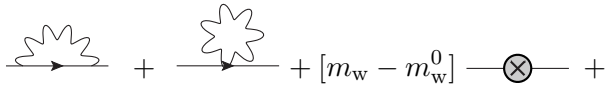 + $[m_{\rm w} - m_{\rm w}^0]$ + $[\mu_q - \mu_0]$

$\equiv \Delta S_q^{\rm self}(pa) + \Delta S_q^{\rm T}(pa) + [m_{\rm w} - m_{\rm w}^0]\, \Delta S^{\rm S}(pa) + [\mu_q - \mu_0]\, \Delta S^{\rm P}(pa)$,

where $[\mu_q - \mu_0] \equiv e_q^2\, \delta\mu_q$ and

$$\Delta S^{\rm P}(x,0) = \mp i \sum_y S^{\rm QCD}(x,y)\, \gamma_5\, S^{\rm QCD}(y,0) \ , \tag{4.3}$$

the sign $\mp$ depending on the component of the twisted quark doublet chosen. The expression of ΔS_q can be compared with the one reported in Eq. (1.45) and obtained in Ref. [3]. Notice that the results of Ref. [3] have been obtained using the Twisted Mass action at maximal twist and in the *physical basis*, this explaining the difference between the mass counterterms defined here in Eq. (4.3) and those in Eq. (1.45) above. We stress here that the difference between *twisted* and *physical* bases has to be carefully taken into account in the calculation of RCs and matrix elements. Indeed, RCs of twisted mass operators computed in the *twisted* basis do not in general coincide with those of twisted mass operators defined in the *physical* basis. This implies that the RCs entering the calculation of physical observables, which are computed in the *physical* basis, have to be properly related to those obtained in the *twisted* basis. The relation between RCs in the two bases, for the bilinear and four-fermion operators considered in this work, are discussed in Sec. 5.1. In the following, RCs are computed for operators in the *twisted* basis.

4.1.2 Tuning of the mass counterterms

The automatic $\mathcal{O}(a)$ improvement in the Twisted Mass regularization of LQCD can be obtained by tuning the quark mass and the twisted mass to the maximal twist

configuration. By defining the twisting angle as

$$\tan\omega = \frac{\hat{\mu}_q}{\hat{m}_{\rm w}} = \frac{Z_\mu\,\mu_q}{Z_m\,(m_{\rm w}-m_{\rm cr})}\ , \tag{4.4}$$

where $\hat{m}_{\rm w}$ and $\hat{\mu}_q$ are the renormalized quark and twisted masses respectively, the maximal twist corresponds to the choice $\omega = \pi/2$ in which the renormalized quark mass $\widehat{m}_{\rm w}$ vanishes. It is common practice to use the complementary angle θ to quantify the deviation from the maximal twist, namely $\theta = \pi/2 - \omega$. In Eq. (4.4) the additive renormalization of the bare quark mass due to the chiral symmetry breaking is made explicit. It follows that the $\mathcal{O}(a)$ improvement can be achieved just by tuning the bare quark mass $m_{\rm w}$ to its critical value $m_{\rm cr}$. An equivalent approach is to find the value of the bare quark mass such that $m_{\rm PCAC}$ vanishes. The $N_f = 4$ gauge ensembles used in this work are generated out of the maximal twist due to instabilities of the simulation and therefore one has to recur to a different strategy to achieve the $\mathcal{O}(a)$ improvement. Since $\mathcal{O}(a)$ effects are odd with respect to the twist angle θ, pairs of ensembles have been produced with opposite θ angles ($\theta_p = -\theta_m$) and the cancellation of the discretization effects in the iso-symmetric QCD analysis is obtained once the RCs, computed within the two sets of ensembles, are averaged [68]. The relation between the renormalized quark and twisted masses in the two sets of ensembles is schematically depicted in Fig. 4.1, the red squares corresponding to the configuration in pure QCD ($\theta_p = -\theta_m$). When introducing the QED interaction we must ensure that the symmetry condition $\theta'_p = -\theta'_m$ is preserved. The shift in the additive (QED) renormalization is the same in the two sets of ensembles (p and m) and therefore, in the absence of appropriate counterterms, the twist angles get modified in a non-symmetric way ($\theta'_p \neq -\theta'_m$), as schematically depicted in Fig. 4.1.

In order to restore the equality and exploit the θ-average to achieve $\mathcal{O}(a)$ improvement we need to properly tune the e.m. corrections to the masses. A possible

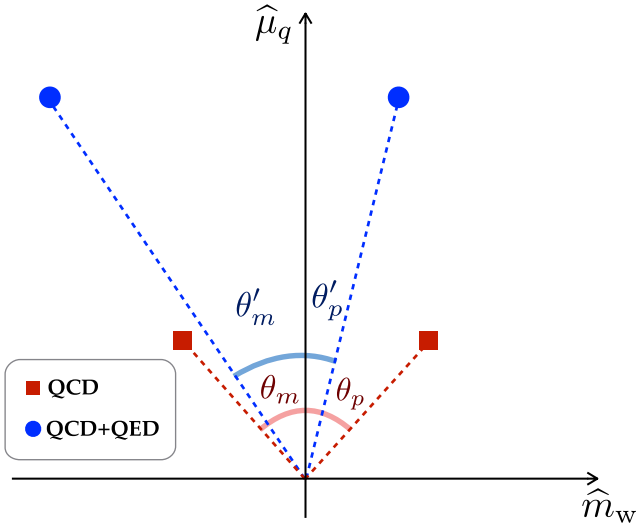

Figure 4.1. Relation between the renormalized quark and twisted masses before the introduction of counterms. In pure QCD (red squares), the angles are tuned to be equal and opposite ($\theta_p = -\theta_m$). In QCD+QED (blue dots), the shift of $m_{\rm w}$ induced by e.m. corrections modifies the angles in a non-symmetric way ($\theta'_p \neq -\theta'_m$).

way is to match the renormalized quark masses of the QCD and QCD+QED theory. This is achieved by imposing that the form factors Σ_2 and Σ_3 of the QCD quark propagator,

$$(S^{\mathrm{QCD}}(ap))^{-1} = -i\not{p}\,\Sigma_1(ap) + \Sigma_2(ap) + \gamma_5\,\Sigma_3(ap) \tag{4.5}$$

coincide in the limit $p^2 \to 0$ with those in the full theory, thus by imposing that their QED corrections vanish in such limit, namely

$$\lim_{p^2\to 0} \Delta\Sigma_2(ap) = \frac{1}{12} \lim_{p^2\to 0} \mathrm{Tr}\left[\Delta\Sigma_q\, \mathbb{1}\right] = 0 \ , \quad \lim_{p^2\to 0} \Delta\Sigma_3 = \frac{1}{12} \lim_{p^2\to 0} \mathrm{Tr}\left[\Delta\Sigma_q\, \gamma_5\right] = 0 \ , \tag{4.6}$$

with $\Delta\Sigma_q$ defined in Eq. (3.27). The needed counterterms are thus obtained by solving, for each set of ensembles, the system of equations

$$\begin{cases} \lim\limits_{p^2\to 0} \left(\Delta\Sigma_2^{\mathrm{self+T}} + \delta m_{\mathrm{w}}\, \Delta\Sigma_2^{\mathrm{S}} + \delta\mu_q\, \Delta\Sigma_2^{\mathrm{P}}\right) = 0 \\ \lim\limits_{p^2\to 0} \left(\Delta\Sigma_3^{\mathrm{self+T}} + \delta m_{\mathrm{w}}\, \Delta\Sigma_3^{\mathrm{S}} + \delta\mu_q\, \Delta\Sigma_3^{\mathrm{P}}\right) = 0 \end{cases} , \tag{4.7}$$

where the components $\Delta\Sigma_{2,3}^{\mathrm{self+T,S,P}}$ are related to the e.m. corrections to the quark propagator defined in Eq. (4.3).

This procedure has been proven to work nicely in the pure QED analysis, in which Wilson fermions have been used. In this case Σ_3 is absent in the propagator and the Wilson mass counterterm is simply given by

$$\delta m_{\mathrm{w}} = -\frac{\Delta\Sigma_2^{\mathrm{self+T}}}{\Delta\Sigma_2^{\mathrm{S}}} = \frac{e_q^2}{12}\, \mathrm{Tr}\left[S_{\mathrm{free}}^{-1}\, \left(\Delta S^{\mathrm{self+T}}\right)\, S_{\mathrm{free}}^{-1}\right] \ . \tag{4.8}$$

By taking the limit $a^2p^2 \to 0$, the quantity δm_{w} results to be in good agreement with the corresponding value computed at one loop in lattice perturbation theory, namely $\delta m_{\mathrm{w}}^{\mathrm{pert}} = -e_q^2 \cdot 0.325714$ [72], as shown in Fig. 4.2.

4.2 Numerical Procedure

The procedure adopted in the present analysis follows the one described in Ref. [61], with appropriate changes due to the different gauge ensembles used.

The core of the non-perturbative calculation of RCs in QCD+QED is the evaluation of the non-factorizable contribution η (see Eq. (3.15)), which can be obtained according to Eq. (3.46) as the difference between the e.m. correction ΔZ computed on the lattice in the full QCD+QED theory and the analogue correction ΔZ^{QED} evaluated in pure QED. As already mentioned above, ΔZ^{QED} can be in principle computed analytically in perturbation theory. However, in this work we decide to compute it numerically on the lattice. This has the clear advantage that, as explained in Sec. 3.1.2, by computing ΔZ^{QED} with the same lattice setup used for the calculation of ΔZ (but with gauge links set to 1), it is possible to make η free from all pure QCD and pure $\mathcal{O}(\alpha_{\mathrm{em}})$ QED cut-off effects. Moreover, the use of the *same* stochastic photon fields in the calculation of the two corrections $\Delta Z^{(\mathrm{QED})}$

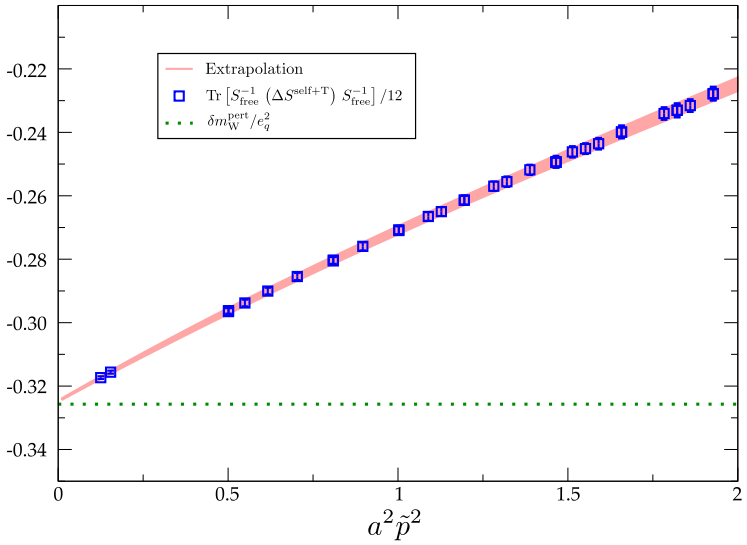

Figure 4.2. Comparison between the mass counterterm δm_{w} obtained in pure QED using the tuning in Eq. (4.6) and the one obtained in lattice perturbation theory in Ref. [72].

yields a significant reduction of statistical uncertainty on η. Therefore, two different analyses are required: one in the full theory and one in pure QED.

In this Section we describe all steps necessary to compute the RCs, their e.m. corrections and the non-factorizable part η, starting from propagators and Green functions. All steps are labelled with capital letters and a summarizing flow chart of the complete analysis is depicted in Fig. 4.3.

Lattice estimator of the RCs are computed from appropriate propagators and Green functions using the RI'-MOM conditions defined in Sec. 3.1 for each lattice coupling β, momentum p, sea quark mass, value of the Wilson parameter r, θ angle and valence quark mass (for Z_q) or combination of masses (in the case of RCs of composite operators). Therefore, the basic ingredients of our calculation are lattice RC *estimators* of the form

$$Z_q^{\mathrm{QCD}}\left(\beta,\theta,\mu^{\mathrm{sea}},\mu^{\mathrm{val}},r,p^2\right)\ , \tag{4.9}$$

$$\Delta Z_q\left(\beta,\theta,\mu^{\mathrm{sea}},\mu^{\mathrm{val}},r,p^2\right)\ , \tag{4.10}$$

$$\Gamma_O^{\mathrm{QCD}}\left(\beta,\theta,\mu^{\mathrm{sea}},\left\{\mu_1^{\mathrm{val}},\mu_2^{\mathrm{val}},\dots\right\},\{r_1,r_2,\dots\},p^2\right)\ , \tag{4.11}$$

$$\Delta\Gamma_O\left(\beta,\theta,\mu^{\mathrm{sea}},\left\{\mu_1^{\mathrm{val}},\mu_2^{\mathrm{val}},\dots\right\},\{r_1,r_2,\dots\},p^2\right)\ . \tag{4.12}$$

In the pure QED calculation, given the absence of non-perturbative dynamics, the same ingredients are computed in the free theory (see Sec. 3.4) and directly in the massless limit[1] with a fixed value of the Wilson parameter ($r = 1$), in order to avoid additional irrelevant steps in the calculation. Furthermore, in the free-theory analysis there is no dependence on the gauge coupling β and the angle θ either.

[1] The appearance of zero modes of fermion propagators is prevented by the anti-periodic boundary conditions adopted, the minimum momentum being equal to the shift $\Delta p_4 = \pi/T$.

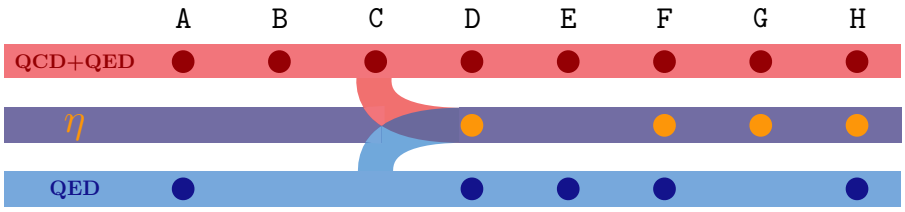

Figure 4.3. Flow chart of the complete analysis for the non-perturbative calculation of RCs in QCD+QED. All steps of the numerical analysis are labelled with capital letters A-H, as defined in Sec. 4.2. The three branches of the analysis (full QCD+QED, pure QED and calculation of η) are depicted to show the sequence of all steps.

Therefore, the RC estimators have the form

$$\Delta Z_q^{\mathrm{QED}}\left(p^2\right), \quad \Delta\Gamma_O^{\mathrm{QED}}\left(p^2\right) \ . \tag{4.13}$$

The same arguments hold for the lepton self-energy ΔZ_ℓ, but its actual calculation will be avoided in the study of leptonic decay rates, as it will be described in Sec. 4.3.1 and 5.2.

After each step described below, the RCs Z_O, its corrections in QCD+QED and in pure QED, $\Delta Z_O^{(\mathrm{QED})}$, and the non-factorizable RC η_O are computed according to the RI-MOM conditions in Sec. 3.1.

A. Average on equivalent momenta Given the momentum $p = (p_1, p_2, p_3, p_4)$, fifteen extra equivalent momenta configurations can be computed on the lattice by considering the copies of p obtained with a reflection about one axis ($\mathbb{Z}_2$ symmetry), i.e. all momenta having components $(\pm p_1, \pm p_2, \pm p_3, \pm p_4)$. The RC estimators computed at such momenta are therefore equivalent with each other and can be averaged to reduce statistical uncertainty. Moreover, on an hypercubic lattice one can also exploit $H(4)$ symmetry, corresponding to 90° rotations about an axis. However, on our $L^3 \times T$ lattices, the symmetry to be considered is the subgroup $H(3)_L \in H(4)$ of spatial 90° rotations, since the lattice extent in temporal direction is twice longer than in spatial ones. Therefore, the symmetry employed in our analysis for the average of equivalent momenta is

$$\hat{H}(4) \equiv H(3)_L \times [\mathbb{Z}_2]^4 \ . \tag{4.14}$$

In previous analyses [56, 61], a different choice was adopted instead. Equivalence classes were indeed identified by the value of $\tilde{p}^2$, which is a naive lattice version of the $O(4)$ Lorentz symmetry, but it does not correspond to any symmetry on the lattice. Note that given two momenta p_1 and p_2 having $\tilde{p}_1^2 = \tilde{p}_2^2$, they are not necessarily $\hat{H}(4)$-equivalent, e.g. $n_1 = (6,4,4,4)$ and $n_2 = (6,3,4,5)$[2]. Since the $O(4)$ rotation symmetry is broken down to $\hat{H}(4)$ hypercubic symmetry, there are lattice artifacts which are only invariant under $\hat{H}(4)$ but not under $O(4)$. Therefore, the average of estimators in equivalence classes different from those obtained using Eq. (4.14),

[2] The vectors $n = (n_t, n_x, n_y, n_z)$ are related to p as $p_0 = 2\pi(n_0 + 0.5)/T$ and $p_i = 2\pi n_i/L$ when using anti-periodic boundary conditions on time.

yields a wrong treatment of such Lorentz non-invariant discretization effects.

Lattice estimators in different equivalence classes are averaged, thus obtaining

$$Z_q^{\mathrm{A}}\left(\beta,\theta,\mu^{\mathrm{sea}},\mu^{\mathrm{val}},p^2\right)=\frac{1}{\mathcal{N}_p}\sum_{p_i\sim p}Z_q\left(\beta,\theta,\mu^{\mathrm{sea}},\mu^{\mathrm{val}},p_i^2\right)\ , \tag{4.15}$$

where $\mathcal{N}_p$ is the number of equivalent momenta in the equivalence class of p. The same form holds for all other ingredients.

B. Average on Wilson parameter r In order to further improve the statistical accuracy of RCs, we have averaged the results obtained from correlation functions with equal quark masses but different values of Wilson parameters. It results that, for example,

$$Z_q^{\mathrm{B}}\left(\beta,\theta,\mu^{\mathrm{sea}},\mu^{\mathrm{val}},p^2\right)\equiv\frac{1}{2}\left[Z_q^{\mathrm{A}}\left(\beta,\theta,\mu^{\mathrm{sea}},\mu^{\mathrm{val}},r_u,p^2\right)+Z_q^{\mathrm{A}}\left(\beta,\theta,\mu^{\mathrm{sea}},\mu^{\mathrm{val}},r_d,p^2\right)\right]\ , \tag{4.16}$$

where Z_q^{A} is the quark RC estimator evaluated at the previous Step A and $r_{u,d}$ are the two possible values of the Wilson parameter. The procedure used for composite operators is the same as for Z_q. The operators studied in this work are composed by two quarks and hence vertices will depend on four indices $(\mu_1^{\mathrm{val}},r_1)(\mu_2^{\mathrm{val}},r_2)$. The dependence on r is removed in this case by averaging over the equivalent combinations of μ^{val} and r, where the equivalence is meant in the sense that the combinations

$$(\mu_A^{\mathrm{val}},r_u)(\mu_B^{\mathrm{val}},r_u)\sim(\mu_B^{\mathrm{val}},r_u)(\mu_A^{\mathrm{val}},r_u)\sim(\mu_A^{\mathrm{val}},r_d)(\mu_B^{\mathrm{val}},r_d)\sim(\mu_B^{\mathrm{val}},r_d)(\mu_A^{\mathrm{val}},r_d) \tag{4.17}$$

correspond to the same effective mass. Here μ_A^{val} and μ_B^{val} are two arbitrary values of the valence quark masses.

In pure QED the calculation is purely perturbative and propagators are generated in the free theory. In this analysis, we decide to fix the value of the Wilson parameter, $r=1$. Such conventional choice corresponds to certain cut-off effects that solve the problem of fermion doubling, pushing the undesired copies to higher scales, and vanish in the continuum limit. The same choice is adopted for the lepton as well, $r_\ell=1$, both in the pure QED and the QCD+QED analyses.

C. Valence chiral extrapolation The RC estimators so far computed are still mass-dependent quantities. The RI-MOM scheme is instead a mass independent renormalization scheme, thus an extrapolation of the results to the chiral limit, i.e. to the limit in which $m_q=0$, must be performed. Once extrapolated to the chiral limit, RCs only depend on the subtraction scale $p^2=\mu^2$, the coupling constant β and the angle θ. The validity of the RI-MOM approach relies on the fact that non perturbative contributions to Green functions vanish asymptotically at large p^2 [54] so, in this region (as long as $p^2<1/a^2$ to keep discretization effects under control), Green functions are expected to be smooth functions of the quark masses. However, particular care must be taken when psuedoscalar currents are involved, e.g. in the calculation of the bilinear vertex Γ_P of the operator $O_P=\bar{q}_2\gamma_5 q_1$, since in this case, due to the coupling with the Goldstone boson (GB), the leading power

suppressed contribution $\sim 1/p^2$ is divergent in the chiral limit and the condition $\mu \gg \Lambda_{\rm QCD}$ may not be enough. The existence of this GB-pole contribution can be understood as follows. Let us consider the Green function constructed from bilinear operators with incoming and outgoing quarks having different momenta, p and p' respectively, and let define $q = p - p'$ the momentum transfer. At asymptotically large p^2 scales, non perturbative effects giving contributions potentially divergent in the chiral limit to the Green function do vanish and the latter turns out to have a polynomial dependence on the quark masses. However, at finite values of p^2, the contributions to the spectral decomposition of these Green functions from one GB intermediate state with momentum q and mass M_P give rise to terms proportional to $(q^2 + M_P^2)^{-1}$ suppressed by some power of $1/p^2$. Such non-perturbative contributions to the Green function, although suppressed by a factor $1/p^2$, are divergent in the chiral limit when using exceptional momenta ($p = p'$ and hence $q^2 = 0$) and therefore they must be disentangled and removed. Moreover, for twisted mass fermions, the explicit breaking of parity at finite lattice spacing can induce a coupling of the GB also with the scalar operator $O_S = \bar{q}_2 q_1$, but it is suppressed by $O(a^2)$ and its effects are almost negligible, as it will be shown in Sec. 4.3.

In pure QCD, the chiral limit in the *valence* sector is achieved through a fit of the amputated and projected Green functions, in a fixed gauge ensemble and at fixed momentum, using the linear Ansatz

$$\Gamma_O^{\rm QCD} = a_O^{(0)} + b_O^{(0)}\, M_P^2 \ , \tag{4.18}$$

where $M_P \equiv M_P(\mu_1, \mu_2)$ is the mass of the pseudoscalar meson composed of valence quarks with masses μ_1 and μ_2 and computed in pure QCD, $\Gamma_O^{\rm QCD}$ is the amputated and projected Green function of an operator O that does not involve pseudoscalar or scalar currents and $\{a_O^{(0)}, b_O^{(0)}\}$ are the fit parameters. The same linear fit ansatz is used for the valence chiral extrapolation of $Z_q^{\rm QCD}$, but in this case the variable of the fit is the effective mass $M_P^2(\mu, \mu)$ constructed from two quarks with equal valence masses. The GB-pole contamination in vertex functions involving pseudoscalar (P) or scalar (S) currents is removed using the following alternative fit Ansatz

$$\Gamma_O^{\rm QCD} = a_O^{(0)} + b_O^{(0)}\, M_P^2 + \frac{c_O^{(0)}}{M_P^2} \ , \tag{4.19}$$

where $O = P, S$ and the additional parameter $c_O^{(0)}$ is the residue at the pole.

When including QED in the calculation, Eqs. (4.18) and (4.19) have to be modified to take into account the e.m. corrections to the meson mass[3],

$$\left[M_P^2\right]^{\rm QCD+QED} = M_P^2 + \frac{\alpha_{\rm em}}{4\pi}\, \Delta M_P^2 \ . \tag{4.20}$$

Considering the Ansatz of Eq. (4.18) in QCD+QED and expanding it in terms of $\alpha_{\rm em}$ one obtains

$$\Delta\Gamma_O = a_O^{(1)} + b_O^{(1)}\, M_P^2 + b_O^{(0)}\, \Delta M_P^2 \ , \tag{4.21}$$

[3]Strong IB corrections to the meson mass can be neglected here, since they vanish in the chiral limit.

while, in the case of Eq. (4.19), the GB poles occurring in QCD generate double poles in the correction to the Green functions $\Delta\Gamma_{P(S)}$ and the fit Ansatz has to be modified into

$$\Delta\Gamma_O = a_O^{(1)} + b_O^{(1)}\, M_P^2 + \frac{c_O^{(1)}}{M_P^2} + b_O^{(0)}\, \Delta M_P^2 - c_O^{(0)}\, \frac{\Delta M_P^2}{M_P^4}\ , \tag{4.22}$$

with $O = P, S$. In Eqs. (4.21) and (4.22) only the coefficients $a_O^{(1)}$, $b_O^{(1)}$ and $c_O^{(1)}$ have to be fitted, since the values of $b_O^{(0)}$ and $c_O^{(0)}$ are known from the fit in pure QCD of Eqs. (4.18) or (4.19). When the amputated and projected vertices and their e.m. corrections are matrices due to operator mixing, the fit is performed on each of their components and the above equations have to be understood as component-wise.

We remind that the pure QED calculation is done, on the other hand, directly in the chiral limit, since no hadronic contamination or GB-pole contribution arise, and hence no chiral extrapolation is needed. The charged lepton is computed directly in the massless limit as well.

In conclusion, the extrapolated RC estimators in the limit $\mu^{\rm val} \to 0$ are obtained from the fit as

$$\left[Z_q^{\rm QCD}\right]^{\rm C}\left(\beta, \theta, \mu^{\rm sea}, p^2\right) \equiv \left[a_q^{(0)}\right]^{\rm B}\left(\beta, \theta, \mu^{\rm sea}, p^2\right)\ , \tag{4.23}$$

$$\left[\Delta Z_q\right]^{\rm C}\left(\beta, \theta, \mu^{\rm sea}, p^2\right) \equiv \left[a_q^{(1)}\right]^{\rm B}\left(\beta, \theta, \mu^{\rm sea}, p^2\right)\ , \tag{4.24}$$

where $\left[a_q^{(0)}\right]^{\rm B}$ and $\left[a_q^{(1)}\right]^{\rm B}$ are the parameters of the fit performed on the data computed at the previous Step B.

After the valence chiral extrapolation, the quantities ΔZ and $\Delta Z^{\rm QED}$, computed respectively in the full theory and in pure QED, are combined to form the non-factorizable RC η as defined in Eq. (3.46), namely

$$\left[\eta\right]^{\rm C}\left(\beta, \theta, \mu^{\rm sea}, p^2\right) \equiv \left[\Delta Z\right]^{\rm C}\left(\beta, \theta, \mu^{\rm sea}, p^2\right) - \left[\Delta Z^{\rm QED}\right]^{\rm C}\left(p^2\right)\ . \tag{4.25}$$

The electromagnetic correction to the squared mass ΔM_P^2 in the above equations, can be rewritten as

$$\Delta M_P^2 \equiv 2 M_P\, \Delta M_P \tag{4.26}$$

and the quantity ΔM_P has been determined following the procedure of Ref. [26].

D. Perturbative evolution Once the RCs have been extrapolated to the (valence) chiral limit, we investigate their dependence on the renormalization scale by evolving, at fixed coupling β, the RCs to a reference scale. This operation is necessary to discern whether the scale dependence of the RC comes from the anomalous dimension of the operator or it is due to lattice artifacts. The evolution of RCs is done using the evolution operator $\hat{U}$ computed in perturbation theory and discussed in detail later in Chapter 6. The evolution matrix relates renormalized operators evaluated at two different scales and it is defined as

$$\vec{O}_{\rm R}(\mu_2) = \hat{U}(\mu_2, \mu_1; \alpha_{\rm em})\ \vec{O}_{\rm R}(\mu_1)\ . \tag{4.27}$$

Since scale dependence of the renormalized operator is encoded in its renormalization constant, namely $\vec{O}_{\rm R}(\mu) = Z_O(\mu)\,\vec{O}_{\rm B}$, it follows that RCs evolve accordingly as

$$Z(\mu_2) = \hat{U}(\mu_2, \mu_1; \alpha_{\rm em})\; Z(\mu_1)\;. \tag{4.28}$$

The perturbative evolution is applied to RCs and not to the amputated and projected Green functions. Therefore, the ingredients computed in the previous Step C are combined to form the RCs according to RI'-MOM conditions in Sec. 3.1 and the analysis proceeds with the quantities $Z^{\rm QCD}$, $\Delta Z^{\rm (QED)}$ and η.

When including e.m. corrections, RCs are defined according to Eq. (3.14) as

$$Z(\mu) = Z^{\rm QCD}(\mu) + \frac{\alpha_{\rm em}}{4\pi}\,\Delta Z^{\rm QED}(\mu) Z^{\rm QCD}(\mu) + \frac{\alpha_{\rm em}}{4\pi}\eta(\mu) Z^{\rm QCD}(\mu)\;, \tag{4.29}$$

where $Z^{\rm QCD}$, $\Delta Z^{\rm QED}$ and η are in general non-commuting matrices. The definition of Z is crucial for a consistent evolution of the non-factorizable contribution η, since it depends on whether Z is defined as in Eq. (3.14) or with $Z^{\rm QCD}$ multiplied on the left. In this work we adopt the convention of Eq. (3.14) with $Z^{\rm QCD}$ multiplied on the right. Inserting the evolution operator (see Eq. (6.50))

$$\hat{U}(\mu_2, \mu_1; \alpha_{\rm em}) = \hat{U}_{\rm QCD}(\mu_2, \mu_1) + \frac{\alpha_{\rm em}}{4\pi}\,\Delta\hat{U}_1(\mu_2, \mu_1) + \frac{\alpha_{\rm em}\alpha_{\rm s}(\mu_1)}{(4\pi)^2}\,\Delta\hat{U}_2(\mu_2, \mu_1) \tag{4.30}$$

into Eq. (4.28) we obtain the following evolution rules[4]

$$Z^{\rm QCD}(\mu_2) \;=\; \hat{U}_{\rm QCD}(\mu_2, \mu_1)\, Z^{\rm QCD}(\mu_1)\;, \tag{4.34}$$

$$\Delta Z^{\rm QED}(\mu_2) \;=\; \Delta Z^{\rm QED}(\mu_1) + \Delta\hat{U}_1^{\rm QED}(\mu_2, \mu_1)\;, \tag{4.35}$$

$$\begin{aligned} \eta(\mu_2) \;=\;& \hat{U}_{\rm QCD}(\mu_2, \mu_1)\,\eta(\mu_1)\,\left[\hat{U}_{\rm QCD}(\mu_1, \mu_2)\right]^{-1} + \\ &+ \hat{U}_{\rm QCD}(\mu_2, \mu_1)\,\Delta Z^{\rm QED}(\mu_1)\,\left[\hat{U}_{\rm QCD}(\mu_2, \mu_1)\right]^{-1} + \\ &- \Delta Z^{\rm QED}(\mu_1) + \Delta\hat{U}_1(\mu_2, \mu_1)\left[\hat{U}_{\rm QCD}(\mu_2, \mu_1)\right]^{-1} + \\ &- \Delta\hat{U}_1(\mu_2, \mu_1) + \frac{\alpha_{\rm s}(\mu_1)}{4\pi}\,\Delta\hat{U}_2(\mu_2, \mu_1)\left[\hat{U}_{\rm QCD}(\mu_2, \mu_1)\right]^{-1}\;. \end{aligned} \tag{4.36}$$

[4] If one defines instead e.m. corrections to RCs as

$$Z = Z^{\rm QCD}\left(1 + \frac{\alpha_{\rm em}}{4\pi}\,\Delta Z^{\rm QED} + \frac{\alpha_{\rm em}}{4\pi}\,\tilde{\eta}\right)\;, \tag{4.31}$$

then the non-factorizable RC $\tilde{\eta}$ would evolve as

$$\begin{aligned} \tilde{\eta}(\mu_2) \;=\;& \tilde{\eta}(\mu_1) + \frac{\alpha_{\rm s}(\mu_1)}{4\pi}\,[Z^{\rm QCD}(\mu_1)]^{-1}\,[U_{\rm QCD}(\mu_2, \mu_1)]^{-1}\,\Delta U_2(\mu_2, \mu_1) Z^{\rm QCD}(\mu_1) + \\ &+ [Z^{\rm QCD}(\mu_1)]^{-1}\,[U_{\rm QCD}(\mu_2, \mu_1)]^{-1}\,\Delta U_1(\mu_2, \mu_1) Z^{\rm QCD}(\mu_1) - \Delta U_1(\mu_2, \mu_1)\;. \end{aligned} \tag{4.32}$$

The relation between $\tilde{\eta}$ and η is the following:

$$\tilde{\eta} = [Z^{\rm QCD}]^{-1}\,\left(\eta + \Delta Z^{\rm QED}\right)\,Z^{\rm QCD} - \Delta Z^{\rm QED}\;, \tag{4.33}$$

from which it is evident that the two definitions are equivalent in the case of non-mixing operators.

If operators do not mix under renormalization, as in the case of bilinear operators, the evolution for η gets the simpler form

$$\begin{aligned}\eta_O(\mu_2) &= \eta_O(\mu_1) + \Delta U_1(\mu_2,\mu_1)\,[U_{\rm QCD}(\mu_2,\mu_1)]^{-1} \\ &\quad - \Delta U_1(\mu_2,\mu_1) + \frac{\alpha_{\rm s}(\mu_1)}{4\pi}\,\Delta U_2(\mu_2,\mu_1)\,[U_{\rm QCD}(\mu_2,\mu_1)]^{-1}\ ,\end{aligned} \tag{4.37}$$

where this time $U_{\rm QCD}$, ΔU_1 and ΔU_2 are scalar functions, as well as η_O. Notice that the pure QED correction $\Delta Z^{\rm QED}$ contributes to the evolution of η only in the case of mixing operators, while it is absent in Eq. (4.37)[5]. As described in Chap. 3, the quantity $\eta = \Delta Z - \Delta Z^{\rm QED}$ is automatically free from pure QCD and pure QED cut-off effects and is only affected by subleading terms of order $\mathcal{O}(\alpha_{\rm em}\alpha_{\rm s}a^2)$. Furthermore, since we have computed the corrections ΔZ and $\Delta Z^{\rm QED}$ using the same stochastic photon fields, we have significantly reduced the statistical uncertainty of η due to the photon sampling. In order to avoid the re-introduction of such effects in the evolution of η, we implement the perturbative evolution substituting in Eq. (4.36) the quantity $\Delta Z^{\rm QED}$, which is computed on the lattice, with the corresponding analytical result $\Delta Z^{\rm QED}_{\rm an}$ computed at one-loop in perturbation theory.

The evolution matrix $\Delta\hat{U}_1$ depends on the one-loop QED anomalous dimension of the operator, $\hat{\gamma}_e^{(0)}$, while $\Delta\hat{U}_2$ depends also on the one-loop strong anomalous dimension $\hat{\gamma}_s^{(0)}$ and the mixed anomalous dimension $\hat{\gamma}_{se}^{(1)}$ of $\mathcal{O}(\alpha_{\rm s}\alpha_{\rm em})$. The computation of such anomalous dimensions for the operators studied in this work is discussed in Chapter 7. On the other hand, the QCD evolution matrix $\hat{U}_{\rm QCD}$ involves the strong anomalous dimensions, which are known at different orders in $\alpha_{\rm s}$ depending on the operator. The specific operators studied in this work are quark bilinear operators and the semi-leptonic operator O_1 entering the weak effective Hamiltonian of Eq. (2.3). In the latter case, since in the absence of e.m. corrections the leptonic part of the four-fermion operator does not contribute to the calculation of RCs, the strong anomalous dimensions are easily related to those of bilinear operators. These have been computed in the RI' scheme up to four loops for Z_q, Z_P and Z_S (in the Landau gauge) in Ref. [73] and up to three loops for Z_T in Ref. [74]. The other bilinears, namely Z_A and Z_V, do not have strong anomalous dimensions due to the QCD Ward identities valid at all orders of $\alpha_{\rm s}$. The calculation of the four-loop QCD evolution matrix of non-mixing operators is discussed in Chap. 6.

Since η evolves in a different way with respect to $\Delta Z^{\rm QED}$ and $Z^{\rm QCD}$, the analysis splits up into a third branch, as schematically depicted in Fig. 4.3, in which we focus on the calculation of η.

We choose to evolve RCs computed at different values of $(ap)^2$ to the reference scale $\mu_0 = 1/a$. Therefore, the RC estimators $\left[Z_O\right]^{\rm D}$ are obtained by applying the evolution operator $\hat{U}(1/a^2, p^2; \alpha_{\rm em})$ to the RC estimators $\left[Z_O\right]^{\rm C}$ obtained at the previous step, according to the evolution rules in Eqs. (4.34)-(4.36).

E. Perturbative subtraction of $\mathcal{O}(g^2a^2)$ cut-off effects In the numerical calculation, the RCs evolved to the reference scale $\mu_0 = 1/a$ still have a dependence on the

[5]The contribution of $\Delta Z^{\rm QED}$ is absent in the evolution of $\tilde{\eta}$, in both the mixing and non-mixing cases.

Table 4.2. Parameters used for the evaluation of the perturbative expansion of quark propagator and amputated bilinear/four-fermion vertices, corresponding to the lattice setup of this work: improved Iwasaki action for gluons, Wilson gauge action for photons, both in Landau gauge ($\lambda = 0$), and twisted mass action at maximal twist for quarks.

Analysis	C_F	c_0	c_1	c_3	$c_{\rm SW}$	λ
QCD	4/3	3.648	−0.331	0	0	0
QED	1	1.0	0	0	0	0

renormalization scale a^2p^2 at which they have been initially computed. Such residual dependence signals the presence of either $\mathcal{O}(a^2)$ discretization effects or higher-order perturbative corrections not included in the evolution function $\hat{U}(1/a^2, p^2; \alpha_{\rm em})$. In order to reduce discretization effects on the RCs we can analytically subtract from the perturbative $\mathcal{O}(a^2)$ contributions. They have been computed at one loop in lattice perturbation theory in Ref. [75] for the quark propagator and the amputated Green functions of bilinear operators, and in Ref. [76] for four-fermion operators. The calculations of Refs. [75, 76] employ the Wilson/clover action for massless fermions and the Symanzik improved action for gluons. Their results exhibit a rather nontrivial dependence on the external momentum (p), and they are explicit functions of the color factor (C_F), gauge parameter (λ), lattice spacing (a), clover coefficient ($c_{\rm SW}$) and coupling constant (g); furthermore, most numerical coefficients depend on the Symanzik parameters of the gluon action (c_i). We notice that the same perturbative results can be used to subtract cut-off effects to RCs computed in pure QCD and in pure QED, with appropriate changes of the parameters and coupling constants. The results of Refs. [75, 76] are valid for twisted mass fermions at maximal twist and the maximal twist configuration, in our case, is achieved through the θ-average of the RC estimators. Given the linearity of the average, we can apply the perturbative subtraction separately to the RC estimators evaluated at opposite θ angles, i.e. before the average, obtaining the same final result. The values of the parameters used in the analysis, according to our lattice setup, are shown in Table 4.2. We observe that the perturbative corrections to RCs in the RI'-MOM scheme start at order $\mathcal{O}(\alpha_{\rm s}a^2)$ in QCD and $\mathcal{O}(\alpha_{\rm em}a^2)$ in QED. As a consequence, the non-factorizable part of the RCs η is free from pure QCD and QED cut-off effects and is only affected by subleading corrections of order $\mathcal{O}(\alpha_{\rm s}\alpha_{\rm em}a^2)$. The subtraction of such discretization effects would require a two-loop calculation in lattice perturbation theory with different couplings, which (to our knowledge) is not present in the literature. Therefore, we do not apply any perturbative subtraction on η.

Using the RI' renormalization conditions on the results of Refs. [75, 76], we determine the $\mathcal{O}(\alpha_{\rm s}a^2)$ and $\mathcal{O}(\alpha_{\rm em}a^2)$ corrections to $Z_O^{\rm QCD}$ and $\Delta Z_O^{\rm QED}$ respectively, namely $\mathcal{F}_O^{\rm QCD}$ and $\mathcal{F}_O^{\rm QED}$, and we compute the subtracted RC estimators as follows

$$\begin{aligned}
&[Z_O^{\rm QCD}]^{\rm E}\left(\beta,\theta,\mu^{\rm sea},p^2\right) = [Z_O^{\rm QCD}]^{\rm D}\left(\beta,\theta,\mu^{\rm sea},p^2\right) - \frac{\alpha_{\rm s}^{(0)}}{4\pi}\,\mathcal{F}_O^{\rm QCD}(\beta,p)\\
&[\Delta Z_O^{\rm QED}]^{\rm E}\left(\beta,\theta,\mu^{\rm sea},p^2\right) = [\Delta Z_O^{\rm QED}]^{\rm D}\left(\beta,\theta,\mu^{\rm sea},p^2\right) - \mathcal{F}_O^{\rm QED}(\beta,p)\\
&[\eta_O]^{\rm E}\left(\beta,\theta,\mu^{\rm sea},p^2\right) = [\eta_O]^{\rm D}\left(\beta,\theta,\mu^{\rm sea},p^2\right)\ .
\end{aligned} \tag{4.38}$$

Here the coupling $\alpha_{\rm s}^{(0)}$ is the *boosted* coupling proposed in Refs. [59, 77] and defined as

$$\alpha_{\rm s}^{(0)} = \frac{1}{4\pi} \frac{g_0^2}{\langle W^{1\times 1}\rangle} \ , \tag{4.39}$$

where $g_0^2 \equiv 6/\beta$ is the standard lattice coupling and $\langle W^{1\times 1}\rangle$ is the value of the plaquette, computed non-perturbatively and averaged on the gauge configurations.

F. Evaluation of residual cut-off effects In order to account for the residual discretization effects in the calculation of the RCs, we follow two different approaches:

- *Extrapolation method* (M1) After subtraction of the $\mathcal{O}(a^2)$ at one loop in perturbation theory, according to Eq. (4.38), we extrapolate the RCs linearly to $a^2p^2 \to 0$. Specifically we fit the RCs computed at the Step E in the large momentum region

$$1.0 \lesssim a^2\tilde{p}^2 \lesssim 3.0 \tag{4.40}$$

  with the fit Ansatz

$$[Z_O]^{\rm E}\left(\beta,\theta,\mu^{\rm sea},p^2\right) = [Z_O]^{\rm F}_{\rm M1}\left(\beta,\theta,\mu^{\rm sea}\right) + \lambda_O\ a^2\tilde{p}^2 \ , \tag{4.41}$$

  and we take the intercept $[Z_O]^{\rm F}\left(\beta,\theta,\mu^{\rm sea}\right)$ as the new result for the RC estimator. We refer to this method as M1.

- *Interpolation method* (M2) In this approach we do not attempt any additional subtraction of discretization effects, besides the perturbative one. The final estimates of RCs are obtained by taking directly the results of $[Z_O]^{\rm E}\left(\beta,\theta,\mu^{\rm sea},p^2\right)$ at a fixed value of $\tilde{p}^2$, namely $\tilde{p}^2_{\rm ref} = 13\ {\rm GeV}^2$. In practice, this is done by fitting the RCs to a constant in a small momentum interval around $\tilde{p}^2_{\rm ref}$, determined by its 5 nearest neighbours. Therefore, symbolically we have that

$$[Z_O]^{\rm F}_{\rm M2}\left(\beta,\theta,\mu^{\rm sea}\right) = [Z_O]^{\rm E}\left(\beta,\theta,\mu^{\rm sea},p^2\right)\Big|_{\tilde{p}^2=\tilde{p}^2_{\rm ref}} \ . \tag{4.42}$$

  The idea behind this approach is that, once RCs are combined with bare quantities, so as to construct the physical observables of interest, the residual $\mathcal{O}(a^2)$ effects, which are present in both RCs and bare quantities, will be extrapolated away in the continuum limit. We refer to this method as M2.

G. Combined sea chiral extrapolation The RC estimators so far computed still have a dependence on the sea quark mass. The RCs are usually extrapolated with a linear fit in $(M_P^{\rm sea})^2$, in a similar way as in the valence sector. In our analysis, however, we only have two ensembles available at $\beta = 1.90$, namely A4 and A5 (see Table 4.1), and a linear fit on just two points is not reliable. In order to overcome this problem, we exploit the facts that the dependence on the pseudoscalar sea meson mass (or, equivalently, on the sea quark masses) is in general very mild and that it does not vary sensibly with the coupling β. Therefore, we perform a *combined* chiral extrapolation in which we force the slope to be the same for all three β's, with the fit Ansatz

$$[Z_O]^{\rm F}\left(\beta,\theta,\mu^{\rm sea}\right) = a_O(\beta,\theta) + b_O^{\rm fixed}\ (M_P^{\rm sea})^2 \ . \tag{4.43}$$

The chirally extrapolated RC estimators are then obtained from the intercept of the fit, namely

$$[Z_O]^{\mathrm{G}}(\beta,\theta) = a_O(\beta,\theta)\ . \tag{4.44}$$

Since in the pure QED analysis, fermion propagators are generated already in the massless limit, this step is skipped in that case.

H. Average on the twist angle θ The last step of the calculation is the average on the twist angle θ, which is necessary to achieve the $\mathcal{O}(a)$ improvement of RCs out of maximal twist, which is proven in Ref. [56, 68].

Finally, the results for the RCs are obtained as

$$Z_O(\beta) \equiv [Z_O]^{\mathrm{H}}(\beta) = \frac{1}{2}\left([Z_O]^{\mathrm{G}}(\beta,\theta_p) + [Z_O]^{\mathrm{G}}(\beta,\theta_m)\right)\ . \tag{4.45}$$

4.3 Numerical results

In this section we present the numerical results of the QCD+QED RI'-MOM analysis of renormalization constants for quark bilinear operators in Eq. (3.47) and the semi-leptonic weak operators in Eq. (3.61) involved in the calculation of light-meson leptonic decay rates.
The RCs are extracted following the procedure outlined in the previous Section 4.2 and with the lattice setup described in Sec. 4.1. We remind that the above procedure is specific for the $N_f = 4$ gauge configurations produced by ETMC and used in this work, which require, among others, an average over the twist angle θ to achieve the $\mathcal{O}(a)$ improvement of lattice correlators. We review here all steps of the analysis showing their application to the calculation of RCs of bilinear and weak four-fermion operators.

The RCs and their e.m. corrections are computed in the RI'-MOM scheme applying the renormalization conditions derived up to $\mathcal{O}(\alpha_{\mathrm{em}})$ in Chap. 3.1. They have been evaluated at different renormalization scales $\mu^2 = p^2$, where p is the lattice four-momentum of the external fermion fields. The first step (step A) of the analysis consists in averaging results obtained at values of p equivalent under the (exact) $\hat{H}(4)$ discrete lattice symmetry, consisting in 90° rotations of spatial components of a four-vector and its reflection along the temporal axis. The effect of such operation is shown in Fig. 4.4, where we show the results for the RCs ΔZ_q, ΔZ_P and ΔZ_{11} computed in QCD+QED and in QED. The average, as expected, yields a reduction of the statistical uncertainty. The $\hat{H}(4)$-averages are obtained at fixed masses and values of the Wilson r parameter. In order to remove the dependence on the Wilson parameter, RCs obtained at opposite values of r ($r = \pm 1$) are averaged (step B). The dependence on the valence quark masses in then removed by extrapolating the RCs (step C) to the chiral limit, with a fit ansatz that takes into account the eventual presence of a Goldstone pole contamination to the amputated and projected vertex. As explained in the previous section, Goldstone poles ($\sim 1/M_P^2$) occurring in QCD vertices, induce double poles ($\sim 1/M_P^4$) in the corresponding e.m. corrections. The valence chiral extrapolation at fixed a momentum scale $(a\tilde{p})^2 \sim 1$ is reported in Figs. 4.5 and 4.6 for a subset of bilinear and semi-leptonic vertices, respectively.

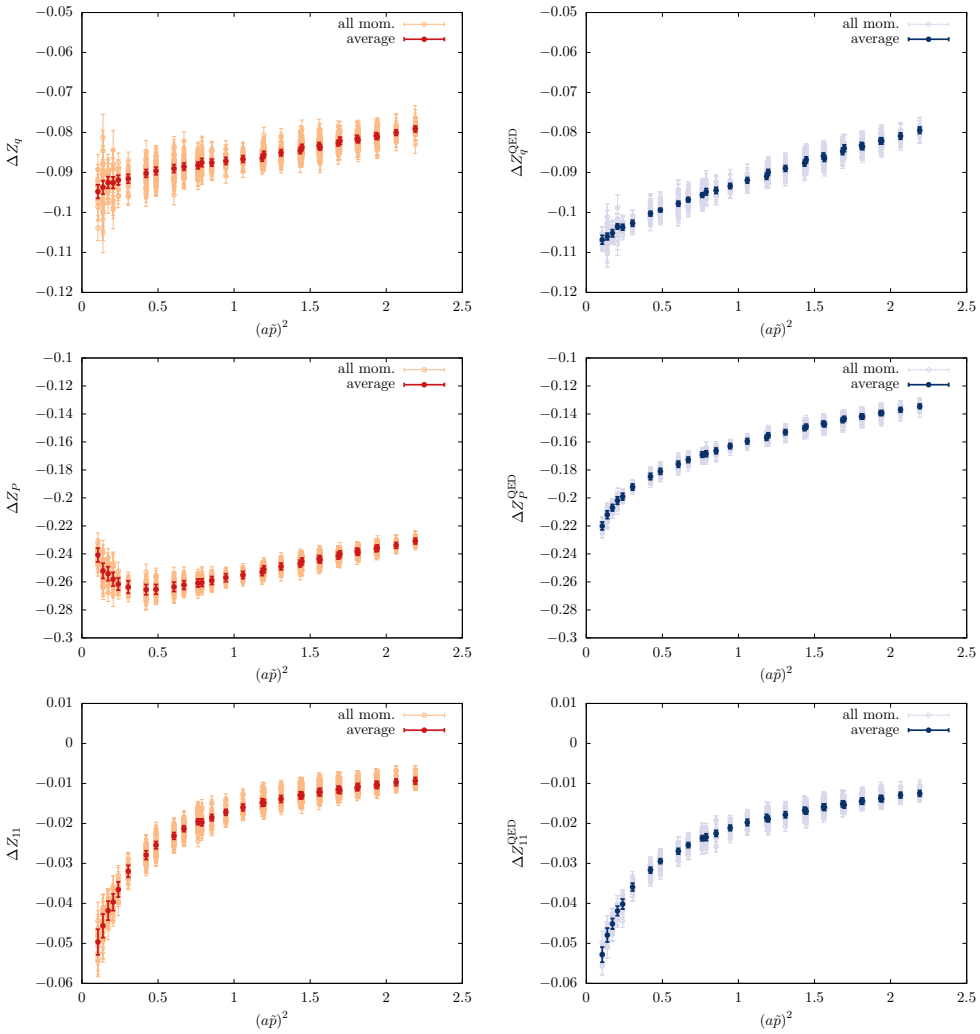

Figure 4.4. [A] *Average of equivalent momenta:* electromagnetic corrections to the RCs Z_q, Z_P and Z_{11} evaluated in the full QCD+QED theory (left panels) and in pure QED (right panels) for the ensemble B2m (see Table 4.1). Results obtained for the complete set of momenta (see Sec. 4.1.1) are reported in light colours, while dark points correspond to the $\hat{H}(4)$ averaged RCs.

While the dependence on M_P^2 is perfectly linear for Γ_V, Γ_{12} and their e.m. corrections, the presence of GB contributions is instead evident in the extrapolation of Γ_P and Γ_{33}, which are constructed from pseudoscalar currents. It is interesting to notice the behaviour of the scalar vertex Γ_S in Fig. 4.5: the operator O_S appears to be mildly coupled with the GB, due to the explicit breaking of parity at finite lattice spacing induced by the twisted mass regularization. However, the coefficient of the pole is much more suppressed with respect to the case of the pseudoscalar vertex. Indeed, for the ensemble B2m and at $(a\tilde{p})^2 = 1.06$ we find (in lattice units):

$$c_S^{(0)}\big|_{\mathrm{B2m},\,(a\tilde{p})^2\sim 1} = -6\,(2)\cdot 10^{-4} \quad \text{and} \quad c_P^{(0)}\big|_{\mathrm{B2m},\,(a\tilde{p})^2\sim 1} = 16\,(1)\cdot 10^{-3}\,. \tag{4.46}$$

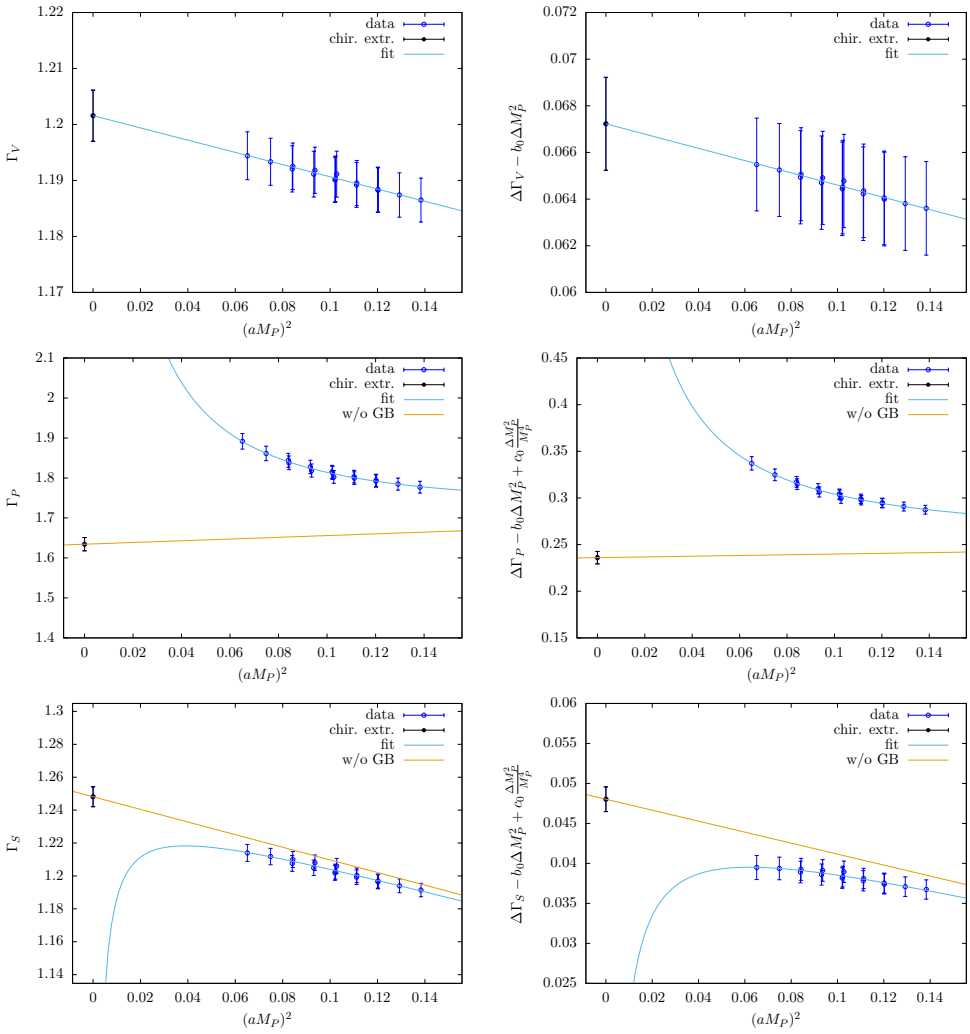

Figure 4.5. [C] *Valence chiral extrapolation* of a subset of bilinear vertices (Γ_V, Γ_P and Γ_S) and their e.m. corrections at fixed momentum $(a\tilde{p})^2 \simeq 1.06$ and for the ensemble B2m. The empty (blue) dots represent the data obtained at Step B, while the full (black) dot is the extrapolation at $M_P = 0$. The curve obtained fitting the data is reported in light blue ("fit") and, when the GB contamination is present, we also show the linear (orange) curve obtained removing the pole ("w/o GB").

Although very small, we decide to keep the coefficient c_S in the fit Ansatz since it yields a better χ^2 value. Once the RCs, computed in both QCD+QED and in QED, are extrapolated to the chiral limit, they are used to construct the non-factorizable parameter η according to Eq. (3.46). In Fig. 4.7 we show the result of this operation for the four-fermion RCs η_{11} and η_{12}, which are essential ingredients for the calculation of e.m. corrections to light-meson leptonic decay rates (see Chap. 5). As discussed in Sec. 3.4, the RCs ΔZ and ΔZ^{QED} have been computed using the *same* stochastic photon fields, in such a way that their statistical uncertainties are maximally correlated. This increases, as a consequence, the numerical precision of η: the relative statistical uncertainty is reduced by approximately a factor $\sim 2 - 10$

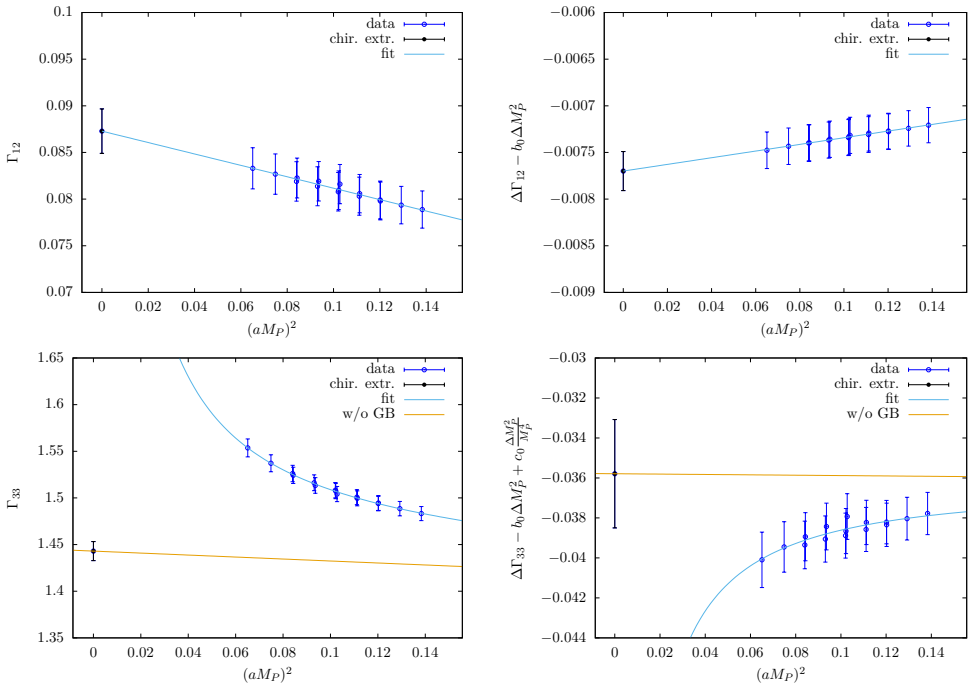

Figure 4.6. [C] *Valence chiral extrapolation* of a subset of semileptonic vertices (Γ_{12} and Γ_{33}) and their e.m. corrections at fixed momentum $(a\tilde{p})^2 \simeq 1.06$ and for the ensemble B2m. The empty (blue) dots represent the data obtained at Step B, while the full (black) dot is the extrapolation at $M_P = 0$. The curve obtained fitting the data is reported in light blue ("fit") and, when the GB contamination is present, we also show the linear (orange) curve obtained removing the pole ("w/o GB").

depending on the operator insertion. The effect of such reduction is reported in Fig. 4.8, where we compare the results of η_{11}, η_{33}, η_V and η_P computed with either correlated or uncorrelated photon fields. We notice that the reduction of the statistical uncertainty is more enhanced in the case of RCs of operators involving either vector, axial-vector or tensor currents. Scale dependent RCs are then evolved to the reference scale $\mu = 1/a$ (step D), in order to better study the impact of

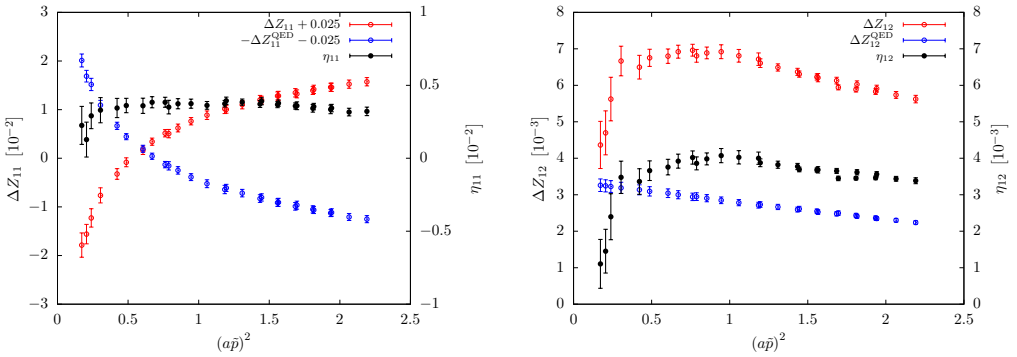

Figure 4.7. Determination of the non-factorizable RCs η_{11} and η_{12} in the ensemble B2m. The e.m. corrections ΔZ (red) and $\Delta Z^{\rm QED}$ (blue) are also reported in the plots.

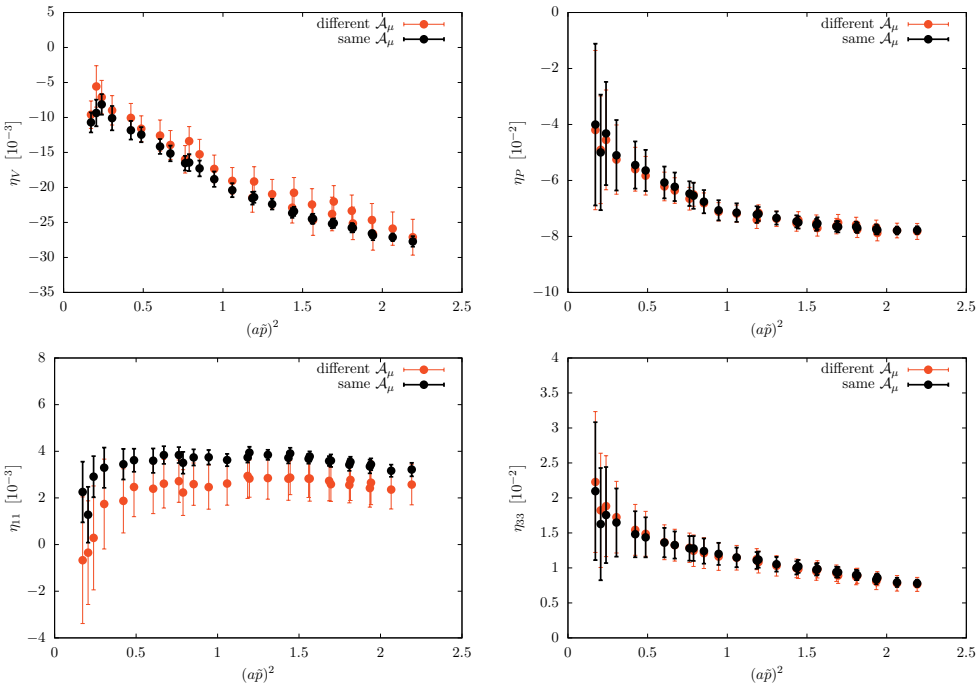

Figure 4.8. Results of η_{11}, η_{33}, η_V and η_P computed with either correlated (black dots) or uncorrelated (orange dots) photon fields [ensemble B2m]. The statistical uncertainty is significantly reduced. Such effect appears to be more pronounced when vector currents are involved (see left panels).

discretization effects, which would result in an eventual residual dependence on the renormalization scale. In the pure QCD and QED calculations, the subtraction of $\mathcal{O}(\alpha_s a^2)$ and $\mathcal{O}(\alpha_{em} a^2)$ cut-off effects can be done by using lattice perturbation theory (step E). On the other hand, an analogue subtraction is impossible for η since a two-loop calculation of $\mathcal{O}(\alpha_s \alpha_{em} a^2)$ corrections is not available in the literature. The application of these operations to the scale-dependent RCs Z_P and Z_{33} is shown in Fig. 4.9. The residual dependence on the renormalization scale a^2p^2 is ascribed to higher order cut-off effects and, in the case of scale non-invariant quantities (such as Z_P and Z_{33} in Fig. 4.9), to the effect of higher order anomalous dimensions non included in the perturbative calculations. In the high-momentum region $(a\tilde{p})^2 \gtrsim 1$, however, the scale-dependence appears to be linear and therefore it can be attributed to residual $\mathcal{O}(a^2)$ effects. In order to account for such effects we extract the RCs by applying the methods M1 and M2 described above in Section 4.2 (step F). As an example, we report in Fig. 4.10 the application of the two methods to the RCs η_P and η_{12} within the ensemble C2m. Once the RCs are determined in each ensemble, we remove their dependence on the sea quark masses by fitting the data (step G). Due to the problem outlined in the previous section, relative to the availability of only two ensembles for the coarsest lattice spacing $\beta = 1.90$, we performed a combined chiral extrapolation by requiring the slope to be equal for all three β's. The linear extrapolation in $(M_P^{\rm sea})^2$ of the RC η_{12} is reported in Fig. 4.11 for the two values of the twist angle θ. The extrapolated values are finally averaged on the angle θ (step H).

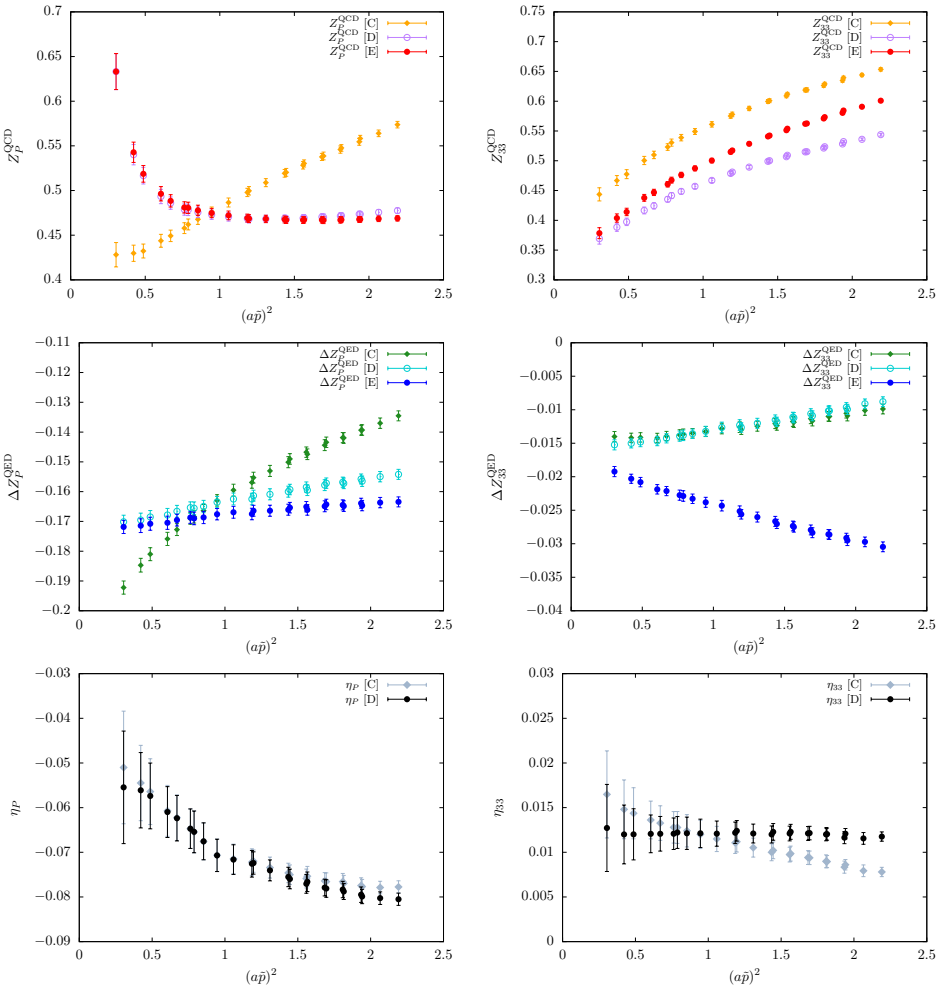

Figure 4.9. [D] *Perturbative evolution* of the RCs Z_P and Z_{33} and [E] *subtraction of discretization effects* of order $\mathcal{O}(\alpha_s a^2, \alpha_{em} a^2)$ [ensemble B2m].

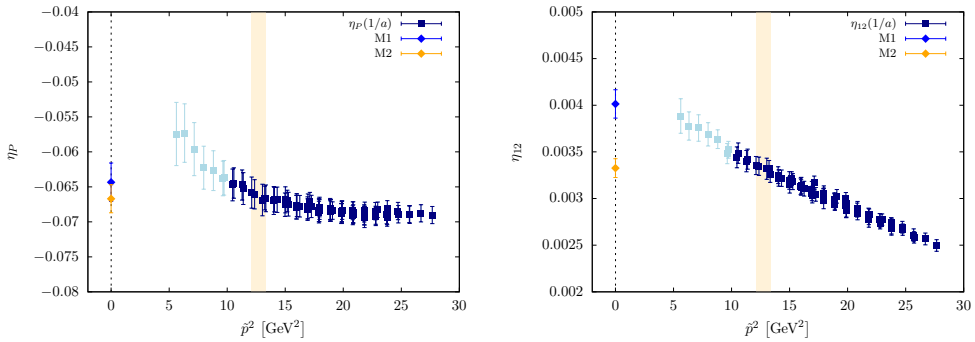

Figure 4.10. [F] *Application of methods* M1 *and* M2 to the RCs η_P and η_{12} within the ensemble C2m. Darker (blue) points corresponds to the momentum region in which the extrapolation method M1 is applied, while the orange band around ($\tilde{p}^2 \sim 13$ GeV^2 highlights the region where the data are interpolated according to the method M2. The value obtained using the method M1 (M2) is reported in blue (orange) at $\tilde{p}^2 = 0$.

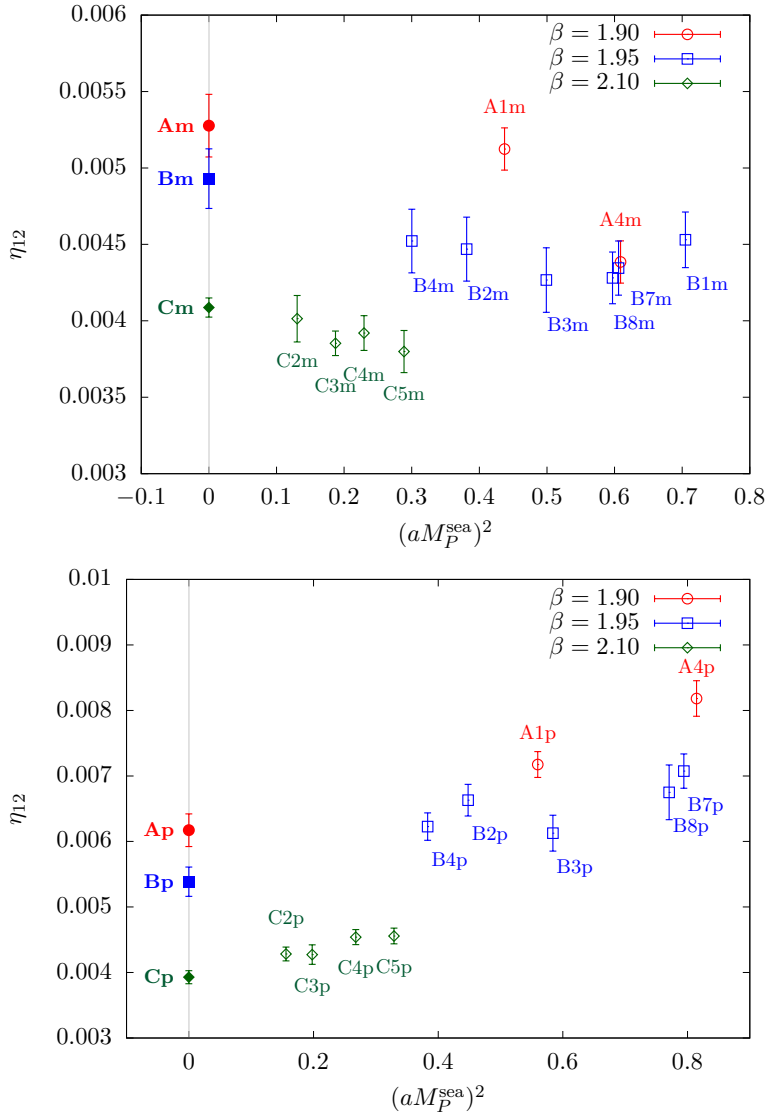

Figure 4.11. [G] *Combined sea chiral extrapolation* of η_{12} at fixed value of the twist angle: θ_m (θ_p) on the above (below) panel. The data shown in the figures are obtained at previous step F with the method M1. Results obtained at different lattice couplings are reported in different colours and shapes. The filled points at $aM_P^{\rm sea} = 0$ are the results of the combined extrapolation performed on the empty points.

In the following subsections we report the final results of the non-perturbative RCs of the bilinear and semileptonic four-fermion operators, evaluated at the scale $\mu = 1/a$ following the procedure described in the last two sections. We only show the results of the non-factorizable corrections η. As regards the QCD RCs, we adopt the values obtained in Ref. [56] since they have been computed using two additional ensembles at the coarsest lattice spacing $\beta = 1.90$ with respect to our analysis. On the other hand, the lattice determinations of QED RCs at $\mathcal{O}(\alpha_{\rm em})$ are not actually used in the calculation: they can be computed in continuum perturbation theory without discretization effects.

4.3.1 Results for quark bilinear operators

Table 4.3. Results of the non-factorizable RCs η for the quark field and the bilinear operators of Eq. (3.47), evaluated in the RI'-MOM scheme at the scale $\mu = 1/a$. The number in parentheses is the statistical uncertainty on the last significant digit.

β	Method	η_q	η_V	η_A	η_S	η_P	η_T
1.90	M1	0.0062 (11)	-0.0153 (17)	0.0142 (16)	-0.0029 (29)	-0.0921 (58)	0.0068 (15)
	M2	-0.0001 (5)	-0.0306 (8)	0.0011 (10)	-0.0093 (14)	-0.0934 (17)	-0.0115 (8)
1.95	M1	0.0082 (7)	-0.0127 (17)	0.0127 (12)	-0.0113 (21)	-0.0766 (47)	0.0069 (13)
	M2	0.0003 (5)	-0.0271 (7)	0.0020 (7)	-0.0093 (14)	-0.0873 (16)	-0.0086 (7)
2.10	M1	0.0064 (3)	-0.0123 (8)	0.0091 (6)	-0.0140 (11)	-0.0708 (24)	0.0052 (6)
	M2	0.0031 (3)	-0.0186 (4)	0.0042 (4)	-0.0120 (6)	-0.0712 (8)	-0.0024 (4)

4.3.2 Results for semileptonic weak-operators

Table 4.4. Results of the non-factorizable RCs η for semileptonic four-fermion operators of Eq. (3.61), evaluated in the RI'-MOM scheme at the scale $\mu = 1/a$. The number in parentheses is the statistical uncertainty on the last significant digit.

β	Method	$\hat{\eta}$
1.90	M1	$\begin{pmatrix} 5.16\,(61) & 5.72\,(13) & 4.39\,(76) & -7.11\,(77) & -0.22\,(7) \\ 5.60\,(12) & 5.87\,(52) & -6.44\,(61) & 5.05\,(80) & 0.19\,(3) \\ -0.70\,(4) & 0.23\,(9) & -4.4\,(27) & 18.1\,(27) & 0.04\,(1) \\ 0.21\,(10) & -0.73\,(4) & 16.7\,(36) & -1.5\,(35) & -0.01\,(1) \\ -8.06\,(91) & -4.5\,(11) & 0.07\,(60) & -12.6\,(11) & 3.60\,(63) \end{pmatrix} \cdot 10^{-3}$
	M2	$\begin{pmatrix} 3.99\,(32) & 3.45\,(15) & 3.70\,(23) & -8.49\,(15) & 0.13\,(3) \\ 3.22\,(9) & 3.08\,(34) & -8.40\,(19) & 3.80\,(23) & 0.12\,(2) \\ -0.63\,(2) & 1.02\,(3) & 8.97\,(95) & -1.31\,(89) & 0.021\,(4) \\ 1.05\,(3) & -0.63\,(1) & -1.47\,(10) & 8.6\,(11) & -0.97\,(1) \\ -8.27\,(37) & -3.37\,(47) & -0.45\,(19) & 31.93\,(39) & 1.83\,(32) \end{pmatrix} \cdot 10^{-3}$
1.95	M1	$\begin{pmatrix} 4.59\,(43) & 5.16\,(14) & 4.95\,(61) & -6.00\,(70) & 0.04\,(6) \\ 5.10\,(13) & 6.03\,(39) & -5.16\,(48) & 5.62\,(67) & 0.27\,(3) \\ -0.82\,(4) & 0.44\,(9) & 5.2\,(20) & 2.9\,(21) & 0.03\,(1) \\ 0.47\,(8) & -0.86\,(3) & 5.8\,(23) & 4.3\,(19) & 0.12\,(1) \\ -5.45\,(71) & -4.93\,(92) & 1.25\,(59) & -18.6\,(10) & 4.20\,(45) \end{pmatrix} \cdot 10^{-3}$
	M2	$\begin{pmatrix} 3.48\,(20) & 3.46\,(13) & 3.65\,(18) & -7.63\,(16) & 0.05\,(2) \\ 3.20\,(10) & 2.90\,(24) & -7.63\,(15) & 3.73\,(19) & 0.11\,(2) \\ -0.59\,(1) & 0.80\,(2) & 9.48\,(68) & -4.97\,(73) & 0.025\,(3) \\ 0.80\,(3) & -0.59\,(1) & -4.31\,(69) & 8.46\,(67) & -0.759\,(4) \\ -8.13\,(32) & -3.45\,(34) & -0.30\,(20) & 21.80\,(40) & 1.59\,(25) \end{pmatrix} \cdot 10^{-3}$
2.10	M1	$\begin{pmatrix} 3.65\,(24) & 4.01\,(6) & 3.61\,(28) & -4.77\,(37) & -0.06\,(3) \\ 3.75\,(6) & 4.58\,(17) & -4.36\,(22) & 3.96\,(36) & 0.15\,(1) \\ -0.63\,(2) & 0.29\,(3) & 8.52\,(82) & -6.33\,(80) & 0.038\,(3) \\ 0.29\,(4) & -0.67\,(2) & -4.02\,(92) & 7.83\,(91) & 0.046\,(6) \\ -4.93\,(34) & -3.36\,(41) & 0.27\,(26) & -10.92\,(51) & 3.22\,(22) \end{pmatrix} \cdot 10^{-3}$
	M2	$\begin{pmatrix} 3.17\,(13) & 3.36\,(6) & 3.23\,(12) & -5.40\,(11) & 0.01\,(1) \\ 3.11\,(5) & 3.30\,(14) & -5.28\,(7) & 3.34\,(13) & 0.12\,(1) \\ -0.56\,(1) & 0.50\,(1) & 8.13\,(35) & -5.07\,(33) & 0.028\,(2) \\ 0.50\,(2) & -0.58\,(1) & -4.21\,(33) & 7.66\,(36) & -0.326\,(3) \\ -6.04\,(13) & -3.22\,(18) & -0.06\,(9) & 4.25\,(23) & 2.13\,(15) \end{pmatrix} \cdot 10^{-3}$

5 | Light-meson leptonic decay rates in QCD+QED: results

In Chapter 3 we have extensively presented a new technique to include QED corrections at $\mathcal{O}(\alpha_{\rm em})$ to the non-perturbative evaluation of RCs of lattice operators. Then in Chapter 4 we have applied such framework to quark bilinear operators and the complete set of weak four-fermion operators entering the calculation of light-meson leptonic decay rates. The numerical analysis has been performed in the electro-quenched approximation using twisted mass fermions and $N_f = 4$ gauge configurations produced by the ETM Collaboration.

According to Eq. (2.33), the IB correction to the leptonic decay rate δR_P, defined in Eq. (2.16), gets two kind of contributions, namely

$$\delta R_P = \delta R_P^{\rm ren} + \delta R_P^{\rm ampl} \ . \tag{5.1}$$

The term $\delta R_P^{\rm ampl}$ is related to the strong IB and e.m. corrections to the decay rate, evaluated with the insertion of the QCD-renormalized weak four fermion operator into the amplitude. Its derivation from lattice correlators has been described in Sec. 2.4. In this Chapter we describe the calculation of the term $\delta R_P^{\rm ren}$, which derives instead from the e.m. corrections to the renormalization of the operator $O_1^{\text{W-reg}}$. Before computing explicitely the term $\delta R_P^{\rm ren}$, we discuss how four-fermion operators constructed with twisted mass fermions mix under renormalization due to chiral symmetry breaking and clarify the relation between the twisted and physical bases.

5.1 Chirality mixing and Twisted Mass fermions

Physical amplitudes have been computed using twisted mass fermions at maximal twist in the *physical* basis. On the other hand, the RCs of bilinear and four-fermion operators have been computed in Chap. 4 using twisted mass fermions in the *twisted* basis. The relevant observation is that the lattice action for twisted mass fermions at maximal twist in the twisted basis only differs from the standard Wilson fermion lattice action for the twisted rotation of the fermion mass term. The two actions become identical in the chiral limit. It then follows that, in any mass-independent renormalization scheme, the RCs for twisted mass operators in the twisted basis are the same as those of the corresponding operators with standard Wilson fermions. It is customary to denote these RCs, for a generic operator O, as Z_O. They are valid for both standard Wilson and twisted mass operators in the twisted basis and differ,

in general, from the RCs for twisted mass operators in the physical basis, that we denote as $\mathcal{Z}_O$.

At maximal twist the rotation from the twisted to the physical basis for both quark and lepton fields is given by

$$q_{\rm tw} = \frac{1}{\sqrt{2}}\,(1+i\gamma_5 r_q)\,q\ , \qquad \ell_{\rm tw} = \frac{1}{\sqrt{2}}\,(1+i\gamma_5 r_\ell)\,\ell\ , \tag{5.2}$$

$$\bar{q}_{\rm tw} = \frac{1}{\sqrt{2}}\,\bar{q}\ (1+i\gamma_5 r_q)\ \ , \qquad \bar{\ell}_{\rm tw} = \frac{1}{\sqrt{2}}\,\bar{\ell}\ (1+i\gamma_5 r_\ell)\ \ , \tag{5.3}$$

where q and ℓ are the quark and lepton fields in the physical basis and r_q and r_ℓ are the corresponding r-parameters. In our simulations we use opposite values of the r-parameter for the two valence quarks, $r_2 = -r_1$ ($r_i = \pm 1$). The quark and lepton bilinears then transform as

$$\begin{aligned}
\left[\overline{q}_2\gamma_\mu(1\pm\gamma_5)q_1\right]_{\rm tw} &= \pm i r_1\left[\overline{q}_2\gamma_\mu(1\pm\gamma_5)q_1\right]\ , \\
\left[\overline{q}_2(1\pm\gamma_5)q_1\right]_{\rm tw} &= \left[\overline{q}_2(1\pm\gamma_5)q_1\right]\ , \\
\left[\overline{q}_2\sigma_{\mu\nu}(1+\gamma_5)q_1\right]_{\rm tw} &= \left[\overline{q}_2\sigma_{\mu\nu}(1+\gamma_5)q_1\right]\ ;
\end{aligned} \tag{5.4}$$

$$\begin{aligned}
\left[\overline{\nu}\gamma_\mu(1-\gamma_5)\ell\right]_{\rm tw} &= \frac{1}{\sqrt{2}}\,(1-i r_\ell)\left[\overline{\nu}\gamma_\mu(1-\gamma_5)\ell\right]\ , \\
\left[\overline{\nu}(1+\gamma_5)\ell\right]_{\rm tw} &= \frac{1}{\sqrt{2}}\,(1+i r_\ell)\left[\overline{\nu}(1+\gamma_5)\ell\right]\ , \\
\left[\overline{\nu}\sigma_{\mu\nu}(1+\gamma_5)\ell\right]_{\rm tw} &= \frac{1}{\sqrt{2}}\,(1+i r_\ell)\left[\overline{\nu}\sigma_{\mu\nu}(1+\gamma_5)\ell\right]\ .
\end{aligned} \tag{5.5}$$

From Eqs. (5.4) one readily derives the relations between the quark vector and axial vector current in the two basis,

$$\begin{aligned}
(O_V)_{\rm tw} &= \left[\overline{q}_2\gamma_\mu q_1\right]_{\rm twisted} = i\,r_1\ \left[\overline{q}_2\gamma_\mu\gamma_5 q_1\right] = i\,r_1\,O_A\ , \\
(O_A)_{\rm tw} &= \left[\overline{q}_2\gamma_\mu\gamma_5 q_1\right]_{\rm twisted} = i\,r_1\ \left[\overline{q}_2\gamma_\mu q_1\right] = i\,r_1\,O_V\ ,
\end{aligned} \tag{5.6}$$

with the other bilinear operators remaining unaltered, namely $(O_\Gamma)_{\rm tw} = O_\Gamma$, with $\Gamma = \{S, P, T\}$. In turn, one determines the relation between the RCs in the two basis

$$\begin{aligned}
\hat{O}_V = \mathcal{Z}_V\,O_V = -i\,r_1\,(\hat{O}_A)_{\rm tw} = -i\,r_1\,Z_A\,(O_A)_{\rm tw} = Z_A\,O_V\ , \\
\hat{O}_A = \mathcal{Z}_A\,O_V = -i\,r_1\,(\hat{O}_V)_{\rm tw} = -i\,r_1\,Z_V\,(O_V)_{\rm tw} = Z_V\,O_A\ ,
\end{aligned} \tag{5.7}$$

where the hat ($\hat{}$) denotes the generic renormalized operator. One then sees from Eq. (5.7) that the RC $\mathcal{Z}_V$ of the vector current in the physical basis, with $r_1 = -r_2$, is simply the RC of the axial current in the twisted basis, which in turn is just Z_A computed with Wilson fermions in the chiral limit. Analogously, $\mathcal{Z}_A$ in the physical basis, with $r_1 = -r_2$, corresponds to Z_V computed with Wilson fermions in the chiral limit. For the other bilinear operators it holds the identity $\mathcal{Z}_\Gamma = Z_\Gamma$.

From the transformations (5.4) and (5.5) one can also derive the relations between the four-fermion operators $O_1 - O_5$ of Eq. (3.61) in the physical and twisted basis,

$$[\vec{O}]_{\rm tw} = \mathcal{S}\cdot\vec{O} \tag{5.8}$$

where

$$\mathcal{S} = \frac{1}{\sqrt{2}} \begin{pmatrix} -i\,r_1\,(1-ir_\ell) & 0 & 0 & 0 & 0 \\ 0 & +i\,r_1\,(1-ir_\ell) & 0 & 0 & 0 \\ 0 & 0 & (1+ir_\ell) & 0 & 0 \\ 0 & 0 & 0 & (1+ir_\ell) & 0 \\ 0 & 0 & 0 & 0 & (1+ir_\ell) \end{pmatrix} \tag{5.9}$$

As a consequence, the set of operators $\vec{O}$ defined in the *physical* basis and renormalized in the RI'-MOM scheme will be related to the corresponding bare ones as follows

$$\begin{aligned} \vec{O}^{\rm RI'} &= \mathcal{S}^{-1}\big[\vec{O}^{\rm RI'}\big]_{\rm tw} = \mathcal{S}^{-1}\,Z_O\,\big[\vec{O}\big]_{\rm tw} = \mathcal{S}^{-1}\,Z_O\,\mathcal{S}\,\vec{O} \\ &\equiv \mathcal{Z}_O\,\vec{O}\,. \end{aligned} \tag{5.10}$$

In particular, for the weak operator $O_1^{\rm RI'}$ in Eq. (2.13), one finds

$$O_1^{\rm RI'} = \sum_{j=1}^{5} \mathcal{Z}_{1j}\,O_j = Z_{11}\,O_1 - Z_{12}\,O_2 - \overline{r}\,\sum_{j=3}^{5} Z_{1j} O_j\ , \tag{5.11}$$

with $\overline{r} \equiv r_1 r_\ell = -r_2 r_\ell$. From Eq. (5.11) we deduce in particular that the mixing coefficients of O_1 with the operators $O_{3,4,5}$ are odd in the parameter $\overline{r}$, defined as the product of the Wilson r parameters of the valence quarks and the lepton. Thus, we can eliminate the mixing with these operators by simply averaging the numerical results of the $\mathcal{O}(\alpha_{\rm em})$ amplitudes over the two possible values $\overline{r} = \pm 1$. Moreover, the matrix element of the operator O_5 between a pseudoscalar meson and the vacuum vanishes, so that the mixing with the operator O_5 cannot contribute to the decay rate.

Therefore, neglecting the mixing with operators $O_{3,4,5}$, Eq. (5.11) for the renormalized operator $O_1^{\rm RI'}$ can be rewritten as

$$\begin{aligned} O_1^{\rm RI'}(\mu) &= \left[\,1 + \frac{\alpha_{\rm em}}{4\pi}\left(\Delta Z^{\rm QED}(\mu a)_{11} + \eta(\mu a, \alpha_s(1/a))_{11}\right)\right] O_1^\chi(a) \\ &\quad - \frac{\alpha_{\rm em}}{4\pi}\left(\Delta Z_{12}^{\rm QED} + \eta(\alpha_s(1/a))_{12}\right) O_2^\chi(a)\,, \end{aligned} \tag{5.12}$$

where we have expanded the RCs at first order in $\alpha_{\rm em}$ and introduced the QCD-renormalized operators in the *physical* basis

$$\begin{aligned} O_1^\chi = (\mathcal{Z}_O^{\rm QCD}\,\vec{O})_1 &= \bar{q}_2\gamma^\mu\left(\mathcal{Z}_V^{\rm QCD} - \mathcal{Z}_A^{\rm QCD}\,\gamma_5\right) q_1\ \bar{\nu}_\ell\gamma_\mu(1-\gamma_5)\ell \\ &= \bar{q}_2\gamma^\mu\left(Z_A^{\rm QCD} - Z_V^{\rm QCD}\,\gamma_5\right) q_1\ \bar{\nu}_\ell\gamma_\mu(1-\gamma_5)\ell\ , \end{aligned} \tag{5.13}$$

$$\begin{aligned} O_2^\chi = (\mathcal{Z}_O^{\rm QCD}\,\vec{O})_2 &= \bar{q}_2\gamma^\mu\left(\mathcal{Z}_V^{\rm QCD} + \mathcal{Z}_A^{\rm QCD}\,\gamma_5\right) q_1\ \bar{\nu}_\ell\gamma_\mu(1-\gamma_5)\ell \\ &= \bar{q}_2\gamma^\mu\left(Z_A^{\rm QCD} + Z_V^{\rm QCD}\,\gamma_5\right) q_1\ \bar{\nu}_\ell\gamma_\mu(1-\gamma_5)\ell\ . \end{aligned} \tag{5.14}$$

In Eq. (5.12) we have explicitly indicated the dependence of the various terms on $\alpha_{\rm s}$ and the renormalization scale μ. Since the mixing of the *bona fide* $(8,1)$ operator O_1^χ with O_2^χ is a consequence of the explicit chiral symmetry breaking of Wilson-like fermions on the lattice, the corresponding coefficient is due to lattice artefacts and can only be a function of the lattice bare coupling constant $\alpha_s(1/a)$ [64]. The RCs $Z_{V,A}^{\rm QCD}$, $\Delta Z^{\rm QED}$ and η in the equations above are defined in the *twisted* basis.

5.2 Calculation of $\delta R_P^{\rm ren}$

The correction to the decay rate $\delta R_P^{\rm ren}$ can be computed in analogy with $\delta R_P^{\rm ampl}$ as

$$\delta R_P^{\rm ren} = 2\,\frac{\delta A_P^W}{A_P^{(0)}}\ , \tag{5.15}$$

where δA_P^W is the e.m. correction from both the matching of the four-fermion lattice weak operator to the W-renormalization scheme and from the mixing with several bare lattice four-fermion operators generated by the breaking of chiral symmetry with the twisted-mass fermion action which we are using. The e.m. correction δA_P^W can be evaluated inserting into the expression for the amplitude of the decay $P \to \ell\nu$, the term of order $\alpha_{\rm em}$ of the renormalized operator $O_1^{\text{W-reg}}(M_W)$. Combining Eqs. (2.13) and (5.12) and choosing $\mu = 1/a$ as renormalization scale in the intermediate RI'-MOM scheme, we obtain

$$\begin{aligned} O_1^{\text{W-reg}}(M_W) \;=\; & O_1^\chi(a) + \frac{\alpha_{\rm em}}{4\pi}\left[2\left(1-\frac{\alpha_s(1/a)}{4\pi}\right)\log\left(a^2M_W^2\right) + C^{\text{W-RI'}}\right] O_1^\chi(a) + \\ & + \frac{\alpha_{\rm em}}{4\pi}\left[\Delta Z_{11}^{\rm QED}(1/a) + \eta_{11}(\alpha_s(1/a))\right] O_1^\chi(a) - \\ & - \frac{\alpha_{\rm em}}{4\pi}\left[\Delta Z_{12}^{\rm QED} + \eta_{12}(\alpha_s(1/a))\right] O_2^\chi(a)\ . \end{aligned} \tag{5.16}$$

The matching coefficient $C^{\text{W-RI'}}$, as well as the pure QED corrections $\Delta Z_{11,12}^{\rm QED}$ are evaluated in perturbation theory at order $\mathcal{O}(\alpha_{\rm s}^0)$. In a generic covariant gauge we have

$$\begin{aligned} C^{\text{W-RI'}} &= -5.7825 + 1.2373\,\xi\ , \\ \Delta Z_{11}^{\rm QED}(1/a) &= -9.7565 - 1.2373\,\xi\ , \\ \Delta Z_{12}^{\rm QED} &= 0.5357\ , \end{aligned} \tag{5.17}$$

where ξ is the photon gauge parameter, with $\xi = 0\,(1)$ in the Feynman (Landau) gauge. It is worth noting that the renormalized operator in the W-regularization scheme is gauge independent, at any order of perturbation theory. In particular, as shown by Eq. (5.17), at first order in $\alpha_{\rm em}$ and at zero order in $\alpha_{\rm s}$ the gauge dependence of the matching coefficient of O_1^χ cancels in the sum $C^{\text{W-RI'}} + \Delta Z_{11}^{\rm QED} = -15.539$. By contrast, for the matching coefficient of O_2^χ, the two terms $\Delta Z_{12}^{\rm QED}$ and η_{12} are separately gauge independent.

The e.m. correction $\delta A_P^{\rm W}$ can be evaluated as follows,

$$\delta A_P^{\rm W} = \frac{\langle 0|\,\text{Tr}\left\{\delta O_1^{\text{W-reg}}(M_W)\ \bar\ell\gamma_0(1-\gamma_5)\nu\right\}|P^{(0)}\rangle}{\langle 0|\,\text{Tr}\left\{O_1^\chi(a)\ \bar\ell\gamma_0(1-\gamma_5)\nu\right\}|P^{(0)}\rangle}\ A_P^{(0)} \tag{5.18}$$

where $\delta O_1^{\text{W-reg}}(M_W) \equiv O_1^{\text{W-reg}}(M_W) - O_1^\chi$ and $A_P^{(0)}$ is the QCD renormalized axial current in Eq. (2.42). We then note that O_1^χ and O_2^χ entering Eq. (5.16) give opposite contributions to the tree-level amplitude, i.e.

$$\begin{aligned} \langle 0|\,\text{Tr}\left\{O_1^\chi(a)\ \bar\ell\gamma_0(1-\gamma_5)\nu\right\}|P^{(0)}\rangle &= -\,\langle 0|\,\text{Tr}\left\{O_2^\chi(a)\ \bar\ell\gamma_0(1-\gamma_5)\nu\right\}|P^{(0)}\rangle \\ &= -A_P^{(0)}\,X_P^{\ell,0}\ . \end{aligned} \tag{5.19}$$

Therefore one obtains

$$\delta A_P^W = Z^{\text{W-reg}} A_P^{(0)} \ , \tag{5.20}$$

with

$$\begin{aligned} Z^{\text{W-reg}} &= \frac{\alpha_{\rm em}}{4\pi}\left[2\left(1-\frac{\alpha_s(1/a)}{4\pi}\right)\log\left(a^2M_W^2\right) - 15.0033 + \right. \\ &\left. \eta_{11}(\alpha_s(1/a)) + \eta_{12}(\alpha_s(1/a))\right] \ . \end{aligned} \tag{5.21}$$

As already noted, the contribution δA_P^W of the matching factor at order $\alpha_{\rm em}$ to the decay amplitude, expressed by Eqs. (5.20) and (5.21), is gauge independent. It then follows that also the order $\alpha_{\rm em}$ contribution of the bare diagrams to the amplitude, expressed by the other terms in Eq. (2.37), is by itself gauge independent. Therefore, we can numerically evaluate the two contributions separately by making different choices for the gluon and the photon gauge in the two cases[1]. In particular, we have chosen to compute the matching factor $Z^{\text{W-reg}}$ of Eq. (5.21) in the Landau gauge for both gluons and photons, because this makes the RI' scheme equivalent to RI up to higher orders in the perturbative expansions. On the other hand, in the calculation of the physical amplitudes described in Sec. 2.4 (and already computed in Ref. [6]) a stochastic photon generated in the Feynman gauge has been used, which has been adopted also in the calculation of $\Gamma_0^{\rm pt}(L)$ in Ref. [49].

5.2.1 Dealing with the lepton self-energy

As discussed in Ref. [14], when we compute the difference $\Gamma_0(L) - \Gamma_0^{\rm pt}(L)$ in Eq. (2.2) at leading order in $\alpha_{\rm em}$, the contribution from the lepton wave function RC cancels out provided, of course, it is evaluated in both $\Gamma_0(L)$ and $\Gamma_0^{\rm pt}(L)$ in the same W-regularization scheme and in the same photon gauge. Since $\Gamma_0^{\rm pt}(L)$ has been computed in Ref. [49] by omitting the lepton wave function RC contribution in the Feynman gauge, we have to subtract the analogous contribution from Eq. (5.21) in the Feynman gauge. The QCD and QED corrections to the the lepton wave function RC at $O(\alpha_{\rm em})$ factorize, so that their contribution does not enter into the non-perturbative determination of the matrix η, which only contains, by its definition, non-factorisable QCD+QED contributions. Therefore, as discussed in Ref. [14], the subtraction of the lepton wave function RC only requires the replacement of $Z^{\text{W-reg}}$ in Eq. (5.21) by the subtracted matching factor

$$\tilde{Z}^{\text{W-reg}} = Z^{\text{W-reg}} - \frac{1}{2}\Delta Z_\ell^{\text{W-reg}}, \tag{5.22}$$

where

$$\Delta Z_\ell^{\text{W-reg}} = \frac{\alpha_{\rm em}}{4\pi}\left[-\log\left(a^2M_W^2\right) - 13.3524\right] \ . \tag{5.23}$$

The final expression to be used in Eq. (5.15) is therefore

$$\delta A_P^W = \tilde{Z}^{\text{W-reg}} A_P^{(0)} \ , \tag{5.24}$$

[1]It should be noted, however, that while $Z^{\text{W-reg}}$ of Eq. (5.21) is gauge independent at any order of perturbation theory, its actual numerical value may display a residual gauge dependence due to higher order terms in the non-perturbative determination of η_{11} which are neglected in the perturbatively evaluated matching coefficient.

with

$$\tilde{Z}^{\text{W-reg}} = \frac{\alpha_{\text{em}}}{4\pi}\left[\left(\frac{5}{2} - 2\,\frac{\alpha_s(1/a)}{4\pi}\right)\log\left(a^2 M_W^2\right) - 8.3271 + \eta_{11}(\alpha_s(1/a)) + \eta_{12}(\alpha_s(1/a))\right] . \tag{5.25}$$

To make contact with the factorization approximation introduced in Refs. [4, 26], we rewrite Eq. (5.25) as

$$\tilde{Z}^{\text{W-reg}} \equiv Z^{\,\text{fact}} \cdot Z^{\text{W-reg}}_{\eta=0} \tag{5.26}$$

where $Z^{\text{W-reg}}_{\eta=0}$ is the result in the factorization approximation (i.e with $\eta = 0$ and $Z^{\,\text{fact}} = 1$),

$$Z^{\text{W-reg}}_{\eta=0} = \frac{\alpha_{\text{em}}}{4\pi}\left[\left(\frac{5}{2} - 2\frac{\alpha_s(1/a)}{4\pi}\right)\log\left(a^2 M_W^2\right) - 8.3271\right] , \tag{5.27}$$

and $Z^{\,\text{fact}}$ is the factor correcting the result for $\tilde{Z}^{\text{W-reg}}$ to include the entries of the matrix η determined in Chap. 4

$$Z^{\,\text{fact}} \equiv 1 + \frac{\alpha_{\text{em}}}{4\pi}\,\frac{\eta_{11}(\alpha_s(1/a)) + \eta_{12}(\alpha_s(1/a))}{Z^{\text{W-reg}}_{\eta=0}} . \tag{5.28}$$

The values of the coefficients $Z^{\text{W-reg}}_{\eta=0}$ and Z^{fact} are collected in Table 5.1 for the three values of the inverse coupling β adopted in this work and for $\mu = 1/a$. We remind that the two methods M1 and M2, introduced in Sec. 4.2, correspond to different treatments of the $\mathcal{O}(a^2\mu^2)$ discretisation effects in the computation of η. The difference of the results obtained with these two methods will enter into the systematic uncertainty labelled as $()_{input}$ in Sec. 5.4 below. The results for $\eta_{11}(\alpha_s(1/a))$ and $\eta_{12}(\alpha_s(1/a))$ are reported in Tab. 4.4. The results in Table 5.1 show that the factorization approximation is not justified, the non-factorizable corrections being of order $\mathcal{O}$(12-18%) for $Z^{\text{W-reg}}$.

Table 5.1. Values of the coefficients $Z^{\text{W-reg}}_{\eta=0}$ (see Eq. (5.27)) and Z^{fact} (see Eq. (5.28)) calculated for the three values of the inverse coupling β adopted in this work and at the scale $\mu = 1/a$. The evaluation of the RCs in the RI'-MOM scheme has been carried out in Chap. 4 using the methods M1 and M2.

β	$Z^{\text{W-reg}}_{\eta=0}$	Z^{fact}	
		M1	M2
1.90	0.00542 (11)	1.184 (11)	1.126 (7)
1.95	0.00519 (10)	1.172 (9)	1.123 (5)
2.10	0.00440 (7)	1.160 (6)	1.136 (4)

We close this section by noting that Eq. (5.15) implies that the contribution to δR_P from the matching factor in Eq. (5.24) amounts to

$$\delta R_P^{\text{ren}} = 2\tilde{Z}^{\text{W-reg}} . \tag{5.29}$$

Such a term is mass independent and only depends on the operator mediating the process. It follows that all the matching and mixing contributions to the axial amplitude contributing to $\delta R_P^{\rm ren}$ cancel exactly in the difference between the corrections corresponding to two different channels, e.g. $\delta R_K^{\rm ren} = \delta R_\pi^{\rm ren}$ cancel in the difference $\delta R_{K\pi} = \delta R_K - \delta R_\pi$. A similar cancellation also occurs in the difference between the corrections to the amplitudes corresponding to the meson P decaying into two different final-state leptonic channels. In Ref. [6] this property has been exploited to compute the leading IB correction to the ratio $\Gamma(K_{\mu_2})/\Gamma(\pi_{\mu_2})$. However, the calculation of Ref. [6], although insensitive to $\delta R_P^{\rm ren}$, is affected by a systematical uncertainty due to the factorization approximation adopted in the renormalization of quark masses, which enters the calculation of $\delta R_P^{\rm ampl}$. As we have shown in Table 2.1, non-factorizable contributions to the mass RC $\mathcal{Z}_m^f$ are significant and therefore have to be included in the calculation.

5.3 Finite volume effects at order $\mathcal{O}(\alpha_{\rm em})$

The subtraction $\Gamma_0(L) - \Gamma_0^{\rm pt}(L)$ in Eq. (2.2) cancels both the IR divergences and the structure-independent FVEs, i.e. those of order $\mathcal{O}(1/L)$. The point-like decay rate $\Gamma_0^{\rm pt}(L)$ is given by

$$\Gamma_0^{\rm pt}(L) = \left(1 + 2\frac{\alpha_{\rm em}}{4\pi}\, Y_P^\ell(L)\right)\, \Gamma_P^{\rm tree}\ , \tag{5.30}$$

where

$$Y_P^\ell(L) = b_{\rm IR}\, \log(M_P L) + b_0 + \frac{b_1}{M_P L} + \frac{b_2}{(M_P L)^2} + \frac{b_3}{(M_P L)^3} + \mathcal{O}(\mathrm{e}^{-M_P L}) \tag{5.31}$$

with the coefficients b_j ($j = {\rm IR}, 0, 1, 2, 3$) depending on the dimensionless ratio m_ℓ/M_P and given explicitly in Eq. (98) of Ref. [49] (see also Ref. [78]) after the subtraction of the lepton self-energy contribution in the Feynman gauge. An important result of Ref. [49] is that the structure-dependent FVEs start at order $\mathcal{O}(1/(M_P L)^2)$. As a consequence the coefficients $b_{\rm IR,0,1}$ in the factor $Y_P^\ell(L)$ are "universal", i.e. they are the same as in the full theory when the structure of the meson P is considered[2].

Therefore, Eq. (5.1) is replaced by

$$\delta R_P = \delta R_P^{\rm ren} + \delta R_P^{\rm ampl} - 2Y_P^\ell(L)\ , \tag{5.32}$$

where $\delta R_P^{\rm ren}$ is defined in Eq. (5.29) and $\delta R_P^{\rm ampl}$ has been obtained above in Sec. 2.4. The residual FVEs after the subtraction of the universal terms as in Eq. (5.32) are illustrated in the plots in Fig. 5.1 for δR_π and δR_K in the fully inclusive case, i.e. where the energy of the final-state photon is integrated over the full phase space. In this case $\Delta E_\gamma = \Delta E_\gamma^{{\rm max},P} = M_P(1 - m_\mu^2/M_P^2)/2$, which corresponds to $\Delta E_\gamma^{{\rm max},K} \simeq 235$ MeV and $\Delta E_\gamma^{{\rm max},\pi} \simeq 29$ MeV, respectively. With a muon as the final state lepton, the contribution from photons with energy greater than about 20 MeV is negligible and hence the point-like approximation is valid. In the top

[2]Notice that the decay rate in the full theory, $\Gamma_0(L)$, can be affected also by non-universal FVEs of order $\mathcal{O}[1/(M_P L)^n]$ with $n \geq 4$ that do not appear in $\Gamma_0^{pt}(L)$.

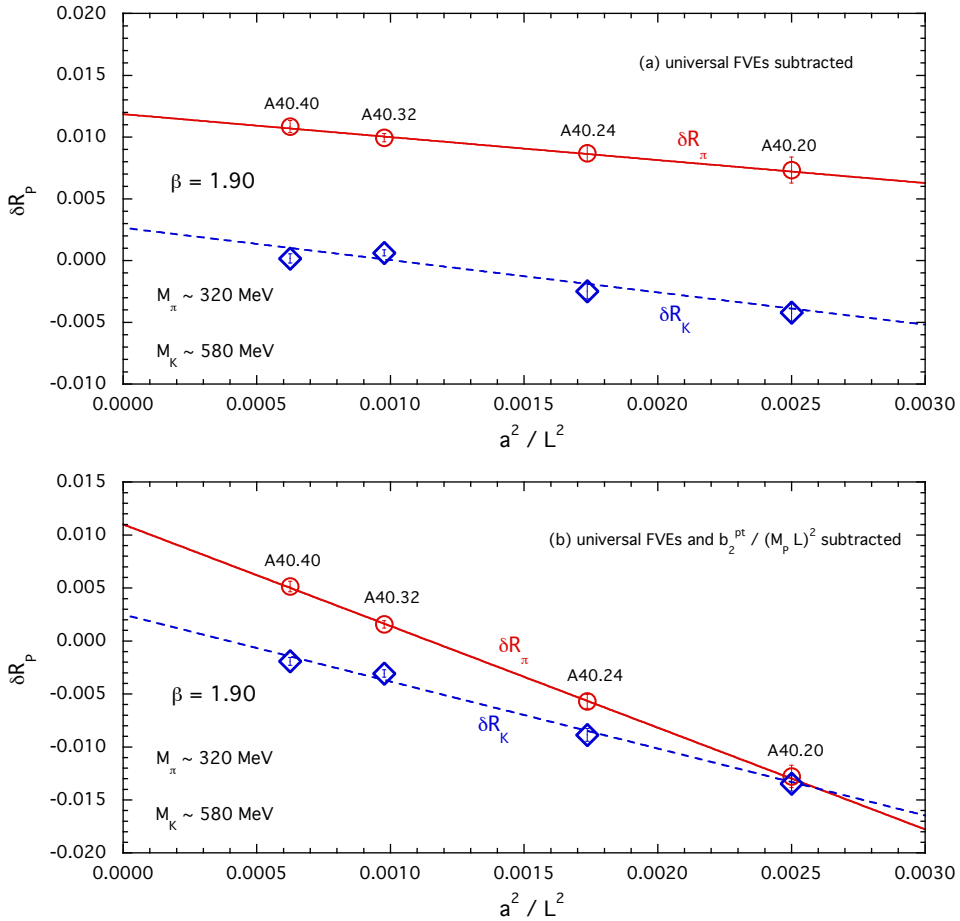

Figure 5.1. Results for the corrections δR_π and δR_K for the gauge ensembles A40.20, A40.24, A40.32 and A40.40 sharing the same lattice spacing, pion, kaon and muon masses, but with different lattice sizes (see Appendix A of Ref. [7]). TOP PANEL (a): the universal FVEs, i.e. the terms up to order $\mathcal{O}(1/M_P L)$ in Eq. (5.31), are subtracted from each quantity. BOTTOM PANEL (b): the same as in (a), but in addition to the subtraction of the universal terms, $b_2^{\rm pt}/(M_P L)^2$ is also removed. Here $b_2^{\rm pt}$ is the pointlike contribution to b_2 in Eq. (5.31) [78]. The solid and dashed lines are linear fits in $1/L^2$. The maximum photon energy ΔE_γ corresponds to the fully inclusive case $\Delta E_\gamma = \Delta E_\gamma^{max,P} = M_P(1 - m_\mu^2/M_P^2)/2$.

plot the universal FV corrections have been subtracted and so we would expect the remaining effects to be of order $\mathcal{O}(1/(M_P L)^2)$ and this is indeed what we see. In the bottom plot of Fig. 5.1, in addition to subtracting the universal FVEs, we also subtract the contribution to the order $\mathcal{O}(1/(M_P L)^2)$ corrections from the point-like contribution to b_2, which can be found in Eq. (3.2) of Ref. [78]. We observe that this additional subtraction does not reduce the $\mathcal{O}(1/(M_P L)^2)$ effects, underlining the expectation that these effects are indeed structure dependent. It can be seen that after subtraction of the universal terms the residual structure-dependent FVEs are almost linear in $1/L^2$, which implies that the FVEs of order $\mathcal{O}(1/(M_P L)^3)$ are quite small; indeed they are too small to be resolved with the present statistics. The central value of δR_P is thus obtained by subtracting the universal terms and fitting

the residual $\mathcal{O}(1/L^2)$ corrections to

$$\frac{K_P}{(M_P L)^2} + \frac{K_P^\ell}{(E_P^\ell L)^2} \ , \tag{5.33}$$

where K_P and K_P^ℓ are constant fitting parameters and E_P^ℓ is the energy of the charged lepton in the rest frame of the pseudoscalar P (see Eq. (5.34) below). Such an ansatz is introduced to model the unknown dependence of b_2 on the ratio m_ℓ/M_P. Indeed, for the four points in each of the plots of Fig. 5.1, m_ℓ/M_P takes the same value, but this is not true for all the ensembles used in the analysis. We estimate the uncertainty due to the use of the ansatz in Eq. (5.33) by repeating the same analysis, but on the data in which, in addition to subtracting the universal terms in Eq. 5.31, we also subtract the term $b_2^{\rm pt}/(M_P L)^2$. Since $b_2^{\rm pt}$ depends on m_ℓ/M_P [78], the result obtained with this additional subtraction is a little different from that obtained with only the universal terms removed and we take the difference between the two results as an estimate of the residual FV uncertainty.

5.4 Results for the charged pion and kaon decays into muons

We are now in a position to extract the complete corrections δR_P for the decays $\pi^+ \to \mu^+\nu(\gamma)$ and $K^+ \to \mu^+\nu(\gamma)$. The results for the corrections δR_π and δR_K are shown in Fig. 5.2, where the "universal" FVEs up to order $\mathcal{O}(1/L)$ have been subtracted from the lattice data (see the empty symbols) and all photon energies[3] are included, the experimental data on $\pi_{\ell 2}$ and $K_{\ell 2}$ decays being fully inclusive. Since the rates are fully inclusive in the real photon energy, structure dependent (SD) contributions to real photon emission should be included. According to the ChPT predictions of Ref. [79], however, these contributions are negligible for both kaon and pion decays into muons, while the same does not hold as well for decays into final-state electrons (see Ref. [14])[4].

The combined chiral, continuum and infinite-volume extrapolations are performed using the following SU(2)-inspired fitting function:

$$\begin{aligned} \delta R_P \ &= \ R_P^{(0)} + R_P^{(\chi)} \log(m_{ud}) + R_P^{(1)} m_{ud} + R_P^{(2)} m_{ud}^2 + D_P\, a^2 \\ &\quad + \frac{K_P}{M_P^2 L^2} + \frac{K_P^\ell}{(E_P^\ell)^2 L^2} + \delta\Gamma^{\rm pt}(\Delta E_\gamma^{{\rm max},P}) \ , \end{aligned} \tag{5.34}$$

where $m_{ud} = \mu_{ud}/Z_P$ and μ_{ud} is the bare (twisted) mass (values in Appendix A of Ref. [7]), E_P^ℓ is the lepton energy in the P-meson rest frame, $R_P^{(0),(1),(2)}$, D_P, K_P and K_P^ℓ are free parameters of the fit. In Eq. (5.34) the chiral coefficient $R_P^{(\chi)}$ is

[3] i.e. $\Delta E_\gamma = \Delta E_\gamma^{{\rm max},P} = M_P(1 - m_\mu^2/M_P^2)/2$.

[4] Recently, a dedicated lattice study of the real photon emission amplitudes in light and heavy P-meson leptonic decays has been carried out [47, 48]. In Ref. [48], the authors have shown that by using lattice QCD, even with moderate statistics, it is possible to predict with good precision the SD form factors relevant for $P \to \ell\nu\gamma$ decays for both light and heavy mesons and that it is also possible to extract their momentum dependence. See also Ref. [80] for similar ongoing calculations.

known for both pion and kaon decays from Ref. [81]; in QED the coefficients are

$$R_\pi^{(\chi)} = \frac{\alpha_{\rm em}}{4\pi}\,(3 - 2\mathcal{X}) \ , \qquad R_K^{(\chi)} = -\frac{\alpha_{\rm em}}{4\pi}\mathcal{X} \ , \tag{5.35}$$

while in qQED they are

$$R_\pi^{(\chi)} = \frac{\alpha_{\rm em}}{4\pi}\left(3 - \frac{10}{9}\mathcal{X}\right) \ , \qquad R_K^{(\chi)} = -\frac{\alpha_{\rm em}}{4\pi}\frac{8}{9}\mathcal{X} \ , \tag{5.36}$$

where $\mathcal{X}$ is obtained from the chiral limit of the $\mathcal{O}(\alpha_{\rm em})$ correction to $M^2_{\pi^\pm}$ (namely $\delta M^2_{\pi^\pm} = 4\pi\alpha_{\rm em}\mathcal{X} f_0^2 + \mathcal{O}(m_{ud})$, f_0 being the QCD low energy constant). The value of $\mathcal{X}$ has been computed in the analysis of Ref. [26] and amounts to $\mathcal{X} = 0.658(40)$.

Using Eq. 5.34 we have fitted the data for δR_π and δR_K using a χ^2-minimization procedure with an uncorrelated χ^2, obtaining values of χ^2/d.o.f. always around 0.9. The quality of our fits is illustrated in Fig. 5.2. It can be seen that the residual SD FVEs are still visible in the data and well reproduced by our fitting ansatz in Eq. (5.34). Discretisation effects on the other hand, only play a minor role.

At the physical pion mass in the continuum and infinite-volume limits we obtain

$$\begin{aligned} \delta R_\pi^{\rm phys} &= +0.0153\ (16)_{stat+fit}\ (4)_{input}\ (3)_{chiral}\ (6)_{FVE}\ (2)_{disc}\ (6)_{qQED} \\ &= +0.0153\ (19)\ , \end{aligned} \tag{5.37}$$

$$\begin{aligned} \delta R_K^{\rm phys} &= +0.0024\ (6)_{stat+fit}\ (3)_{input}\ (1)_{chiral}\ (3)_{FVE}\ (2)_{disc}\ (6)_{qQED} \\ &= +0.0024\ (10)\ , \end{aligned} \tag{5.38}$$

where

- $()_{stat+fit}$ indicates the uncertainty induced by the statistical Monte Carlo errors of the simulations and its propagation in the fitting procedure;
- $()_{input}$ is the error coming from the uncertainties of the input parameters of the quark-mass analysis of Ref. [56] and of the non-perturbative RCs;
- $()_{chiral}$ is the difference between including or excluding the chiral logarithm in Eq. (5.34), i.e. taking $R_\chi \neq 0$ or $R_\chi = 0$;
- $()_{FVE}$ is the difference between the analyses of the data corresponding to the FVE subtractions up to the order $\mathcal{O}(1/L)$ alone or by also subtracting the term proportional to $b_2^{\rm pt}/(M_P L)^2$ (see Fig. 5.1 and the discussion at the end of Sec. 5.3);
- $()_{disc}$ is the uncertainty coming from including ($D \neq 0$) or excluding (setting $D = 0$) the discretisation term proportional to a^2 in Eq. (5.34);
- $()_{qQED}$ is our estimate of the uncertainty of the QED quenching. This is obtained using the ansatz (5.34) with the coefficient R_χ of the chiral log fixed either at the value (5.36), which corresponds to the qQED approximation, or at the value (5.35), which includes the effects of the up, down and strange sea-quark charges [81]. The change both in $\delta R_\pi^{\rm phys}$ and in $\delta R_K^{\rm phys}$ is $\simeq 0.0003$, which has been already added in the central values given by Eqs. (5.37) and (5.38). To be conservative, we use twice this value for our estimate of the qQED uncertainty.

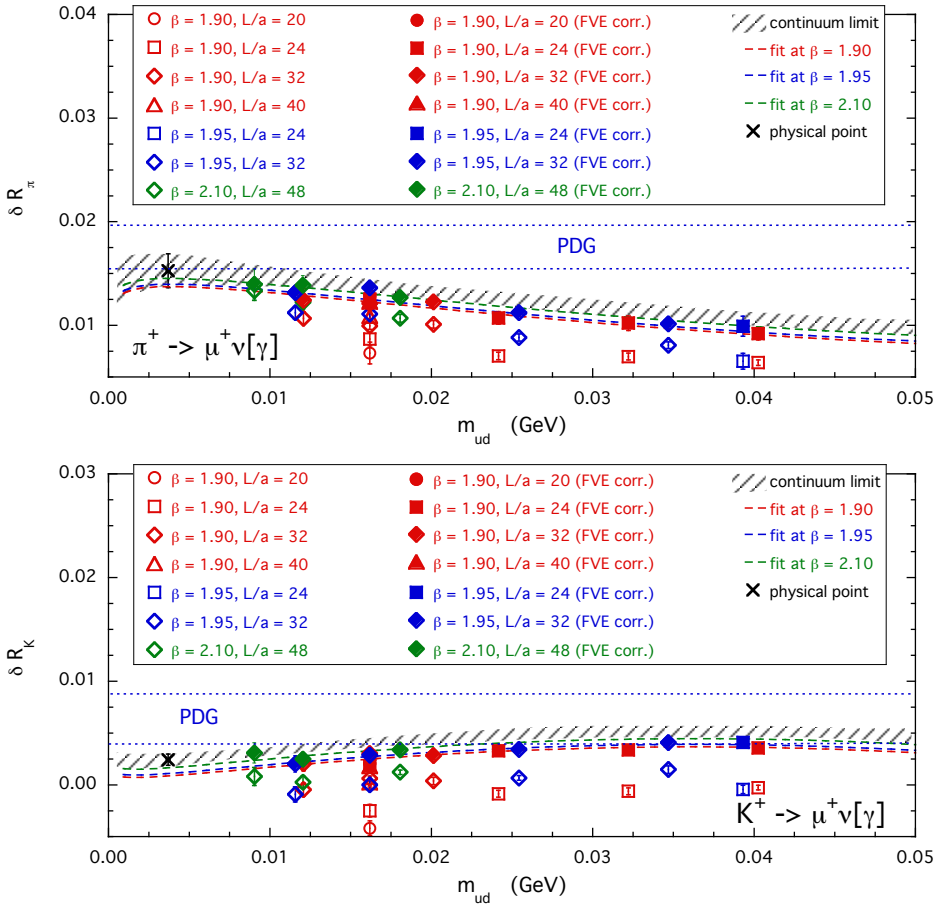

Figure 5.2. Results for the corrections δR_π (TOP PANEL) and δR_K (BOTTOM PANEL) obtained after the subtraction of the "universal" FVE terms up to order $\mathcal{O}(1/L)$ in Eq. (5.31) (empty markers). The full markers correspond to the lattice data corrected by the residual FVEs obtained in the case of the fitting function (5.34) including the chiral log. The dashed lines are the (central) results in the infinite volume limit at each value of the lattice spacing, while the shaded areas identify the results in the continuum limit at the level of one standard deviation. The crosses represent the values $\delta R_\pi^{\rm phys}$ and $\delta R_K^{\rm phys}$ extrapolated at the physical point $m_{ud}^{\rm phys}(\overline{\rm MS}, 2\,{\rm GeV}) = 3.70\ (17)$ MeV [56]. The blue dotted lines correspond to the values $\delta R_\pi^{\rm phys} = 0.0176\ (21)$ and $\delta R_K^{\rm phys} = 0.0064\ (24)$, obtained using ChPT [18] and adopted by the PDG [55].

Our results in Eqs. (5.37) - (5.38) can be compared with the ChPT predictions $\delta R_\pi^{\rm phys} = 0.0176(21)$ and $\delta R_K^{\rm phys} = 0.0064(24)$ obtained in Ref. [18] and adopted by the PDG [9, 55]. The difference is within one standard deviation for $\delta R_\pi^{\rm phys}$, while it is larger for $\delta R_K^{\rm phys}$. Note that the precision of our determination of $\delta R_\pi^{\rm phys}$ is comparable to the one obtained in ChPT, while our determination of $\delta R_K^{\rm phys}$ has a much better accuracy compared to that obtained using ChPT; the improvement in precision is a factor of about 2.2. We stress that the level of precision of our pion and kaon results depends crucially on the non-perturbative determination of the chirality mixing, carried out in Chapters 3 and 4 by including simultaneously QED at first order and QCD at all orders.

As already stressed, the correction δR_P and the QCD quantity $f_P^{(0)}$ separately depend on the prescription used for the separation between QED and QCD corrections [46]. Only the product $f_P^{(0)}\sqrt{1+\delta R_P}$ is independent of the prescription and its value, multiplied by the relevant CKM matrix element, yields the P-meson decay rate. We remind the reader that our results (5.37) - (5.38) are given in the GRS prescription (see the dedicated discussion in sections 1.5.2 and 2.4) in which the renormalized couplings and quark masses in the full theory and in isosymmetric QCD coincide in the $\overline{\rm MS}$ scheme at a scale of 2 GeV [8]. We remind the reader that, to the current level of precision, this GRS scheme can be considered equivalent to the FLAG scheme (see Sec. 2.4).
Taking the experimental values

$$\Gamma(\pi^- \to \mu^- \bar{\nu}_\mu[\gamma]) = 3.8408(7)\cdot 10^7\,{\rm s}^{-1}\,, \tag{5.39}$$
$$\Gamma(K^- \to \mu^- \bar{\nu}_\mu[\gamma]) = 5.134(11)\cdot 10^7\,{\rm s}^{-1} \tag{5.40}$$

from the PDG [9] and using our results in Eqs. (5.37)-(5.38), we obtain

$$f_\pi^{(0)}|V_{ud}| = 127.28\ (2)_{\rm exp}\ (12)_{\rm th}\,{\rm MeV} = 127.28\,(12)\,{\rm MeV}\,, \tag{5.41}$$
$$f_K^{(0)}|V_{us}| = 35.23\ (4)_{\rm exp}\ (2)_{\rm th}\,{\rm MeV} = 35.23\,(5)\,{\rm MeV}\,, \tag{5.42}$$

where the first error is the experimental uncertainty and the second is that from our theoretical calculations. The result for the pion in Eq. (5.41) agrees within the errors with the updated value $f_\pi^{(0)}|V_{ud}| = 127.12(13)\,{\rm MeV}$ [9], obtained by the PDG and based on the model-dependent ChPT estimate of the e.m. corrections from Ref. [18]. Our result for the kaon in Eq. (5.42) however, is larger than the corresponding PDG value $f_K^{(0)}|V_{us}| = 35.09(5)\,{\rm MeV}$ [9], based on the ChPT calculation of Ref. [18], by about 2 standard deviations.

As anticipated in the Introduction and discussed in detail in Sec. 2.4, we cannot use the result (5.41) to determine the CKM matrix element $|V_{ud}|$, since the pion decay constant was used by ETMC [56] to set the lattice scale in isosymmetric QCD and its value, $f_\pi^{(0)} = 130.41(20)$ MeV, was based on the determination of $|V_{ud}|$ obtained from super-allowed β-decays in Ref. [82]. On the other hand, adopting the best lattice determination of the QCD kaon decay constant[5], $f_K^{(0)} = 156.11(21)$ MeV [1, 83–85], we find that Eq. (5.42) implies

$$|V_{us}| = 0.22567(26)_{\rm exp}\,(33)_{\rm th} = 0.22567\,(42)\,, \tag{5.43}$$

which is a result with the excellent precision of $\simeq 0.2\%$.

Since the non-factorizable e.m. corrections to the mass RC (see the coefficient $Z_m^{\rm fact}$ in Table 2.1) were not included in Ref. [6], we update the estimate of the ratio of the kaon and pion decay rates:

$$\delta R_{K\pi}^{\rm phys} = \delta R_K^{\rm phys} - \delta R_\pi^{\rm phys} = -0.0126\,(14)\,. \tag{5.44}$$

[5]The average value of $f_{K^\pm}$ quoted by FLAG [1] includes the strong IB corrections. In order to obtain $f_K^{(0)}$ therefore, we have subtracted this correction which is given explicitly in Refs. [83–85].

Using the pion and kaon experimental decay rates we get

$$\frac{|V_{us}|}{|V_{ud}|}\frac{f_K^{(0)}}{f_\pi^{(0)}} = 0.27683\,(29)_{\rm exp}\,(20)_{\rm th} = 0.27683\,(35)\,. \tag{5.45}$$

Using the best $N_f = 2+1+1$ lattice determination of the ratio of the QCD kaon and pion decay constants, $f_K^{(0)}/f_\pi^{(0)} = 1.1966\ (18)$ [1, 83–85], we find

$$\frac{|V_{us}|}{|V_{ud}|} = 0.23135\,(24)_{\rm exp}\,(39)_{\rm th} = 0.23135\,(46)\,. \tag{5.46}$$

Taking the updated value $|V_{ud}| = 0.97420\,(21)$ from super-allowed nuclear beta decays [10], Eq. (5.46) yields the following value for the CKM element $|V_{us}|$:

$$|V_{us}| = 0.22538\,(24)_{\rm exp}\,(39)_{\rm th} = 0.22538\,(46)\,, \tag{5.47}$$

which agrees with our result (5.43) within the errors. Note that our result (5.47) agrees with the latest estimate $|V_{us}| = 0.2253(7)$, recently updated by the PDG [9], but it improves the error by a factor of approximately 1.5.

Taking the values $|V_{ub}| = 0.00413(49)$ [9] and $|V_{ud}| = 0.97420(21)$ [10] our result in Eq. (5.47) implies that the unitarity of the first-row of the CKM matrix is confirmed to better than the per-mille level

$$|V_{ud}|^2 + |V_{us}|^2 + |V_{ub}|^2 = 0.99988\,(46)\,. \tag{5.48}$$

With the same value $|V_{ud}| = 0.97420(21)$ from super-allowed nuclear beta decays [10], our result (5.41) implies for the QCD pion decay constant (in the GRS prescription) the following value

$$f_\pi^{(0)} = 130.65\,(12)_{\rm exp+th}\,(3)_{V_{ud}}\,{\rm MeV} = 130.65\,(12)\,{\rm MeV}\ , \tag{5.49}$$

which, as anticipated in Sec. 2.4, agrees within the errors with the value $f_\pi^{(0)} = 130.41\,(20)$ MeV adopted in Ref. [56] to set the lattice scale in the isosymmetric QCD theory. This demonstrates the equivalence of the GRS and PDG schemes within the precision of our simulation.

In a recent paper [86] the hadronic contribution to the electroweak radiative corrections to neutron and super-allowed nuclear β decays has been analyzed in terms of dispersion relations and neutrino scattering data. With respect to the result $V_{ud} = 0.97420(21)$ from Ref. [10] a significant shift in the central value and a reduction of the uncertainty have been obtained, namely $V_{ud} = 0.97370(14)$ [86]. The impact of the new value of V_{ud} on our determinations of V_{us} and $f_\pi^{(0)}$ is $V_{us} = 0.22526\,(46)$ and $f_\pi^{(0)} = 130.72\,(12)$ MeV, i.e. well within the uncertainties shown in Eqs. (5.47) and (5.49), respectively. On the contrary, the first-row CKM unitarity (5.48) will be significantly modified into

$$|V_{ud}|^2 + |V_{us}|^2 + |V_{ub}|^2 = 0.99885(34)\ , \tag{5.50}$$

which would imply a $\simeq 3.4\sigma$ tension with unitarity. The $\simeq 3.4\sigma$ deviation, if confirmed, is large enough to start taking new physics extensions of the SM seriously

into account [87]. A confirmation of the new calculation of the radiative corrections made in Ref. [86] is therefore urgently called for. The authors of Ref. [10] have recently updated their analysis of super-allowed nuclear β decays in Ref. [88], including new results for nucleus-independent radiative corrections [89, 90]. They confirm an appreciable reduction in the unitarity sum of the first row of the CKM matrix, yielding a possible tension with the SM. However, further new independent determinations of V_{ud}, perhaps from lattice QCD calculations of neutron β decay, could shed a light on such inconsistency.

Before closing this section, we comment briefly about the comparison between our result $\delta R_K^{\rm phys} = 0.0024(10)$ and the corresponding model-dependent ChPT prediction $\delta R_K^{\rm phys} = 0.0064(24)$ from Ref. [18]. The latter is obtained by adding a model-dependent QED correction of 0.0107(21) and a model-independent next-to-leading strong IB contribution equal to $-0.0043(12)$. Our result on the other hand, obtained in the GRS prescription, stems from a QED correction equal to 0.0088(9) and a strong IB term equal to $-0.0064(7)$ (see also Ref. [26]). The difference between our result and the ChPT prediction of Ref. [18] appears to be mainly due to a different strong IB contribution. Thus, in the present $N_f = 2 + 1 + 1$ study, we confirm for the strong IB term a discrepancy at the level of about 2 standard deviations, which was already observed at $N_f = 2$ in Ref. [3].

Part II

Perturbative calculations

6 | Perturbative evolution in QCD+QED

In this Chapter we derive in full details the renormalization group evolution (RGE) function for the renormalization constants at next-to-leading order (NLO) in QCD+QED. The evolution function, which relates renormalization constants evaluated at two different energy scales, has been used in the present work in Sec. 2.3 and Sec. 4.2. In the first case we evolved the operator $O_1^{\mathrm{RI'}}(\mu)$, computed in the RI'-MOM scheme at a given scale μ, to the scale M_W, in order to match it to the corresponding operator renormalized in the W-regularization scheme. In the second case, instead, the evolution function enters the calculation of non-perturbative RCs on the lattice since the RCs, evaluated at different renormalization scales $\mu^2 = p^2$, have to be evolved to a common reference scale μ_{ref} in order to study their scale-dependence. The use of the evolution function is different in the two cases. While in the former case, the evolution function is applied to a single operator $O_1^{\mathrm{RI'}}(\mu)$, in the latter it is used on RCs which are in general matrices, since bare lattice operators can mix under renormalization. In the following we will describe how to compute the evolution function for a generic set of operators and we will consider them mixing with each other under renormalization. The evolution function for non-mixing operators can be trivially derived from the general case.
The following discussion follows the line of Refs. [12, 13], although in these papers the authors compute the evolution matrix for Wilson coefficients of the $\Delta F = 1$ effective Hamiltonian.

6.1 General formalism

Let us consider a set of renormalized composite operators $\vec{O}_{\mathrm{R}}$ and let define

$$\vec{O}_{\mathrm{R}}(\mu) = \hat{Z}(\mu)\, \vec{O}_{\mathrm{B}} \ , \tag{6.1}$$

where $\hat{Z}(\mu)$ is the renormalization matrix relating bare operators $\vec{O}_{\mathrm{B}}$ with renormalized ones. Since $\vec{O}_{\mathrm{B}}$ do not depend on the renormalization scale μ, we have

$$\frac{\mathrm{d}}{\mathrm{d}\ln\mu^2}\ \vec{O}_{\mathrm{R}}(\mu) = \frac{\mathrm{d}\hat{Z}(\mu)}{\mathrm{d}\ln\mu^2}\ \vec{O}_{\mathrm{B}} = \frac{\mathrm{d}\hat{Z}(\mu)}{\mathrm{d}\ln\mu^2}\ \hat{Z}^{-1}(\mu)\, \vec{O}_{\mathrm{R}}(\mu) \ . \tag{6.2}$$

By defining

$$\hat{\gamma} = -\frac{\mathrm{d}\hat{Z}}{\mathrm{d}\ln\mu}\ \hat{Z}^{-1} \tag{6.3}$$

as the *anomalous dimension matrix* of the operators $\vec{O}$, we obtain the following renormalization group (RG) equation

$$\frac{\mathrm{d}\vec{O}_{\mathrm{R}}(\mu)}{\mathrm{d}\ln\mu^2} = -\frac{\hat{\gamma}(\alpha_{\mathrm{s}},\alpha_{\mathrm{em}})}{2}\,\vec{O}_{\mathrm{R}}(\mu)\ . \tag{6.4}$$

It is worth to underline that anomalous dimensions are commonly computed in perturbation theory from the inverse renormalization constants $\hat{\mathbb{Z}}$, defined as

$$\vec{O}_{\mathrm{B}} = \hat{\mathbb{Z}}(\mu)\,\vec{O}_{\mathrm{R}}(\mu). \tag{6.5}$$

The anomalous dimension matrix can be expressed in terms of the matrix $\hat{\mathbb{Z}}$ as

$$\hat{\gamma} = \hat{\mathbb{Z}}^{-1}\,\frac{\mathrm{d}\hat{\mathbb{Z}}}{\mathrm{d}\ln\mu} \tag{6.6}$$

and this relation will be used in Chap. 7 to perturbatively evaluate the anomalous dimensions in QCD+QED for bilinear and semileptonic operators.

The RG equation (6.4) can be rewritten as

$$\frac{\mathrm{d}\vec{O}_{\mathrm{R}}(\mu)}{\mathrm{d}\ln\mu^2} = \left(\frac{\partial}{\partial\ln\mu^2} + \beta(\alpha_{\mathrm{s}},\alpha_{\mathrm{em}})\,\frac{\partial}{\partial\alpha_{\mathrm{s}}}\right)\,\vec{O}_{\mathrm{R}}(\mu) = -\frac{\hat{\gamma}(\alpha_{\mathrm{s}},\alpha_{\mathrm{em}})}{2}\,\vec{O}_{\mathrm{R}}(\mu)\ , \tag{6.7}$$

where we made the dependence of the strong coupling α_{s} on the scale μ explicit, neglected the running of α_{em} and introduced the QCD *beta function*, which is defined as

$$\beta(\alpha_{\mathrm{s}},\alpha_{\mathrm{em}}) = \frac{d\alpha_{\mathrm{s}}}{d\ln\mu^2} = -\beta_0\frac{\alpha_{\mathrm{s}}^2}{4\pi} - \beta_1\frac{\alpha_{\mathrm{s}}^3}{(4\pi)^2} - \beta_1^{se}\frac{\alpha_{\mathrm{s}}^2\alpha_{\mathrm{em}}}{(4\pi)^2}\ , \tag{6.8}$$

with

$$\beta_0 = 11 - \frac{2}{3}N_f\ ,\quad \beta_1 = 102 - \frac{38}{3}N_f\ ,\quad \beta_1^{se} = -\frac{8}{9}\left(N_u + \frac{N_d}{4}\right)\ , \tag{6.9}$$

where N_f denotes the number of active flavours, and N_u and N_d denote the number of uplike and downlike active quarks, respectively ($N_u + N_d = N_f$). We stress that to the order considered in this work also the e.m. correction of order $\mathcal{O}(\alpha_{\mathrm{s}}^2\alpha_{\mathrm{em}})$ to the QCD beta function, β_1^{se}, should be *in principle* taken into account[1]. However, we will show that the contribution of β_1^{se} vanishes in the final result for the evolution function.

The NLO anomalous dimension matrix can be expanded in powers of the coupling constants as follows:

$$\hat{\gamma}(\alpha_{\mathrm{s}},\alpha_{\mathrm{em}}) = \frac{\alpha_{\mathrm{s}}}{4\pi}\,\hat{\gamma}_s^{(0)} + \frac{\alpha_{\mathrm{s}}^2}{(4\pi)^2}\,\hat{\gamma}_s^{(1)} + \frac{\alpha_{\mathrm{em}}}{4\pi}\,\hat{\gamma}_e^{(0)} + \frac{\alpha_{\mathrm{s}}\alpha_{\mathrm{em}}}{(4\pi)^2}\,\hat{\gamma}_{se}^{(1)} + \ \ldots\ , \tag{6.10}$$

where the ellipsis stands for higher order terms in α_{s} and α_{em}. In the following we only consider first order corrections in α_{em}. On the other hand, higher order QCD corrections up to $\mathcal{O}(\alpha_{\mathrm{s}}^3)$ will be taken into account later in Sec. 6.4.

[1] This terms has been neglected in Refs. [12, 13].

Let define the evolution operator $U(\mu_2, \mu_1)$ that evolves renormalized operators from the scale μ_1 to $\mu_2 < \mu_1$ as[2]

$$\vec{O}_{\rm R}(\mu_2) = \hat{U}(\mu_2, \mu_1; \alpha_{\rm em})\ \vec{O}_{\rm R}(\mu_1)\ . \tag{6.11}$$

By substituting Eq. (6.11) into the RG equation (6.7) we find

$$\left(\frac{\partial}{\partial \ln \mu_2^2} + \beta(\alpha_{\rm s}(\mu_2), \alpha_{\rm em})\,\frac{\partial}{\partial \alpha_{\rm s}}\right)\ \hat{U}(\mu_2, \mu_1; \alpha_{\rm em}) = -\frac{\hat{\gamma}(\alpha_{\rm s}(\mu_2), \alpha_{\rm em})}{2}\ \hat{U}(\mu_2, \mu_1; \alpha_{\rm em})\ , \tag{6.12}$$

with initial condition $\hat{U}(\mu_1, \mu_1; \alpha_{\rm em}) = \hat{1}$. This differential equation for $\hat{U}$ can be converted into an integral equation and solved iteratively,

$$\hat{U}(\mu_2, \mu_1; \alpha_{\rm em}) = T_{\alpha_{\rm s}}\ \exp\left[-\int_{\alpha_{\rm s}(\mu_1)}^{\alpha_{\rm s}(\mu_2)} {\rm d}\alpha_{\rm s}\ \frac{\hat{\gamma}(\alpha_{\rm s}, \alpha_{\rm em})}{2\beta(\alpha_{\rm s}, \alpha_{\rm em})}\right]\ , \tag{6.13}$$

where the time ordered product $T_{\alpha_{\rm s}}$ has to be intended in terms of the Taylor expansion of the exponential function with increasing coupling from right to left[3].

The evolution matrix $\hat{U}(\mu_2, \mu_1; \alpha_{\rm em})$ in Eq. (6.13) is consistent with the one found in Refs. [12, 13] for the evolution of Wilson coefficients. In order to prove it, we start by observing that an Effective Lagrangian is by construction μ-independent and therefore $\vec{C}^T(\mu_2)\,\vec{O}(\mu_2) \equiv \vec{C}^T(\mu_1)\,\vec{O}(\mu_1)$. Using the evolution matrix on $\vec{O}(\mu_2)$ we get $(\mu_2 < \mu_1)$

$$\begin{aligned} \vec{C}^T(\mu_2)\,\vec{O}(\mu_2) &= \vec{C}^T(\mu_2)\,\hat{U}(\mu_2, \mu_1; \alpha_{\rm em})\,\vec{O}(\mu_1) && (6.14)\\ &\equiv \vec{C}^T(\mu_1)\,\vec{O}(\mu_1)\ . && (6.15) \end{aligned}$$

It follows that

$$\vec{C}^T(\mu_2) = \left[\hat{U}^T(\mu_2, \mu_1; \alpha_{\rm em})\right]^{-1}\,\vec{C}^T(\mu_1) \equiv \hat{U}_C(\mu_2, \mu_1; \alpha_{\rm em})\ , \tag{6.16}$$

where we have defined the evolution operator for the Wilson coefficients as $\hat{U}_C(\mu_2, \mu_1; \alpha_{\rm em})$, which using our result in Eq. (6.13) takes the form

$$\begin{aligned} \hat{U}_C(\mu_2, \mu_1; \alpha_{\rm em}) &= T_{\alpha_{\rm s}}\ \exp\left[\int_{\alpha_{\rm s}(\mu_1)}^{\alpha_{\rm s}(\mu_2)} {\rm d}\alpha_{\rm s}\ \frac{\hat{\gamma}^T(\alpha_{\rm s}, \alpha_{\rm em})}{2\beta(\alpha_{\rm s}, \alpha_{\rm em})}\right]\\ &= T_g\ \exp\left[\int_{g(\mu_1)}^{g(\mu_2)} {\rm d}g\ \frac{\hat{\gamma}^T(g, e)}{\beta(g, e)}\right]\ . \end{aligned} \tag{6.17}$$

Here we have used the relation

$$\frac{{\rm d}\alpha_{\rm s}}{\beta(\alpha_{\rm s})} = 2\frac{{\rm d}g}{\beta(g)} \tag{6.18}$$

[2]Restricting the evolution operator to run towards the IR avoids algebraic technicalities. The running towards the UV can be obtained by taking $[\hat{U}(\mu_2, \mu_1; \alpha_{\rm em})]^{-1}$.

[3]Explicitly, for a generic matrix function $\hat{F}$, one has

$$T_x\ \exp\left[\int_{x_-}^{x_+} {\rm d}x\,\hat{F}(x)\right] = \hat{1} + \int_{x_-}^{x_+} {\rm d}x\,\hat{F}(x) + \int_{x_-}^{x_+} {\rm d}x_1\,\hat{F}(x_1)\int_{x_-}^{x_1} {\rm d}x_2\,\hat{F}(x_2) + \ldots$$

between the beta function $\beta(\alpha_s)$ defined in Eq. (6.8) and the one defined in terms of g [13], namely

$$\beta(g) = \frac{\mathrm{d}g}{\mathrm{d}\ln\mu} \ . \tag{6.19}$$

The expression for $\hat{U}_C(\mu_2, \mu_1; \alpha_{\rm em})$ in Eq. (6.17) is exactly the one obtained in Refs. [12, 13]. All formulas derived below can be then easily compared with those obtained for Wilson coefficient in Refs. [12, 13] by substituting $\hat{\gamma} \to -\hat{\gamma}^T$.

It is useful to rewrite the evolution matrix $\hat{U}$ as

$$\hat{U}(\mu_2, \mu_1; \alpha_{\rm em}) = \hat{W}(\mu_2)\, \hat{U}^{(0)}(\mu_2, \mu_1)\, \hat{W}^{-1}(\mu_1) \ , \tag{6.20}$$

where the matrix

$$\hat{U}^{(0)}(\mu_2, \mu_1) = \left[\frac{\alpha_s(\mu_2)}{\alpha_s(\mu_1)}\right]^{\frac{\hat{\gamma}_s^{(0)}}{2\beta_0}} \tag{6.21}$$

is the leading order (LO) QCD evolution matrix and $\hat{W}(\mu)$ is a generic unitary and scale dependent matrix which takes into account higher order terms in α_s and $\alpha_{\rm em}$. Hence, the definition of $\hat{W}(\mu)$ depends on the orders one wants to include in the perturbative expansion.
By differentiating Eqs. (6.13) and (6.20) with respect to $\alpha_s(\mu_2)$ we obtain respectively

$$\begin{aligned}
\partial_{\alpha_s}\hat{U} &= -\frac{\hat{\gamma}(\alpha_s(\mu_2), \alpha_{\rm em})}{2\beta(\alpha_s, \alpha_{\rm em}))} \cdot \hat{U}(\mu_2, \mu_1; \alpha_{\rm em}) \\
&= -\frac{\hat{\gamma}(\alpha_s(\mu_2), \alpha_{\rm em})}{2\beta(\alpha_s, \alpha_{\rm em}))} \cdot \hat{W}(\mu_2)\, \hat{U}^{(0)}(\mu_2, \mu_1)\hat{W}^{-1}(\mu_1) \ , \qquad (6.22) \\
\partial_{\alpha_s}\hat{U} &= \left(\partial_{\alpha_s}\hat{W}(\mu_2) + \hat{W}(\mu_2)\frac{\hat{\gamma}_s^{(0)}}{2\beta_0}\frac{1}{\alpha_s(\mu_2)}\right)\hat{U}^{(0)}(\mu_2, \mu_1)\hat{W}^{-1}(\mu_1) \ . \qquad (6.23)
\end{aligned}$$

and equating the right-hand sides we get the following equation for $\hat{W}(\mu_2)$,

$$\partial_{\alpha_s}\hat{W}(\mu_2) + \frac{1}{\alpha_s(\mu_2)}\left[\hat{W}(\mu_2), \frac{\hat{\gamma}_s^{(0)}}{2\beta_0}\right] = \left(-\frac{\hat{\gamma}(\alpha_s(\mu_2), \alpha_{\rm em})}{2\beta(\alpha_s(\mu_2), \alpha_{\rm em})} - \frac{1}{\alpha_s(\mu_2)}\frac{\hat{\gamma}_s^{(0)}}{2\beta_0}\right)\hat{W}(\mu_2) \ . \tag{6.24}$$

6.2 Determination of the matrix $\hat{W}$

Following Ref. [12], we define the matrix $\hat{W}$ as

$$\begin{aligned}
\hat{W}(\mu_2) &= \left(\hat{1} + \frac{\alpha_{\rm em}}{4\pi}\hat{K}\right)\left(\hat{1} + \frac{\alpha_s(\mu_2)}{4\pi}\hat{J}\right)\left(\hat{1} + \frac{\alpha_{\rm em}}{\alpha_s(\mu_2)}\hat{P}\right) \ , \qquad (6.25) \\
\hat{W}^{-1}(\mu_1) &= \left(\hat{1} - \frac{\alpha_{\rm em}}{\alpha_s(\mu_1)}\hat{P}\right)\left(\hat{1} - \frac{\alpha_s(\mu_1)}{4\pi}\hat{J}\right)\left(\hat{1} - \frac{\alpha_{\rm em}}{4\pi}\hat{K}\right) \ . \qquad (6.26)
\end{aligned}$$

In order to obtain the expression of $\hat{K}$, $\hat{J}$ and $\hat{P}$ we need to solve order by order Eq. (6.24). The derivative of $\hat{W}(\mu_2)$ with respect to $\alpha_{\rm s}(\mu_2)$ gives in this case

$$\begin{aligned}\partial_{\alpha_{\rm s}}\hat{W}(\mu_2) &= \frac{1}{4\pi}\left(\hat{1}+\frac{\alpha_{\rm em}}{4\pi}\hat{K}\right)\hat{J}\left(\hat{1}+\frac{\alpha_{\rm em}}{\alpha_{\rm s}(\mu_2)}\hat{P}\right)- \\ &\quad -\frac{\alpha_{\rm em}}{\alpha_{\rm s}^2(\mu_2)}\left(\hat{1}+\frac{\alpha_{\rm em}}{4\pi}\hat{K}\right)\left(\hat{1}+\frac{\alpha_{\rm s}(\mu_2)}{4\pi}\hat{J}\right)\hat{P}\ . \end{aligned} \tag{6.27}$$

Eq. (6.24) can be easily solved multiplying it by $\alpha_{\rm s}(\mu_2)$ and expanding the ratio $\hat{\gamma}_s/\beta$ as

$$\begin{aligned}\alpha_{\rm s}(\mu_2)\,\frac{\hat{\gamma}_s(\alpha_{\rm s}(\mu_2),\alpha_{\rm em})}{2\,\beta(\alpha_{\rm s}(\mu_2),\alpha_{\rm em})} &\approx -\frac{\hat{\gamma}_s^{(0)}}{2\beta_0}+\frac{\alpha_{\rm s}(\mu_2)}{4\pi}\left(\frac{\beta_1}{2\beta_0^2}\hat{\gamma}_s^{(0)}-\frac{\hat{\gamma}_s^{(1)}}{2\beta_0}\right)-\frac{\alpha_{\rm em}}{\alpha_{\rm s}(\mu_2)}\frac{\hat{\gamma}_e^{(0)}}{2\beta_0}+ \\ &\quad +\frac{\alpha_{\rm em}}{4\pi}\left(\frac{\beta_1}{2\beta_0^2}\hat{\gamma}_e^{(0)}+\frac{\beta_1^{se}}{2\beta_0^2}\hat{\gamma}_s^{(0)}-\frac{\hat{\gamma}_{se}^{(1)}}{2\beta_0}\right)+ \\ &\quad +\mathcal{O}(\alpha_{\rm s}^2,\alpha_{\rm em}^2,\alpha_{\rm s}\alpha_{\rm em})\ . \end{aligned} \tag{6.28}$$

Notice that the first term in Eq. (6.29) cancels with the second term appearing in the r.h.s. of Eq. (6.24). We do not include higher order terms like $\mathcal{O}(\alpha_{\rm s}\alpha_{\rm em})$ in the expansion, because they require the knowledge of the anomalous dimension matrix and the beta function at three loops. Equating order by order terms of Eqs. (6.24) and (6.27) one obtains the following relations,

$$2\hat{J}-\left[\frac{\hat{\gamma}_s^{(0)}}{\beta_0},\hat{J}\right]=-\frac{\beta_1}{\beta_0^2}\hat{\gamma}_s^{(0)}+\frac{\hat{\gamma}_s^{(1)}}{\beta_0}\ , \tag{6.29}$$

$$-2\hat{P}-\left[\frac{\hat{\gamma}_s^{(0)}}{\beta_0},\hat{P}\right]=\frac{\hat{\gamma}_e^{(0)}}{\beta_0}\ , \tag{6.30}$$

$$\left[\hat{K},\hat{\gamma}_s^{(0)}\right]=\left[\hat{\gamma}_s^{(0)},\hat{J}\hat{P}\right]+2\beta_1\hat{P}-\frac{\beta_1}{\beta_0}\hat{P}\hat{\gamma}_s^{(0)}+\hat{\gamma}_s^{(1)}\hat{P}+\hat{\gamma}_{se}^{(1)}+\hat{\gamma}_e^{(0)}\hat{J}\ -\frac{\beta_1^{se}}{\beta_0}\hat{\gamma}_s^{(0)}, \tag{6.31}$$

in accordance with Eq. (14-16) of Ref. [12]. In order to solve the above equations it is useful to work in the basis in which the matrix $\hat{\gamma}_s^{(0)}$ is diagonal,

$$\left(\hat{\gamma}_s^{(0)}\right)_D\equiv\hat{V}^{-1}\hat{\gamma}_s^{(0)}\hat{V}=\mathrm{diag}\left(\gamma_{s,1}^{(0)},\ldots,\gamma_{s,n}^{(0)}\right)\ . \tag{6.32}$$

In such basis the leading order QCD operator (6.21) becomes the diagonal matrix

$$\hat{R}^{(0)}(\mu_2,\mu_1)=\hat{V}^{-1}\,\hat{U}^{(0)}(\mu_2,\mu_1)\,\hat{V}=\left(\frac{\alpha_{\rm s}(\mu_2)}{\alpha_{\rm s}(\mu_1)}\right)^{\vec{a}}\ ,\quad\text{with}\quad\vec{a}=\frac{\vec{\gamma}_s^{(0)}}{2\beta_0}\ . \tag{6.33}$$

By defining also the following rotated matrices,

$$\begin{aligned}\hat{G}&\equiv\hat{V}^{-1}\hat{\gamma}_s^{(1)}\hat{V}\ , & \hat{S}_J&\equiv\hat{V}^{-1}\hat{J}\,\hat{V}\ , \\ \hat{M}^{(0)}&\equiv\hat{V}^{-1}\hat{\gamma}_e^{(0)}\hat{V}\ , & \hat{S}_P&\equiv\hat{V}^{-1}\hat{P}\,\hat{V}\ , \\ \hat{M}^{(1)}&\equiv\hat{V}^{-1}\hat{\gamma}_{se}^{(1)}\hat{V}\ , & \hat{S}_K&\equiv\hat{V}^{-1}\hat{K}\,\hat{V}\ . \end{aligned} \tag{6.34}$$

we obtain from Eq. (6.29) the relation

$$2(\hat{S}_J)_{ij} - \frac{1}{\beta_0}(\hat{S}_J)_{ij}\left(\gamma_{s,i}^{(0)} - \gamma_{s,j}^{(0)}\right) = -\delta_{ij}\,\frac{\beta_1}{\beta_0^2}\,\gamma_{s,i}^{(0)} + \frac{\hat{G}_{ij}}{\beta_0}\ , \tag{6.35}$$

and hence

$$(\hat{S}_J)_{ij} = -\delta_{ij}\,a_i\,\frac{\beta_1}{\beta_0} + \frac{\hat{G}_{ij}}{2\beta_0(1-a_i+a_j)}\ . \tag{6.36}$$

From Eq. (6.30) we obtain

$$2(\hat{S}_P)_{ij} + 2(\hat{S}_P)_{ij}(a_i - a_j) = -\frac{\hat{M}_{ij}^{(0)}}{\beta_0}\ , \tag{6.37}$$

$$(\hat{S}_P)_{ij} = -\frac{1}{2\beta_0}\,\frac{\hat{M}_{ij}^{(0)}}{(1+a_i-a_j)}\ . \tag{6.38}$$

Analogously, from Eq. (6.31), by expliciting the matrix $\hat{S}_P$ and using the definition of $\hat{S}_J$, we obtain

$$2\beta_0(\hat{S}_K)_{ij}(a_j - a_i) = -\frac{\beta_1}{\beta_0}\hat{M}_{ij}^{(0)} + \hat{M}_{ij}^{(1)} - (\hat{S}_J)_{ik}\hat{M}_{kj}^{(0)} + \hat{M}_{ik}^{(0)}(\hat{S}_J)_{kj} - 2\beta_1^{se}\delta_{ij}\,a_i\ , \tag{6.39}$$

so that, if one defines the matrix

$$\hat{H} \equiv \hat{V}^{-1}\left(\hat{\gamma}_{se}^{(1)} - \frac{\beta_1}{\beta_0}\hat{\gamma}_e^{(0)} + \left[\hat{\gamma}_e^{(0)}, \hat{J}\right]\right)\hat{V}\ , \tag{6.40}$$

the above equation reduces to

$$(\hat{S}_K)_{ij} = \frac{1}{2\beta_0}\,\frac{\left(\hat{H}_{ij} - 2\beta_1^{se}\delta_{ij}\,a_i\right)}{(a_j - a_i)}\ . \tag{6.41}$$

Notice that the matrix $\hat{S}_K$ is singular for $a_i = a_j$, but this singularity cancels out in the final expression for $\hat{U}[\mu_2, \mu_1, \alpha_{\rm em}]$, as we will show in the following.

6.3 Evolution matrix at NLO in QCD+QED

6.3.1 Pure QCD evolution matrix

The pure QCD evolution matrix at NLO in $\alpha_{\rm s}$ can be obtained from Eq. (6.20) and Eqs. (6.25)-(6.26) by taking the limit $\alpha_{\rm em} \to 0$. Defining the NLO QCD operator in analogy with Eq. (6.33) as

$$\hat{R}^{\rm QCD}(\mu_2, \mu_1) = \hat{V}^{-1}\,\hat{U}_{\rm QCD}(\mu_2, \mu_1)\,\hat{V}\ , \tag{6.42}$$

one gets

$$\hat{R}_{ij}^{\rm QCD}(\mu_2, \mu_1) \equiv \hat{R}_{ij}^{(0)}(\mu_2, \mu_1) + (\hat{S}_J)_{ij}\left[\frac{\alpha_{\rm s}(\mu_2)}{4\pi}\left(\frac{\alpha_{\rm s}(\mu_2)}{\alpha_{\rm s}(\mu_1)}\right)^{a_j} - \frac{\alpha_{\rm s}(\mu_1)}{4\pi}\left(\frac{\alpha_{\rm s}(\mu_2)}{\alpha_{\rm s}(\mu_1)}\right)^{a_i}\right]\ , \tag{6.43}$$

where $\hat{R}^{(0)}$ is defined in Eq. (6.33). The matrix $\hat{S}_J$ presents a singularity when $a_j = a_i - 1$, in this case the (non-singular) evolution matrix $\hat{R}^{\rm QCD}_{ij}$ can be rewritten as

$$\hat{R}^{\rm QCD}_{ij}(\mu_2,\mu_1) = \hat{R}^{(0)}_{ij}(\mu_2,\mu_1) + \frac{\alpha_{\rm s}(\mu_1)}{4\pi}\,\frac{\hat{G}_{ij}}{2\beta_0}\left(\frac{\alpha_{\rm s}(\mu_2)}{\alpha_{\rm s}(\mu_1)}\right)^{a_i}\log\left(\frac{\alpha_{\rm s}(\mu_2)}{\alpha_{\rm s}(\mu_1)}\right) \quad [a_j = a_i - 1]\,. \tag{6.44}$$

6.3.2 QED correction

When including QED corrections, the operator $\hat{U}(\mu_2,\mu_1,\alpha_{\rm em})$, rotated in the basis in which $\hat{\gamma}^{(0)}_s$ is diagonal, can be written as

$$\hat{R}(\mu_2,\mu_1;\alpha_{\rm em}) = \hat{R}^{\rm QCD}(\mu_2,\mu_1) + \hat{R}^{\rm QED}(\mu_2,\mu_1;\alpha_{\rm em})\,, \tag{6.45}$$

where

$$\hat{R}^{\rm QED} = \hat{R}^{\rm QED}_{(\alpha_{\rm em}/\alpha_{\rm s})} + \hat{R}^{\rm QED}_{(\alpha_{\rm em})} \tag{6.46}$$

and $\hat{R}^{\rm QED}_{(\kappa)}$ contain terms of order $\mathcal{O}(\kappa)$. We find that

$$\left(\hat{R}^{\rm QED}_{(\alpha_{\rm em}/\alpha_{\rm s})}\right)_{ij} = \alpha_{\rm em}\times\begin{cases}\frac{\hat{M}^{(0)}_{ij}}{2\beta_0(1+a_i-a_j)}\left[\frac{1}{\alpha_{\rm s}(\mu_1)}\left(\frac{\alpha_{\rm s}(\mu_2)}{\alpha_{\rm s}(\mu_1)}\right)^{a_i} - \frac{1}{\alpha_{\rm s}(\mu_2)}\left(\frac{\alpha_{\rm s}(\mu_2)}{\alpha_{\rm s}(\mu_1)}\right)^{a_j}\right] & \\ \frac{\hat{M}^{(0)}_{ij}}{2\beta_0}\,\frac{1}{\alpha_{\rm s}(\mu_1)}\left(\frac{\alpha_{\rm s}(\mu_2)}{\alpha_{\rm s}(\mu_1)}\right)^{a_i}\log\left(\frac{\alpha_{\rm s}(\mu_2)}{\alpha_{\rm s}(\mu_1)}\right) & [a_j = a_i + 1]\end{cases} \tag{6.47}$$

$$\begin{aligned}\left(\hat{R}^{\rm QED}_{(\alpha_{\rm em})}\right)_{ij} = {}& \frac{\alpha_{\rm em}}{4\pi}\times\begin{cases}\frac{\left(\hat{H}_{ij}-2\beta_1^{se}\delta_{ij}\,a_i\right)}{2\beta_0(a_i-a_j)}\left[\left(\frac{\alpha_{\rm s}(\mu_2)}{\alpha_{\rm s}(\mu_1)}\right)^{a_i} - \left(\frac{\alpha_{\rm s}(\mu_2)}{\alpha_{\rm s}(\mu_1)}\right)^{a_j}\right] & \\ \frac{\left(\hat{H}_{ij}-2\beta_1^{se}\delta_{ij}\,a_i\right)}{2\beta_0}\left(\frac{\alpha_{\rm s}(\mu_2)}{\alpha_{\rm s}(\mu_1)}\right)^{a_i}\log\left(\frac{\alpha_{\rm s}(\mu_2)}{\alpha_{\rm s}(\mu_1)}\right) & [a_j = a_i]\end{cases} \\ & + \\ & + \frac{1}{4\pi}\left[\alpha_{\rm s}(\mu_2)\,\hat{S}_J\hat{R}^{\rm QED}_{(\alpha_{\rm em}/\alpha_{\rm s})} - \alpha_{\rm s}(\mu_1)\,\hat{R}^{\rm QED}_{(\alpha_{\rm em}/\alpha_{\rm s})}\hat{S}_J\right]_{ij}\end{aligned} \tag{6.48}$$

6.3.3 Expanding the resummed logarithms

The formulas reported in previous sections can be simplified by using the two loops recursive solution for the running of $\alpha_s(\mu_2)$, namely

$$\frac{1}{\alpha_{\rm s}(\mu_2)} = \frac{1}{\alpha_{\rm s}(\mu_1)} + \frac{\hat{\beta}_0}{4\pi}\log\left(\frac{\mu_2^2}{\mu_1^2}\right) + \frac{1}{4\pi}\,\frac{\beta_1}{\hat{\beta}_0}\log\left(\frac{\frac{4\pi}{\alpha_{\rm s}(\mu_2)}+\frac{\beta_1}{\hat{\beta}_0}}{\frac{4\pi}{\alpha_{\rm s}(\mu_1)}+\frac{\beta_1}{\hat{\beta}_0}}\right)\,, \tag{6.49}$$

where $\hat{\beta}_0 \equiv \beta_0 + \frac{\alpha_{\rm em}}{4\pi}\,\beta_1^{se}$ has been introduced in order to take into account first-order e.m. corrections to the QCD beta function. Using Eq. (6.49) we can obtain the evolution matrix at order $\mathcal{O}\left(\alpha_{\rm em}\alpha_{\rm s}\log\left(\mu_2/\mu_1\right)\right)$, which has the form

$$\hat{U}(\mu_2,\mu_1;\alpha_{\rm em}) = \hat{U}_{\rm QCD}(\mu_2,\mu_1) + \frac{\alpha_{\rm em}}{4\pi}\,\Delta\hat{U}_1(\mu_2,\mu_1) + \frac{\alpha_{\rm em}\alpha_{\rm s}(\mu_1)}{(4\pi)^2}\,\Delta\hat{U}_2(\mu_2,\mu_1)\,. \tag{6.50}$$

The matrix $\hat{U}_{\rm QCD}$ is the NLO QCD evolution function, which is obtained by applying Eq. (6.49) to $\hat{R}^{\rm QCD}$ in Eq. (6.43). The matrices $\Delta\hat{U}_1$ and $\Delta\hat{U}_2$ are given by

$$\left[\Delta\hat{U}_1(\mu_2,\mu_1)\right]_{ij} = -\frac{1}{2}\left[\hat{\gamma}_e^{(0)}\right]_{ij}\log\left(\frac{\mu_2^2}{\mu_1^2}\right) , \tag{6.51}$$

$$\begin{aligned}\left[\Delta\hat{U}_2(\mu_2,\mu_1)\right]_{ij} &= -\frac{1}{2}\left[\gamma_{se}^{(1)}\right]_{ij}\log\left(\frac{\mu_2^2}{\mu_1^2}\right) \\ &\quad + \frac{1}{8}(\gamma_{s,i}^{(0)}+\gamma_{s,j}^{(0)})\left[\hat{\gamma}_e^{(0)}\right]_{ij}\left(\log\left(\frac{\mu_2^2}{\mu_1^2}\right)\right)^2 ,\end{aligned} \tag{6.52}$$

where $\gamma_{s,i}^{(0)}$ are the entries of the diagonalized matrix $(\hat{\gamma}_s^{(0)})_D$.

Notice that, when expanding the resummed logarithms at LO in QCD, since we have used $\hat{\beta}_0$ instead of β_0 in Eq. (6.49), a correction of order $\mathcal{O}(\alpha_{\rm s}\alpha_{\rm em})$ will appear. This amounts to

$$\frac{\alpha_{\rm em}\alpha_{\rm s}(\mu_1)}{(4\pi^2)}\left[-\frac{1}{2}\frac{\beta_1^{se}}{\beta_0}\,\hat{\gamma}_s^{(0)}\,\log\left(\frac{\mu_2^2}{\mu_1^2}\right)\right] , \tag{6.53}$$

but such contribution cancels exactly with a term coming from the expansion of $\hat{R}^{\rm QED}_{(\alpha_{\rm em})}$ in Eq. (6.48). Therefore the contribution of β_1^{se}, although appearing in intermediate steps of the calculation, vanishes in the final result. The results obtained in Eqs. (6.50), (6.51) and (6.52) hold also when $\mu_2 > \mu_1$, since $\left[\hat{U}(\mu_2,\mu_1)\right]^{-1} = \hat{U}(\mu_1,\mu_2)$.

6.4 Evolution matrix in pure QCD

The pure QCD evolution matrix is known for most of the operators beyond NLO. Here we discuss the calculation of $U_{\rm QCD}$ in the case of non-mixing operators at N^{3}LO in $\alpha_{\rm s}$. In pure QCD, the strong anomalous dimension and the β function can be expanded in powers of $\alpha_{\rm s}$ as

$$\gamma(\alpha_{\rm s}) = \sum_{i=0}^{\infty}\gamma_s^{(i)}\left(\frac{\alpha_{\rm s}}{4\pi}\right)^{i+1} , \qquad \beta(\alpha_{\rm s}) = \alpha_{\rm s}\sum_{i=0}^{\infty}\beta_i\left(\frac{\alpha_{\rm s}}{4\pi}\right)^{i+1} . \tag{6.54}$$

It is common practice to express the evolution operator $U^{\rm QCD}$ in terms of two evolution functions $c(\mu_1)$ and $c(\mu_2)$, namely

$$U_{\rm QCD}(\mu_2,\mu_1) = \frac{c(\mu_2)}{c(\mu_1)} . \tag{6.55}$$

To obtain the expression for $c(\mu)$, we can rewrite the evolution operator in Eq. (6.13) (evaluated with $\alpha_{\rm em}=0$) as follows,

$$\begin{aligned}U_{\rm QCD}(\mu_2,\mu_1) &= \exp\left[\int_{\alpha_{\rm s}(\mu_1)}^{\alpha_{\rm s}(\mu_2)}\frac{{\rm d}\alpha_{\rm s}}{\alpha_{\rm s}}\frac{\gamma_0}{2\beta_0\alpha_{\rm s}}\right]\times\exp\left[-\int_{\alpha_{\rm s}(\mu_1)}^{\alpha_{\rm s}(\mu_2)}{\rm d}\alpha_{\rm s}\left(\frac{\gamma(\alpha_{\rm s})}{2\beta(\alpha_{\rm s})}-\frac{\gamma_0}{2\beta_0\alpha_{\rm s}}\right)\right] \\ &= \left[\frac{\alpha_{\rm s}(\mu_2)}{\alpha_{\rm s}(\mu_1)}\right]^{\frac{\gamma_s^{(0)}}{2\beta_0}}\times\exp\left[-\int_{\alpha_{\rm s}(\mu_1)}^{\alpha_{\rm s}(\mu_2)}{\rm d}\alpha_{\rm s}\left(\frac{\gamma(\alpha_{\rm s})}{2\beta(\alpha_{\rm s})}-\frac{\gamma_0}{2\beta_0\alpha_{\rm s}}\right)\right] ,\end{aligned} \tag{6.56}$$

where we have factorized the LO contribution $U^{(0)}(\mu_2,\mu_1)$. The advantage of having rewritten $U_{\rm QCD}$ in this way is that now the integral in the exponential is finite as either integration limit is taken to zero ($\alpha_{\rm s}(\mu)\to 0 \;\Leftrightarrow\; \mu\to\infty$). As a consequence, the function $c(\mu)$ can be defined as

$$c(\mu) \;=\; \left[\frac{\alpha_{\rm s}(\mu)}{4\pi}\right]^{\frac{\gamma_s^{(0)}}{2\beta_0}} \times \exp\left[-\int_0^{\alpha_{\rm s}(\mu)} {\rm d}\alpha_{\rm s}\left(\frac{\gamma(\alpha_{\rm s})}{2\beta(\alpha_{\rm s})}-\frac{\gamma_0}{2\beta_0}\right)\right] . \qquad (6.57)$$

Inserting Eq. (6.54) into Eq. (6.57) and expanding the result of the integral in powers of $a_{\rm s}\equiv\alpha_{\rm s}/(4\pi)$, we obtain

$$\begin{aligned} c(\mu) \;=\;& [a_{\rm s}(\mu)]^{\bar\gamma_0}\Big\{1+(\bar\gamma_1-\bar\beta_1\bar\gamma_0)\,a_{\rm s}(\mu) \\ &+\frac{1}{2}\Big[(\bar\gamma_1-\bar\beta_1\bar\gamma_0)^2+\bar\gamma_2+\bar\beta_1^2\bar\gamma_0-\bar\beta_1\bar\gamma_1-\bar\beta_2\bar\gamma_0\Big]\;a_{\rm s}^2(\mu) \\ &+\Big[\frac{1}{6}(\bar\gamma_1-\bar\beta_1\bar\gamma_0)^3+\frac{1}{2}(\bar\gamma_1-\bar\beta_1\bar\gamma_0)(\bar\gamma_2+\bar\beta_1^2\bar\gamma_0-\bar\beta_1\bar\gamma_1-\bar\beta_2\bar\gamma_0) \\ &\quad+\frac{1}{3}\Big(\bar\gamma_3-\bar\beta_1^3\bar\gamma_0+2\bar\beta_1\bar\beta_2\bar\gamma_0-\bar\beta_3\bar\gamma_0+\bar\beta_1^2\bar\gamma_1-\bar\beta_2\bar\gamma_1-\bar\beta_1\bar\gamma_2\Big)\Big]\;a_{\rm s}^3(\mu) \\ &+O(a_{\rm s}^4)\Big\}\ , \end{aligned} \qquad (6.58)$$

where we have defined $\bar\beta_i\equiv\beta_i/\beta_0$ and $\bar\gamma_i\equiv\gamma_s^{(i)}/(2\beta_0)$. The four-loop QCD β-function has been computed in the $\overline{\rm MS}$ scheme in Ref. [91] and coefficients β_2 and β_3 are given by

$$\begin{aligned} \beta_2^{\overline{\rm MS}} \;=\;& \frac{2857}{2}-\frac{5033}{18}\,N_f+\frac{325}{54}\,N_f^2\ , \\ \beta_3^{\overline{\rm MS}} \;=\;& \left(\frac{149753}{6}+3564\,\zeta_3\right)-\left(\frac{1078361}{162}+\frac{6508}{27}\,\zeta_3\right)N_f \\ &+\left(\frac{50065}{162}+\frac{6472}{81}\,\zeta_3\right)N_f^2+\frac{1093}{729}\,N_f^3\ , \end{aligned} \qquad (6.59)$$

where ζ is the Riemann zeta-function ($\zeta_3=1.202056903\ldots$). The coefficients β_2 and β_3 of the QCD β-function, and in general all β_i with $i\geq 2$, are scheme-dependent. Strong anomalous dimensions beyond the LO are scheme-dependent quantities as well, and have to be computed for the specific operator of interest. Therefore, the evolution function $c(\mu)$ must be evaluated in the same scheme in which the RCs are computed. In Sec. 4.2, we applied the evolution function to RCs of operators renormalized in the RI' scheme. In this case, since the four loop RI' β-function is equivalent to the four loop $\overline{\rm MS}$ β-function in all gauges [74], the expression in Eq. (6.58) can be used with $\gamma^{\rm RI'}(\alpha_{\rm s})$ computed in the RI'-MOM scheme and the coefficients β_i given in Eqs. (6.9) and (6.59).

The evaluation of the strong coupling constant at the scale μ is done using the

following approximate analytical solution

$$\begin{aligned}\alpha_{\rm s}(\mu) \;=\; & \frac{4\pi}{\beta_0\,\log(\mu^2/\Lambda^2)}\left[1-\frac{\beta_1}{\beta_0^2}\frac{\log[\log(\mu^2/\Lambda^2)]}{\log(\mu^2/\Lambda^2)}+\right. \\ & +\frac{\beta_1^2}{\beta_0^4\log^2(\mu^2/\Lambda^2)}\left(\Big(\log[\log(\mu^2/\Lambda^2)]\Big)^2-\log[\log(\mu^2/\Lambda^2)]-1+\frac{\beta_2\beta_0}{\beta_1^2}\right)+ \\ & +\frac{\beta_1^3}{\beta_0^6\log(\mu^2/\Lambda^2)}\left(-\Big(\log[\log(\mu^2/\Lambda^2)]\Big)^3+\frac{5}{2}\,\Big(\log[\log(\mu^2/\Lambda^2)]\Big)^2+\right. \\ & \left.+\,2\,\log[\log(\mu^2/\Lambda^2)]-\frac{1}{2}-3\,\frac{\beta_2\beta_0}{\beta_1^2}\log[\log(\mu^2/\Lambda^2)]+\frac{\beta_3\beta_0^2}{2\beta_1^3}\right)+ \\ & \left.+\,\mathcal{O}\left(\frac{(\log[\log(\mu^2/\Lambda^2)])^4}{\log(\mu^2/\Lambda^2)}\right)\right]\;, \end{aligned} \tag{6.60}$$

where for $\Lambda \equiv \Lambda_{\rm QCD}$ we have used the value quoted by the PDG [9] and computed in the $\overline{\rm MS}$ scheme for $N_f = 4$ flavours of quarks,

$$\Lambda^{(4)}_{\overline{\rm MS}} = 0.292\ {\rm GeV}\ . \tag{6.61}$$

Notice that the contribution of the e.m. correction β_1^{se} to the QCD β-function has been neglected in Eqs. (6.58) and (6.60) because such term is absent in the electro-quenched theory adopted in the numerical analysis.

7 | Two-loop anomalous dimensions in QCD+QED

In this Chapter we describe the calculation of the anomalous dimension matrix of a set of operators at NLO in QCD+QED. The anomalous dimension matrix describes the evolution of a set of operators (and their mixing) when changing the renormalization scale. It has been introduced in the previous Chapter 6 and used in Part I of this thesis to evolve renormalization constants of bilinear and semileptonic four-fermion operators from one scale to another. Here we give the details of the calculation of the anomalous dimension matrix at two-loops in the $\overline{\text{MS}}$-scheme in the *naive dimensional regularization* (NDR) for the two sets of operators used in this work. For details on dimensional regularization we refer to Refs. [92–95].
The anomalous dimension matrix for a generic set of operators $\vec{O}$ is defined from the operator renormalization matrix as

$$\hat{\gamma} = \hat{Z}^{-1} \frac{\mathrm{d}\hat{Z}}{\mathrm{d}\ln\mu} \tag{7.1}$$

where $\hat{Z}$ is defined by the relation

$$\vec{O}_{\mathrm{B}} = \hat{Z}(\mu)\,\vec{O}_{\mathrm{R}}(\mu). \tag{7.2}$$

These correspond to the relations of Eqs. (6.5) and (6.6), but in the following we will use the symbol $\hat{Z}$ instead of $\hat{\mathbb{Z}}$ to simplify the notation. In a mass independent renormalization scheme, such as the $\overline{\text{MS}}$, the only μ-dependence of $\hat{Z}(\mu)$ resides in the coupling constants. For this reason, we start this discussion by studying the scale dependence of QCD and QED coupling constants in NDR with $D = 4 - 2\epsilon$ dimensions. In order to maintain the action adimensional (in natural units), the renormalized couplings must be related to the bare ones as

$$\alpha_0 = Z_\alpha\,\alpha\,\mu^{2\epsilon}\ , \tag{7.3}$$

where α_0 and α are the bare and renormalized couplings respectively, Z_α the renormalization constant and μ the renormalization scale. It follows that, in NDR the β-function for the coupling α has the form

$$\begin{aligned}
\frac{\mathrm{d}\alpha}{\mathrm{d}\ln\mu^2} &\equiv \beta(\alpha;\epsilon) = \frac{\mathrm{d}}{\mathrm{d}\ln\mu^2}\left[\alpha_0\, Z_\alpha^{-1}\mu^{-2\epsilon}\right] \\
&= -\epsilon\alpha - \alpha_{\mathrm{s}} Z_\alpha \frac{\mathrm{d}Z_\alpha}{\mathrm{d}\ln\mu^2} \\
&= -\epsilon\alpha + \beta(\alpha)\ ,
\end{aligned}$$

where we have exploited the μ-independence of the bare coupling constant α_0 and called $\beta(\alpha)$ the β-function in $D = 4$ dimensions obtained in the limit $\epsilon \to 0$. Therefore, for the QCD and QED coupling constants we have the following relations

$$\beta(\alpha_{\rm s}, \alpha_{\rm em}; \epsilon) = -\epsilon\alpha_{\rm s} + \beta(\alpha_{\rm s}, \alpha_{\rm em}) \ , \tag{7.4}$$

$$\beta_e(\alpha_{\rm em}, \alpha_{\rm s}; \epsilon) = -\epsilon\alpha_{\rm em} + \beta_e(\alpha_{\rm em}, \alpha_{\rm s}) \ , \tag{7.5}$$

where $\beta(\alpha_{\rm s}, \alpha_{\rm em})$ is the QCD β-function defined in Eq. (6.8) and $\beta_e(\alpha_{\rm em}, \alpha_{\rm s})$ is the analogue QED β-function in $D = 4$ dimensions. In our work we have neglected the running of the electromagnetic coupling, i.e. we have adopted the approximation $\beta_e(\alpha_{\rm em}, \alpha_{\rm s}) \sim 0$. However, from Eq. (7.5) we see that even using such approximation, a residual scale dependence of $\alpha_{\rm em}(\mu)$ is induced by the dimensional regularization when $D \neq 4$, yielding

$$\beta_e(\alpha_{\rm em}; \epsilon) = -\epsilon\alpha_{\rm em} \ . \tag{7.6}$$

7.1 The master formulae

We can use the above definitions to rewrite Eq. (7.1) as follows,

$$\hat{Z} \cdot \hat{\gamma} = \frac{{\rm d}\hat{Z}}{{\rm d}\ln\mu} = 2\beta(\alpha_{\rm s}, \alpha_{\rm em}; \epsilon)\, \frac{{\rm d}\hat{Z}}{{\rm d}\alpha_{\rm s}} + 2\beta_e(\alpha_{\rm em}; \epsilon)\, \frac{{\rm d}\hat{Z}}{{\rm d}\alpha_{\rm em}} \ . \tag{7.7}$$

In the $\overline{\rm MS}$-scheme we have that RC matrices can be written as an expansion in inverse powers of ϵ, namely

$$\hat{Z} = 1 + \sum_{k=1}^{\infty} \frac{1}{\epsilon^k}\, \hat{Z}_k(\alpha_{\rm s}, \alpha_{\rm em}) \ . \tag{7.8}$$

As a consequence, by inserting the ϵ-expansions of Eqs (7.4), (7.6) and (7.8) into Eq. (7.7) and requiring $\hat{\gamma}$ to be finite in the limit $\epsilon = 0$ one obtains

$$\hat{\gamma} = -2\alpha_{\rm s}\, \frac{{\rm d}\hat{Z}_1}{{\rm d}\alpha_{\rm s}} - 2\alpha_{\rm em}\, \frac{{\rm d}\hat{Z}_1}{{\rm d}\alpha_{\rm em}} \ , \tag{7.9}$$

where $\hat{Z}_1 = \hat{Z}_1(\alpha_{\rm s}, \alpha_{\rm em})$ is the coefficient of the single pole $1/\epsilon$ of the RC matrix $\hat{Z}$.

At NLO the anomalous dimension matrix can be written as in Eq. (6.10), namely

$$\hat{\gamma}(\alpha_{\rm s}, \alpha_{\rm em}) = \frac{\alpha_{\rm s}}{4\pi}\, \hat{\gamma}_s^{(0)} + \frac{\alpha_{\rm s}^2}{(4\pi)^2}\, \hat{\gamma}_s^{(1)} + \frac{\alpha_{\rm em}}{4\pi}\, \hat{\gamma}_e^{(0)} + \frac{\alpha_{\rm s}\alpha_{\rm em}}{(4\pi)^2}\, \hat{\gamma}_{se}^{(1)} \ . \tag{7.10}$$

In a similar way, $\hat{Z}_1$ can be expanded in powers of the coupling constants

$$\hat{Z}_1 = \sum_{k=1}^{\infty} \left(\frac{\alpha_{\rm s}}{4\pi}\right)^k \hat{Z}_1^{(k)} + \frac{\alpha_{\rm em}}{4\pi}\, \hat{Z}_1^{(e)} + \frac{\alpha_{\rm s}\alpha_{\rm em}}{(4\pi)^2}\, \hat{Z}_1^{(se)} \ . \tag{7.11}$$

Each term in Eq. (7.11) can be evaluated from the computation of amputated Green functions with the insertions of the operators $\vec{O}$. Let us denote $\Gamma_B^{(n)}(\vec{O}_B)$ and $\Gamma^{(n)}(\vec{O})$ the bare and renormalized one-particle irreducible (1PI) Green functions with the

inserions of the n-fermion operators $\vec{O}$. They are in general matrices, since the insertion of a single operator O_i into a given diagram results in a linear combination of operators. The two green functions are related by

$$\begin{aligned} \Gamma_B^{(n)}(\vec{O}_B) &= \left[\prod_{i=1}^{n} Z_{\psi_i}^{-1/2}\right] \hat{Z}\, \Gamma^{(n)}(\vec{O}) \\ &\equiv Z_{\rm GF}\, \Gamma^{(n)}(\vec{O}) \end{aligned} \tag{7.12}$$

where $Z_\psi^{1/2}$ is the fermion field RC, $\hat{Z}$ the RC matrix of the operators $\vec{O}$ and $Z_{\rm GF}$ is defined above. By expanding the RCs in the above equation in inverse powers of ϵ as in Eq. (7.11) we get

$$\hat{Z}_1 = \frac{1}{2}\left[\sum_{i=1}^{n} Z_{\psi_i,1}\right] \hat{\mathbb{1}} + \hat{Z}_{\rm GF,1}\ . \tag{7.13}$$

Since the Green functions $\Gamma^{(n)}(\vec{O})$ are finite, the singularities in $Z_{\rm GF}$ are found directly from the calculation of the unrenormalized Green functions. At two-loops the matrix $\hat{Z}_1$ has to be computed subtracting $1/\epsilon$ divergences of one-loop subdiagrams. The anomalous dimension matrices for bilinear and the semileptonic operators in our interest will be computed from n-point Green functions with $n = 2$ and $n = 4$ respectively and the calculation is described in Sec.7.4. The combination of Eq. (7.1) and (7.13) allows one to obtain the following *master formulae* for the anomalous dimension matrices in Eq. (7.10),

$$\hat{\gamma}_s^{(0)} = -2\, Z_1^{(1)} = -2\left[\frac{1}{2}\left(\sum_{i=1}^{n} Z_{\psi_i,1}^{(1)}\right) \hat{\mathbb{1}} + \hat{Z}_{\rm GF,1}^{(1)}\right]\ , \tag{7.14}$$

$$\hat{\gamma}_e^{(0)} = -2\, Z_1^{(e)} = -2\left[\frac{1}{2}\left(\sum_{i=1}^{n} Z_{\psi_i,1}^{(e)}\right) \hat{\mathbb{1}} + \hat{Z}_{\rm GF,1}^{(e)}\right]\ , \tag{7.15}$$

$$\hat{\gamma}_s^{(1)} = -4\, Z_1^{(2)} = -4\left[\frac{1}{2}\left(\sum_{i=1}^{n} Z_{\psi_i,1}^{(2)}\right) \hat{\mathbb{1}} + \hat{Z}_{\rm GF,1}^{(2)}\right]\ , \tag{7.16}$$

$$\hat{\gamma}_{se}^{(1)} = -4\, Z_1^{(se)} = -4\left[\frac{1}{2}\left(\sum_{i=1}^{n} Z_{\psi_i,1}^{(se)}\right) \hat{\mathbb{1}} + \hat{Z}_{\rm GF,1}^{(se)}\right]\ . \tag{7.17}$$

Clearly $Z_{\psi,1}^{(n)} = Z_{\psi,1}^{(se)} = 0$ for each n if the fermion ψ is a charged lepton. In the case of neutrinos one also have $Z_{\nu,1}^{(e)} = 0$. Before entering the discussion on how to compute the Green functions at one- and two-loops, we should discuss a complication arising in dimensional regularizations: the presence of the so-called *evanescent* operators [96–98].

7.2 Evanescent operators

Evanescent operators (EOs) are independent operators which are present in D dimensions, but disappear in the physical basis of operators in four dimensions. Such operators, which are an artifact of using dimensional regularization, must be taken

carefully into account in the calculation of two-loop anomalous dimensions. Indeed, in the intermediate steps of the calculation EOs can mix with physical operators and affect the final result. One-loop diagrams might contain a $1/\epsilon$ divergence proportional to the matrix element of an evanescent operator, which is of $\mathcal{O}(\epsilon)$ by definition. While this does not affect one-loop anomalous dimensions, when inserted as a subdiagram in a higher-loop diagram, such evanescent operators can generate both UV divergent and finite contributions. These effects must be taken into account in order to correctly extract two-loop UV divergences and their associated anomalous dimensions. For a detailed discussion of the mixing between physical and evanescent operators see Refs. [96–99]. Therefore, we introduce non-singular terms in the ϵ-expansion of RCs in order to be able to incorporate the effects of evanescent operators, namely by expanding $\hat{Z}$ as

$$\hat{Z} = \sum_{k=1}^{\infty} \left(\frac{\alpha_{\rm s}}{4\pi}\right)^k \hat{Z}^{(k)} + \frac{\alpha_{\rm em}}{4\pi}\,\hat{Z}^{(e)} + \frac{\alpha_{\rm s}\alpha_{\rm em}}{(4\pi)^2}\,\hat{Z}^{(se)} \ , \tag{7.18}$$

we consider

$$\hat{Z}^{(k)} = \sum_{i=0}^{k} \frac{\hat{Z}_i^{(k)}}{\epsilon^i} \ , \quad \hat{Z}^{(e)} = \sum_{i=0}^{1} \frac{\hat{Z}_i^{(e)}}{\epsilon^i} \ , \quad \hat{Z}^{(se)} = \sum_{i=0}^{2} \frac{\hat{Z}_i^{(se)}}{\epsilon^i} \ . \tag{7.19}$$

Inserting such relations into Eq. (7.7) we derive the following relations

$$\begin{aligned} \hat{\gamma}_s^{(0)} &= -2\epsilon\hat{Z}^{(1)} \ , \qquad \hat{\gamma}_e^{(0)} = -2\epsilon\hat{Z}^{(e)} \ , \\ \hat{\gamma}_s^{(1)} &= -4\epsilon\hat{Z}^{(2)} - 2\beta_0\hat{Z}^{(1)} + 2\epsilon\hat{Z}^{(1)}\hat{Z}^{(1)} \ , \\ \hat{\gamma}_{se}^{(1)} &= -4\epsilon\hat{Z}^{(se)} + 2\epsilon\left(\hat{Z}^{(e)}\hat{Z}^{(1)} + \hat{Z}^{(1)}\hat{Z}^{(e)}\right) \ , \end{aligned} \tag{7.20}$$

and hence

$$\begin{aligned} \hat{\gamma}_s^{(0)} &= -2\hat{Z}_1^{(1)} \ , \qquad \hat{\gamma}_e^{(0)} = -2\hat{Z}_1^{(e)} \ , \\ \hat{\gamma}_s^{(1)} &= -4\hat{Z}_1^{(2)} - 2\beta_0\hat{Z}_0^{(1)} + 2\left(\hat{Z}_0^{(1)}\hat{Z}_1^{(1)} + \hat{Z}_1^{(1)}\hat{Z}_0^{(1)}\right) \ , \\ \hat{\gamma}_{se}^{(1)} &= -4\hat{Z}_1^{(se)} + 2\left(\hat{Z}_1^{(e)}\hat{Z}_0^{(1)} + \hat{Z}_0^{(e)}\hat{Z}_1^{(1)} + \hat{Z}_1^{(1)}\hat{Z}_0^{(e)} + \hat{Z}_0^{(1)}\hat{Z}_1^{(e)}\right) \ . \end{aligned} \tag{7.21}$$

As we can see, one-loop anomalous dimensions are not affected by the presence of EOs, while they enter the calculation of two-loop anomalous dimensions instead. Indeed, the products of the matrices $\hat{Z}_j^{(i)}$ in Eq. (7.21) have to be done by summing indices over the full set of operators, including EOs. We notice that the first terms in the expressions of the two-loops anomalous dimension matrices $\hat{\gamma}_s^{(1)}$ and $\hat{\gamma}_{se}^{(1)}$ in Eq. (7.21) correspond to the master formulae of Eqs. (7.16) - (7.17), while the remaining terms are the corrections we are looking for. Therefore, the inclusion of EOs in the calculation results in the addition of a proper counterterm to the two loop diagrams. Notice that the correction to the master formulae for two-loop anomalous dimensions due to EOs is twice as smaller than the corresponding counter-terms present in the main terms. Translated in the language of diagrams, this means that in calculating $\gamma_s^{(1)}$ and $\gamma_{se}^{(1)}$ the contributions to the counter-diagrams involving an evanescent operator should be multiplied by a factor 1/2.

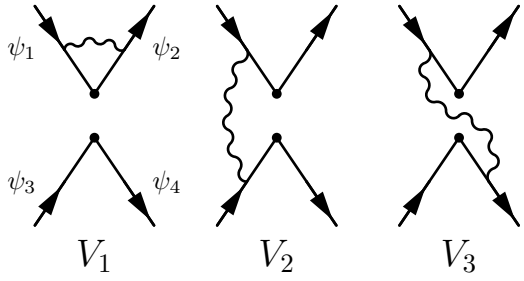

Figure 7.1. Current-current diagrams at one-loop.

7.3 Diagrams and counterterms

In this section we describe the explicit calculation of the anomalous dimension matrix $\hat{\gamma}(\alpha_s, \alpha_{em})$ from four fermion current-current diagrams, with a focus on the mixed term $\hat{\gamma}_{se}^{(1)}$ of $\mathcal{O}(\alpha_s \alpha_{em})$. The operators we are interested in are those described in Part I of this thesis, namely quark bilinear operators and weak four-fermion operators made of two quarks and a lepton-neutrino pair entering the lattice calculation of leptonic decay rates of light mesons. We notice that anomalous dimensions for the two sets of operators can be derived from the evaluation of the same set of *current-current* diagrams, which are then combined in different ways and with different colour and charge factors. The complete set of current-current diagrams at one-loop are reported in Fig. 7.1, while the two-loops diagrams are collected in Fig. 7.2, assuming curly lines to be, in general, non-abelian gauge bosons, e.g. gluons. The blob appearing in diagrams $V_{29,30,31}$ corresponds to the sum of a fermion, a gluon and a ghost loop. Diagrams obtainable through up-down or left-right reflections from those reported in Figs. 7.1 and 7.2 are not shown, but contribute to the multiplicity of the diagrams. We will refer to the fermionic lines in the diagrams using the enumeration reported in Fig. 7.1. In addition to current-current diagrams, we need to compute also self-energy diagrams contributing to the fermionic RCs Z_ψ. Their computation has been already done by several authors, see for example Refs. [12, 97], and it will be discussed later in this Section. The explicit calculation of the anomalous dimensions described in the following has been carried out using Wolfram Mathematica [100].

Bilinear operators In the case of *bilinear operators* defined in Eq. (3.47), anomalous dimensions can be obtained from the diagrams with vertex corrections only. We remind that, both in QCD and QED, bilinear operators do not mix with each and therefore the anomalous dimension matrix reduces to a number. At one loop only diagram V_1 contributes to the QCD and QED anomalous dimensions, while at two loops a subset of the diagrams in Fig. 7.2 has to be considered. The pure QCD two-loop anomalous dimension $\gamma_s^{(1)}$ gets contributions from the diagrams $\{V_4, V_7, V_{10}, V_{13}, V_{25}, V_{29}\}$ at $\mathcal{O}(\alpha_s^2)$, i.e. considering both bosons as gluons. On the other hand, the mixed QCD+QED matrix $\gamma_{se}^{(1)}$ is obtained from $\mathcal{O}(\alpha_s \alpha_{em})$ diagrams. This means that only the subset of "abelian" diagrams $\{V_4, V_7, V_{10}, V_{13}\}$ has to be taken into account. Clearly, the nature of the two bosons has to be

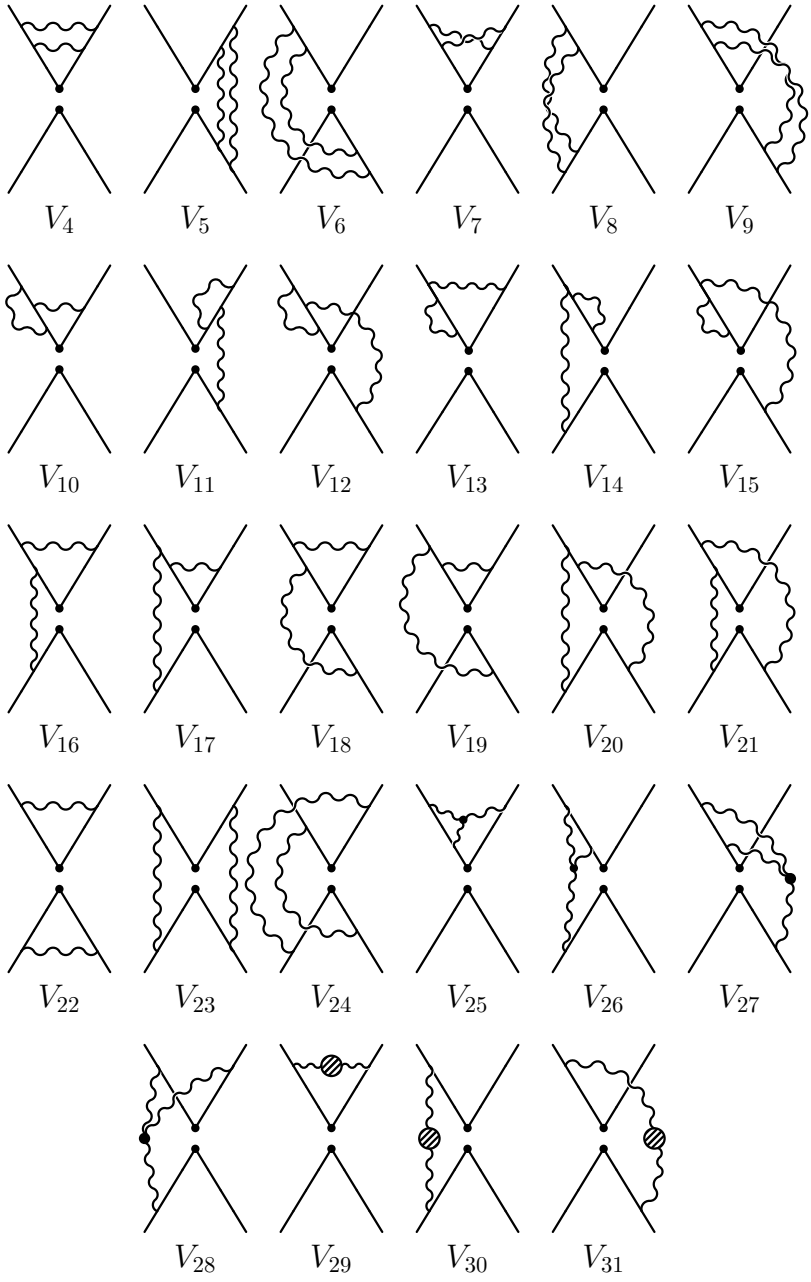

Figure 7.2. Current-current diagrams at two-loops. The directions of external momenta are chosen as in Fig. 7.1.

distinguished in this case, thus doubling the multiplicity of the diagrams. In the following we will focus only on the calculation of the matrix $\gamma_{se}^{(1)}$, since the strong anomalous dimensions are already known and have been computed in the RI' scheme up to four loops for Z_P and Z_S (in the Landau gauge) in Ref. [73] and up to three loops for Z_T in Ref. [74]. We refer to such strong anomalous dimensions at order $\mathcal{O}(\alpha_s^{k+1})$ as $\gamma_{s,P}^{(k)}$, $\gamma_{s,S}^{(k)}$ and $\gamma_{s,T}^{(k)}$ respectively. The anomalous dimensions for the

vector and axial vector current vanish at all order due to QCD Ward identities in the massless limit. Furthermore, the pure QED one-loop anomalous dimension $\gamma_e^{(0)}$ can be straightforwardly deduced from $\gamma_s^{(0)}$. Indeed, the exchange of a gluon with a photon in diagram V_1 simply results in a different overall colour factor, namely ($\Gamma = S, P, T$)

$$\gamma_{s,\Gamma}^{(0)} = C_F\, \gamma_{e,\Gamma}^{(0)} \,, \tag{7.22}$$

with $C_F = (N^2-1)/2N = 4/3$. We remind that the bilinear operators used in this work are considered to be made of quarks with unitary fractional electric charge, namely $e_{q_1} = e_{q_2} = 1$.

Four-fermion operators Also in the case of the weak four-fermion operators in Eq. (3.61) we have to deal only with a subset of diagrams. If we consider the upper and lower fermions in Figs. 7.1 and 7.2 to be respectively quarks and leptons, then it follows that strong anomalous dimensions receive contributions from the same set of diagrams considered for bilinear operators, although with different operator insertions. From Eq. (3.72) we deduce that the QCD anomalous dimension matrix at order $\mathcal{O}(\alpha_{\rm s}^{k+1})$ has the form

$$\hat{\gamma}_s^{(k)} = \mathrm{diag}\left(0, 0, \gamma_{s,P}^{(k)}, \gamma_{s,P}^{(k)}, \gamma_{s,T}^{(k)}\right) \,, \tag{7.23}$$

the strong anomalous dimensions $\gamma_{s,P}$ and $\gamma_{s,T}$ being defined above. When computing the matrices $\hat{\gamma}_e^{(0)}$ and $\hat{\gamma}_{se}^{(1)}$, instead, one has to consider also diagrams with *one* photon exchange between upper quarks and the charged lepton. The multiplicity of the diagrams will have to be then consistently counted, recalling that the neutrino is electrically neutral. The set of two-loop diagrams contributing at $\mathcal{O}(\alpha_{\rm s}\alpha_{\rm em})$ is then $\{V_4, V_7, V_{10} - V_{19}, V_{22}\}$.

In the following we report the calculation of the one-loop and two-loop diagrams in NDR. We use as a benchmark for our calculation the one performed in Ref. [12], where only the insertions of the operators $\gamma_\mu(1-\gamma_5)\otimes\gamma^\mu(1-\gamma_5)$ and $\gamma_\mu(1-\gamma_5)\otimes\gamma^\mu(1+\gamma_5)$ have been considered.

Table 7.1. Set of operators and corresponding set of projectors adopted in our calculation.

Operators		$X \otimes Y$	$P_X \otimes P_Y$
Bilinears	O_S	$\mathbb{1} \otimes \mathbb{1}$	$\mathbb{1} \otimes \mathbb{1}$
	O_V	$\gamma^\mu \otimes \mathbb{1}$	$\gamma_\mu \otimes \mathbb{1}$
	O_P	$\gamma_5 \otimes \mathbb{1}$	$\gamma_5 \otimes \mathbb{1}$
	O_A	$\gamma^\mu\gamma^5 \otimes \mathbb{1}$	$\gamma_\mu\gamma^5 \otimes \mathbb{1}$
	O_T	$\sigma^{\mu\nu} \otimes \mathbb{1}$	$-\sigma_{\mu\nu} \otimes \mathbb{1}$
Four fermions	O_1	$\gamma^\mu(1-\gamma_5) \otimes \gamma_\mu(1-\gamma_5)$	$\gamma^\nu(1+\gamma_5) \otimes \gamma_\nu(1+\gamma_5)$
	O_2	$\gamma^\mu(1+\gamma_5) \otimes \gamma_\mu(1-\gamma_5)$	$(1+\gamma_5) \otimes (1-\gamma_5)$
	O_3	$(1-\gamma_5) \otimes (1+\gamma_5)$	$\gamma^\nu(1+\gamma_5) \otimes \gamma_\nu(1-\gamma_5)$
	O_4	$(1+\gamma_5) \otimes (1+\gamma_5)$	$(1+\gamma_5) \otimes (1+\gamma_5)$
	O_5	$\sigma^{\mu\nu}(1+\gamma_5) \otimes \sigma_{\mu\nu}(1+\gamma_5)$	$\sigma^{\alpha\beta}(1+\gamma_5) \otimes \sigma_{\alpha\beta}(1+\gamma_5)$

7.3.1 Current-current diagrams at one-loop

Let us consider the diagrams in Fig. 7.1, where the wavy lines can be due to a gluon or a photon exchange. The difference will result in a different colour-charge factor. We denote the Dirac structur of a generic four fermion operator

$$O = \bar{\psi}_2 X \psi_1 \; \bar{\psi}_4 Y \psi_3 \tag{7.24}$$

with the short notation $X \otimes Y$. The Dirac structures inserted in the vertices are reported in Table 7.1. In the case of bilinear operators, we trasform them into four-fermion operators with the trivial insertion of the Dirac identity matrix on the additional fermionic line, i.e. $(\bar{\psi}_4 \mathbb{1} \psi_3)$. In general, the insertion of an operator into a given diagram at one or two loops results in a linear combination of basis operators and hence the corresponding amputated Green function will be in general a matrix. In order to compute the coefficients of such linear combination, we introduce a set of projectors $\mathcal{P} \equiv P_X \otimes P_Y$, consisting in a combination of Dirac gamma matrices. The projectors adopted for the set of operators used in this work are reported in the right column of Table 7.1. By denoting the 1PI Green function with the insertion of the operator O_i as $\langle O_i \rangle$ we have in general that

$$\langle O_i \rangle = c_{ij} \, \langle O_j \rangle^{(0)} \; , \tag{7.25}$$

where the coefficients c_{ij} contains the divergences $1/\epsilon^n$ contributing to the renormalization constants we are interested in and $\langle O_j \rangle^{(0)}$ is the tree-level Green function of the operator O_j. In order to extract the coefficient C_{ij} we trace $\langle O_i \rangle$ with a projector $\mathcal{P}_k$,

$$\begin{aligned} \mathrm{Tr}[\langle O_i \rangle \, \mathcal{P}_k] &= c_{ij} \, \mathrm{Tr}[\langle O_j \rangle^{(0)} \mathcal{P}_k] \\ &\equiv c_{ij} \, N_{jk} \; , \end{aligned} \tag{7.26}$$

where the trace is done over the Dirac indices and in D dimensions as follows

$$N_{ij} = \mathrm{Tr}[\langle O_i \rangle^{(0)} \, \mathcal{P}_j] \equiv \mathrm{Tr}[X_i P_{X_j} Y_i P_{Y_j}] \; . \tag{7.27}$$

As a consequence, the coefficients of the linear combination are given by

$$c_{ij} = \mathrm{Tr}[\langle O_i \rangle \, \mathcal{P}_k] \, (N^{-1})_{kj} \equiv \mathrm{Tr}[\langle O_i \rangle \, \mathcal{P}_k] \, \mathcal{N}_{kj} \; . \tag{7.28}$$

The *normalization* matrices $\mathcal{N} \equiv N^{-1}$ for bilinear operators (bil) and the weak four-fermion operators (ff) result to be

$$\mathcal{N}_{\mathrm{bil}} = \begin{pmatrix} \frac{1}{4} & 0 & 0 & 0 & 0 \\ 0 & \frac{1}{16} + \frac{\epsilon}{32} & 0 & 0 & 0 \\ 0 & 0 & \frac{1}{4} & 0 & 0 \\ 0 & 0 & 0 & \frac{1}{16} + \frac{\epsilon}{32} & 0 \\ 0 & 0 & 0 & 0 & \frac{1}{48} + \frac{7\epsilon}{288} \end{pmatrix} \; , \tag{7.29}$$

$$\mathcal{N}_{\mathrm{ff}} = \begin{pmatrix} -\frac{1}{256} - \frac{3\epsilon}{512} & 0 & 0 & 0 & 0 \\ 0 & \frac{1}{128} + \frac{\epsilon}{256} & 0 & 0 & 0 \\ 0 & 0 & \frac{1}{128} + \frac{\epsilon}{256} & 0 & 0 \\ 0 & 0 & 0 & \frac{1}{128} + \frac{\epsilon}{256} & -\frac{1}{512} - \frac{\epsilon}{512} \\ 0 & 0 & 0 & -\frac{1}{512} - \frac{\epsilon}{512} & -\frac{1}{6144} - \frac{13\epsilon}{36864} \end{pmatrix} \; . \tag{7.30}$$

It has to be stressed that the projection on the physical basis of four-fermion operators does not take into account the contribution of EOs to the Green function $\langle O_i \rangle$. Therefore the coefficients c_{ij} obtained at two loops will require an appropriate correction. We now discuss, as an example, the explicit calculation of the one-loop diagram V_2 in Fig. 7.1 with the insertion of the operator O_1. By choosing equal external momenta p and setting fermion masses to zero, the diagram V_2 is given by

$$\begin{aligned} D^{(2)}(O_1) &= ig^2\bar{\mu}^{2\epsilon}\mathcal{C}^{(2)} \int \frac{\mathrm{d}^D q}{(2\pi)^D} \frac{X_1 \not{q} \gamma^\mu \otimes Y_1 \not{q} \gamma_\mu}{(q^2)^2 (p-q)^2} \\ &= ig^2\bar{\mu}^{2\epsilon}\mathcal{C}^{(2)} \int \frac{\mathrm{d}^D q}{(2\pi)^D} \frac{q^\alpha q^\beta}{(q^2)^2 (p-q)^2} \left\{ X_1 \gamma_\alpha \gamma^\mu \otimes Y_1 \gamma_\beta \gamma_\mu \right\} \end{aligned} \tag{7.31}$$

where the Feynman gauge for the boson has been chosen and

$$\bar{\mu}^2 \equiv \mu^2 \frac{e^{\gamma_E}}{4\pi} \tag{7.32}$$

defines the $\overline{\mathrm{MS}}$-scheme subtraction scale, which removes spurious terms in the ϵ-expansion, which are simply artifacts of the dimensional regularization. Charge-colour factors are contained in the coefficient $\mathcal{C}^{(2)}$ and g is a generic coupling constant. By solving the D-dimensional integral[1] and expanding the result in powers of ϵ, the diagram V_2 takes the form

$$D^{(2)}(O_1) = -\frac{\alpha}{4\pi} \left(\frac{\mu^2}{-p^2} \right)^\epsilon \mathcal{C}^{(2)} \left[\frac{1}{4\epsilon} + \frac{5}{8} \right] \left\{ X_1 \gamma^\alpha \gamma^\mu \otimes Y_1 \gamma_\alpha \gamma_\mu \right\} \ . \tag{7.33}$$

In D dimensions, the string of gamma matrices in Eq. (7.33) cannot be reduced to the physical insertion $X_1 \otimes Y_1$, contrary to four dimensional case. Indeed, the relation

$$\gamma_\mu \gamma_\nu \gamma_\alpha = g_{\mu\nu}\gamma_\alpha - g_{\mu\alpha}\gamma_\nu + g_{\nu\alpha}\gamma_\nu + i\varepsilon_{\mu\nu\alpha\beta}\gamma^\beta\gamma_5 \tag{7.34}$$

only holds in $D = 4$ dimensions, the Dirac algebra of gamma matrices becoming formally infinite dimensional in a $D = 4 - 2\epsilon$ dimensional space-time for arbitrary ϵ. The problem is clearly the lack of an extension of the completely antisymmetric tensor $\varepsilon_{\mu\nu\alpha\beta}$ away from $D = 4$. However we can parametrize the difference between a higher product of gamma matrices and its four-dimensional limit with an evanescent operator, namely

$$X_1 \gamma^\alpha \gamma^\mu \otimes Y_1 \gamma_\alpha \gamma_\mu = 4(4-\epsilon)\, X_1 \otimes Y_1 + E^{(2)} \ . \tag{7.35}$$

As a consequence,

$$\begin{aligned} D^{(2)}(O_1) &= -\frac{\alpha}{4\pi} \left(\frac{\mu^2}{-p^2} \right)^\epsilon \mathcal{C}^{(2)} \left[\frac{1}{4\epsilon} + \frac{5}{8} \right] \left\{ 4(4-\epsilon)\, X_1 \otimes Y_1 + E^{(2)} \right\} \\ &\equiv D^{(2)}_{\mathrm{bare}}(O_1) + D^{(2)}_E(O_1) \ . \end{aligned} \tag{7.36}$$

[1] We do not report the explicit calculation of D-dimensional integrals, but refer to Ref. [101] for a very good review on the subject.

with

$$D^{(2)}_{\rm bare}(O_1) = \frac{\alpha}{4\pi}\left(\frac{\mu^2}{-p^2}\right)^{\epsilon}\mathcal{C}^{(2)}\left[-\frac{4}{\epsilon}-9\right]\; X_1\otimes Y_1 \tag{7.37}$$

$$D^{(2)}_{E}(O_1) = \frac{\alpha}{4\pi}\left(\frac{\mu^2}{-p^2}\right)^{\epsilon}\mathcal{C}^{(2)}\left[\frac{1}{4\epsilon}+\frac{5}{8}\right] E^{(2)}\;. \tag{7.38}$$

Notice that, when projecting the result of $D^{(2)}$ on the physical set of operators with the projector $\mathcal{P}_1$, the contribution of $D^{(2)}_E$ vanishes. For diagrams V_1 and V_3 we obtain analogous results

$$D^{(1)}(O_1) = \frac{\alpha}{4\pi}\left(\frac{\mu^2}{-p^2}\right)^{\epsilon}\mathcal{C}^{(1)}\left[\frac{1}{4\epsilon}+\frac{5}{8}\right]\left\{4(1-2\epsilon)\,X_1\otimes Y_1 + E^{(1)}\right\} \tag{7.39}$$

$$D^{(3)}(O_1) = \frac{\alpha}{4\pi}\left(\frac{\mu^2}{-p^2}\right)^{\epsilon}\mathcal{C}^{(3)}\left[\frac{1}{4\epsilon}+\frac{5}{8}\right]\left\{4(1-2\epsilon)\,X_1\otimes Y_1 + E^{(3)}\right\} \tag{7.40}$$

The coefficient preceding the tree-level insertions $X_i\otimes Y_i$ in previous equations will be different, in general, for each operator. By defining as $\mathcal{F}^{(n)}_{ij}$ the coefficient of the tree-level structure $X_j\otimes Y_j$ obtained when the operator O_i is inserted in the diagram V_n $(n=1,2,3)$, they can be explicitely computed as

$$\begin{aligned}
\mathcal{F}^{(1)}_{ij}(\epsilon) &= {\rm Tr}\left[\gamma^\mu\gamma^\nu X_i\gamma^\nu\gamma^\mu P_{X_k}\; Y_i P_{Y_k}\right]\mathcal{N}_{kj}\;,\\
\mathcal{F}^{(2)}_{ij}(\epsilon) &= {\rm Tr}\left[X_i\gamma^\nu\gamma^\mu P_{X_k}\; Y_i\gamma^\nu\gamma^\mu P_{Y_k}\right]\mathcal{N}_{kj}\;,\\
\mathcal{F}^{(3)}_{ij}(\epsilon) &= {\rm Tr}\left[X_i\gamma^\nu\gamma^\mu P_{X_k}\; \gamma^\mu\gamma^\nu Y_i P_{Y_k}\right]\mathcal{N}_{kj}\;.
\end{aligned} \tag{7.41}$$

Obviously, such choice for the coefficients $\mathcal{F}^{(n)}_{ij}$ is not unique. In principle we could take them of the form $\mathcal{F}^{(0)}_{ij} + a_{ij}\,\epsilon$, with arbitrary values of a_{ij}. Different values of a_{ij} result in a different definition of the evanescent operators $E^{(n)}$.

The pole and finite terms coming from the calculation of diagrams $V_{1,3}$ are collected in Tables 7.2 and 7.3 respectively for the insertions of the bilinear operators and the weak four fermion operators reported in Table 7.1. The corresponding charge-colour factors and multiplicity are not shown. In the case of weak four-fermion operator the 1PI Green function is a matrix and all elements not reported in Table 7.3 are zero. Our results for $O_{1,1}$ and $O_{2,2}$ in Table 7.3 are in agreement with those obtained in Ref. [12]. From Eqs. (7.36), (7.39) and (7.40), we can define the counterterms

$$\begin{aligned}
D^{(1)}_C(O_1) &= \frac{\alpha}{4\pi}\mathcal{C}^{(i)}\left[\frac{1}{4\epsilon}\right]\left\{\mathcal{F}^{(1)}_{11}(0)\,X_1\otimes Y_1\right\}\;,\\
D^{(2)}_C(O_1) &= -\frac{\alpha}{4\pi}\mathcal{C}^{(2)}\left[\frac{1}{4\epsilon}\right]\left\{\mathcal{F}^{(2)}_{11}(0)\,X_1\otimes Y_1\right\}\;,\\
D^{(3)}_C(O_1) &= \frac{\alpha}{4\pi}\mathcal{C}^{(3)}\left[\frac{1}{4\epsilon}\right]\left\{\mathcal{F}^{(3)}_{11}(0)\,X_1\otimes Y_1\right\}\;,
\end{aligned} \tag{7.42}$$

By subtracting the counterterms in Eq. (7.42) from the result of the calculation of the diagrams in Fig. 7.1, we thus obtain the renormalized operator matrix elements

Table 7.2. Singular and finite terms for diagrams in Fig. 7.1, with the insertion of bilinear operators. Multiplicity and colour-charge factors are not reported and an overall factor $\alpha/4\pi$ is understood.

V_n	O_S, O_P		O_V, O_A		O_T	
	$\mathcal{O}(1/\epsilon)$	$\mathcal{O}(1)$	$\mathcal{O}(1/\epsilon)$	$\mathcal{O}(1)$	$\mathcal{O}(1/\epsilon)$	$\mathcal{O}(1)$
V_1	4	6	1	$\frac{1}{2}$	0	0
V_2	2	2	-1	$-\frac{7}{2}$	-2	-4
V_3	4	6	1	$\frac{1}{2}$	0	0

Table 7.3. Singular and finite terms for diagrams in Fig. 7.1, with the insertion of weak four-fermion operators. Multiplicity and colour-charge factors are not reported and an overall factor $\alpha/4\pi$ is understood. The notation $O_{i,j}$ means that the diagram with the insertion of the operator O_i is projected on the Dirac structure of operator O_j.

V_n	$O_{1,1}$		$O_{2,2}$		$O_{3,3}$		$O_{4,4}$	
	$\mathcal{O}(1/\epsilon)$	$\mathcal{O}(1)$	$\mathcal{O}(1/\epsilon)$	$\mathcal{O}(1)$	$\mathcal{O}(1/\epsilon)$	$\mathcal{O}(1)$	$\mathcal{O}(1/\epsilon)$	$\mathcal{O}(1)$
V_1	1	$\frac{1}{2}$	1	$\frac{1}{2}$	4	6	4	6
V_2	-4	-9	-1	$-\frac{7}{2}$	-1	$-\frac{7}{2}$	-1	-2
V_3	1	$\frac{1}{2}$	4	6	1	$\frac{1}{2}$	1	2

V_n	$O_{4,5}$		$O_{5,4}$		$O_{5,5}$	
	$\mathcal{O}(1/\epsilon)$	$\mathcal{O}(1)$	$\mathcal{O}(1/\epsilon)$	$\mathcal{O}(1)$	$\mathcal{O}(1/\epsilon)$	$\mathcal{O}(1)$
V_1	0	0	0	0	0	0
V_2	$-\frac{1}{4}$	$-\frac{5}{8}$	-12	-10	-3	-6
V_3	$-\frac{1}{4}$	$-\frac{5}{8}$	-12	-10	3	4

expressed in terms of the tree-level ones. From the counterterms $D_C^{(i)}$ we extract the contribution to the one-loop anomalous dimension, by taking the residues at the pole $1/\epsilon$. Moreover, $D_C^{(i)}$ will be used in the two-loop calculation to compute the two-loop counter-diagram.

7.3.2 Current-current diagrams at two loops

After the detailed study of the one-loop diagrams, we are ready to show the construction of a "complete" two loop diagram, including all necessary counterterms. In general, the computation of any diagram or sum of diagrams D, including the effect of the corresponding first-order counterterms D_C leads to a total result of the form

$$D - D_C = \frac{\alpha}{4\pi}\left(\frac{\mu^2}{-p^2}\right)^{2\epsilon}\left[\frac{F}{\epsilon^2} + \frac{G}{\epsilon} + \cdots\right] - \frac{\alpha}{4\pi}\left(\frac{\mu^2}{-p^2}\right)^{\epsilon}\left[\frac{F_C}{\epsilon^2} + \frac{G_C}{\epsilon} + \cdots\right] , \quad (7.43)$$

where only singular terms in the brackets were shown. The first term is the contribution to the unrenormalized vertex function, without counterterm subtraction. The second term comes from the insertion of first-order counterterms. Note that the

power of μ^2 in the counter-diagram is ϵ and not 2ϵ as in D, because the first order counter-term (see for example Eq. (7.42)) does not contain the factor $(\mu^2/p^2)^\epsilon$. In order to obtain the renormalized vertices at two-loops the double and single poles should be subtracted away from Eq. (7.43), by properly defining RCs. By expanding the exponential in Eq. (7.43) we find for the pole part

$$(D - D_C)_{\rm poles} = \frac{\alpha}{4\pi}\left[\frac{F - F_C}{\epsilon^2} + \frac{(2F - F_C)\ell + (G - G_C)}{\epsilon}\right] , \tag{7.44}$$

with $\ell = \log(\mu^2/(-p^2))$. Since in the $\overline{\rm MS}$ the RC cannot depend explicitely on ℓ, we have that diagram by diagram the relation $F_C = 2F$ must be satisfied. We have verified that such relation holds for all the diagrams in Fig. 7.2. Therefore Eq. (7.44) reduces to

$$(D - D_C)_{\rm poles} = \frac{\alpha}{4\pi}\left[\frac{-F}{\epsilon^2} + \frac{G - G_C}{\epsilon}\right] . \tag{7.45}$$

In the MS scheme, counterterms are usually obtained by retaining only the $1/\epsilon$ parts in the subdiagrams. There is, however, the subtlety related to the mixing in $D \neq 4$ of physical and evanescent operators, as discussed in the previous section. Therefore, in addiction to the usual counter-diagram subtraction we will have to evaluate the correction introduced by the insertion of evanescent operators in sub-divergent diagrams. Let us consider as an example the diagram V_5 of Fig. 7.2, where we insert the operator O_1. We denote as $D^{(5)}$ the double and single pole contribution from this diagram. The external momenta are set all equal to p and their direction is the same as in Fig. 7.1. This is computed similarly to the one-loop case, by using the projection method. Strings of Dirac matrices, which are independent operators in D dimensions, are projected on the physical operator basis. Then we solve the two-loop D-dimensional integrals and expand the result in inverse powers of ϵ. The projection method allows one to reduce the calculation of difficult tensor integrals to the evaluation of few scalar ones. Once $D^{(5)}$ is computed, we subtract the corresponding counter-diagrams. They are computed by substituting internal subdiagrams with the suitable one-loop divergent counter-terms $D_C^{(i)}$. In our case, the two-loop diagram V_5 can be visualized as the convolution of two nested one-loop diagrams V_2. Therefore by taking the results of Eqs. (7.37) and (7.42), and neglecting for the moment the contribution of EOs at one-loop, the counterdiagram $D_C^{(5)}$ can be obtained as

$$\begin{aligned} D_C^{(5)}(O_1) &= \left(\frac{\alpha}{4\pi}\right)^2 \left(\frac{\mu^2}{-p^2}\right)^\epsilon \mathcal{C}^{(5)} \left[-\frac{4}{\epsilon} - 9\right] \left(-\frac{4}{\epsilon}\right) \; X_1 \otimes Y_1 \\ &= \left(\frac{\alpha}{4\pi}\right)^2 \left(\frac{\mu^2}{-p^2}\right)^\epsilon \mathcal{C}^{(5)} \left[\frac{16}{\epsilon^2} + \frac{36}{\epsilon}\right] \; X_1 \otimes Y_1 \; , \end{aligned} \tag{7.46}$$

where $\mathcal{C}^{(5)}$ is the colour-charge factor of $D^{(5)}$. We then calculate the contribution of the evanescent operator to the counter-diagram by simply inserting the appropriate structure $E^{(n)}$, defined as in Eq. (7.35), into the remaining one-loop sub-diagram and projecting the result onto the physical operator basis. For diagram V_5 we would

obtain

$$
\begin{aligned}
D_E^{(5)} &= \frac{\alpha}{4\pi}\left(\frac{\mu^2}{-p^2}\right)^{\epsilon} \mathcal{C}^{(5)} \left[\frac{1}{4\epsilon}+\frac{5}{8}\right]^2 E^{(2)}(X_1\gamma^\alpha\gamma^\mu \otimes Y_1\gamma_\alpha\gamma_\mu) \qquad (7.47)\\
&= \frac{\alpha}{4\pi}\left(\frac{\mu^2}{-p^2}\right)^{\epsilon} \mathcal{C}^{(5)} \left[\frac{1}{4\epsilon}+\frac{5}{8}\right]^2 \{X_1\gamma^\alpha\gamma^\mu\gamma^\nu\gamma^\rho \otimes Y_1\gamma_\alpha\gamma_\mu\gamma_\nu\gamma_\rho \\
&\qquad\qquad - [4(4-\epsilon)]^2\ X_1\gamma^\alpha\gamma^\mu \otimes Y_1\gamma_\alpha\gamma_\mu\Big\} \\
&= \frac{\alpha}{4\pi}\left(\frac{\mu^2}{-p^2}\right)^{\epsilon} \mathcal{C}^{(5)} \left[-\frac{6}{\epsilon}\right] . \qquad (7.48)
\end{aligned}
$$

We observe that the $1/\epsilon^2$ singularity, as expected, is unaffected by the evanescent contribution. The "complete" diagram is thus obtained by combining the tree different contributions as

$$\overline{D}^{(5)} = D^{(5)} - D_C^{(5)} - \frac{1}{2}D_E^{(5)} , \qquad (7.49)$$

where the factor 1/2 comes from the relation in Eq. (7.21). The contribution proportional to the first coefficient of the beta function β_0 in Eq. (7.21) is absent for diagram V_5. It will only give contribution for those diagrams which contain an internal loop corresponding to the renormalization of α_s, as for example V_{12}. The term $\sim \beta_0$ is automatically taken into account by subtractng the counterterm corresponding to the renormalization of the strong vertex. In order to compare our results with those obtained in Ref. [12] we find it useful to redefine the complete diagram $\overline{D}^{(5)}$ as follows

$$\overline{D}^{(5)} \equiv D^{(5)} - C^{(5)} + E^{(5)} , \qquad (7.50)$$

where $C^{(5)} \equiv D_C^{(5)} + D_E^{(5)}$ corresponds to the result of the counter-diagram obtained by substituting divergent sub-diagrams with counterterms, including those proportional to EOs, as done by the authors of Ref. [12], and $E^{(5)} = D_E^{(5)}/2$. In Tables A.1-A.10 of Appendix A we report, in units of $(\alpha/4\pi)^2$, the double and single pole contributions of all the two-loop current-current diagrams and the corresponding counterterms for all possible operator insertions, specifying the contribution of EO counterterms when present and using the notation of Eq. (7.50). The coupling α, although generic, has to be read as $\alpha_{\rm s}$ in the case of non-abelian diagrams contributing to $\gamma_s^{(1)}$ only. Our two-loop results for $O_{1,1}$ and $O_{2,2}$ in Tables A.4 and A.5 are in agreement with those obtained in Ref. [12].

7.3.3 Self-energy diagrams at one and two loops

The calculation of the quark self-energy diagrams is much simpler and has already been done by several authors (e.g. in Refs. [96, 97, 102]). We do not discuss the calculation in detail, but report in Tables 7.4 and 7.5 the results of the different diagrams at one and two loops shown in Figs. 7.3 and 7.4, respectively. In the calculation of the non-abelian diagram S_3 we include also the contribution of the ghost field loop. In the last two columns of Tables 7.4 and 7.5 we also report the

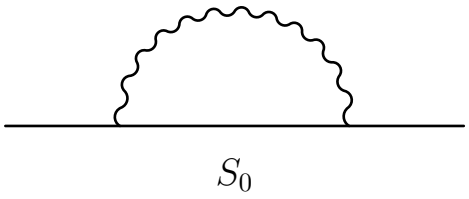

Figure 7.3. Self-energy diagram at one loop.

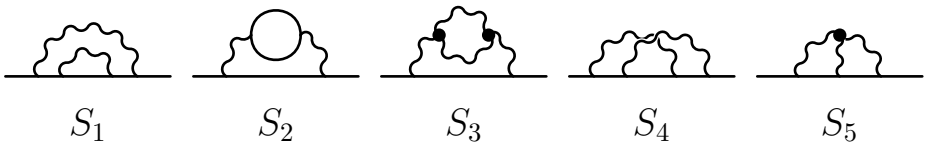

Figure 7.4. Quark self-energy diagram at two loops.

colour-charge factors of the diagrams, when evaluated at $\mathcal{O}(\alpha_s)$, $\mathcal{O}(\alpha_{em})$, $\mathcal{O}(\alpha_s^2)$ or $\mathcal{O}(\alpha_s\alpha_{em})$. They are expressed in terms of $C_F = (N^2-1)/2N = 4/3$, $T_F = 1/2$, $C_A = N$ and e_q, where $N = 3$ is the number of colours, N_f the number of flavours and e_q the fractional charge of the fermion.

Table 7.4. Singular and finite terms for the diagram in Fig. 7.3. Colour-charge factors are reported in the case of a $\mathcal{O}(\alpha_s)$ ($\mathcal{C}_s$) or $\mathcal{O}(\alpha_{em})$ ($\mathcal{C}_e$) calculation. An overall factor $\alpha/4\pi$ is understood.

S_n	$\mathcal{O}(1/\epsilon)$	$\mathcal{O}(1)$	$\mathcal{C}_s$	$\mathcal{C}_e$
S_0	-1	$-\frac{1}{2}$	C_F	e_q^2

Table 7.5. Two-loop pole contributions of the self-energy diagrams in Fig. 7.4. Colour-charge factors, inclusive of multiplicity, are reported in the case of either an $\mathcal{O}(\alpha_s^2)$ ($\mathcal{C}_s$) or $\mathcal{O}(\alpha_s\alpha_{em})$ ($\mathcal{C}_{se}$) calculation. An overall factor $(\alpha/4\pi)^2$ is understood.

S_n	D		C		$\overline{D}$		$\mathcal{C}_s$	$\mathcal{C}_{se}$
	$\mathcal{O}(1/\epsilon^2)$	$\mathcal{O}(1/\epsilon)$	$\mathcal{O}(1/\epsilon^2)$	$\mathcal{O}(1/\epsilon)$	$\mathcal{O}(1/\epsilon^2)$	$\mathcal{O}(1/\epsilon)$		
S_1	$\frac{1}{2}$	$\frac{3}{4}$	1	$\frac{1}{2}$	$-\frac{1}{2}$	$\frac{1}{4}$	C_F^2	$2\,C_F e_q^2$
S_2	0	1	0	0	0	1	$T_F C_F N_f$	0
S_3	0	$-\frac{5}{4}$	0	0	0	$-\frac{5}{4}$	$C_A C_F$	0
S_4	-1	$-\frac{1}{2}$	-2	-1	1	$\frac{1}{2}$	$C_F^2 - \frac{C_A C_F}{2}$	$2\,C_F e_q^2$
S_5	-3	$-\frac{17}{2}$	-6	-3	3	$-\frac{11}{2}$	$\frac{C_A C_F}{2}$	0

7.4 Anomalous dimension matrices

7.4.1 One-loop anomalous dimension matrix $\hat{\gamma}_e^{(0)}$

The one-loop QED anomalous dimension matrix $\hat{\gamma}_e^{(0)}$ can be straightforwardly obtained by combining Eq. (7.15) and the results of the above sections. One-loop results are already well known both for bilinear and four-fermion operators. However, it is important to make a remark on the calculation of $\hat{\gamma}_e^{(0)}$ when weak-four fermion operators are studied and the lepton field renormalization is neglected. This is the situation we face in the calculation of light-meson leptonic decay rates, as discussed in Sections 4.3 and 5.2. For the weak-four fermion operators considered in Eq. (3.61), Eq. (7.15) takes the form

$$\hat{\gamma}_e^{(0)} = -2\left[\frac{1}{2}\left(Z^{(e)}_{q_1,1} + Z^{(e)}_{q_1,1} + Z^{(e)}_{\ell,1}\right)\hat{\mathbb{1}} + \hat{Z}^{(e)}_{\mathrm{GF},1}\right] . \tag{7.51}$$

where $Z^{(e)}_{q_i,1} = -e^2_{q_i}$ and $Z^{(e)}_{\ell,1} = -e^2_\ell = -1$ are the $1/\epsilon$ poles of the quark and lepton fields RCs respectively, evaluated at $\mathcal{O}(\alpha_{\mathrm{em}})$. For weak four-fermion operators and including the lepton self-energy contribution, the result of $\hat{\gamma}_e^{(0)}$ is

$$\hat{\gamma}_e^{(0)} = \begin{pmatrix} -4 & 0 & 0 & 0 & 0 \\ 0 & -2 & 0 & 0 & 0 \\ 0 & 0 & \frac{4}{3} & 0 & 0 \\ 0 & 0 & 0 & \frac{4}{3} & -\frac{1}{6} \\ 0 & 0 & 0 & -8 & -\frac{40}{9} \end{pmatrix} . \tag{7.52}$$

Notice that if the lepton renormalization is neglected in the calculation, then the anomalous dimension $\gamma_e^{(0)}$ must be modified into

$$\tilde{\gamma}_e^{(0)} \equiv \hat{\gamma}_e^{(0)} - \mathbb{1} = \begin{pmatrix} -5 & 0 & 0 & 0 & 0 \\ 0 & -3 & 0 & 0 & 0 \\ 0 & 0 & \frac{1}{3} & 0 & 0 \\ 0 & 0 & 0 & \frac{1}{3} & -\frac{1}{6} \\ 0 & 0 & 0 & -8 & -\frac{49}{9} \end{pmatrix} . \tag{7.53}$$

For completeness, we report here also the results of $\gamma_e^{(0)}$ for Z_q and quark bilinear operators:

$$\begin{aligned} \gamma^{(0)}_{e,q} = 2\ , \quad \gamma^{(0)}_{e,V} = \gamma^{(0)}_{e,A} = 0\ , \\ \gamma^{(0)}_{e,S} = \gamma^{(0)}_{e,P} = -6\ , \quad \gamma^{(0)}_{e,T} = 2\ . \end{aligned} \tag{7.54}$$

7.4.2 Two-loop anomalous dimension matrix $\hat{\gamma}_{se}^{(1)}$

As discussed in Sec. 7.3, strong anomalous dimensions for the set of weak four-fermion operators used in this work reduce to a combination of anomalous dimensions of bilinear operators, which are known at three or four loops [73, 74]. Therefore, we

focus now on the calculation of the mixed $\mathcal{O}(\alpha_s\alpha_{em})$ contribution $\gamma_{se}^{(1)}$ for both bilinear and semi-leptonic operators. From the result of Eq. (7.17), we can write

$$\hat{\gamma}_{se}^{(1)} = -4\left[\frac{1}{2}\left(\sum_{i=1}^{n} Z_{\psi_i,1}^{(se)}\right)\hat{\mathbb{1}} + \hat{Z}_{\mathrm{GF},1}^{(se)}\right] , \tag{7.55}$$

where n is the number of external fermions and the $1/\epsilon$ divergences of the RCs $Z_{\psi_i}^{(se)}$ and $\hat{Z}_{\mathrm{GF}}^{(se)}$ are computed as in the previous section, i.e. by subtracting counter-diagrams, including those related to EOs. For quark bilinear operators we have that $n = 2$, while $n = 4$ for the semi-leptonic operators. We recall that for bilinear operators we have $e_{q_1} = e_{q_2} = 1$, and for semi-leptonic operators $e_{q_1} = 2/3$, $e_{q_1} = -1/3$, $e_\ell = -1$ and $e_\nu = 0$. The results for the fermionic RCs $Z_{\psi_i,1}^{(se)}$ can be obtained by summing the $1/\epsilon$ results in the column $\overline{D}$ of Table 7.5, with the appropriate colour-charge factors $\mathcal{C}_{se}$. On the other hand, the matrix $\hat{Z}_{\mathrm{GF},1}^{(se)}$ can be computed from the $1/\epsilon$ poles in column $\overline{D}$ of Tables A.1-A.3 for bilinear operators and Tables A.4-A.10 for semi-leptonic ones. The colour-charge factors for two-loop current-current diagrams involved in the $\mathcal{O}(\alpha_s\alpha_{em})$ calculation are reported in Table A.11.

By combining all the above results, we obtain the following anomalous dimensions for the RCs of fermion fields and the quark bilinear operators defined in Eq. (3.47):

$$\begin{aligned} \gamma_{se,q}^{(1)} &= -8 , \quad \gamma_{se,V}^{(1)} = \gamma_{se,A}^{(1)} = 0 , \\ \gamma_{se,S}^{(1)} &= \gamma_{se,P}^{(1)} = -8 , \quad \gamma_{se,T}^{(1)} = -\tfrac{152}{3} . \end{aligned} \tag{7.56}$$

On the other hand, for the weak four-fermion operators of Eq. (3.61), the anomalous dimension matrix takes the form

$$\hat{\gamma}_{se}^{(1)} = \begin{pmatrix} 4 & 0 & 0 & 0 & 0 \\ 0 & -4 & 0 & 0 & 0 \\ 0 & 0 & \frac{484}{9} & 0 & 0 \\ 0 & 0 & 0 & \frac{412}{9} & -\frac{38}{9} \\ 0 & 0 & 0 & -\frac{928}{9} & -\frac{428}{27} \end{pmatrix} . \tag{7.57}$$

The result obtained for the first entry of $\hat{\gamma}_{se}^{(1)}$, namely $[\hat{\gamma}_{se}^{(1)}]_{11} = 4$ is in agreement with the one quoted in Ref. [103] . Notice that, in this case, the matrix $\hat{\gamma}_{se}^{(1)}$ is insensitive to the omission of the lepton self-energy, since it only contributes at $\mathcal{O}(\alpha_{em})$.

7.5 Scheme dependence of the matrix $\hat{\gamma}_{se}^{(1)}$

Before closing this Chapter it is important to study the scheme-dependence of the anomalous dimension matrix computed at NLO in QCD+QED. In general, different renormalization prescriptions will define different renormalized operators. This is clearly shown in Ref. [12], where anomalous dimensions have been computed in both the NDR and the 't Hooft-Veltman (HV) regularization schemes, which differ in the treatment of γ_5 in D dimensions. This dependence arises because the renormalization

prescription involves an arbitrariness in the finite parts to be subtracted along with the ultraviolet singularities. Let us define the renormalized one-loop matrix elements as

$$\langle \vec{O} \rangle = \left(\mathbb{1} + \frac{\alpha_{\rm s}}{4\pi}\, \hat{r} + \frac{\alpha_{\rm em}}{4\pi}\, \hat{s} \right) \langle \vec{O} \rangle^{(0)} \ . \tag{7.58}$$

If $\hat{Z}_A$ and $\hat{Z}_B$ are the renormalization matrices computed in two different schemes A and B, then

$$\hat{Z}_A = \hat{Z}_B \left(\mathbb{1} + \frac{\alpha_{\rm s}}{4\pi}\, \Delta\hat{r} + \frac{\alpha_{\rm em}}{4\pi}\, \Delta\hat{s} \right) \ , \tag{7.59}$$

where

$$\Delta\hat{r} \equiv (\hat{r})_B - (\hat{r})_A \ , \qquad \Delta\hat{s} \equiv (\hat{s})_B - (\hat{s})_A \ . \tag{7.60}$$

By inserting Eq. (7.59) into the definition of $\hat{\gamma}$ in Eq. (7.1) and comparing terms order by order we obtain the following relations between anomalous dimensions in the two schemes. At one loop we find the well known results

$$\left(\hat{\gamma}_s^{(0)}\right)_B = \left(\hat{\gamma}_s^{(0)}\right)_A \ , \qquad \left(\hat{\gamma}_e^{(0)}\right)_B = \left(\hat{\gamma}_e^{(0)}\right)_A \ , \tag{7.61}$$

denoting the scheme-independence of anomalous dimensions at LO in $\alpha_{\rm s}$ and $\alpha_{\rm em}$. At two loops we obtain instead the following relations:

$$\left(\hat{\gamma}_s^{(1)}\right)_B = \left(\hat{\gamma}_s^{(1)}\right)_A - 2\beta_0 \Delta\hat{r} + \left[\hat{\gamma}_s^{(0)}, \Delta\hat{r}\right] \ , \tag{7.62}$$

$$\left(\hat{\gamma}_{se}^{(1)}\right)_B = \left(\hat{\gamma}_{se}^{(1)}\right)_A + \left[\hat{\gamma}_e^{(0)}, \Delta\hat{r}\right] + \left[\hat{\gamma}_s^{(0)}, \Delta\hat{s}\right] \ . \tag{7.63}$$

From Eq. (7.63) follows that the anomalous dimension matrix $\hat{\gamma}_{se}^{(1)}$ is scheme independent in the two following cases:

- The set of operators do not mix under renormalization. In this case the one-loop anomalous dimension matrices and the matrices $\Delta\hat{r}$ and $\Delta\hat{s}$ are diagonal and hence as a consequence the commutators vanish;
- The one-loop QCD and QED anomalous dimensions vanish.

The former case applies to the quark bilinear operators of Eq. (3.47), since they do not mix under renormalization. As a consequence, the anomalous dimensions (7.56) have been used in the numerical analysis to evolve RCs, evaluated in the RI'-MOM scheme, from one scale to another. The latter case applies instead, for example, to the semi-leptonic four-fermion operator $O_1^{\rm RI'}$ appearing in Eq. (2.13), which is renormalized non-perturbatively on the lattice in the RI'-MOM scheme. Since one-loop anomalous dimensions vanish for such operator, then the anomalous dimension $[\hat{\gamma}_{se}^{(1)}]_{11}$ computed above in the $\overline{\rm MS}$-scheme can be used in Eq. (2.12) to evolve $O_1^{\rm RI'}$ to the scale $\mu = M_W$. Moreover, as in the case of bilinear operators, the matrix (7.57) has been also used in the numerical analysis to evolve RCs of four-fermion operators from one scale to another.

8 | Future perspectives

In the second part of this thesis we have extensively discussed the perturbative calculation of anomalous dimensions of composite operators at order $\mathcal{O}(\alpha_s\alpha_{em})$ and how they enter the renormalization group evolution at NLO in QCD+QED. We focused on quark bilinear operators and the weak four-fermion operators involved in the calculation of light-meson leptonic decay rates. However, the procedure presented above and the Mathematica package produced for the calculation of anomalous dimensions can be applied to different set of operators. A possible interesting extension of the present work could be the application of the above procedure to penguin operators. This has been done in Refs. [12, 13] for the case of the $\Delta F = 1$ effective Hamiltonian within the Standard Model. However, penguin operators can enter different kind of calculations and, among all, leptonic or semileptonic decay of B mesons are of particular interest. Indeed, apparent tensions between experimental data and SM predictions in B decays mediated by Flavour Changing Neutral Currents have been found in the last few years (and recently reviewed in Ref. [104]), hinting at a possible violation of Lepton Flavour Universality. Effects of new physics beyond the SM can be studied using effective field theories, in which such effects may manifest themselves either by modifying the Wilson coefficients of SM operators or by generating new operators. Since semileptonic operators (made of two quarks and two leptons), including semileptonic penguin operators, mediate decays such as $B \to K^{(*)}\ell^+\ell^-$, to which the $R_K^{(*)}$ tension is related, they play an important role in the study of the B-anomalies. The values of the Wilson coefficients of such operators, defined within and beyond the SM, are usually extracted from global fit analyses of observables related to several weak processes. Such analyses require the knowledge of the operator mixing in the RG evolution from the electroweak scale down to the typical scale of B physics. This is currently done at NNLO in QCD and NLO in QED [105, 106] and a step forward would be the introduction of the mixed QCD+QED anomalous dimension matrix in the RG evolution, including the contribution of penguin operators. Since interactions beyond the SM can generate new operators in the effective hamiltonian (e.g. scalar and tensor operators) [107] one cannot rely just on the SM results of Refs. [12, 13] and a new systematic calculation of penguin diagrams at $\mathcal{O}(\alpha_s\alpha_{em})$ is necessary. The calculation is rather more complicated with respect to current-current diagrams: in this case the set of two-loops diagrams to be computed present one additional scale and require a careful treatment of γ_5 when using NDR. The extension of the Mathematica package with the inclusion of penguin diagrams is currently ongoing.

Conclusions

In this thesis work we have presented the details of the *first* lattice computation of the leading e.m. and strong IB corrections to $\pi^+ \to \mu^+\nu_\mu$ and $K^+ \to \mu^+\nu_\mu$ leptonic decay rates, following the method proposed in Ref. [14], that properly deals with the infrared divergences appearing in the intermediate stages of the calculation. The results are obtained using the gauge ensembles produced by the ETM Collaboration with $N_f = 2 + 1 + 1$ dynamical quarks. A fundamental novel feature of this work is the renormalization of the effective weak Hamiltonian with a consistent treatment of the non-perturbative dynamics of QCD and the inclusion of first order QED corrections. The effective Hamiltonian in the W-regularization scheme appropriate for the calculation of leptonic decay rates is obtained from the bare lattice operators in two stages. First of all, the lattice operators are renormalized non-perturbatively on the lattice at $\mathcal{O}(\alpha_{\rm em})$ and to all orders in the strong coupling $\alpha_{\rm s}$, including non-factorizable contributions of $\mathcal{O}(\alpha_{\rm s}\alpha_{\rm em})$ which were neglected in previous calculations. This renormalization procedure is presented here within the RI'-MOM scheme, although it is general and easily applicable to different renormalization schemes. The RCs for quark bilinears and the weak four-fermion operators involved in the calculation of the decay rates have been computed using $N_f = 4$ gauge configurations produced by the ETM Collaboration. Because of the breaking of chiral symmetry in the twisted mass formulation of QCD, one needs to take into account the mixing under renormalization of the lattice four-fermion operators with other four-fermion operators of different chirality. In the second step, we perform the matching from the RI'-MOM scheme to the W-regularization scheme perturbatively. The matching procedure to the W boson mass scale, as well as the evolution of RCs from one scale to another in the numerical calculation, required the calculation of the two-loop anomalous dimensions of the corresponding operators at $\mathcal{O}(\alpha_{\rm s}\alpha_{\rm em})$, which we have computed for the first time for the complete sets of quark bilinear and weak four-fermion operators. By calculating and including the mixed anomalous dimension, we have improved the residual truncation error of the matching to the W-regularization from $\mathcal{O}(\alpha_{\rm em}\alpha_{\rm s}(1/a))$ of Ref. [6, 14] to $\mathcal{O}(\alpha_{\rm em}\alpha_{\rm s}(M_W))$. Since the typical value of $1/a$ is of order $\mathcal{O}$(2-4) GeV and $M_W \sim 80$ GeV, it follows that $\alpha_{\rm s}(M_W) < \alpha_{\rm s}(1/a)$. As a consequence, we expect that higher order corrections will be smaller at a larger scale.

When computing IB "corrections" a definition of QCD without such corrections is necessary. Since IB effects change hadronic masses and other physical quantities, a prescription is needed to define QCD, whether isosymmetric or not, and in Sec. 1.5 we discuss this issue in detail. In particular, the correction δR_P and the QCD

quantity $f_P^{(0)}$ depend separately on the prescription used [46]. However, the product $f_P^{(0)}\sqrt{1+\delta R_P}$ is prescription independent and its value, multiplied by the relevant CKM matrix element, yields the P-meson decay rate. In this work we have decided to adopt the GRS prescription (see the dedicated discussion in 1.5.2 and 2.4) in which the renormalized quark masses and couplings in the full QCD+QED theory coincide in the $\overline{\text{MS}}$ at a scale of 2 GeV with the ones defined in isosymmetric QCD [8]. However, the use of "hadronic" schemes, in which QCD is defined by requiring that a set of hadronic quantities take their physical value in QCD and in QCD+QED, is suggested for future studies.

The main results of the calculation are presented in Sec. 5.4 together with a detailed discussion of their implications. In summary, after extrapolation of the data to the physical pion mass, and to the continuum and infinite-volume limits, the isospin-breaking corrections to the leptonic decay rates can be written in the form:

$$\begin{aligned}\Gamma(\pi^\pm \to \mu^\pm \nu_\ell[\gamma]) &\equiv (1+\delta R_\pi^{\text{phys}})\,\Gamma^{(0)}(\pi^\pm \to \mu^\pm \nu_\ell) \\ &= (1.0153 \pm 0.0019)\,\Gamma^{(0)}(\pi^\pm \to \mu^\pm \nu_\ell), \qquad (8.1)\\ \Gamma(K^\pm \to \mu^\pm \nu_\ell[\gamma]) &\equiv (1+\delta R_K^{\text{phys}})\,\Gamma^{(0)}(\pi^\pm \to \mu^\pm \nu_\ell) \\ &= (1.0024 \pm 0.0010)\,\Gamma^{(0)}(K^\pm \to \mu^\pm \nu_\ell)\,, \qquad (8.2)\end{aligned}$$

where $\Gamma^{(0)}$ is the leptonic decay rate at tree level in the GRS scheme (see Eqs. (5.37) and (5.38)). These results can be compared with the ChPT predictions $\delta R_\pi^{\text{phys}} = 0.0176(21)$ and $\delta R_K^{\text{phys}} = 0.0064(24)$ obtained in Ref. [18] and adopted by the PDG [9, 55]. The difference is within one standard deviation for $\delta R_\pi^{\text{phys}}$, while it is larger for δR_K^{phys}. We also underline that our result $|V_{us}| = 0.22538(46)$ in Eq. (5.47), together with the value of V_{ud} determined in Ref. [10] and $|V_{ub}|$ from the PDG [9], implies that the unitarity of the first row of the CKM matrix is satisfied at the per-mille level (see Eq. (5.48)). In addition to testing the CKM unitarity, our results allows also to update other stringent tests of the SM which have been done in the past [108–110], that can provide new bounds on possible interactions allowed beyond the SM (see for example Ref. [108], where the minimal supersymmetric extension of the SM is taken into account).

The results obtained in our ab initio lattice calculation are at the moment the most precise in the literature and they have been included in the review on leptonic decays of charged pseudoscalar mesons by the PDG [9].

Although the work presented in this thesis has allowed to determine some IB effects with unprecedented precision, still further important improvements and developments are possible.

In our calculation of the relevant amplitudes, contributions from disconnected diagrams and from diagrams present in unquenched QED have been neglected. The only way to precisely quantify the systematic error associated to this approximation is to actually compute the neglected contributions. A theoretical study that discusses how twisted mass lattice QCD can be conveniently combined with the RM123 approach beyond the quenched-QED approximation is currently underway [111], as well as numerical simulations.

Another source of systematic uncertainty is associated to the chiral extrapolation. Only recently, thanks to the increased computational power, the first lattice

computations at physical light quark mass have been presented. An important improvement of the present work would consist in performing the same calculation with simulations at the physical point. In this respect new ETMC gauge ensembles at the physical pion mass will soon become available [112, 113].

As regards the calculation of the renormalization constants of lattice operators, a possible improvement of the results presented in this thesis could be the use of different renormalization schemes. In Sec. 3.7 we briefly describe the SMOM scheme, in which the contamination of the Goldstone boson in pseudoscalar vertices has a milder effect due to the non-exceptional kinematics. In this case, however, anti-periodic boundary conditions in time cannot be adopted for fermions. Indeed, such choice would not satisfy the SMOM condition on momenta $p_1^2 = p_2^2 = (p_1 - p_2)^2$. As a consequence, pure QED simulations and the calculation of leptonic propagators cannot be done in the massless limit, due to the contribution of fermionic zero modes. Furthermore, it would be interesting to better investigate how small are the finite volume effects (FVE) in the evaluation of RCs at $\mathcal{O}(\alpha_{\rm em}\alpha_{\rm s})$ (the pure QED and QCD FVEs are cancelled in the ratio that defines η), that we have neglected in this work. This could be possible by reproducing the same analysis on two different lattice volumes at a fixed value of the lattice spacing. This would definitively clarify the issue raised in Ref. [29] about the uncertain separation of IR and UV divergences when the (non-local) $\mathrm{QED_L}$ regularization of the photon is used. The $N_f = 4$ gauge ensembles used in this work, however, have been generated with only one volume per lattice spacing and thus do not allow for such a test. Nevertheless, an exploratory analysis on the $N_f = 2 + 1 + 1$ gauge ensembles is ongoing and preliminary results show a perfect agreement of the data obtained at different lattice volumes, this implying that FVEs are actually negligible.

The procedure described above to compute the leading IB corrections to hadronic processes, that we successfully applied to the calculation of light-meson leptonic decay rates, can be in principle extended to other classes of processes.

In Ref. [114] a possible extension to the computation of radiative corrections to semileptonic decay rates has been proposed, focusing on the $K_{\ell 3}$ decay. New issues appears in this context, in particular the presence of unphysical terms which grow exponentially with the time separation between the insertion of the weak Hamiltonian and the sink for the final-state meson-lepton pair. Such terms must be identified and subtracted. The method still needs to be implemented and tested numerically and could lead to improved precision in the determination of the corresponding CKM matrix elements and other tests of the SM. Moreover, the generality of the strategy proposed in Chap. 3 for the QCD+QED calculation of the mixing matrix of the lattice weak four-fermion operators, allows one to use the results obtained in this work in many other contexts. Since renormalization is independent on the external states, the same RCs can be used in semileptonic decays of light-mesons and in (semi)leptonic decays of heavy particles such as D and B mesons.

The perturbative calculation of the mixed anomalous dimension $\hat{\gamma}_{se}$ of order $\mathcal{O}(\alpha_{\rm s}\alpha_{\rm em})$ can be extended to different classes of operators. In Chap. 8 we briefly discuss the case of penguin operators, which play an important role in (semi)leptonic decays of B mesons. The contribution of penguin operators to the RG evolution at order $\mathcal{O}(\alpha_{\rm s}\alpha_{\rm em})$ is currently neglected. Their inclusion could in principle improve the precision of the calculation and help to shed a light on the recently observed

tensions between experimental data and SM predictions for physical observables related to B decays. We are currently extending the Mathematica package that computes anomalous dimension matrices with the inclusion of the contribution of penguin diagrams at $\mathcal{O}(\alpha_s \alpha_{em})$.

A | Divergent part of two-loop current-current diagrams

We report here the results of the two-loop current-current diagrams in Fig. 7.2 computed in the $\overline{\text{MS}}$ in NDR, with the insertion of the bilinear operators and the weak four-fermion operators of Table 7.1. Multiplicity and charge-factors are not shown and an overall $(\alpha/4\pi)^2$ factor is understood. Results are reported according to the definition of the "complete" diagram given in Eq. (7.50) and adopted in Ref. [12]. For diagrams V_{29}, V_{30} and V_{31}, the results proportional to the number of colours N (V^N) and flavours N_f (V^f) are reported separately.

A.1 Bilinear operators

Table A.1. Two-loop pole contributions for the subgroup of bilinear-like diagrams in Fig. 7.2 with the insertion of operators O_S and O_P.

O_S, O_P							
V_n	D		C		E	$\overline{D}$	
	$\mathcal{O}(1/\epsilon^2)$	$\mathcal{O}(1/\epsilon)$	$\mathcal{O}(1/\epsilon^2)$	$\mathcal{O}(1/\epsilon)$	$\mathcal{O}(1/\epsilon)$	$\mathcal{O}(1/\epsilon^2)$	$\mathcal{O}(1/\epsilon)$
V_4	8	32	16	24	0	-8	8
V_7	0	-2	0	0	0	0	-2
V_{10}	2	4	4	6	0	-2	-2
V_{13}	-2	-7	-4	-6	0	2	-1
V_{25}	-6	-23	-12	-18	0	6	-5
V_{29}^f	-2	-8	-4	$-\frac{16}{3}$	0	2	$-\frac{8}{3}$
V_{29}^N	$\frac{5}{2}$	11	5	$\frac{20}{3}$	0	$-\frac{5}{2}$	$\frac{13}{3}$

Table A.2. Two-loop pole contributions for the subgroup of bilinear-like diagrams in Fig. 7.2 with the insertion of operators O_V and O_A.

$\boldsymbol{O_V}$, $\boldsymbol{O_A}$							
V_n	D		C		E	$\overline{D}$	
	$\mathcal{O}(1/\epsilon^2)$	$\mathcal{O}(1/\epsilon)$	$\mathcal{O}(1/\epsilon^2)$	$\mathcal{O}(1/\epsilon)$	$\mathcal{O}(1/\epsilon)$	$\mathcal{O}(1/\epsilon^2)$	$\mathcal{O}(1/\epsilon)$
V_4	$\frac{1}{2}$	$\frac{7}{4}$	1	$\frac{1}{2}$	0	$-\frac{1}{2}$	$\frac{5}{4}$
V_7	0	-2	0	0	0	0	-2
V_{10}	$\frac{1}{2}$	$\frac{5}{4}$	1	$\frac{1}{2}$	0	$-\frac{1}{2}$	$\frac{3}{4}$
V_{13}	$-\frac{1}{2}$	$-\frac{5}{4}$	-1	$-\frac{1}{2}$	0	$\frac{1}{2}$	$-\frac{3}{4}$
V_{25}	$-\frac{3}{2}$	$-\frac{17}{4}$	-3	$-\frac{3}{2}$	0	$\frac{3}{2}$	$-\frac{11}{4}$
V_{29}^f	0	-1	0	0	0	0	-1
V_{29}^N	0	$\frac{5}{4}$	0	0	0	0	$\frac{5}{4}$

Table A.3. Two-loop pole contributions for the subgroup of bilinear-like diagrams in Fig. 7.2 with the insertion of operators O_V and O_A.

$\boldsymbol{O_T}$							
V_n	D		C		E	$\overline{D}$	
	$\mathcal{O}(1/\epsilon^2)$	$\mathcal{O}(1/\epsilon)$	$\mathcal{O}(1/\epsilon^2)$	$\mathcal{O}(1/\epsilon)$	$\mathcal{O}(1/\epsilon)$	$\mathcal{O}(1/\epsilon^2)$	$\mathcal{O}(1/\epsilon)$
V_4	0	0	0	0	0	0	0
V_7	0	2	0	0	0	0	2
V_{10}	0	1	0	0	0	0	1
V_{13}	0	0	0	0	0	0	0
V_{25}	0	0	0	0	0	0	0
V_{29}^f	$\frac{2}{3}$	$\frac{4}{9}$	$\frac{4}{3}$	0	0	$-\frac{2}{3}$	$\frac{4}{9}$
V_{29}^N	$-\frac{5}{6}$	$-\frac{8}{9}$	$-\frac{5}{3}$	0	0	$\frac{5}{6}$	$-\frac{8}{9}$

A.2 Weak four-fermions operators

Table A.4. Two-loop pole contributions for the current-current diagrams in Fig. 7.2 with the insertion of operator O_1 and projected onto O_1.

$O_{1,1}$							
V_n	D		C		E	$\overline{D}$	
	$\mathcal{O}(1/\epsilon^2)$	$\mathcal{O}(1/\epsilon)$	$\mathcal{O}(1/\epsilon^2)$	$\mathcal{O}(1/\epsilon)$	$\mathcal{O}(1/\epsilon)$	$\mathcal{O}(1/\epsilon^2)$	$\mathcal{O}(1/\epsilon)$
V_4	$\frac{1}{2}$	$\frac{7}{4}$	1	$\frac{1}{2}$	0	$-\frac{1}{2}$	$\frac{5}{4}$
V_5	8	41	16	30	-3	-8	8
V_6	$\frac{1}{2}$	$\frac{7}{4}$	1	$\frac{1}{2}$	0	$-\frac{1}{2}$	$\frac{5}{4}$
V_7	0	-2	0	0	0	0	-2
V_8	0	-2	0	0	0	0	-2
V_9	0	-2	0	0	0	0	-2
V_{10}	$\frac{1}{2}$	$\frac{5}{4}$	1	$\frac{1}{2}$	0	$-\frac{1}{2}$	$\frac{3}{4}$
V_{11}	-2	$-\frac{11}{2}$	-4	-9	0	2	$\frac{7}{2}$
V_{12}	$\frac{1}{2}$	$\frac{5}{4}$	1	$\frac{1}{2}$	0	$-\frac{1}{2}$	$\frac{3}{4}$
V_{13}	$-\frac{1}{2}$	$-\frac{5}{4}$	-1	$-\frac{1}{2}$	0	$\frac{1}{2}$	$-\frac{3}{4}$
V_{14}	2	$\frac{17}{2}$	4	9	0	-2	$-\frac{1}{2}$
V_{15}	$-\frac{1}{2}$	$-\frac{5}{4}$	-1	$-\frac{1}{2}$	0	$\frac{1}{2}$	$-\frac{3}{4}$
V_{16}	-2	$-\frac{17}{2}$	-4	-8	-3	2	$-\frac{7}{2}$
V_{17}	-2	$-\frac{11}{2}$	-4	-9	0	2	$\frac{7}{2}$
V_{18}	$\frac{1}{2}$	$-\frac{7}{4}$	1	$-\frac{11}{2}$	-3	$-\frac{1}{2}$	$\frac{3}{4}$
V_{19}	$\frac{1}{2}$	$\frac{5}{4}$	1	$\frac{1}{2}$	0	$-\frac{1}{2}$	$\frac{3}{4}$
V_{20}	-2	$-\frac{17}{2}$	-4	-15	-3	2	$\frac{7}{2}$
V_{21}	-2	$-\frac{11}{2}$	-4	-2	0	2	$-\frac{7}{2}$
V_{22}	1	1	2	1	0	-1	0
V_{23}	16	66	32	60	-6	-16	0
V_{24}	1	1	2	1	0	-1	0
V_{25}	$-\frac{3}{2}$	$-\frac{17}{4}$	-3	$-\frac{3}{2}$	0	$\frac{3}{2}$	$-\frac{11}{4}$
V_{26}	-6	$-\frac{55}{2}$	-12	-27	0	6	$-\frac{1}{2}$
V_{27}	$\frac{3}{2}$	$\frac{17}{4}$	3	$\frac{3}{2}$	0	$-\frac{3}{2}$	$\frac{11}{4}$
V_{28}	0	0	0	0	0	0	0
V_{29}^f	0	-1	0	0	0	0	-1
V_{29}^N	0	$\frac{5}{4}$	0	0	0	0	$\frac{5}{4}$
V_{30}^f	2	10	4	$\frac{28}{3}$	0	-2	$\frac{2}{3}$
V_{30}^N	$-\frac{5}{2}$	$-\frac{27}{2}$	-5	$-\frac{35}{3}$	0	$\frac{5}{2}$	$-\frac{11}{6}$
V_{31}^f	0	-1	0	0	0	0	-1
V_{31}^N	0	$\frac{5}{4}$	0	0	0	0	$\frac{5}{4}$

Table A.5. Two-loop pole contributions for the current-current diagrams in Fig. 7.2 with the insertion of operator O_2 and projected onto O_2.

$O_{2,2}$							
V_n	D		C		E	$\overline{D}$	
	$\mathcal{O}(1/\epsilon^2)$	$\mathcal{O}(1/\epsilon)$	$\mathcal{O}(1/\epsilon^2)$	$\mathcal{O}(1/\epsilon)$	$\mathcal{O}(1/\epsilon)$	$\mathcal{O}(1/\epsilon^2)$	$\mathcal{O}(1/\epsilon)$
V_4	$\frac{1}{2}$	$\frac{7}{4}$	1	$\frac{1}{2}$	0	$-\frac{1}{2}$	$\frac{5}{4}$
V_5	$\frac{1}{2}$	$\frac{31}{4}$	1	$\frac{19}{2}$	3	$-\frac{1}{2}$	$\frac{5}{4}$
V_6	8	32	16	24	0	-8	8
V_7	0	-2	0	0	0	0	-2
V_8	0	-2	0	0	0	0	-2
V_9	0	-2	0	0	0	0	-2
V_{10}	$\frac{1}{2}$	$\frac{5}{4}$	1	$\frac{1}{2}$	0	$-\frac{1}{2}$	$\frac{3}{4}$
V_{11}	$-\frac{1}{2}$	$-\frac{11}{4}$	-1	$-\frac{7}{2}$	0	$\frac{1}{2}$	$\frac{3}{4}$
V_{12}	2	4	4	6	0	-2	-2
V_{13}	$-\frac{1}{2}$	$-\frac{5}{4}$	-1	$-\frac{1}{2}$	0	$\frac{1}{2}$	$-\frac{3}{4}$
V_{14}	$\frac{1}{2}$	$\frac{11}{4}$	1	$\frac{7}{2}$	0	$-\frac{1}{2}$	$-\frac{3}{4}$
V_{15}	-2	-7	-4	-6	0	2	-1
V_{16}	$-\frac{1}{2}$	$\frac{1}{4}$	-1	$\frac{11}{2}$	3	$\frac{1}{2}$	$-\frac{9}{4}$
V_{17}	$-\frac{1}{2}$	$-\frac{11}{4}$	-1	$-\frac{7}{2}$	0	$\frac{1}{2}$	$\frac{3}{4}$
V_{18}	2	7	4	8	3	-2	2
V_{19}	2	4	4	6	0	-2	-2
V_{20}	-2	-7	-4	-8	3	2	4
V_{21}	-2	-10	-4	-6	0	2	-4
V_{22}	1	1	2	1	0	-1	0
V_{23}	1	13	2	19	6	-1	0
V_{24}	16	48	32	48	0	-16	0
V_{25}	$-\frac{3}{2}$	$-\frac{17}{4}$	-3	$-\frac{3}{2}$	0	$\frac{3}{2}$	$-\frac{11}{4}$
V_{26}	$-\frac{3}{2}$	$-\frac{35}{4}$	-3	$-\frac{21}{2}$	0	$\frac{3}{2}$	$\frac{7}{4}$
V_{27}	6	23	12	18	0	-6	5
V_{28}	0	0	0	0	0	0	0
V_{29}^f	0	-1	0	0	0	0	-1
V_{29}^N	0	$\frac{5}{4}$	0	0	0	0	$\frac{5}{4}$
V_{30}^f	0	3	0	4	0	0	-1
V_{30}^N	0	$-\frac{15}{4}$	0	-5	0	0	$\frac{5}{4}$
V_{31}^f	-2	-8	-4	$-\frac{16}{3}$	0	2	$-\frac{8}{3}$
V_{31}^N	$\frac{5}{2}$	11	5	$\frac{20}{3}$	0	$-\frac{5}{2}$	$\frac{13}{3}$

Table A.6. Two-loop pole contributions for the current-current diagrams in Fig. 7.2 with the insertion of operator O_3 and projected onto O_3.

$\boldsymbol{O_{3,3}}$							
V_n	D		C		E	$\overline{D}$	
	$\mathcal{O}(1/\epsilon^2)$	$\mathcal{O}(1/\epsilon)$	$\mathcal{O}(1/\epsilon^2)$	$\mathcal{O}(1/\epsilon)$	$\mathcal{O}(1/\epsilon)$	$\mathcal{O}(1/\epsilon^2)$	$\mathcal{O}(1/\epsilon)$
V_4	8	32	16	24	0	-8	8
V_5	$\frac{1}{2}$	$\frac{31}{4}$	1	$\frac{19}{2}$	3	$-\frac{1}{2}$	$\frac{5}{4}$
V_6	$\frac{1}{2}$	$\frac{7}{4}$	1	$\frac{1}{2}$	0	$-\frac{1}{2}$	$\frac{5}{4}$
V_7	0	-2	0	0	0	0	-2
V_8	0	-2	0	0	0	0	-2
V_9	0	-2	0	0	0	0	-2
V_{10}	2	4	4	6	0	-2	-2
V_{11}	$-\frac{1}{2}$	$-\frac{11}{4}$	-4	-14	0	$\frac{7}{2}$	$\frac{45}{4}$
V_{12}	$\frac{1}{2}$	$\frac{5}{4}$	4	2	0	$-\frac{7}{2}$	$-\frac{3}{4}$
V_{13}	-2	-7	-4	-6	0	2	-1
V_{14}	$\frac{1}{2}$	$\frac{11}{4}$	1	$\frac{7}{2}$	0	$-\frac{1}{2}$	$-\frac{3}{4}$
V_{15}	$-\frac{1}{2}$	$-\frac{5}{4}$	-1	$-\frac{1}{2}$	0	$\frac{1}{2}$	$-\frac{3}{4}$
V_{16}	-2	-7	-4	0	3	2	-4
V_{17}	-2	-10	-4	-14	0	2	4
V_{18}	2	7	4	12	3	-2	-2
V_{19}	2	4	4	2	0	-2	2
V_{20}	$-\frac{1}{2}$	$\frac{1}{4}$	-1	$\frac{5}{2}$	3	$\frac{1}{2}$	$\frac{3}{4}$
V_{21}	$-\frac{1}{2}$	$-\frac{11}{4}$	-1	$-\frac{1}{2}$	0	$\frac{1}{2}$	$-\frac{9}{4}$
V_{22}	16	48	32	48	0	-16	0
V_{23}	1	13	2	19	6	-1	0
V_{24}	1	1	2	1	0	-1	0
V_{25}	-6	-23	-12	-18	0	6	-5
V_{26}	$-\frac{3}{2}$	$-\frac{35}{4}$	-3	$-\frac{21}{2}$	0	$\frac{3}{2}$	$\frac{7}{4}$
V_{27}	$\frac{3}{2}$	$\frac{17}{4}$	3	$\frac{3}{2}$	0	$-\frac{3}{2}$	$\frac{11}{4}$
V_{28}	0	0	0	0	0	0	0
V_{29}^f	-2	-8	-4	$-\frac{16}{3}$	0	2	$-\frac{8}{3}$
V_{29}^N	$\frac{5}{2}$	11	5	$\frac{20}{3}$	0	$-\frac{5}{2}$	$\frac{13}{3}$
V_{30}^f	0	3	0	4	0	0	-1
V_{30}^N	0	$-\frac{15}{4}$	0	-5	0	0	$\frac{5}{4}$
V_{31}^f	0	-1	0	0	0	0	-1
V_{31}^N	0	$\frac{5}{4}$	0	0	0	0	$\frac{5}{4}$

Table A.7. Two-loop pole contributions for the current-current diagrams in Fig. 7.2 with the insertion of operator O_4 and projected onto O_4.

$O_{4,4}$							
V_n	D		C		E	$\overline{D}$	
	$\mathcal{O}(1/\epsilon^2)$	$\mathcal{O}(1/\epsilon)$	$\mathcal{O}(1/\epsilon^2)$	$\mathcal{O}(1/\epsilon)$	$\mathcal{O}(1/\epsilon)$	$\mathcal{O}(1/\epsilon^2)$	$\mathcal{O}(1/\epsilon)$
V_4	8	32	16	24	0	-8	8
V_5	2	9	1	$\frac{9}{2}$	$\frac{5}{4}$	1	$\frac{23}{4}$
V_6	2	9	1	$\frac{9}{2}$	$\frac{5}{4}$	1	$\frac{23}{4}$
V_7	0	-2	0	0	0	0	-2
V_8	0	1	0	0	0	0	1
V_9	0	1	0	0	0	0	1
V_{10}	2	4	4	6	0	-2	-2
V_{11}	$-\frac{1}{2}$	-2	-4	-8	0	$\frac{7}{2}$	6
V_{12}	$\frac{1}{2}$	2	4	8	0	$-\frac{7}{2}$	-6
V_{13}	-2	-7	-4	-6	0	2	-1
V_{14}	$\frac{1}{2}$	2	1	2	0	$-\frac{1}{2}$	0
V_{15}	$-\frac{1}{2}$	-2	-1	-2	0	$\frac{1}{2}$	0
V_{16}	-2	-7	-4	-6	0	2	-1
V_{17}	-2	-7	-4	-8	0	2	1
V_{18}	2	7	4	6	0	-2	1
V_{19}	2	7	4	8	0	-2	-1
V_{20}	1	3	-1	$\frac{1}{2}$	$\frac{5}{4}$	2	$\frac{15}{4}$
V_{21}	1	3	-1	$\frac{1}{2}$	$\frac{5}{4}$	2	$\frac{15}{4}$
V_{22}	16	48	32	48	0	-16	0
V_{23}	4	14	2	9	$\frac{5}{2}$	2	$\frac{15}{2}$
V_{24}	4	14	2	9	$\frac{5}{2}$	2	$\frac{15}{2}$
V_{25}	-6	-23	-12	-18	0	6	-5
V_{26}	$-\frac{3}{2}$	$-\frac{13}{2}$	-3	-6	0	$\frac{3}{2}$	$-\frac{1}{2}$
V_{27}	$\frac{3}{2}$	$\frac{13}{2}$	3	6	0	$-\frac{3}{2}$	$\frac{1}{2}$
V_{28}	0	0	0	0	0	0	0
V_{29}^f	-2	-8	-4	$-\frac{16}{3}$	0	2	$-\frac{8}{3}$
V_{29}^N	$\frac{5}{2}$	11	5	$\frac{20}{3}$	0	$-\frac{5}{2}$	$\frac{13}{3}$
V_{30}^f	0	2	0	2	0	0	0
V_{30}^N	0	$-\frac{5}{2}$	0	$-\frac{5}{2}$	0	0	0
V_{31}^f	0	-2	0	-2	0	0	0
V_{31}^N	0	$\frac{5}{2}$	0	$\frac{5}{2}$	0	0	0

Table A.8. Two-loop pole contributions for the current-current diagrams in Fig. 7.2 with the insertion of operator O_4 and projected onto O_5.

$\boldsymbol{O_{4,5}}$							
V_n	D		C		E	$\overline{D}$	
	$\mathcal{O}(1/\epsilon^2)$	$\mathcal{O}(1/\epsilon)$	$\mathcal{O}(1/\epsilon^2)$	$\mathcal{O}(1/\epsilon)$	$\mathcal{O}(1/\epsilon)$	$\mathcal{O}(1/\epsilon^2)$	$\mathcal{O}(1/\epsilon)$
V_4	0	0	0	0	0	0	0
V_5	$\frac{1}{2}$	$\frac{11}{4}$	$\frac{1}{16}$	2	$\frac{59}{64}$	$\frac{7}{16}$	$\frac{107}{64}$
V_6	$-\frac{1}{2}$	$-\frac{5}{2}$	$\frac{1}{16}$	$-\frac{3}{2}$	$-\frac{53}{64}$	$-\frac{9}{16}$	$-\frac{117}{64}$
V_7	0	0	0	0	0	0	0
V_8	0	$-\frac{1}{4}$	0	0	0	0	$-\frac{1}{4}$
V_9	0	$\frac{1}{4}$	0	0	0	0	$\frac{1}{4}$
V_{10}	0	0	0	0	0	0	0
V_{11}	$-\frac{1}{8}$	$-\frac{5}{16}$	0	0	0	$-\frac{1}{8}$	$-\frac{5}{16}$
V_{12}	$-\frac{1}{8}$	$-\frac{5}{16}$	0	0	0	$-\frac{1}{8}$	$-\frac{5}{16}$
V_{13}	0	0	0	0	0	0	0
V_{14}	$\frac{1}{8}$	$\frac{9}{16}$	$\frac{1}{4}$	$\frac{5}{8}$	0	$-\frac{1}{8}$	$-\frac{1}{16}$
V_{15}	$\frac{1}{8}$	$\frac{9}{16}$	$\frac{1}{4}$	$\frac{5}{8}$	0	$-\frac{1}{8}$	$-\frac{1}{16}$
V_{16}	0	0	0	0	0	0	0
V_{17}	$-\frac{1}{2}$	-2	0	0	0	$-\frac{1}{2}$	-2
V_{18}	0	0	0	0	0	0	0
V_{19}	$-\frac{1}{2}$	-2	0	0	0	$-\frac{1}{2}$	-2
V_{20}	$\frac{1}{4}$	$\frac{9}{8}$	$\frac{1}{16}$	1	$\frac{27}{64}$	$\frac{3}{16}$	$\frac{35}{64}$
V_{21}	$-\frac{1}{4}$	$-\frac{7}{8}$	$\frac{1}{16}$	$-\frac{1}{2}$	$-\frac{21}{64}$	$-\frac{5}{16}$	$-\frac{45}{64}$
V_{22}	0	0	0	0	0	0	0
V_{23}	1	$\frac{9}{2}$	$\frac{1}{8}$	4	$\frac{59}{32}$	$\frac{7}{8}$	$\frac{75}{32}$
V_{24}	-1	-4	$\frac{1}{8}$	-3	$-\frac{53}{32}$	$-\frac{9}{8}$	$-\frac{85}{32}$
V_{25}	0	0	0	0	0	0	0
V_{26}	$-\frac{3}{8}$	$-\frac{29}{16}$	$-\frac{3}{4}$	$-\frac{15}{8}$	0	$\frac{3}{8}$	$\frac{1}{16}$
V_{27}	$-\frac{3}{8}$	$-\frac{29}{16}$	$-\frac{3}{4}$	$-\frac{15}{8}$	0	$\frac{3}{8}$	$\frac{1}{16}$
V_{28}	0	0	0	0	0	0	0
V_{29}^f	0	0	0	0	0	0	0
V_{29}^N	0	0	0	0	0	0	0
V_{30}^f	$\frac{1}{6}$	$\frac{25}{36}$	$\frac{1}{3}$	$\frac{2}{3}$	0	$-\frac{1}{6}$	$\frac{1}{36}$
V_{30}^N	$-\frac{5}{24}$	$-\frac{137}{144}$	$-\frac{5}{12}$	$-\frac{5}{6}$	0	$\frac{5}{24}$	$-\frac{17}{144}$
V_{31}^f	$\frac{1}{6}$	$\frac{25}{36}$	$\frac{1}{3}$	$\frac{2}{3}$	0	$-\frac{1}{6}$	$\frac{1}{36}$
V_{31}^N	$-\frac{5}{24}$	$-\frac{137}{144}$	$-\frac{5}{12}$	$-\frac{5}{6}$	0	$\frac{5}{24}$	$-\frac{17}{144}$

Table A.9. Two-loop pole contributions for the current-current diagrams in Fig. 7.2 with the insertion of operator O_5 and projected onto O_4.

$O_{5,4}$							
V_n	D		C		E	$\overline{D}$	
	$\mathcal{O}(1/\epsilon^2)$	$\mathcal{O}(1/\epsilon)$	$\mathcal{O}(1/\epsilon^2)$	$\mathcal{O}(1/\epsilon)$	$\mathcal{O}(1/\epsilon)$	$\mathcal{O}(1/\epsilon^2)$	$\mathcal{O}(1/\epsilon)$
V_4	0	0	0	0	0	0	0
V_5	24	68	144	208	44	-120	-96
V_6	-24	-80	144	248	64	-168	-264
V_7	0	0	0	0	0	0	0
V_8	0	-12	0	0	0	0	-12
V_9	0	12	0	0	0	0	12
V_{10}	0	0	0	0	0	0	0
V_{11}	-6	-5	0	0	0	-6	-5
V_{12}	-6	-5	0	0	0	-6	-5
V_{13}	0	0	0	0	0	0	0
V_{14}	6	17	12	10	0	-6	7
V_{15}	6	17	12	10	0	-6	7
V_{16}	-24	-80	0	-40	-20	-24	-60
V_{17}	0	0	0	0	0	0	0
V_{18}	-24	-80	0	-40	-20	-24	-60
V_{19}	0	0	0	0	0	0	0
V_{20}	-12	-46	144	208	44	-156	-210
V_{21}	12	34	144	248	64	-132	-150
V_{22}	0	0	0	0	0	0	0
V_{23}	48	88	288	416	88	-240	-240
V_{24}	-48	-112	288	496	128	-336	-480
V_{25}	0	0	0	0	0	0	0
V_{26}	-18	-57	-36	-30	0	18	-27
V_{27}	-18	-57	-36	-30	0	18	-27
V_{28}	0	0	0	0	0	0	0
V_{29}^f	0	0	0	0	0	0	0
V_{29}^N	0	0	0	0	0	0	0
V_{30}^f	8	20	16	$\frac{16}{3}$	0	-8	$\frac{44}{3}$
V_{30}^N	-10	-29	-20	$-\frac{20}{3}$	0	10	$-\frac{67}{3}$
V_{31}^f	8	20	16	$\frac{16}{3}$	0	-8	$\frac{44}{3}$
V_{31}^N	-10	-29	-20	$-\frac{20}{3}$	0	10	$-\frac{67}{3}$

Table A.10. Two-loop pole contributions for the current-current diagrams in Fig. 7.2 with the insertion of operator O_5 and projected onto O_5.

$\boldsymbol{O_{5,5}}$							
V_n	D		C		E	$\overline{D}$	
	$\mathcal{O}(1/\epsilon^2)$	$\mathcal{O}(1/\epsilon)$	$\mathcal{O}(1/\epsilon^2)$	$\mathcal{O}(1/\epsilon)$	$\mathcal{O}(1/\epsilon)$	$\mathcal{O}(1/\epsilon^2)$	$\mathcal{O}(1/\epsilon)$
V_4	0	0	0	0	0	0	0
V_5	6	27	9	$\frac{33}{2}$	$-\frac{3}{4}$	-3	$\frac{39}{4}$
V_6	6	23	9	$\frac{29}{2}$	$\frac{5}{4}$	-3	$\frac{39}{4}$
V_7	0	2	0	0	0	0	2
V_8	0	-1	0	0	0	0	-1
V_9	0	-1	0	0	0	0	-1
V_{10}	0	1	0	0	0	0	1
V_{11}	$-\frac{3}{2}$	-4	0	0	0	$-\frac{3}{2}$	-4
V_{12}	$\frac{3}{2}$	3	0	0	0	$\frac{3}{2}$	3
V_{13}	0	0	0	0	0	0	0
V_{14}	$\frac{3}{2}$	6	3	6	0	$-\frac{3}{2}$	0
V_{15}	$-\frac{3}{2}$	-5	-3	-4	0	$\frac{3}{2}$	-1
V_{16}	0	-2	0	-4	-2	0	0
V_{17}	0	0	0	0	0	0	0
V_{18}	0	-2	0	-4	-2	0	0
V_{19}	0	0	0	0	0	0	0
V_{20}	-3	-12	-9	$-\frac{39}{2}$	$-\frac{3}{4}$	6	$\frac{27}{4}$
V_{21}	-3	-10	-9	$-\frac{19}{2}$	$\frac{5}{4}$	6	$\frac{3}{4}$
V_{22}	0	0	0	0	0	0	0
V_{23}	12	42	18	33	$-\frac{3}{2}$	-6	$\frac{15}{2}$
V_{24}	12	34	18	29	$\frac{5}{2}$	-6	$\frac{15}{2}$
V_{25}	0	0	0	0	0	0	0
V_{26}	$-\frac{9}{2}$	$-\frac{39}{2}$	-9	-18	0	$\frac{9}{2}$	$-\frac{3}{2}$
V_{27}	$\frac{9}{2}$	$\frac{33}{2}$	9	12	0	$-\frac{9}{2}$	$\frac{9}{2}$
V_{28}	0	0	0	0	0	0	0
V_{29}^f	$\frac{2}{3}$	$\frac{4}{9}$	$\frac{4}{3}$	0	0	$-\frac{2}{3}$	$\frac{4}{9}$
V_{29}^N	$-\frac{5}{6}$	$-\frac{8}{9}$	$-\frac{5}{3}$	0	0	$\frac{5}{6}$	$-\frac{8}{9}$
V_{30}^f	$\frac{4}{3}$	$\frac{62}{9}$	$\frac{8}{3}$	6	0	$-\frac{4}{3}$	$\frac{8}{9}$
V_{30}^N	$-\frac{5}{3}$	$-\frac{167}{18}$	$-\frac{10}{3}$	$-\frac{15}{2}$	0	$\frac{5}{3}$	$-\frac{16}{9}$
V_{31}^f	$-\frac{4}{3}$	$-\frac{50}{9}$	$-\frac{8}{3}$	$-\frac{10}{3}$	0	$\frac{4}{3}$	$-\frac{20}{9}$
V_{31}^N	$\frac{5}{3}$	$\frac{137}{18}$	$\frac{10}{3}$	$\frac{25}{6}$	0	$-\frac{5}{3}$	$\frac{31}{9}$

Table A.11. Colour-charge factors for the subset of two-loop diagrams in Fig. 7.2 contributing at $\mathcal{O}(\alpha_s \alpha_{em})$, inclusive of multiplicity.

V_n	$\mathcal{C}_{se}$
V_4	$2\,C_F\,e_{q_1}e_{q_2}$
V_7	$2\,C_F\,e_{q_1}e_{q_2}$
V_{10}	$C_F\,(e_{q_1}^2 + e_{q_2}^2 + 2\,e_{q_1}e_{q_2})$
V_{11}	$C_F\,(e_{q_1}e_{q_3} + e_{q_2}e_{q_4})$
V_{12}	$C_F\,(e_{q_1}e_{q_4} + e_{q_2}e_{q_3})$
V_{13}	$C_F\,(e_{q_1}^2 + e_{q_2}^2 + 2\,e_{q_1}e_{q_2})$
V_{14}	$C_F\,(e_{q_1}e_{q_3} + e_{q_2}e_{q_4})$
V_{15}	$C_F\,(e_{q_1}e_{q_4} + e_{q_2}e_{q_3})$
V_{16}	$C_F\,(e_{q_1}e_{q_3} + e_{q_2}e_{q_4})$
V_{17}	$C_F\,(e_{q_1}e_{q_3} + e_{q_2}e_{q_4})$
V_{18}	$C_F\,(e_{q_1}e_{q_4} + e_{q_2}e_{q_3})$
V_{19}	$C_F\,(e_{q_1}e_{q_4} + e_{q_2}e_{q_3})$
V_{22}	$C_F\,e_{q_3}e_{q_4}$

Bibliography

[1] S. Aoki et al. "FLAG Review 2019: Flavour Lattice Averaging Group (FLAG)". In: *Eur. Phys. J. C* 80.2 (2020), p. 113. DOI: 10.1140/epjc/s10052-019-7354-7. arXiv: 1902.08191 [hep-lat].

[2] G. M. de Divitiis et al. "Isospin breaking effects due to the up-down mass difference in lattice QCD". In: *Journal of High Energy Physics* 2012.4 (Apr. 2012). ISSN: 1029-8479. DOI: 10.1007/jhep04(2012)124. URL: http://dx.doi.org/10.1007/JHEP04(2012)124.

[3] G. M. de Divitiis et al. "Leading isospin breaking effects on the lattice". In: *Physical Review D* 87.11 (June 2013). ISSN: 1550-2368. DOI: 10.1103/physrevd.87.114505. URL: http://dx.doi.org/10.1103/PhysRevD.87.114505.

[4] D. Giusti et al. "Strange and charm HVP contributions to the muon $(g-2)$ including QED corrections with twisted-mass fermions". In: *JHEP* 10 (2017), p. 157. DOI: 10.1007/JHEP10(2017)157. arXiv: 1707.03019 [hep-lat].

[5] D. Giusti et al. "Electromagnetic and strong isospin-breaking corrections to the muon $g-2$ from Lattice QCD+QED". In: *Phys. Rev. D* 99.11 (2019), p. 114502. DOI: 10.1103/PhysRevD.99.114502. arXiv: 1901.10462 [hep-lat].

[6] D. Giusti et al. "First lattice calculation of the QED corrections to leptonic decay rates". In: *Phys. Rev. Lett.* 120.7 (2018), p. 072001. DOI: 10.1103/PhysRevLett.120.072001. arXiv: 1711.06537 [hep-lat].

[7] M. Di Carlo et al. "Light-meson leptonic decay rates in lattice QCD+QED". In: *Phys. Rev. D* 100.3 (2019), p. 034514. DOI: 10.1103/PhysRevD.100.034514. arXiv: 1904.08731 [hep-lat].

[8] J. Gasser, A. Rusetsky, and I. Scimemi. "Electromagnetic corrections in hadronic processes". In: *Eur. Phys. J. C* 32 (2003), pp. 97–114. DOI: 10.1140/epjc/s2003-01383-1. arXiv: hep-ph/0305260.

[9] Particle Data Group et al. "Review of Particle Physics". In: *Progress of Theoretical and Experimental Physics* 2020.8 (Aug. 2020). 083C01. ISSN: 2050-3911. DOI: 10.1093/ptep/ptaa104. eprint: https://academic.oup.com/ptep/article-pdf/2020/8/083C01/33653179/ptaa104.pdf. URL: https://doi.org/10.1093/ptep/ptaa104.

[10] John Hardy and I.S. Towner. "$|V_{ud}|$ from nuclear β decays". In: *PoS* CKM2016 (2016), p. 028. DOI: 10.22323/1.291.0028.

[11] A. Sirlin. "Large m_W, m_Z Behavior of the $O(\alpha)$ Corrections to Semileptonic Processes Mediated by W". In: *Nucl. Phys. B* 196 (1982), pp. 83–92. DOI: 10.1016/0550-3213(82)90303-0.

[12] Marco Ciuchini et al. "The $\Delta S = 1$ effective Hamiltonian including next-to-leading order QCD and QED corrections". In: *Nucl. Phys. B* 415 (1994), pp. 403–462. DOI: 10.1016/0550-3213(94)90118-X. arXiv: hep-ph/9304257.

[13] Andrzej J. Buras, Matthias Jamin, and Markus E. Lautenbacher. "The Anatomy of ϵ'/ϵ beyond leading logarithms with improved hadronic matrix elements". In: *Nucl. Phys. B* 408 (1993), pp. 209–285. DOI: 10.1016/0550-3213(93)90535-W. arXiv: hep-ph/9303284.

[14] N. Carrasco et al. "QED Corrections to Hadronic Processes in Lattice QCD". In: *Phys. Rev. D* 91.7 (2015), p. 074506. DOI: 10.1103/PhysRevD.91.074506. arXiv: 1502.00257 [hep-lat].

[15] G. Amoros, J. Bijnens, and P. Talavera. "QCD isospin breaking in meson masses, decay constants and quark mass ratios". In: *Nucl. Phys. B* 602 (2001), pp. 87–108. DOI: 10.1016/S0550-3213(01)00121-3. arXiv: hep-ph/0101127.

[16] Johan Bijnens and Karim Ghorbani. "Isospin breaking in $K\pi$ vector form-factors for the weak and rare decays $K_{\ell 3}$, $K \to \pi\nu\overline{\nu}$ and $K \to \pi\ell^+\ell^-$". In: (Nov. 2007). arXiv: 0711.0148 [hep-ph].

[17] A. Kastner and H. Neufeld. "The $K_{\ell 3}$ scalar form factors in the standard model". In: *Eur. Phys. J. C* 57 (2008), pp. 541–556. DOI: 10.1140/epjc/s10052-008-0703-6. arXiv: 0805.2222 [hep-ph].

[18] Vincenzo Cirigliano and Helmut Neufeld. "A note on isospin violation in $P_{\ell 2(\gamma)}$ decays". In: *Phys. Lett. B* 700 (2011), pp. 7–10. DOI: 10.1016/j.physletb.2011.04.038. arXiv: 1102.0563 [hep-ph].

[19] A. Duncan, E. Eichten, and H. Thacker. "Electromagnetic Splittings and Light Quark Masses in Lattice QCD". In: *Physical Review Letters* 76.21 (May 1996), 3894–3897. ISSN: 1079-7114. DOI: 10.1103/physrevlett.76.3894. URL: http://dx.doi.org/10.1103/PhysRevLett.76.3894.

[20] S. Basak et al. "Electromagnetic splittings of hadrons from improved staggered quarks in full QCD". In: *PoS* LATTICE2008 (2008). Ed. by Christopher Aubin et al., p. 127. DOI: 10.22323/1.066.0127. arXiv: 0812.4486 [hep-lat].

[21] T. Blum et al. "Electromagnetic mass splittings of the low lying hadrons and quark masses from 2+1 flavor lattice QCD+QED". In: *Phys. Rev. D* 82 (2010), p. 094508. DOI: 10.1103/PhysRevD.82.094508. arXiv: 1006.1311 [hep-lat].

[22] A. Portelli et al. "Electromagnetic corrections to light hadron masses". In: *PoS* LATTICE2010 (2010). Ed. by Giancarlo Rossi, p. 121. DOI: 10.22323/1.105.0121. arXiv: 1011.4189 [hep-lat].

[23] Sz. Borsanyi et al. "Ab initio calculation of the neutron-proton mass difference". In: *Science* 347 (2015), pp. 1452–1455. DOI: 10.1126/science.1257050. arXiv: 1406.4088 [hep-lat].

[24] P. Boyle et al. "Isospin breaking corrections to meson masses and the hadronic vacuum polarization: a comparative study". In: *JHEP* 09 (2017), p. 153. DOI: 10.1007/JHEP09(2017)153. arXiv: 1706.05293 [hep-lat].

[25] Martin Hansen et al. "Gauge invariant determination of charged hadron masses". In: *JHEP* 05 (2018), p. 146. DOI: 10.1007/JHEP05(2018)146. arXiv: 1802.05474 [hep-lat].

[26] D. Giusti et al. "Leading isospin-breaking corrections to pion, kaon, and charmed-meson masses with twisted-mass fermions". In: *Physical Review D* 95.11 (June 2017). ISSN: 2470-0029. DOI: 10.1103/physrevd.95.114504. URL: http://dx.doi.org/10.1103/PhysRevD.95.114504.

[27] S. Borsanyi et al. "Ab initio calculation of the neutron-proton mass difference". In: *Science* 347.6229 (Mar. 2015), 1452–1455. ISSN: 1095-9203. DOI: 10.1126/science.1257050. URL: http://dx.doi.org/10.1126/science.1257050.

[28] Antonin Portelli. "Inclusion of isospin breaking effects in lattice simulations". In: *PoS* LATTICE2014 (2015), p. 013. DOI: 10.22323/1.214.0013. arXiv: 1505.07057 [hep-lat].

[29] Agostino Patella. "QED Corrections to Hadronic Observables". In: *PoS* LATTICE2016 (2017), p. 020. DOI: 10.22323/1.256.0020. arXiv: 1702.03857 [hep-lat].

[30] Masashi Hayakawa and Shunpei Uno. "QED in finite volume and finite size scaling effect on electromagnetic properties of hadrons". In: *Prog. Theor. Phys.* 120 (2008), pp. 413–441. DOI: 10.1143/PTP.120.413. arXiv: 0804.2044 [hep-ph].

[31] P. Weisz. "Continuum Limit Improved Lattice Action for Pure Yang-Mills Theory. 1." In: *Nucl. Phys. B* 212 (1983), pp. 1–17. DOI: 10.1016/0550-3213(83)90595-3.

[32] Norman H. Christ et al. "Prospects for a lattice computation of rare kaon decay amplitudes II $K \to \pi\nu\bar{\nu}$ decays". In: *Phys. Rev. D* 93.11 (2016), p. 114517. DOI: 10.1103/PhysRevD.93.114517. arXiv: 1605.04442 [hep-lat].

[33] Ziyuan Bai et al. "$K^+ \to \pi^+\nu\bar{\nu}$ decay amplitude from lattice QCD". In: *Phys. Rev. D* 98.7 (2018), p. 074509. DOI: 10.1103/PhysRevD.98.074509. arXiv: 1806.11520 [hep-lat].

[34] Biagio Lucini et al. "Charged hadrons in local finite-volume QED+QCD with C* boundary conditions". In: *JHEP* 02 (2016), p. 076. DOI: 10.1007/JHEP02(2016)076. arXiv: 1509.01636 [hep-th].

[35] Akaki Rusetsky. "Isospin symmetry breaking". In: *PoS* CD09 (2009), p. 071. DOI: 10.22323/1.086.0071. arXiv: 0910.5151 [hep-ph].

[36] Tomomi Ishikawa et al. "Full QED+QCD Low-Energy Constants through Reweighting". In: *Physical Review Letters* 109.7 (Aug. 2012). ISSN: 1079-7114. DOI: 10.1103/physrevlett.109.072002. URL: http://dx.doi.org/10.1103/PhysRevLett.109.072002.

[37] S. Aoki et al. "1+1+1 flavor QCD+QED simulation at the physical point". In: *Physical Review D* 86.3 (Aug. 2012). ISSN: 1550-2368. DOI: 10.1103/physrevd.86.034507. URL: http://dx.doi.org/10.1103/PhysRevD.86.034507.

[38] S. Basak et al. *Finite-volume effects and the electromagnetic contributions to kaon and pion masses*. 2014. arXiv: 1409.7139 [hep-lat].

[39] Michael G. Endres et al. "Massive photons: an infrared regularization scheme for lattice QCD+QED". In: *Phys. Rev. Lett.* 117.7 (2016), p. 072002. DOI: 10.1103/PhysRevLett.117.072002. arXiv: 1507.08916 [hep-lat].

[40] Z. Fodor et al. "Up and down quark masses and corrections to Dashen's theorem from lattice QCD and quenched QED". In: *Phys. Rev. Lett.* 117.8 (2016), p. 082001. DOI: 10.1103/PhysRevLett.117.082001. arXiv: 1604.07112 [hep-lat].

[41] R. Horsley et al. "Isospin splittings of meson and baryon masses from three-flavor lattice QCD + QED". In: *J. Phys. G* 43.10 (2016), 10LT02. DOI: 10.1088/0954-3899/43/10/10LT02. arXiv: 1508.06401 [hep-lat].

[42] Peter Boyle et al. "Electromagnetic Corrections to Meson Masses and the HVP". In: *PoS* LATTICE2016 (2016), p. 172. DOI: 10.22323/1.256.0172. arXiv: 1612.05962 [hep-lat].

[43] Nazario Tantalo. "Isospin Breaking Effects on the Lattice". In: *PoS* LATTICE2013 (2014), p. 007. DOI: 10.22323/1.187.0007. arXiv: 1311.2797 [hep-lat].

[44] F. Bloch and A. Nordsieck. "Note on the Radiation Field of the electron". In: *Phys. Rev.* 52 (1937), pp. 54–59. DOI: 10.1103/PhysRev.52.54.

[45] Johan Bijnens. "Violations of Dashen's theorem". In: *Physics Letters B* 306.3-4 (June 1993), 343–349. ISSN: 0370-2693. DOI: 10.1016/0370-2693(93)90089-z. URL: http://dx.doi.org/10.1016/0370-2693(93)90089-Z.

[46] J. Gasser and G.R.S. Zarnauskas. "On the pion decay constant". In: *Phys. Lett. B* 693 (2010), pp. 122–128. DOI: 10.1016/j.physletb.2010.08.021. arXiv: 1008.3479 [hep-ph].

[47] G.M. de Divitiis et al. "Real photon emissions in leptonic decays". In: (Aug. 2019). arXiv: 1908.10160 [hep-lat].

[48] A. Desiderio et al. "First lattice calculation of radiative leptonic decay rates of pseudoscalar mesons". In: (June 2020). arXiv: 2006.05358 [hep-lat].

[49] V. Lubicz et al. "Finite-Volume QED Corrections to Decay Amplitudes in Lattice QCD". In: *Phys. Rev. D* 95.3 (2017), p. 034504. DOI: 10.1103/PhysRevD.95.034504. arXiv: 1611.08497 [hep-lat].

[50] S.M. Berman. "Radiative corrections to muon and neutron decay". In: *Phys. Rev.* 112 (1958), pp. 267–270. DOI: 10.1103/PhysRev.112.267.

[51] Toichiro Kinoshita and Alberto Sirlin. "Radiative corrections to Fermi interactions". In: *Phys. Rev.* 113 (1959), pp. 1652–1660. DOI: 10.1103/PhysRev.113.1652.

[52] A. Sirlin. "Radiative Corrections in the $SU(2)_L \times U(1)$ Theory: A Simple Renormalization Framework". In: *Phys. Rev. D* 22 (1980), pp. 971–981. DOI: 10.1103/PhysRevD.22.971.

[53] Eric Braaten and Chong-Sheng Li. "Electroweak radiative corrections to the semihadronic decay rate of the tau lepton". In: *Phys. Rev. D* 42 (1990), pp. 3888–3891. DOI: 10.1103/PhysRevD.42.3888.

[54] G. Martinelli et al. "A General method for nonperturbative renormalization of lattice operators". In: *Nucl. Phys. B* 445 (1995), pp. 81–108. DOI: 10.1016/0550-3213(95)00126-D. arXiv: hep-lat/9411010.

[55] Jonathan L. Rosner, Sheldon Stone, and Ruth S. Van de Water. "Leptonic Decays of Charged Pseudoscalar Mesons - 2015". In: (Sept. 2015). arXiv: 1509.02220 [hep-ph].

[56] N. Carrasco et al. "Up, down, strange and charm quark masses with $N_f = 2+1+1$ twisted mass lattice QCD". In: *Nucl. Phys. B* 887 (2014), pp. 19–68. DOI: 10.1016/j.nuclphysb.2014.07.025. arXiv: 1403.4504 [hep-lat].

[57] G. Martinelli and Yi-Cheng Zhang. "The Connection Between Local Operators on the Lattice and in the Continuum and Its Relation to Meson Decay Constants". In: *Phys. Lett. B* 123 (1983), p. 433. DOI: 10.1016/0370-2693(83)90987-5.

[58] Sinya Aoki et al. "Perturbative renormalization factors of bilinear quark operators for improved gluon and quark actions in lattice QCD". In: *Phys. Rev. D* 58 (1998), p. 074505. DOI: 10.1103/PhysRevD.58.074505. arXiv: hep-lat/9802034.

[59] G.Peter Lepage and Paul B. Mackenzie. "On the viability of lattice perturbation theory". In: *Phys. Rev. D* 48 (1993), pp. 2250–2264. DOI: 10.1103/PhysRevD.48.2250. arXiv: hep-lat/9209022.

[60] C. Sturm et al. "Renormalization of quark bilinear operators in a momentum-subtraction scheme with a nonexceptional subtraction point". In: *Phys. Rev. D* 80 (2009), p. 014501. DOI: 10.1103/PhysRevD.80.014501. arXiv: 0901.2599 [hep-ph].

[61] M. Constantinou et al. "Non-perturbative renormalization of quark bilinear operators with $N_f = 2$ (tmQCD) Wilson fermions and the tree-level improved gauge action". In: *JHEP* 08 (2010), p. 068. DOI: 10.1007/JHEP08(2010)068. arXiv: 1004.1115 [hep-lat].

[62] Jean-Rene Cudell, A. Le Yaouanc, and Carlotta Pittori. "Pseudoscalar vertex, Goldstone boson and quark masses on the lattice". In: *Phys. Lett. B* 454 (1999), pp. 105–114. DOI: 10.1016/S0370-2693(99)00339-1. arXiv: hep-lat/9810058.

[63] Leonardo Giusti and A. Vladikas. "RI / MOM renormalization window and Goldstone pole contamination". In: *Phys. Lett. B* 488 (2000), pp. 303–312. DOI: 10.1016/S0370-2693(00)00837-6. arXiv: hep-lat/0005026.

[64] Marco Bochicchio et al. "Chiral Symmetry on the Lattice with Wilson Fermions". In: *Nucl. Phys. B* 262 (1985), p. 331. DOI: 10.1016/0550-3213(85)90290-1.

[65] Yasumichi Aoki. "Quark mass renormalization with non-exceptional momenta". In: *PoS* LATTICE2008 (2008). Ed. by Christopher Aubin et al., p. 222. DOI: 10.22323/1.066.0222. arXiv: 0901.2595 [hep-lat].

[66] Benoit Blossier et al. "Renormalisation constants of quark bilinears in lattice QCD with four dynamical Wilson quarks". In: *PoS* LATTICE2011 (2011). Ed. by Pavlos Vranas, p. 233. DOI: 10.22323/1.139.0233. arXiv: 1112.1540 [hep-lat].

[67] Petros Dimopoulos et al. "Renormalization constants for Wilson fermion lattice QCD with four dynamical flavours". In: *PoS* LATTICE2010 (2010). Ed. by Giancarlo Rossi, p. 235. DOI: 10.22323/1.105.0235. arXiv: 1101.1877 [hep-lat].

[68] R. Frezzotti and G.C. Rossi. "Chirally improving Wilson fermions. 1. $O(a)$ improvement". In: *JHEP* 08 (2004), p. 007. DOI: 10.1088/1126-6708/2004/08/007. arXiv: hep-lat/0306014.

[69] Bradley Efron. "Bootstrap Methods: Another Look at the Jackknife". In: *Annals Statist.* 7.1 (1979), pp. 1–26. DOI: 10.1214/aos/1176344552.

[70] Bradley Efron. *The Jackknife, the bootstrap and other resampling plans*. CBMS-NSF Reg. Conf. Ser. Appl. Math. Lectures given at Bowling Green State Univ., June 1980. Philadelphia, PA: SIAM, 1982. URL: https://cds.cern.ch/record/98913.

[71] Christof Gattringer and Christian B. Lang. *Quantum chromodynamics on the lattice*. Vol. 788. Berlin: Springer, 2010. ISBN: 978-3-642-01849-7, 978-3-642-01850-3. DOI: 10.1007/978-3-642-01850-3.

[72] Stefano Capitani. "Lattice perturbation theory". In: *Phys. Rept.* 382 (2003), pp. 113–302. DOI: 10.1016/S0370-1573(03)00211-4. arXiv: hep-lat/0211036.

[73] K.G. Chetyrkin and A. Retey. "Renormalization and running of quark mass and field in the regularization invariant and MS-bar schemes at three loops and four loops". In: *Nucl. Phys. B* 583 (2000), pp. 3–34. DOI: 10.1016/S0550-3213(00)00331-X. arXiv: hep-ph/9910332.

[74] J.A. Gracey. "Three loop anomalous dimension of nonsinglet quark currents in the RI-prime scheme". In: *Nucl. Phys. B* 662 (2003), pp. 247–278. DOI: 10.1016/S0550-3213(03)00335-3. arXiv: hep-ph/0304113.

[75] M. Constantinou et al. "$O(a^2)$ corrections to the one-loop propagator and bilinears of clover fermions with Symanzik improved gluons". In: *Journal of High Energy Physics* 2009.10 (Oct. 2009), 064–064. ISSN: 1029-8479. DOI: 10.1088/1126-6708/2009/10/064. URL: http://dx.doi.org/10.1088/1126-6708/2009/10/064.

[76] Martha Constantinou et al. "Perturbative renormalization factors and $O(a^2)$ corrections for lattice four-fermion operators with improved fermion/gluon actions". In: *Physical Review D* 83.7 (Apr. 2011). ISSN: 1550-2368. DOI: 10.1103/physrevd.83.074503. URL: http://dx.doi.org/10.1103/PhysRevD.83.074503.

[77] G. Parisi. "Recent Progresses in Gauge Theories". In: *AIP Conf. Proc.* 68 (1980). Ed. by Loyal Durand and Lee G. Pondrom, pp. 1531–1568. DOI: 10.1063/1.2948626.

[78] N. Tantalo et al. "Electromagnetic corrections to leptonic decay rates of charged pseudoscalar mesons: finite-volume effects". In: (Dec. 2016). arXiv: 1612.00199 [hep-lat].

[79] Vincenzo Cirigliano and Ignasi Rosell. "$\pi/K \to e\bar{\nu}_e$ branching ratios to $O(e^2p^4)$ in Chiral Perturbation Theory". In: *JHEP* 10 (2007), p. 005. DOI: 10.1088/1126-6708/2007/10/005. arXiv: 0707.4464 [hep-ph].

[80] Christopher Kane et al. "Radiative leptonic decays on the lattice". In: *PoS* LATTICE2019 (2019), p. 134. DOI: 10.22323/1.363.0134. arXiv: 1907.00279 [hep-lat].

[81] Johan Bijnens and Niclas Danielsson. "Electromagnetic Corrections in Partially Quenched Chiral Perturbation Theory". In: *Phys. Rev. D* 75 (2007), p. 014505. DOI: 10.1103/PhysRevD.75.014505. arXiv: hep-lat/0610127.

[82] J.C. Hardy and I.S. Towner. "Superallowed $0^+ \to 0^+$ nuclear β decays: 2014 critical survey, with precise results for V_{ud} and CKM unitarity". In: *Phys. Rev. C* 102 (2020), p. 045501. DOI: 10.1103/PhysRevC.91.025501. arXiv: 1411.5987 [nucl-ex].

[83] R.J. Dowdall et al. "V_{us} from π and K decay constants in full lattice QCD with physical u, d, s and c quarks". In: *Phys. Rev. D* 88 (2013), p. 074504. DOI: 10.1103/PhysRevD.88.074504. arXiv: 1303.1670 [hep-lat].

[84] N. Carrasco et al. "Leptonic decay constants f_K, f_D, and f_{D_s} with $N_f = 2+1+1$ twisted-mass lattice QCD". In: *Phys. Rev. D* 91.5 (2015), p. 054507. DOI: 10.1103/PhysRevD.91.054507. arXiv: 1411.7908 [hep-lat].

[85] A. Bazavov et al. "B- and D-meson leptonic decay constants from four-flavor lattice QCD". In: *Phys. Rev. D* 98.7 (2018), p. 074512. DOI: 10.1103/PhysRevD.98.074512. arXiv: 1712.09262 [hep-lat].

[86] Chien-Yeah Seng et al. "Reduced Hadronic Uncertainty in the Determination of V_{ud}". In: *Phys. Rev. Lett.* 121.24 (2018), p. 241804. DOI: 10.1103/PhysRevLett.121.241804. arXiv: 1807.10197 [hep-ph].

[87] Benedetta Belfatto, Revaz Beradze, and Zurab Berezhiani. "The CKM unitarity problem: A trace of new physics at the TeV scale?" In: *Eur. Phys. J. C* 80.2 (2020), p. 149. DOI: 10.1140/epjc/s10052-020-7691-6. arXiv: 1906.02714 [hep-ph].

[88] J.C. Hardy and I.S. Towner. "Superallowed $0^+ \to 0^+$ nuclear β decays: 2020 critical survey, with implications for Vud and CKM unitarity". In: *Phys. Rev. C* 102.4 (2020), p. 045501. DOI: 10.1103/PhysRevC.102.045501.

[89] Chien Yeah Seng, Mikhail Gorchtein, and Michael J. Ramsey-Musolf. "Dispersive evaluation of the inner radiative correction in neutron and nuclear β decay". In: *Phys. Rev. D* 100.1 (2019), p. 013001. DOI: 10.1103/PhysRevD.100.013001. arXiv: 1812.03352 [nucl-th].

[90] Andrzej Czarnecki, William J. Marciano, and Alberto Sirlin. "Radiative Corrections to Neutron and Nuclear Beta Decays Revisited". In: *Phys. Rev. D* 100.7 (2019), p. 073008. DOI: 10.1103/PhysRevD.100.073008. arXiv: 1907.06737 [hep-ph].

[91] T. van Ritbergen, J.A.M. Vermaseren, and S.A. Larin. "The Four loop beta function in quantum chromodynamics". In: *Phys. Lett. B* 400 (1997), pp. 379–384. DOI: 10.1016/S0370-2693(97)00370-5. arXiv: hep-ph/9701390.

[92] Gerard 't Hooft and M.J.G. Veltman. "Regularization and Renormalization of Gauge Fields". In: *Nucl. Phys. B* 44 (1972), pp. 189–213. DOI: 10.1016/0550-3213(72)90279-9.

[93] C.G. Bollini and J.J. Giambiagi. "Dimensional Renormalization: The Number of Dimensions as a Regularizing Parameter". In: *Nuovo Cim. B* 12 (1972), pp. 20–26. DOI: 10.1007/BF02895558.

[94] Gerard 't Hooft. "Dimensional regularization and the renormalization group". In: *Nucl. Phys. B* 61 (1973), pp. 455–468. DOI: 10.1016/0550-3213(73)90376-3.

[95] P. Breitenlohner and D. Maison. "Dimensional Renormalization and the Action Principle". In: *Commun. Math. Phys.* 52 (1977), pp. 11–38. DOI: 10.1007/BF01609069.

[96] Guido Altarelli et al. "QCD Nonleading Corrections to Weak Decays as an Application of Regularization by Dimensional Reduction". In: *Nucl. Phys. B* 187 (1981), pp. 461–513. DOI: 10.1016/0550-3213(81)90473-9.

[97] Andrzej J. Buras and Peter H. Weisz. "QCD Nonleading Corrections to Weak Decays in Dimensional Regularization and 't Hooft-Veltman Schemes". In: *Nucl. Phys. B* 333 (1990), pp. 66–99. DOI: 10.1016/0550-3213(90)90223-Z.

[98] Michael J. Dugan and Benjamin Grinstein. "On the vanishing of evanescent operators". In: *Phys. Lett. B* 256 (1991), pp. 239–244. DOI: 10.1016/0370-2693(91)90680-O.

[99] Stefan Herrlich and Ulrich Nierste. "Evanescent operators, scheme dependences and double insertions". In: *Nucl. Phys. B* 455 (1995), pp. 39–58. DOI: 10.1016/0550-3213(95)00474-7. arXiv: hep-ph/9412375.

[100] Wolfram Research, Inc. *Mathematica, Version 12.1*. Champaign, IL, 2020. URL: https://www.wolfram.com/mathematica.

[101] Vladimir A. Smirnov. *Evaluating Feynman Integrals*. Vol. 211. Berlin: Springer, 2005, p. 250. ISBN: 978-3-540-23933-8, 978-3-642-06297-1. DOI: 10.1007/b95498.

[102] E.G. Floratos, D.A. Ross, and Christopher T. Sachrajda. "Higher Order Effects in Asymptotically Free Gauge Theories: The Anomalous Dimensions of Wilson Operators". In: *Nucl. Phys. B* 129 (1977). [Erratum: Nucl.Phys.B 139, 545–546 (1978)], pp. 66–88. DOI: 10.1016/0550-3213(77)90020-7.

[103] Joachim Brod and Martin Gorbahn. "Electroweak Corrections to the Charm Quark Contribution to $K^+ \to \pi^+ \nu\bar{\nu}$". In: *Phys. Rev. D* 78 (2008), p. 034006. DOI: 10.1103/PhysRevD.78.034006. arXiv: 0805.4119 [hep-ph].

[104] Jason Aebischer et al. "B-decay discrepancies after Moriond 2019". In: *Eur. Phys. J. C* 80.3 (2020), p. 252. DOI: 10.1140/epjc/s10052-020-7817-x. arXiv: 1903.10434 [hep-ph].

[105] Andrzej J. Buras, Mikolaj Misiak, and Jorg Urban. "Two loop QCD anomalous dimensions of flavor changing four quark operators within and beyond the standard model". In: *Nucl. Phys. B* 586 (2000), pp. 397–426. DOI: 10.1016/S0550-3213(00)00437-5. arXiv: hep-ph/0005183.

[106] Jason Aebischer et al. "B physics Beyond the Standard Model at One Loop: Complete Renormalization Group Evolution below the Electroweak Scale". In: *JHEP* 09 (2017), p. 158. DOI: 10.1007/JHEP09(2017)158. arXiv: 1704.06639 [hep-ph].

[107] Christoph Bobeth, Gudrun Hiller, and Giorgi Piranishvili. "Angular distributions of $\bar{B} \to \bar{K}\ell^+\ell^-$ decays". In: *JHEP* 12 (2007), p. 040. DOI: 10.1088/1126-6708/2007/12/040. arXiv: 0709.4174 [hep-ph].

[108] M. Antonelli et al. "An Evaluation of $|V_{us}|$ and precise tests of the Standard Model from world data on leptonic and semileptonic kaon decays". In: *Eur. Phys. J. C* 69 (2010), pp. 399–424. DOI: 10.1140/epjc/s10052-010-1406-3. arXiv: 1005.2323 [hep-ph].

[109] Matthew Moulson. "Experimental determination of V_{us} from kaon decays". In: *8th International Workshop on the CKM Unitarity Triangle*. Nov. 2014. arXiv: 1411.5252 [hep-ex].

[110] Matthew Moulson. "Experimental determination of V_{us} from kaon decays". In: *PoS* CKM2016 (2017), p. 033. DOI: 10.22323/1.291.0033. arXiv: 1704.04104 [hep-ex].

[111] Roberto Frezzotti, Giancarlo Rossi, and Nazario Tantalo. "Sea quark QED effects and twisted mass fermions". In: *PoS* LATTICE2016 (2016), p. 320. DOI: 10.22323/1.256.0320. arXiv: 1612.02265 [hep-lat].

[112] Constantia Alexandrou et al. "Simulating twisted mass fermions at physical light, strange and charm quark masses". In: *Phys. Rev. D* 98.5 (2018), p. 054518. DOI: 10.1103/PhysRevD.98.054518. arXiv: 1807.00495 [hep-lat].

[113] Georg Bergner et al. "Quark masses and decay constants in $N_f = 2 + 1 + 1$ isoQCD with Wilson clover twisted mass fermions". In: *PoS* LATTICE2019 (2020), p. 181. DOI: 10.22323/1.363.0181. arXiv: 2001.09116 [hep-lat].

[114] C.T. Sachrajda et al. "Radiative corrections to semileptonic decay rates". In: *PoS* LATTICE2019 (2019), p. 162. DOI: 10.22323/1.363.0162. arXiv: 1910.07342 [hep-lat].